UNIVERSIDAD DE BURGOS

Study of novel pro-viral activities of non-structural protein 1 (NS1) of influenza A virus

DOCTORAL THESIS

Ms. Sadaf Aslam

DIRECTORS

Dr. Juan Ayllón Barasoain

Dr. Adolfo García-Sastre

UNIVERSIDAD DE BURGOS

Doctorate in Health Sciences

"Vísteme despacio, que tengo prisa."

"The more you study, the more you know; how less you know."

"Compromise for your dream. But never compromise on your dream."

Imran Khan

"Education is not merely acquiring knowledge, but it is about developing the ability to think."
Allama Iqbal

ACKNOWLEDGMENTS

ACKNOWLEDGMENTS

ACKNOWLEDGMENTS

I owe my deepest gratitude to my mentors, Dr. Adolfo García-Sastre and Dr. Juan Ayllón Barasoain. This journey would not have been possible without your support, guidance, and belief in me.

Adolfo, thank you for giving me the incredible opportunity to work on this beautiful project—and many others—under your mentorship. Your generosity in providing the freedom to explore and learn has had a profound impact on my development as a scientist. Before joining your lab, I knew very little about influenza beyond the seasonal flu vaccines. Today, I can design and generate recombinant viruses using reverse genetics—something I never imagined I would be capable of. I am sincerely grateful for your patience, your encouragement, and the trust you placed in me, especially during moments when I doubted myself. Thank you for standing by me when I needed it most. It has been a true honor to learn from you.

Juan, I honestly do not have the words to fully express how thankful I am for your mentorship, which began on the very first day of this journey. When I started working with you as a research associate, I had no prior experience at the bench and only a dream of one day becoming a medical doctor. Working alongside you changed the course of my life. You opened the doors to science for me and helped me discover a passion I didn't know I had. From the moment I realized I wanted to pursue a PhD, I hoped it would be under your guidance. Thank you for your endless patience with all my questions, for teaching me with such kindness and clarity, and for guiding me through every step of the way—both in person at Mount Sinai and remotely during my time at the University of Burgos. You have been a true inspiration to me, not only as a scientist but also as a person. I can only hope to carry forward your example of humility, knowledge, and compassion. *Gracias por todo, de corazón*.

I would like to thank Dr. Silvia Ubillos Landa for being so warm and welcoming and always guiding me with the technical details of the doctoral school.

ACKNOWLEDGMENTS

I would like to thank Dr. Benjamin Hale for his feedback and for kindly allowing me to use the figure from his publication.

I would also like to express my heartfelt thanks to Dr. Sara Cuadrado-Castaño for always being there for me, for your constant support, and for your guidance at every step.

This journey would not have been the same without the people I had the privilege of meeting and working with in the lab. I am especially thankful to Drs. Maite, Tere, Lisa, Melissa and my labmates (Fam 1684): Claire, Dr. Randy, Rebecca, and Dan—as well as Ryan, Richard and Danae—for their camaraderie, support, and encouragement. To all the friends I've made along the way—Alba, Arantza, Amaya, Amy, Jane, and many others—thank you for making this experience so full of joy, laughter, and meaning. I am also grateful to all the past and present members of the García-Sastre laboratory. Thank you for guiding me throughout these years and helping me along the way.

Finally, I want to thank my family for their unconditional love and unwavering support. Thank you to my Nani (grandmother), my mom, my sister, and all my aunts and uncles for giving me the space to dream and the courage to pursue what makes me truly happy. Your love has been the foundation of everything I've accomplished. I carry it with me every day.

ACKNOWLEDGMENTS

Table of Contents

Table of Contents

Table of Contents

Table of Contents

Index of Figures

Index of Figures

Index of Figures

Index of Figures

Index of Tables

Index of Tables

Index of Tables

Index of Tables

List of Abbreviations

List of Abbreviations

List of Abbreviations

NS1	Non-structural 1
PI3K	Phosphoinositide 3-kinase
BiFC	Bimolecular Fluorescence Complementation
IAV	Influenza A virus
HA	Hemagglutinin
NA	Neuraminidase
CDC	Centers for Disease Control and Prevention
PB1	Polymerase basic 1
PB2	Polymerase basic 2
PA	Polymerase acidic
NP	Nucleoprotein
M	Matrix
vRNP	Viral ribonucleoproteins
NLS	Nuclear localization signal
RBD	RNA binding domain
ED	Effector domain
dsRNA	Double stranded RNA
vRNA	Viral RNA
cRNA	Complementary RNA
mRNA	Messenger RNA
snRNA	Small nuclear RNA
NEP	Nuclear export protein
kDa	Kilodalton
ISG	Interferon stimulated gene
Mx	Myxovirus
PKR	Protein kinase R
RIG-I	Retinoic acid-inducible gene I
TRIM25	Tripartite motif-containing 25
RIPLET	RING finger protein leading to RIG-I

List of Abbreviations

CARD	Caspase recruitment domain
PRR	Pattern recognition receptor
IFN	Interferon
MAVS	Mitochondrial antiviral signaling
CPSF	Cleavage and polyadenylation specificity factor
OAS	2'-5'-oligo (A) synthetase
eIF2	Eukaryotic initiation factor 2
GDP	Guanosine diphosphate
ATP	Adenosine triphosphate
SH2	Src homology 2
PKB/Akt	Protein kinase B
PDK-1	Phosphoinositide-dependent kinase-1
mTORC2	Mammalian target of rapamycin complex
pAkt	Phosphorylated Akt
ABD	Adaptor binding domain
RBD	Ras binding domain
HD	Helical domain
SH3	Src homology 3
BH	B-cell receptor homology
iSH2	Inter SH2
RTK	Receptor tyrosine kinase
PIP3	Phosphatidylinositol-3,4,5-trisphosphate
PH	Pleckstrin homology
PTEN	Phosphatase and tensin homologue deleted on chromosome 10
PR8	A/Puerto Rico/8/1934 virus strain
WSN	A/WSN/1933 virus strain
pDZ	Plasmid Dimitry Zamarian
IRES	Internal ribosome entry site
DMEM	Dulbecco's Modified Eagle's Medium
FBS	Fetal bovine serum
MEM	Minimum Essential Medium

List of Abbreviations

BA	Bovine albumin
PS (Pen/Strep)	Penicillin/streptomycin
DEAE-dextran	Diethylaminoethyl-dextran
TPCK-trypsin	N-Tosyl-L-phenylalanyl chloromethyl ketone-treated trypsin
LB	Luria-Bertani
2XYT	2 times Yeast Extract Tryptone medium
SPF	Specific pathogen free
PBS	Phosphate buffered saline
RBC	Red blood cell
HA assay	Hemagglutination assay
HAU	Hemagglutination unit
BSA	Bovine serum albumin
PFA	Paraformaldehyde
HRP	Horseradish peroxidase
RTPCR	Real-time polymerase chain reaction
PCR	Polymerase chain reaction
DNTP	Deoxyribonucleotide triphosphate
cDNA	complementary DNA
ORF	Open reading frame
DAPI	4′,6-diamidino-2-phenylindole
RT	Room temperature
SDS-PAGE	Sodium dodecyl sulfate polyacrylamide gel electrophoresis
PVDF	Polyvinylidene difluoride
PBST	Phosphate buffered saline tween
GFP	Green fluorescent protein
YFP	Yellow fluorescent protein
Co-IP	Co-immunoprecipitation
GST	Glutathione S-Transferase
PEI	Polyethyleneimine
βME	Beta-mercaptoethanol
PC	Phosphatidylcholine

List of Abbreviations

MOI	Multiplicity of infection
pY	Phosphorylated tyrosine
PC	Phosphatidylcholine
PEI	Polyethyleneimine
GST	Glutathione S-Transferase
BAD	Bcl-2-associated death promoter
FOXO	Forkhead box O1
FAK	Focal adhesion kinase
EGFR	Epidermal growth factor receptor
GPCRs	G-protein coupled receptors
VEGFR	Vascular endothelial growth factor
WNV	West Nile virus
DC	Dendritic cell

List of Abbreviations

Summary

Summary

Abstract

The non-structural protein 1 (NS1) of influenza A virus performs a broad variety of pro-viral activities in the infected cell, primarily mediating evasion from the host innate immune response by being the main viral interferon antagonist. However, among the multiple interactions described for this small multifunctional protein, there are several whose biological relevance remains obscure, such as the ability of NS1 to bind and activate class IA phosphoinositide 3-kinases (PI3Ks). PI3Ks are highly regulated lipid kinases that act as critical nodes in multiple cell signaling networks and regulate cellular physiology, including differentiation, growth, survival, trafficking, and immune function. As such, PI3Ks are also important proto-oncogenes whose deregulation lies behind a substantial number of different human cancers. Structurally, class IA PI3Ks are heterodimers formed by a regulatory (p85) and catalytic (p110) subunit, of which there are several isoforms described, adding further layers of complexity to their activity. Activation of PI3K by NS1 is mediated by NS1 binding to the p85 subunit. Interestingly, such binding is specific to the p85β isoform, and PI3K heterodimers containing p85β and any of the other three p110 isoforms are presumably activated by NS1. However, the significance of this p85β specificity, and the contributions of different p110 isoforms, remains unknown.

In order to better understand the consequences of PI3K activation by NS1, we have developed a bimolecular fluorescence complementation (BiFC) assay to selectively track the different PI3K heterodimers according to their specific regulatory and catalytic isoforms, as well as to assess their behavior upon activation. Using this system, we found that NS1 induces an isoform-specific relocation and activation of the different PI3K heterodimers. However, the effects of other known activators of PI3K, such as Ras and Src, were different from those induced by NS1. We found that clinically relevant, oncogenic hyper-activating mutations in both catalytic and regulatory subunits of PI3K could mimic the effect caused by NS1, and partially rescued the loss of viral fitness in a recombinant virus encoding a p85β-binding deficient NS1. We postulate that by mimicking an oncogenic deregulation of the PI3K pathway, influenza A virus induces a transient, transformed-like status in the infected cell to stimulate virus replication.

Keywords: Influenza A virus, Non-structural protein 1 (NS1), Phosphoinositide-3-kinase (PI3K), Bimolecular fluorescence complementation (BiFC)

Summary

1. Introduction

1. Introduction

1. Introduction

1.1 Influenza viruses

Influenza viruses (IAVs) are negative-sense, segmented single-stranded RNA viruses belonging to the *Orthomyxoviridae* family (47). This family consists of seven genera: *Alphainfluenzavirus, Betainfluenzavirus, Deltainfluenzavirus, Gammainfluenzavirus, Isavirus, Quaranjaviros* and *Thogotovirus*, of which we will focus on *influenza A virus* species belonging to the *Alphainfluenzavirus* genus (88, 89, 119). Influenza A and B viruses are the most predominantly studied because they circulate in humans and cause seasonal epidemics. According to Centers for Disease Control and Prevention (CDC), there have been 21-37 million medical visits for flu between October 1, 2024-May 10, 2025, and about a million hospitalizations in the US (1). Moreover, IAVs not only cause infections in humans but other mammalian and avian hosts as well. Due to this diverse range of hosts there is potential for the virus to jump from one species to another, and these zoonotic introductions have also been the cause of several past pandemics (88).

1.1.1 Virion structure. Antigenic drift and antigenic shift of influenza viruses.

Influenza A virus has a genome that consists of eight RNA segments encoding 11-14 proteins. The eight segments are PB1 (polymerase basic 1), PB2 (polymerase basic 2), PA (polymerase acidic), HA (hemagglutinin), NP (nucleoprotein), NA (neuraminidase), M (matrix) and NS (non-structural). These segments produce the following proteins: PB1, PB1-F2, PB1-N40, PB2, PA, PA-X, HA, NP, NA, M1, M2, NS1, NS3 and NEP (21, 26, 89). Influenza virus virions are composed of a viral envelope made of a lipid bilayer that contains two membrane proteins (HA and NA) and one transmembrane protein (M2) (**Figure 1**). M1 is located just below the lipid membrane and forms a matrix that holds the viral ribonucleoproteins (vRNPs). vRNPs are the core of the virus and are composed of a negative strand vRNA (viral RNA), which is wrapped in NP. At one end of the vRNP are the three polymerases: PB1, PB2 and PA. Together, they make up the viral RNA polymerase complex (25, 123, 140).

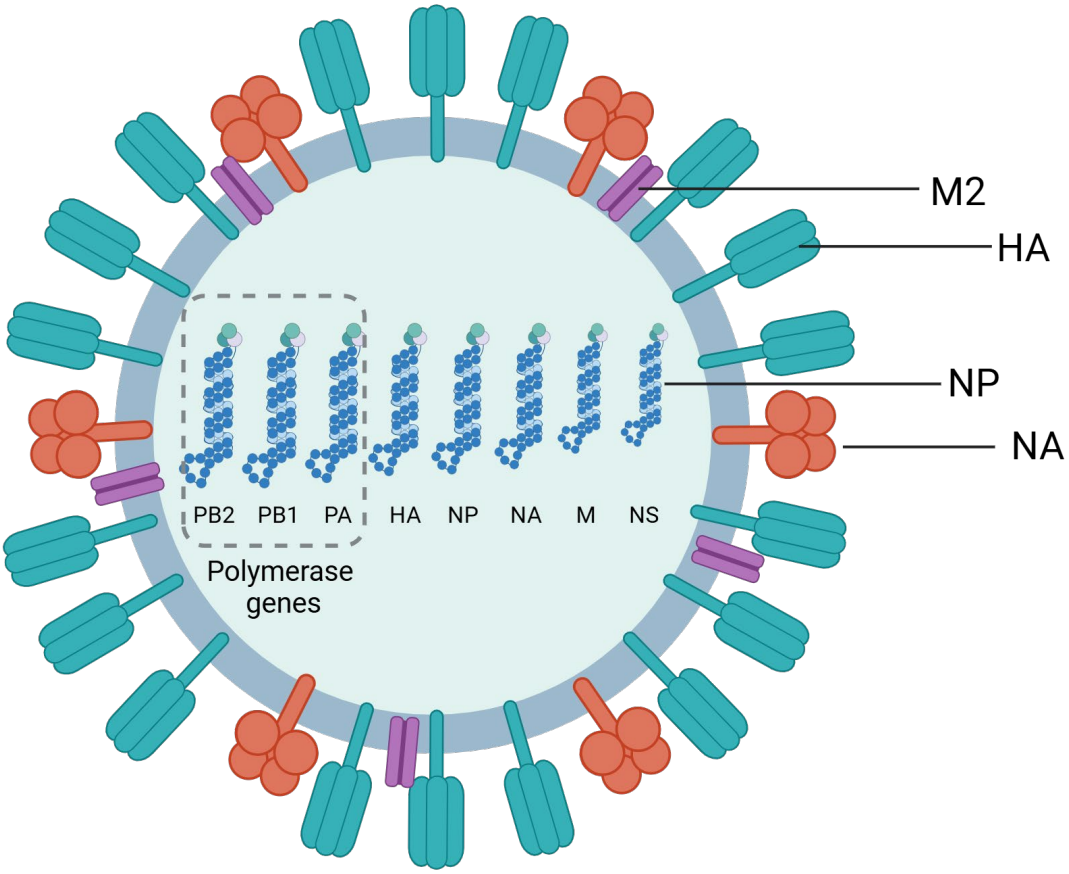

Figure 1. Schematic of influenza A virus virion.
The virion is made of lipid envelope made of the host membrane. HA and NA glycoproteins are expressed on the surface and M2 is a transmembrane protein. The internal structure is made of the M1 structural protein. Eight vRNPs are packed in the core, consisting of vRNA wrapped in NP *(Generated using Biorender).*

IAV are subtyped based on their two surface glycoproteins, hemagglutinin (HA) and neuraminidase (NA). There have been identified 19 different HA and 11 different NA (80, 178) subtypes in nature. Subtypes H1N1 and H3N2 are the most predominant in humans and are the cause of seasonal epidemics every year. The reason for such high rates of infections is due to the nature of the virus and its ability to evolve past population existing immunity. This may be achieved by two phenomena: antigenic shift and antigenic drift. Antigenic drift originates from the gradual accumulation of mutations overtime during replication, due to error prone

polymerase activity (**Figure 2**), and it´s the main source of seasonal variability. Antigenic shift, on the other hand, supposes a far bigger genetic change to the virus and it is due to the segmented nature of influenza virus genome. During co-infection, one or more segments from one virus are combined with segments from another leading to a novel genotype (**Figure 3**). Such events may lead to pandemics because of the lack of immunity to this antigenically novel combination (103, 125, 182). Antigenic shift is rare in comparison to antigenic drift yet, in the last 100 years, there have been four pandemics caused by the emergence in human populations of the following subtypes, H1N1 (1918), H2N2 (1957), H3N2 (1968) and H1N1 (2009) (**Figure 4**), with the 1918 pandemic being the deadliest, killing about 40-50 million people (103, 144).

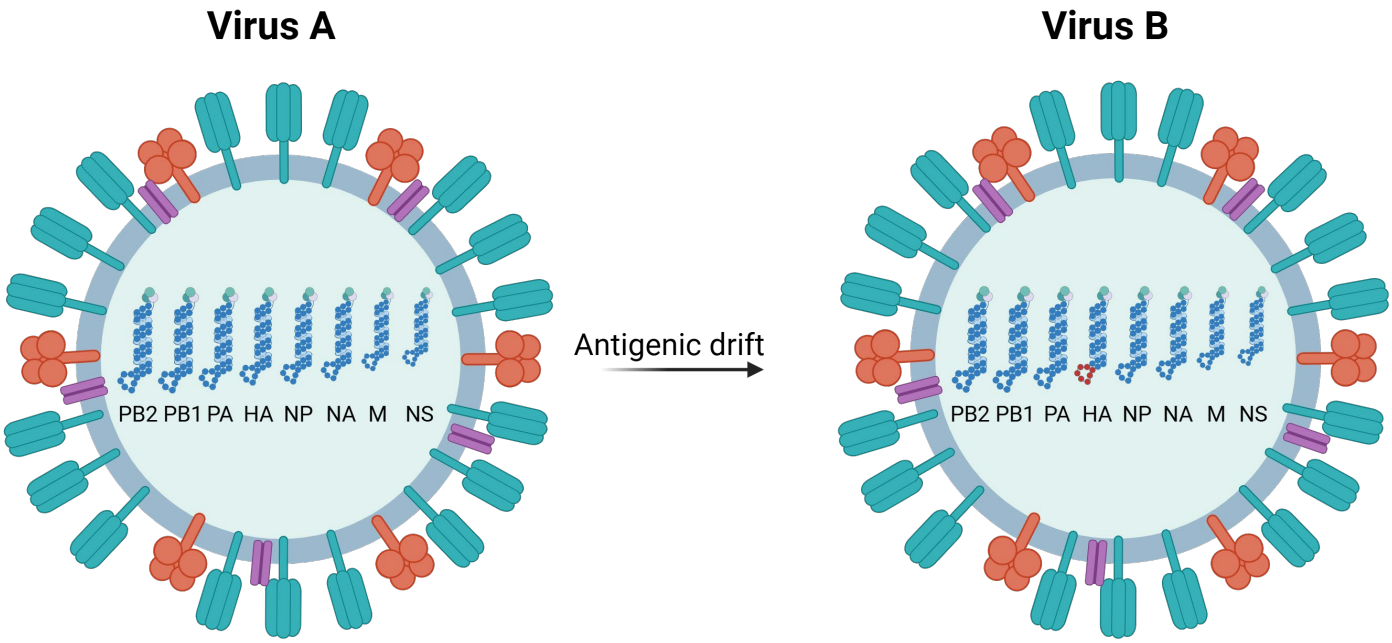

Figure 2. Schematic representation of antigenic drift
Schematic representing an antigenic drift event in influenza A virus. Overtime mutations are accumulated to allow escape from the host immune response. As depicted, there are small changes in the HA protein that differentiate virus A from B *(Generated using Biorender).*

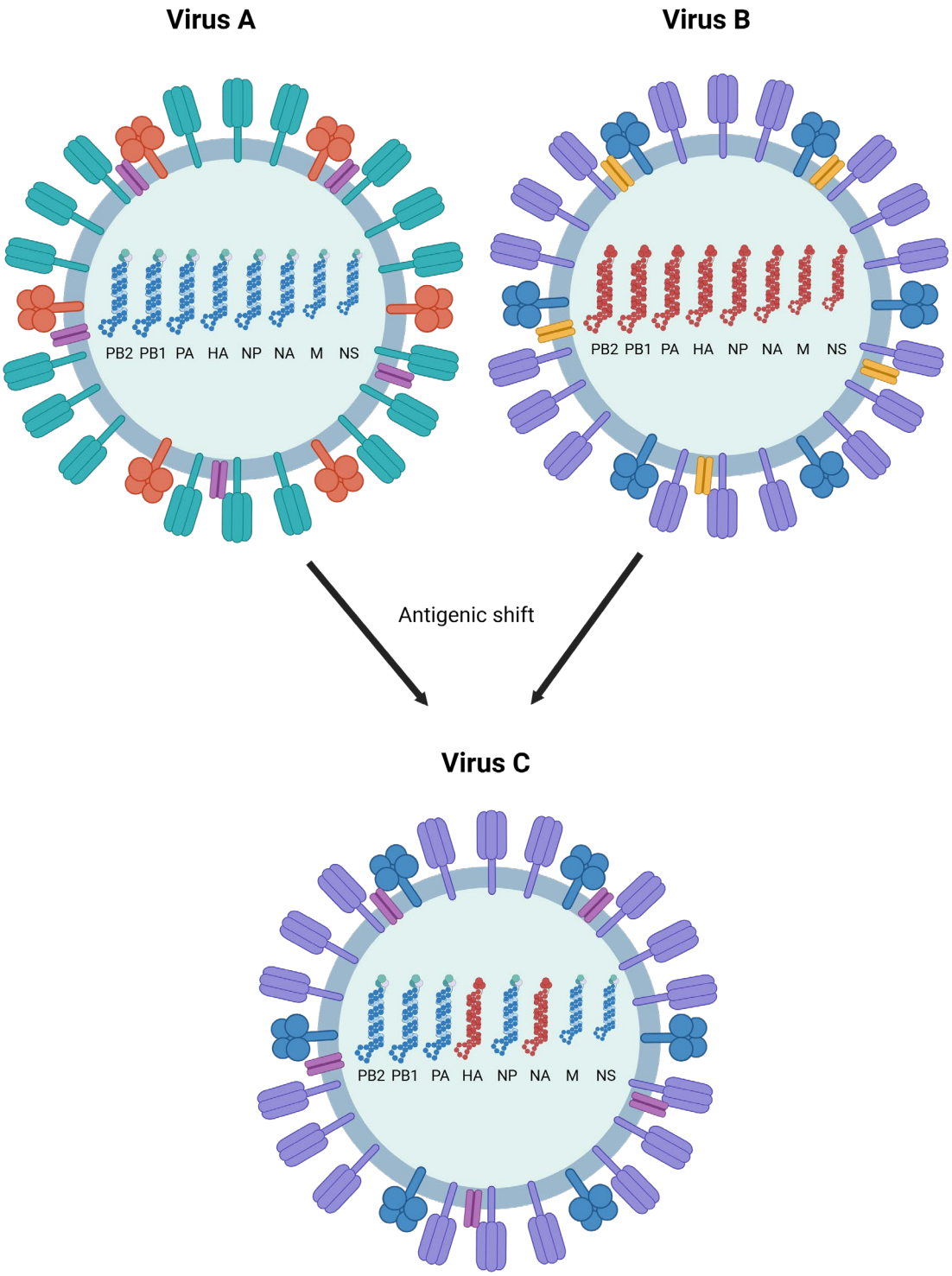

Figure 3. Schematic representation of Antigenic shift
A schematic representation of an antigenic shift event, when a cell is co-infected with two different strains of influenza A virus. There is a potential for a novel reassortant virus to emerge, where 1 or more segments from virus A can mix with segments from virus B to generate a new virus (virus C) that is drastically different and can escape the host immune response *(Generated using Biorender)*.

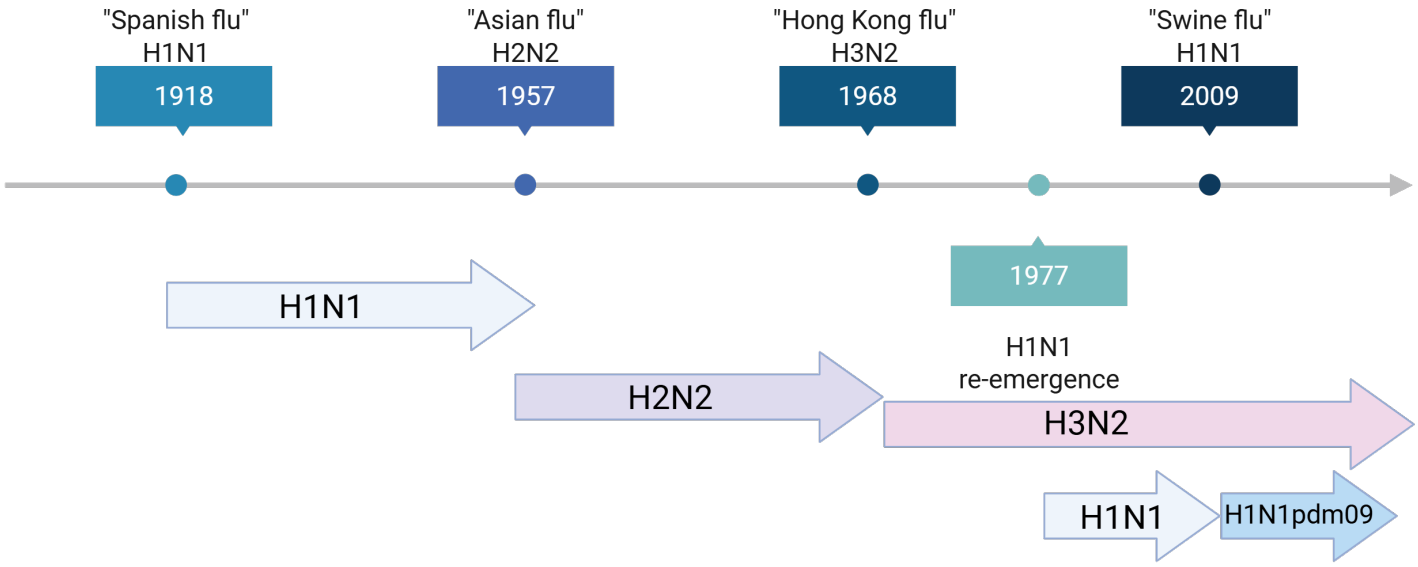

Figure 4. Pandemic timeline
Timeline representing past recorded influenza virus pandemics. These pandemics were emergence of different reassortant viruses and the re-emergence of H1N1 is highlighted as well. *(Generated using Biorender)*

1.1.2 Replication cycle

The replication cycle of the influenza virus has been studied in detail over the years (**Figure 5**). The virus binds to sialylated surface receptors (*N*-acetylneuraminic acid attached to the penultimate galactose sugar by an α2-6–linked sialic acids in humans and α2-3 linkage in avian species) (55), and the virion is endocytosed using the traditional clathrin-mediated pathway (176). Following endocytosis, the low pH of the endosome leads to the fusion of the viral membrane with the endosome, resulting in the release of the vRNPs into the cytoplasm. This fusion activity is triggered by a structural change in the HA. The free RNPs are transported to the nucleus through the nuclear pores and utilize the nucleocytoplasmic trafficking machinery of the host. All proteins in the RNP complex contain nuclear localization signal (NLS); however, the NLSs on NP have been shown to be sufficient and important for the import of vRNA. Importin-α binds to the NLS and recruits importin-β into a trimeric complex that docks at the nuclear pore complex (37).

Influenza virus replication depends on an RNA-dependent RNA polymerase complex comprised of PB1, PB2 and PA. The core of the polymerase is made up of PB1, the C-terminal domain of PA, and the N-terminal domain of PB2. This complex binds to the terminal ends of vRNA and cRNA for initiation of transcription and replication (186). Full length copies of vRNAs are made into positive strand cRNAs that are used as templates for new negative sense genomic vRNAs (121). Newly formed RNP complexes are assembled in the nucleus and then exported to the cytoplasm. M1 and NEP facilitate the export of the new RNP complexes to the cytoplasm.

Initiation of messenger RNA synthesis occurs through "cap snatching" from host pre-mRNA transcripts by PB2, and cleavage of bound mRNAs and small nuclear RNAs (snRNAs) by PA (48). RNA chain elongation is catalyzed by PB1, followed by polyadenylation by the same polymerase. Polyadenylation is dependent on an uninterrupted stretch of five to seven "U" residues (132). Polyadenylation is needed to properly export mRNAs from the nucleus and for their processing and gene expression. Some of the segments code for more than one gene using alternative splicing, ex., NS into NS1 and NEP. Viral mRNA is spliced using the host (cell) splicing machinery. Various viral proteins are synthesized using the host's translation machinery and are produced by both cytosolic and endoplasmic reticulum-associated ribosomes.

Some of the newly synthesized proteins, such as NP and polymerases, are imported back into the nucleus for additional mRNA and vRNA generation. The remaining vRNPs in the cytoplasm are trafficked toward the plasma membrane for assembly via Rab11. The glycoproteins are processed through the ER-associated ribosomes and are folded into their proper configurations. Oligomerization of HA and NA occurs into a trimer and tetramer, respectively. Following folding and oligomerization, HA is cleaved into HA1 and HA2 in the *trans-Golgi* network. The viral components are assembled at the apical plasma membrane sites into a 7+1 configuration, and the virus buds and is released when NA cleaves the local sialic acid residues.

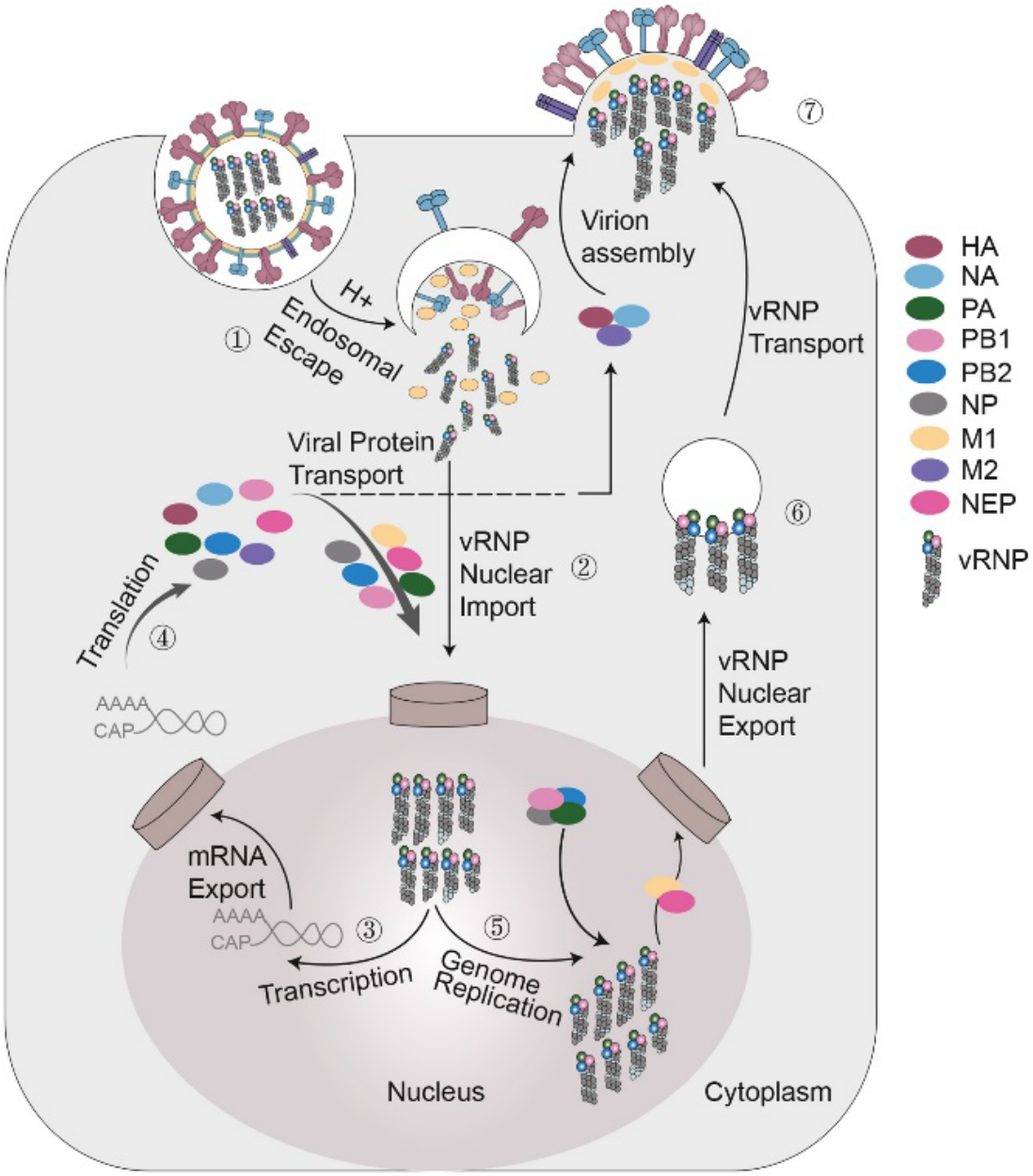

Figure 5. Schematic of influenza A virus replication cycle.
Influenza virus replication cycle starts with the attachment of virus and entry by endocytosis. vRNP are released into the cytoplasm that is transported into the nucleus. Transcription and genome replication occurs in the nucleus. mRNA is exported to the cytoplasm where translation occurs and viral proteins are generated. Newly synthesized vRNA and translated viral proteins form new vRNPS that assemble into virions. *Adapted from Du et al. 2023 (39).*

1.2 The NS1 protein

The main focus of this thesis is the non-structural protein 1 (NS1) of influenza A virus. NS1 is encoded by the smallest of the eight genomic segments of the influenza A virus (148). It was first identified as a non-structural protein in the 1970s (96) and is a highly expressed protein, generated from the collinear mRNA transcribed from the same segment that also encodes NEP (nuclear export protein), through alternative splicing (71, 94). NS1 and NEP share the first 10 amino acids, and bases 503-690 of the NS1 coding sequence with bases 31-221 of NEP (95). A third protein, NS3, has also been described in some influenza A virus isolates, arising through alternative splicing. This protein is mainly found in strains that carry the mutation D125G (A374G), which creates a novel splice donor site (147).

NS1 mRNA is translated into a ~26 kDa polypeptide, and the length may vary slightly among different strains of IAV, typically ranging between 215 and 237 amino acids (63). Based on sequence homology, NS1 proteins are categorized into two subsets, referred to as alleles A and B (8, 105, 161). The polypeptide is comprised of two globular domains: an N-terminal RNA binding domain (RBD) (amino acids 1-73) and a C-terminal effector domain (ED) (185-end), separated by a short linker region and followed by a C-terminal tail (8). Most of the NS1 proteins consist of 11 amino acid long linker regions; however, highly pathogenic H5N1 strains isolated after 2000 exhibit a deletion of 5 amino acids (residues 80-84) (8).

The RNA binding domain consists of three α-helices and homodimerizes to generate a six-helix antiparallel bundle, which serves as the binding site for dsRNA (double stranded RNA) (27, 101, 175) (**Figure 6**). Mutational analysis has shown that dimerization is absolutely required for RNA binding and that the arginine at position 38 is required for this process (175). The effector domain is formed by seven β-strands and three α-helices and is capable of independent homodimerization (20, 59).

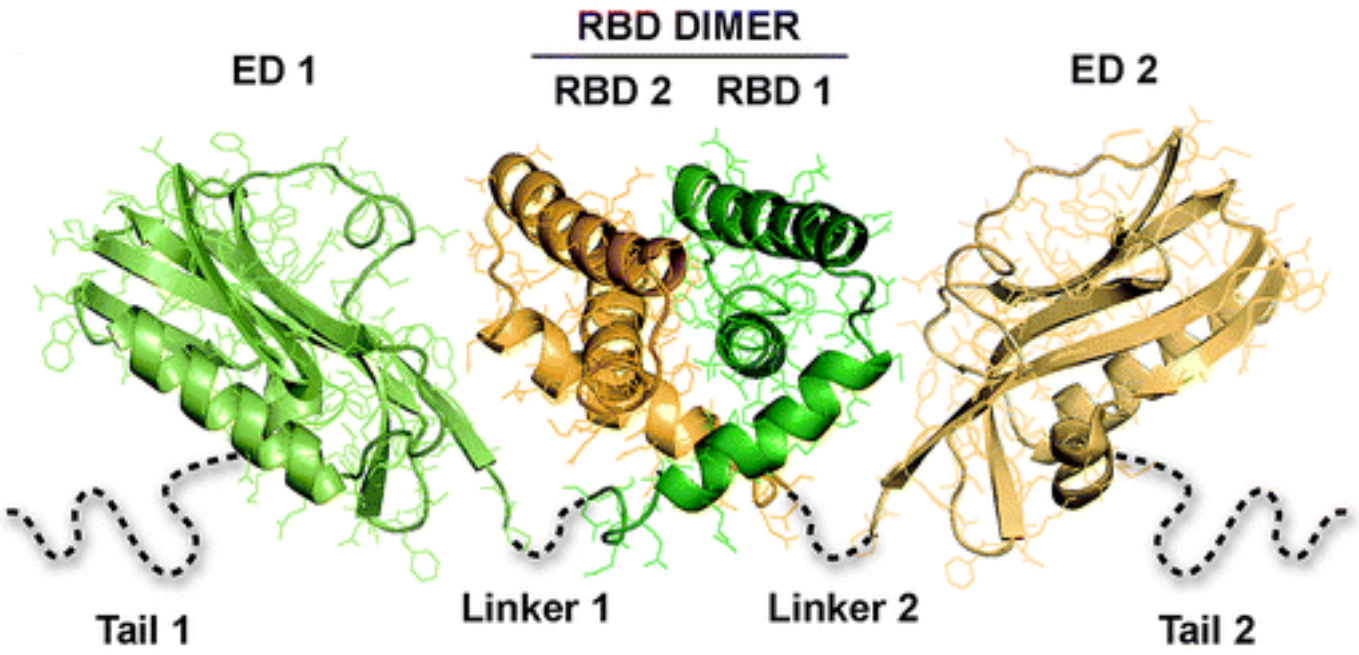

Figure 6. Crystal structure of NS1 homodimer.
NS1 is made of RNA binding domain and effector domain that are connected by a linker region and it also contains a C-terminal tail. Here the crystal structure of a homodimer is represented with one monomer in green (1) and another in gold (2). The RBDs are made of 3 alpha helices and the ED is made of 7 β-strands. *Adapted from Ayllon et al. 2015 (8).*

Structural and biochemical analyses have shown that tryptophan at position 187 is required for the dimerization of NS1 ED (6, 63, 83). Pull-down assays showed that the ability of NS1 ED to form helix-helix dimers was important for the efficient activity of the RBD. When a poly I:C pull-down assay was performed with NS1 WT, NS1 W187A mutant, and NS1 R38A (dsRNA-binding incompetent mutant) was performed, NS1 WT (wild type) bound successfully to poly I:C but NS1 W187A bound less efficiently and as expected no poly I:C was bound to NS1 R38A (**Figure 7**).

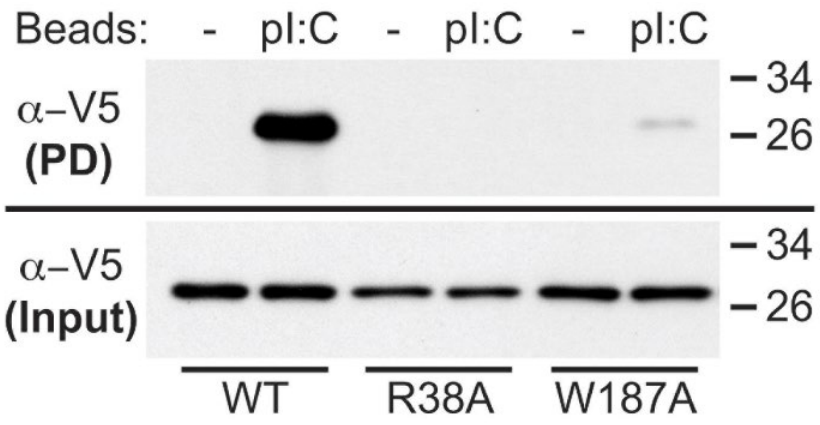

Figure 7. Functionally testing NS1 binding to synthetic dsRNA.
Cells were transfected with NS1 WT, NS1 R38A, and NS1 W187A constructs and pull down assay was performed with beads either conjugated with poly I:C or blank. NS1 WT successfully bound dsRNA while NS1 W187A was not efficiently bound indicating that dimeric NS1 is required for dsRNA binding. R38A was a negative control and did not bind any dsRNA as expected. *Adapted from Kerry et al. 2011* (83).

1.2.1 Functions of the NS1 protein

NS1 is a multifunctional protein that is involved in various mechanisms to aid viral replication, host gene regulation and evasion of the innate immune response (8). Since its discovery in 1971, NS1 has been the focus of extensive research due to its ability to interfere with various cellular processes that would otherwise inhibit viral propagation. One of the first functions of NS1 to be described was its ability to bind different species of RNAs (vRNA, dsRNA, poly(A) tails, and snRNA).Through these interactions, NS1 disrupts host mRNA processing by blocking the splicing of pre-mRNA and the export of polyadenylated mRNAs out of the nucleus (8). NS1 also plays a critical role in antagonizing the host's antiviral defense mechanisms, particularly the interferon (IFN) response. The concept of interferon as a host-derived antiviral factor was first described by Isaacs and Lindenmann in 1957. They demonstrated that cells treated with heat-inactivated viruses developed resistance ("interference") to subsequent infections (72, 73), whereas cells infected with live viruses did not exhibit this effect. Consequently, they termed the phenomenon "reverse interference" (64). As research progressed, the development of reverse genetics techniques (49, 120) and generation of NS1-deficient virus led to the discovery that the NS1 protein is the virally encoded antagonist of the interferon response predicted by Lindenmann

(8, 56). Mammalian cells respond to viral infections by initiating signaling cascades that lead to the production of type I (IFNα and IFNβ) and type III (IFNλ) interferons, which, in turn, induce the expression of interferon-stimulated genes (ISGs) that restrict viral replication. One of the first ISG identified to prevent viral infections in vivo is Mx ("Myxovirus resistance"), which confers resistance to influenza virus infection (67, 100). Another well-characterized ISG is protein kinase R (PKR), a dsRNA-activated kinase that inhibits translation during viral infection (81). NS1 has been shown to directly inhibit PKR activation, and it was one of the first ISG to show that NS1 played an inhibitory effect (104). NS1 exerts its inhibitory effects on the interferon response multiple regulatory levels—pre-transcriptional, co-transcriptional, and post-transcriptional levels and post-translational—thus ensuring efficient suppression of host antiviral signaling (**Figure 8 and Figure 9**).

At the pre-transcriptional level, NS1 inhibits the production of IFN genes: IRF3, NFκB, and Ap-1. It does this by complexing with RIG-I (retinoic acid-inducible gene I) (110). RIG-I is a pattern recognition receptor (PRR) for detecting influenza virus in epithelial cells and leads to downstream production of IFN genes. RIG-I detects and binds dsRNA structures with 5'-triphosphates, which leads to an ATP-dependent conformation change on RIG-I. Residues in RIG-I are ubiquitinated by the E3 ligases TRIM25 and RIPLET leading to oligomerization of RIG-I. Next, RIG-I CARDs bind CARD domains of mitochondrial antiviral signaling (MAVS) and downstream signaling cascade leads to the production of IFN genes. NS1 inhibits the production by complexing with RIG-I and two of its positive regulators: TRIM25 and RIPLET, and thus prevents the oligomerization of the CARD domain of RIG-I and ubiquitination by E3 ligase (54, 134).

At the Co- and post-transcriptionally, NS1 interacts by limiting host gene expression. One of the best described mechanism is by blocking cleavage and polyadenylation specificity factor (CPSF); NS1 inhibits the processing of cellular mRNA and expression of cellular genes such as interferon and ISGs that play a role in host antiviral response. CPSF is composed of four subunits that recognize and bind AAUAAA sequence on nascent mRNA and catalyze the endonucleolytic activity and the subsequent addition of poly(A) tail (31, 170). NS1 binds to two of the zinc fingers of the smallest component of CPSF, CPSF30, and thus inhibits the entire CPSF complex from binding the pre-mRNA (33, 118, 163). However, this phenotype is strain dependent and not all NS1s bind CPSF30, for example, A/PR/8/34 (84, 162).

The third mechanism of invading host immune response is by post-translational inhibition of antiviral genes: *PKR* and *OAS*. PKR is an RNA-binding protein kinase constitutively expressed in an inactive state in cells and upon activation by a stimulus (ex. dsRNA) it leads to a conformational change to the active state and then phosphorylates other substrates that lead to the activation of a chain of signal transduction pathways. One of the best understood mechanism of activation is that PKR phosphorylates the alpha subunit of the eIF2 translation initiation factor and therefore represses the synthesis of all proteins. Phosphorylated eIF2α blocks the recycling of GDP-bound eIF2α to form new initiation complexes, thereby inhibiting the initiation of mRNA translation. This shuts down protein synthesis in the infected cells (32). Studies have shown that NS1 binds PKR through an interaction involving amino acids 123-127 of NS1 and the N-terminal region of PKR (112). It is hypothesized that NS1 prevents PKR from undergoing the conformational change required for activation (97).

Additionally, NS1 inhibits the 2'-5'-oligo (A) synthetase (OAS) pathway, which is an IFN-stimulated gene product that catalyzes the formation of 2'-5'-polyA chains from ATP. These oligomers activate the latent RNAse L, a repressor of viral infection by degrading single-stranded RNA (153). A putative mechanism of action is that NS1 outcompetes OAS in binding of dsRNA and thus hinders the activation of RNAse L (90, 111). NS1 protein has a plethora of functions, some of which are highlighted in the schematic and structure in **Figure 8**, and one such intriguing role is the activation of phosphoinositide 3-kinase (PI3K) pathway.

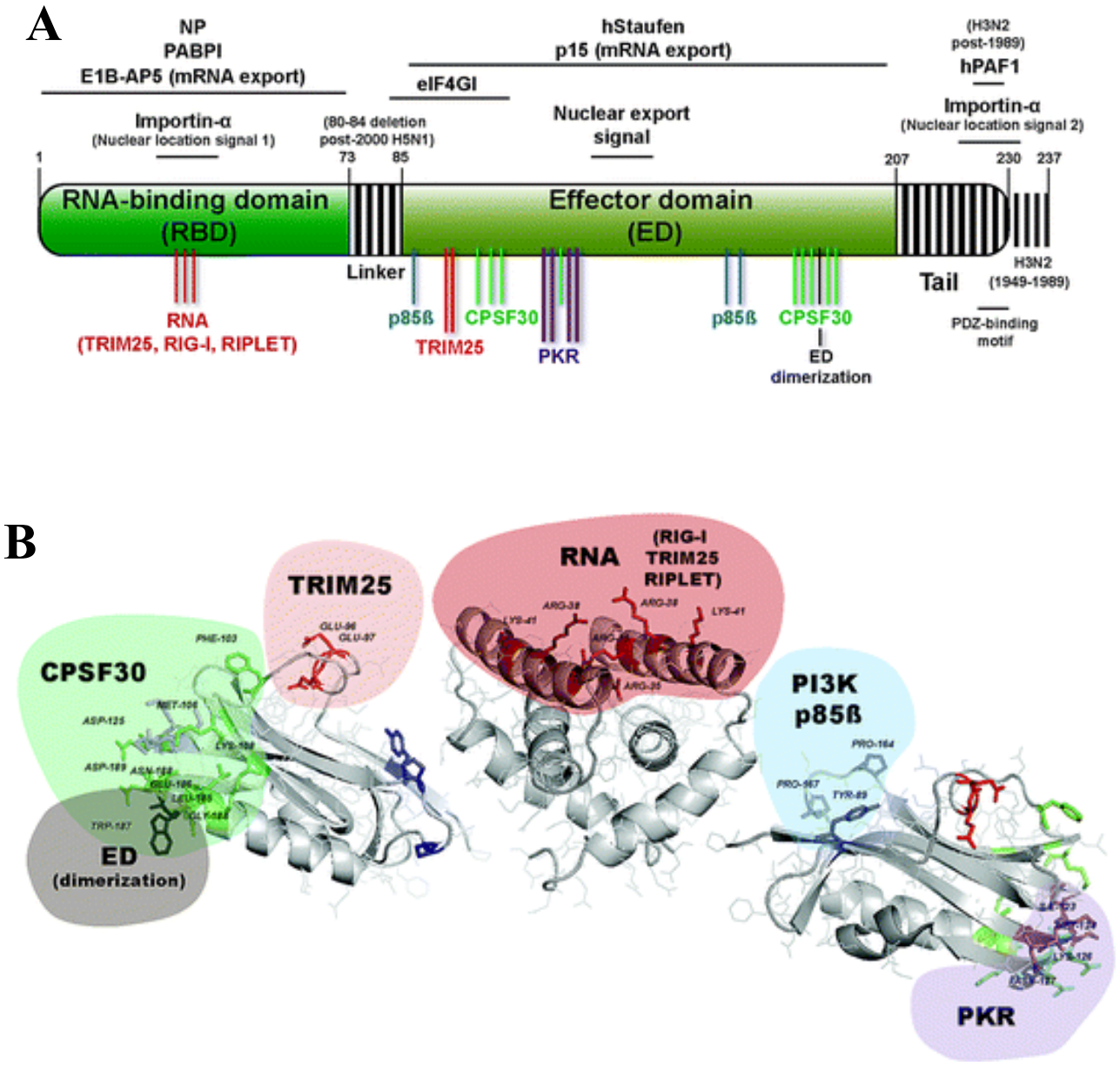

Figure 8. NS1 structure and it's multiple interactors.
A schematic diagram of NS1 highlighting the N-terminus RNA binding domain (RBD), the linker region, effector domain (ED) and the C-terminus tail. Binding sites of various host proteins that NS1 interacts with are highlighted (A). Crystal structure of NS1 homodimer in gray and various regions of interactions with host proteins are highlighted in color. The RNA binding domains are in a dimer while the effector domain is in monomeric state (B). *Adapted from Ayllon et al.2015 (8).*

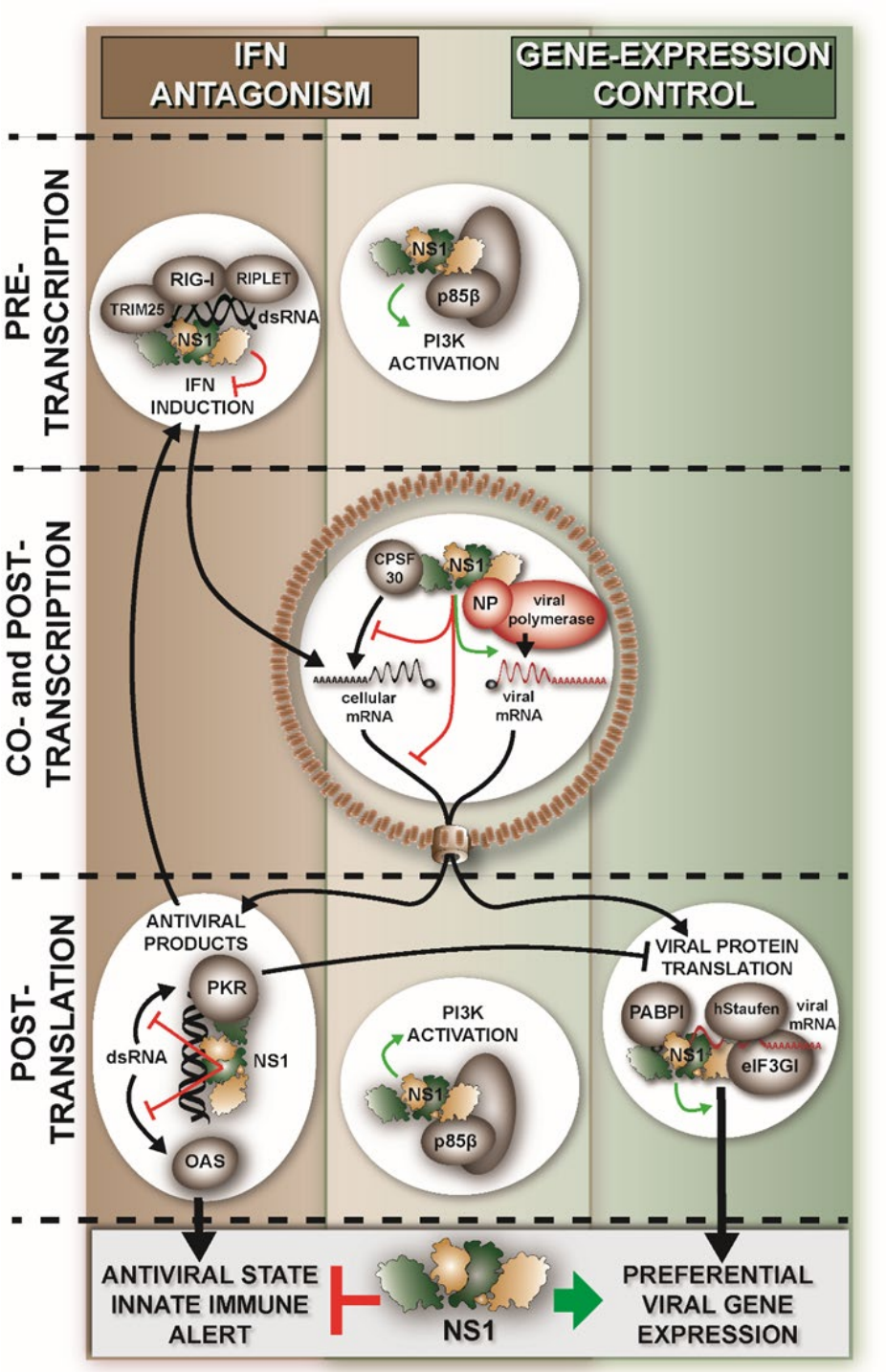

Figure 9. Overview of the multifunctionality of the NS1 protein of influenza A virus.
NS1 plays a wide array of functions in the infected cells, however, one of the main functions ascribed to this protein is as the main IFN antagonist. NS1 inhibits the IFN pathway via three different routes: pre-transcriptional, co- and post-transcriptional and post-translation. The activation of PI3K by NS1 may change the different proteins being expressed and may affect the cellular environment. *Adapted from Ayllon et al. 2015 (8).*

1.3 Phosphoinositide 3-kinase

Phosphoinositide 3-Kinases (PI3K) are lipid kinases involved in cell growth, proliferation, and survival (43). Due to the critical role of these functions in cellular processes, it is also one of the most commonly overactivated pathways in oncogenic transformation (124, 135, 157). PI3K was initially discovered in the 1980s during the studies of Src, a proto-oncogenic tyrosine kinase. It was shown that phosphatidylinositol kinase activity was due to an 85 kDa phosphoprotein bound to the middle T antigen of the polyoma tumor DNA virus (79). Lewis Cantley and colleagues showed that the product of the phosphatidylinositol activity in Src immunoprecipitates migrated slightly differently on thin layer chromatography plates compared to PtdIns-4-P (phosphatidylinositol 4-phosphate), the initially assumed product. Furthermore, their collaborators confirmed that the product was PtdIns-3-P (phosphatidylinositol 3-phosphate), a new phosphoinositide identified 30 years after the discovery of phosphoinositides (177). These discoveries led to the purification and subsequent cloning of p85 by various laboratories (46, 128, 155). It was shown that p85 binds strongly with a 110 kDa polipeptide (23), while Waterfield and colleagues were the first to clone and characterize this protein as the catalytic subunit of PI3K, p110 (66).

1.3.1 Classes and structure

PI3Ks are highly conserved cytoplasmic heterodimeric enzymes, and multiple isoforms exist in mammalian cells (45). PI3Ks are enzymes that phosphorylate phosphatidylinositol, a type of phospholipid with a head group that can be phosphorylated at multiple hydroxyl positions. These phosphorylated derivatives are collectively known as phosphoinositides. The inositol head group contains five free hydroxyls that have the potential to be phosphorylated (53) (**Figure 10**).

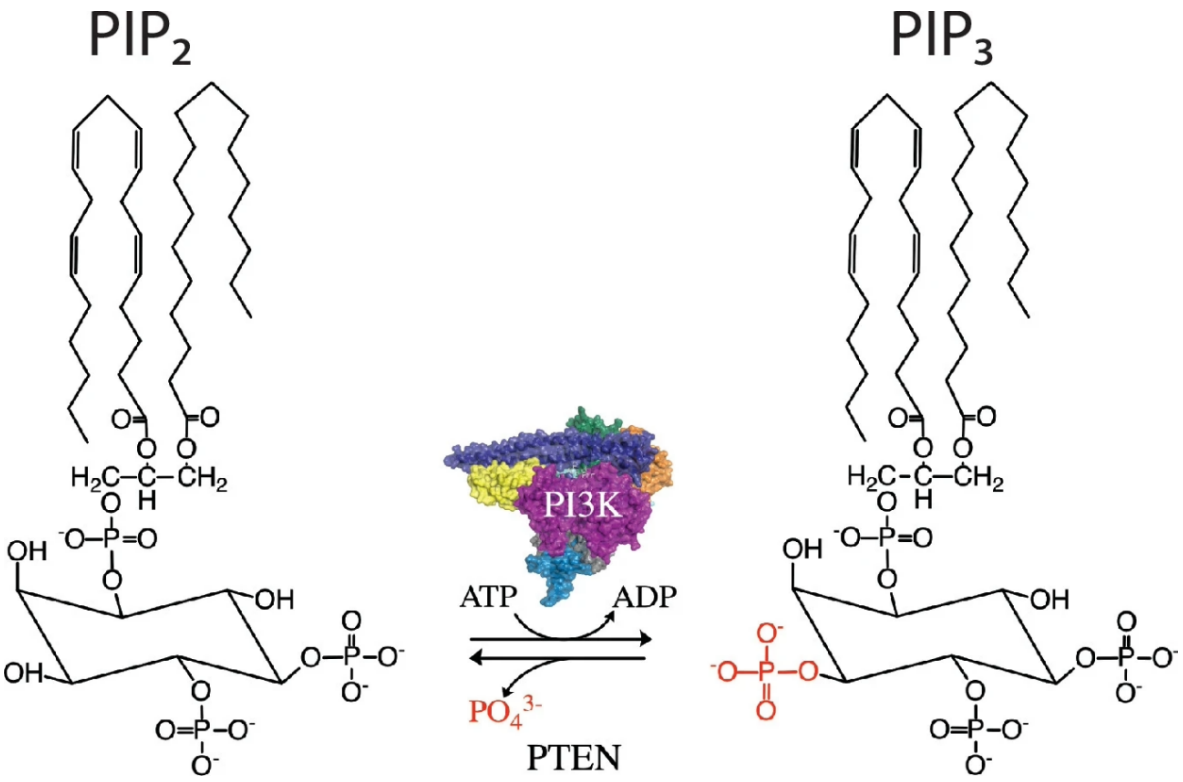

Figure 10. Overview of the reaction catalyzed by PI3K.
Upon activation by upstream stimuli, PI3K catalyzes the ATP-dependent phosphorylation of PIP_2 at the 3' position of the inositol ring, to generate PIP_3. This reaction is reversed by PTEN, which dephosphorylates PIP_3 back to PIP_2. *Adapted from Aytenfisu et al. 2022 (12).*

The various isoforms of PI3K are classified into three classes (22): class IA and IB, class II, and class III (36, 167, 189). **Table 1**, lists the different classes of P3K and their respective catalytic and regulatory subunits. At the time of initial cloning and sequencing of p85, the SH2 domain was discovered (35, 107, 115, 126). Two copies of the SH2 domains were identified in p85 by which PI3K relocalized to sites of activated, phosphorylated receptor tyrosine kinases.

One of the first effectors of PI3K discovered was the Serine/Threonine kinase Akt, also known as PKB (protein kinase B) (51). Akt is phosphorylated at two key residues: Thr308 (T loop segment of the kinase domain) and Ser473 (hydrophobic region at the carboxyl-terminus) (3). Two groups independently identified PDK-1 (phosphoinositide-dependent kinase-1), as the kinase

responsible for phosphorylating Akt at Thr308, while phosphorylation of Ser473 is relevant for mTORC2 complex. Phosphorylation at Ser473 is required for full activation of Akt (2, 114, 143). Although Akt is not directly phosphorylated by PI3K, its post-translational modifications are strictly dependent on PI3K activity. Consequently, phosphorylation of Akt (pAkt) at Ser473 is commonly used as a marker for PI3K activation (42).

Table 1. Classification of PI3K classes
PI3K is classified into three classes I, II and III. The different catalytic and regulatory subunits of each class are listed. *Adapted from Hawkins et al. (65).*

Class	*Catalytic*		*Regulatory*	
	Isoform/Subunit	**Gene**	**Isoform/Subunit**	**Gene**
Class IA	p110α	PIK3CA	p85α	PIK3R1
	p110β	PIK3CB	p55α	
			p50α	
	p110δ	PIK3CD	p85β	PIK3R2
			p55γ	PIK3R3
Class IB	p110γ	PIK3CG	p101	PIK3R5
			p84	PIK3R6
Class II	C2α	PIK3C2A		
	C2β	PIK3C2B		
	C2γ	PIK3C2G		
Class III	VPS34 (hVPS34)	PIK3C3	p150	PIK3R4

Here, we focus on class 1A PI3K, which forms heterodimers consisting of regulatory and catalytic subunits (63). There are three isoforms of the catalytic subunit: p110α, p110β, and p110δ—and five isoforms of the regulatory subunits (**Figure 11**): p85α, p85β, p50α, p55α, and p55γ (9). p50α and p55α are splice variants of p85α. The catalytic subunit (p110) contains five domains: an N-terminal adaptor-binding domain (ABD), a Ras-binding domain (RBD), a C2 domain, a helical domain (HD) and a catalytic kinase domain (18, 168, 171). Similarly, the

regulatory subunit (p85) also contains five domains: a Src homology 3 domain (SH3), a B-cell receptor homology (BH) domain flanked by proline-rich sequences, two SH2 domains (nSH3 and cSH2) and an inter-SH2 (iSH2) region. iSH2 domain contains the p110 binding site.

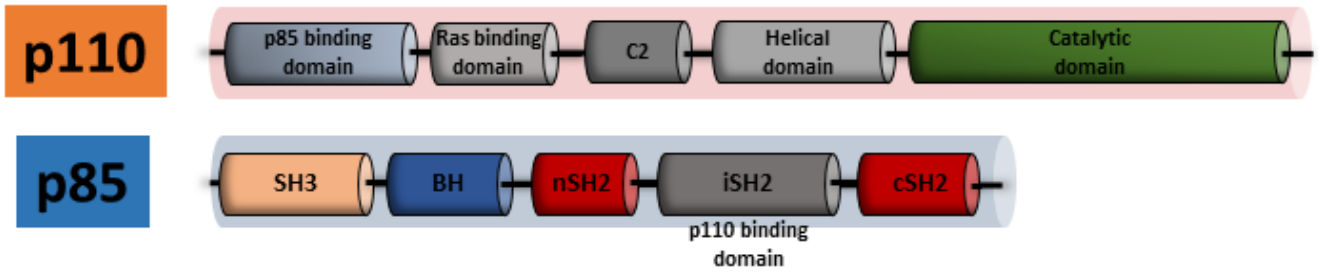

Figure 11. Schematic of the catalytic and regulatory subunit of Class IA PI3K.
Class IA PI3K are heterodimers made of the catalytic subunit (p110) and the regulatory subunit (p85). The different domains of each of the subunits are marked and the domain where p110 binds on p85 is marked as well.

1.3.2 Canonical mode of activation

PI3K is involved in various cellular responses, such as cell proliferation, motility, adhesion, and survival (8, 22). The best-characterized mechanism of activation of class IA PI3K involves its translocation to the membrane upon activation by different stimuli (e.g. growth factors). Thus inducing a conformational change in the heterodimer and releasing inhibition of the active site in p110. The p85 subunit then binds to phosphorylated tyrosine residues in the p-Y-X-X-M motifs on activated receptor tyrosine kinases (RTKs) (156), this, in turn, leads to the production of the intracellular second messenger phosphatidylinositol-3,4,5-trisphosphate (PIP3) (8, 22, 63). PIP3 acts as a docking platform for pleckstrin homology (PH) domains and leads to the activation of downstream effectors such as protein kinase B (PKB or Akt) (4, 52, 127). PTEN (phosphatase and tensin homologue deleted on chromosome 10) is the main regulator of PIP3 levels. It controls PIP3 signaling by dephosphorylating PIP3 at the 3-position of the inositol head (**Figure 12**) (19, 106).

Class IA PI3K activation and regulation is further complicated by the existence of several isoforms of each subunit (p85α, p85β, p110α, p110β, p110δ), some of which vary in abundance across different cell types. p110α and p110β are more broadly present while p110δ is exclusively

present in immune cells (85, 86). This allows for different combinations of catalytic and regulatory subunits with either distinct or redundant functions. The functional consequences of this PI3K diversity are not yet fully understood (18, 30, 139).

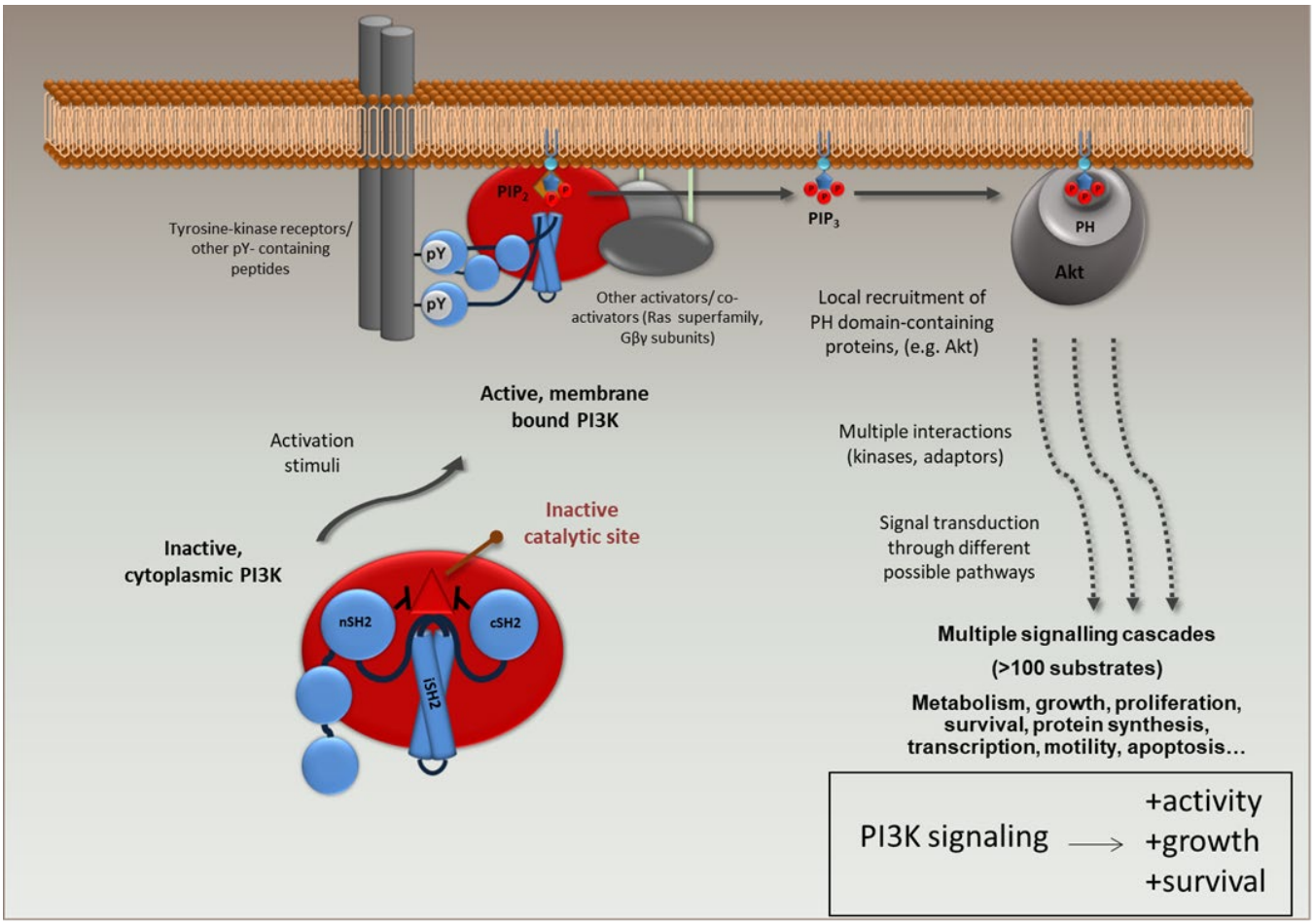

Figure 12. Canonical mode of activation for PI3K heterodimers.
PI3K heterodimers are in the cytoplasm in their inactive state and upon binding of a stimuli there is a conformation change, and the kinase is activated. Activated complex translocate to the membrane where it binds phosphorylated tyrosine kinase receptors. The activated kinase leads to the production of PIP_3 which leads to further downstream activation of Akt which leads to the activation of a plethora of signaling cascades. *Adapted from Ayllon et al. 2012 (9).*

1.3.3 Pharmacological agents

In 1993, multiple groups showed that a furanosteroid metabolite isolated from the fungus *Penicillium funiculosum* known as wortmannin, potently inhibits fMLP-stimulated PtdIns-3,45-P_3 (7, 183). Other labs confirmed the inhibitory activity of wortmannin on PI3K and later Ely Lilly discovered a structurally distinct compound, LY294002, which also directly inhibits PI3K (169). LY294002 was the first artificial inhibitor of PI3K. Wortmannin has irreversible effects on the pathway, whereas LY294002 is reversible (181). Both compounds have been extensively used in studies of the PI3K pathway over the years, and numerous new inhibitors have since been identified. Many of the recent inhibitors have been tested in preclinical developments and some have received FDA approvals for therapeutic use. These include pan-class I PI3K inhibitors, isoform-selective PI3K inhibitors, or dual-PI3K inhibitors that target two isoforms simultaneously (**Table 2**) (15, 181).

Table 2. List of PI3K inhibitors.
A wide array of PI3K inhibitors have been developed, with several receiving FDA approval for clinical use. Representative compounds are outlined below and classified into pan-PI3K inhibitors, isoform-selective inhibitors, and dual PI3K inhibitors. *Adapted from Belli et al. and Wright et al.* (15, 181).

Target	Drug	FDA status
Pan-PI3K Inhibitors	Copanlisib (BAY 80-6946)	Approved
	Duvelisib (IPI-145)	Approved
	Buparlisib (BKM120)	Discontinued
Isoform-Specific PI3K Inhibitors	Alpelisib (BYL719) **p110α**	Approved
	Idelalisib (CAL101) **p110δ**	Approved
Dual-PI3K Inhibitors	Taselisib (GDC-0032)	No
	Duvelisib (IPI-145)	Approved

1.4 PI3K activation by NS1 protein of influenza A virus

Influenza A virus infection activates the PI3K pathway, as measured by downstream phosphorylation of Akt (pAkt) at serine 473 (Ser473) (3, 61). It has been suggested that this activation prevents, or at least delays, virus-induced apoptosis, thereby enhancing viral replication, as it does with other viruses (44). Phosphorylation of Akt was tested in cells infected with influenza A virus, and it was observed that PI3K activation occurred concomitantly with the expression of NS1. Furthermore, when testing pAkt levels in cells constitutively expressing NS1, it was demonstrated that NS1 alone is sufficient to activate the PI3K pathway (61).

Initial studies showed that PI3K plays a double role during influenza virus infection, with "early" activation" (~2hr post infection) and "late" activation (~6hr post infection). During early activation, PI3K is required for efficient virus entry, and this activation is short and transient, In contrast, the "late" activation is sustained and coincides with viral replication (42). It has been shown that when cells treated with PI3K inhibitors are infected with influenza A virus, the progeny virus grows to lower titers than untreated cells. Additionally, immunofluorescence analysis suggested that PI3K may be involved in viral uptake. Inhibition of PI3K results in accumulation of virus particles at the cell surface and fail to traffic to early endosomes during receptor-mediated endocytosis (42, 43). However, the "late" activation of PI3K leads to a decline in IRF-3-dependent promoter activity, misphosphorylation and impaired dimerization of IRF-3 (43).

1.4.1 Isoform specificity and structural binding

Biochemical analyses revealed that NS1 protein of influenza A virus interacts specifically with the β isoform of the p85 regulatory subunit of PI3K, but not with p85α (**Figure 13**). This interaction was consistently observed with NS1 proteins from different strains of influenza A virus. Sequence analysis showed that tyrosine at residue 89 (Y89) is highly conserved among different strains of influenza A viruses and this residue is upstream of a methionine (M93), together forming the classical YXXM motif (61, 156). As described above, tyrosine phosphorylation within the YXXM motif in activated growth factor receptors or substrates provides a docking site for the SH2 domains of p85, triggering a conformational change that activates the kinase. Mutational analysis showed that when the tyrosine is switched to a phenylalanine the interaction is abrogated (61).

Consistently, co-immunoprecipitation experiments demonstrated that wild type NS1, but not the Y89F mutant, successfully precipitated p85β (61).

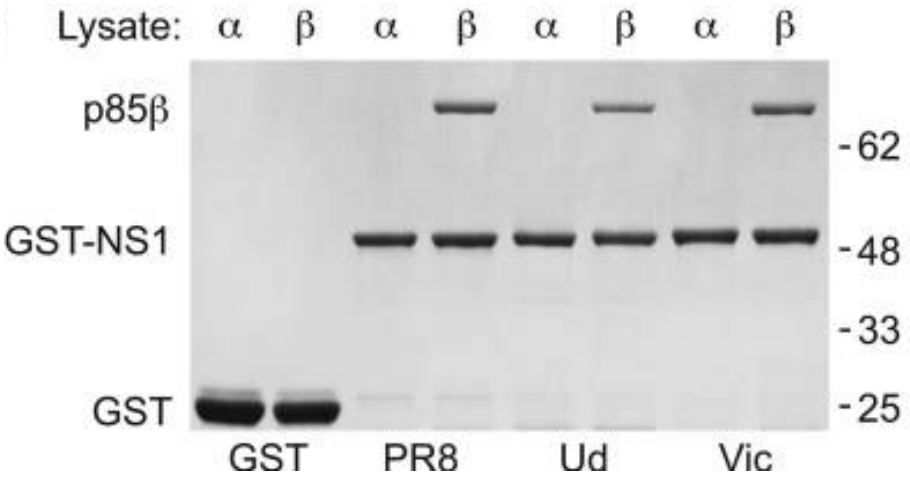

Figure 13. NS1 binds to PI3K in an isoform specific manner.
Soluble Sf9 cell lysates were mixed with NS1 from different strains or GST alone and the complexes were separated on SDS-PAGE. NS1 complexed with p85β isoform only, regardless of the strain and neither protein were present in GST only construct as expected. *Adapted from Hale et al. 2006 (61).*

In order to identify the region of binding, mutational and biochemical studies were performed, which revealed that the C-terminal effector domain of NS1 is sufficient to form a complex with p85β. This finding further supports the relevance of the Y89F mutation, as its located within the effector domain. Pull-down assays using individual subunits of p85β demonstrated that NS1 specifically binds to the iSH2 domain, as only this domain was co-precipitated with NS1 (60). In parallel, another group performed similar assays using infected cells and individual subunits of p85β, reaching the same conclusion. They further identified that valine at position 573 is critical for NS1-p85β binding. Additionally, when valine was introduced to the corresponding position in p85α, they were able to observe NS1 binding with p85α (98).

Structural studies further corroborated these findings and helped generate a potential model for NS1:PI3K heterotrimeric complex. The crystal structure of NS1 ED in complex with p85β iSH2 domain was resolved, and positions of key residues were identified. Tyr89, which is essential for NS1 ED to bind p85β, was positioned at the heart of the complex (**Figure 14**). The

position of Val573 was determined to be at the interface of the complex, highlighting how it may contribute to isoform specificity (62).

Another key finding was that the activation loop of p110 was close to the NS1 ED in the heterotrimeric complex. It was hypothesized that a small acidic α-helix of NS1 ED, which is involved in ED:β-iSH2 binding, might modulate p110 activity. To validate this, a recombinant virus expressing NS1 with charge-disrupting mutations (E96A/E97A) was generated. This virus was defective in activating PI3K and generating downstream products (PIP_3 and pAkt). However, it induced large amounts of IFN, indicating that the acidic α-helix of NS1 plays a dual role during influenza virus infection (62).

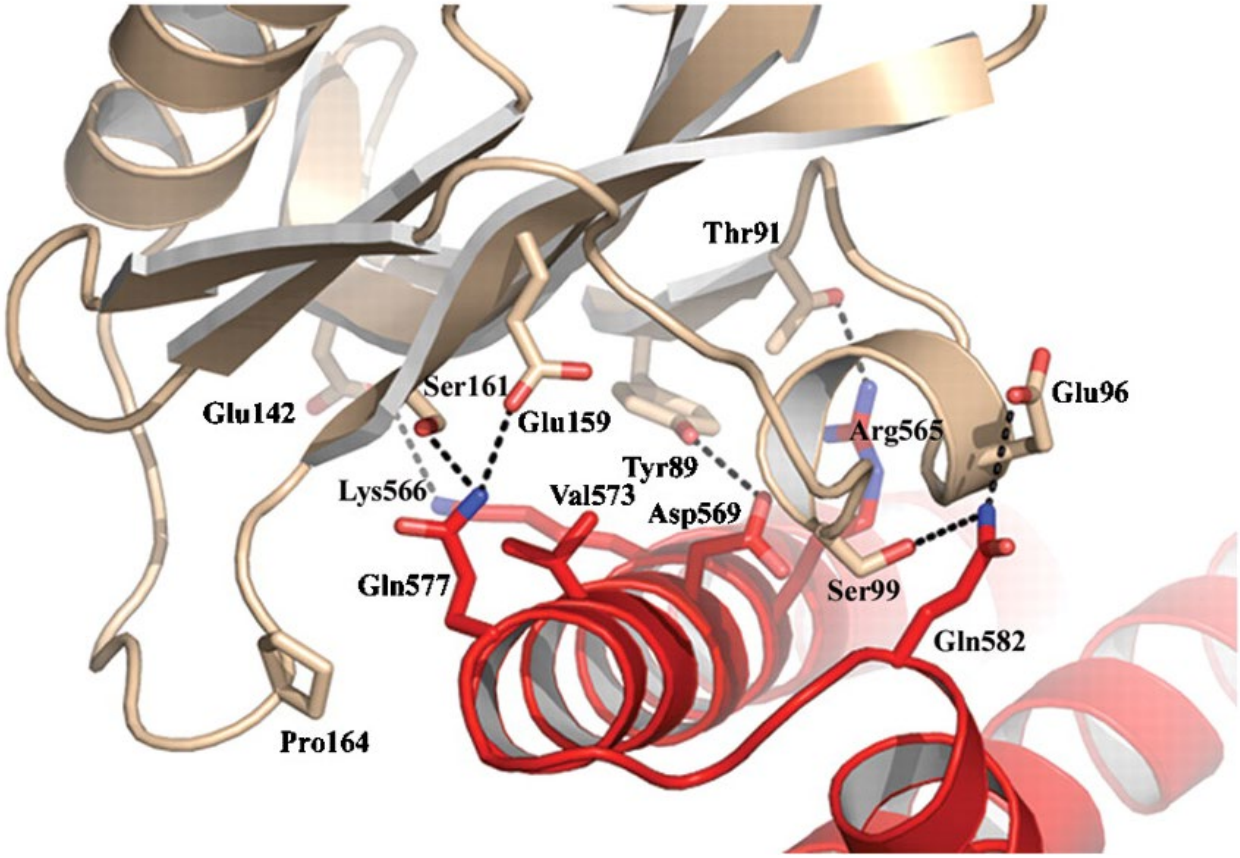

Figure 14. Crystal structure of NS1 ED in complex with β-iSH2 domain of p85β.
Cartoon representation of ED:β-iSH2 complex, NS1 ED is in gold and β-iSH2 in red. Residues at the interface of the complex are represented in stick structures. *Adapted from Hale et al. 2010 (62).*

1.4.2 Strain Specificity

NS1 activation of PI3K is not only isotype-specific, but also strain specific. It has been demonstrated that when Y89F mutation was introduced into two H1N1 strains (PR8 and WSN) and their replication kinetics compared with the wild type viruses, there was difference in morbidity and mortality in mice for one strain (PR8) but not the other (WSN). Similar differences were observed in in vitro assays. However, pAkt activation levels were similar in both viruses, indicating that Y89F mutation was able to abrogate PI3K interaction in both viruses but it affected virus growth and phenotype differently (**Figure 15**) (10, 61). Despite this knowledge about the NS1-PI3K interaction (**Figure 9**), the mechanisms and biological meaning of this pro-viral function remains elusive, and as such it will be our objective to further characterize it and to compare influenza virus-mediated activation of PI3K at the cellular levels with other physiological and physiopathological stimuli.

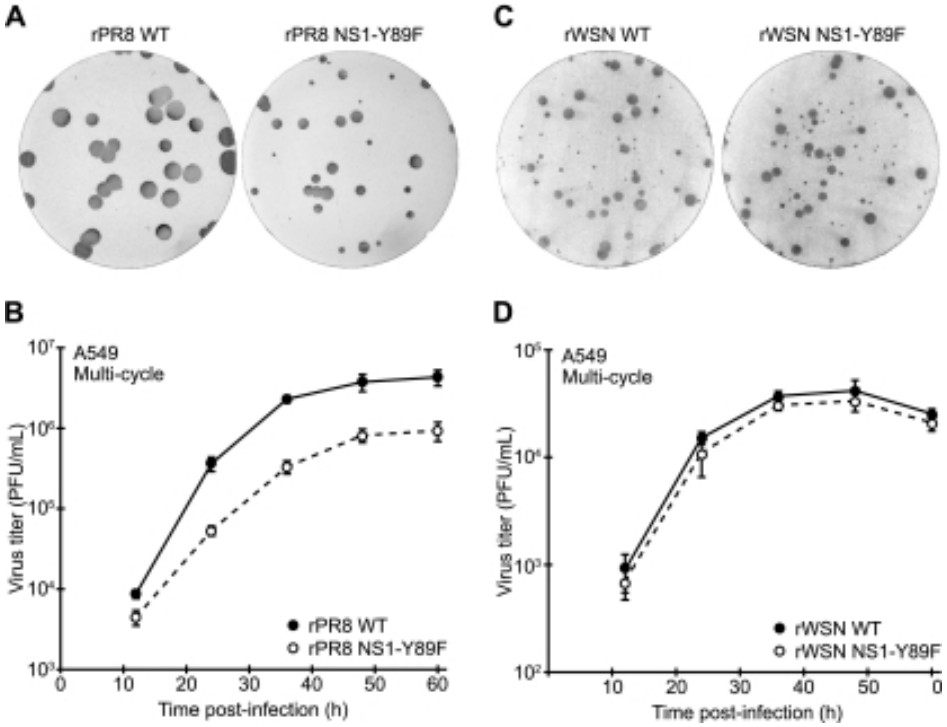

Figure 15. PI3K activation is strain specific and affects virus phenotype.
PI3K activation abrogating mutation (Y89F) is introduced to two different H1N1 strains and plaque phenotype is compared to wild type viruses. PR8 wt produces large plaques in comparison to PR8 Y89F virus (A), while there is no difference in plaque size between WSN Y89F and WSN wt viruses (B). Growth kinetics were performed for PR8 WT and PR8 Y89F (C) and WSN WT and WSN Y89F (D) in A549 cells and there was a difference in growth kinetics for PR8 WT and PR8 Y89F but not with WSN WT and mutant. *Adapted from Ayllon et al. 2012 (10).*

1. Introduction

2. Objectives

2. Objectives

2. Objectives

Given the variety of processes regulated by PI3K, including cell survival, translation, endocytosis, vesicle trafficking, cell motility, innate immunity and oncogenesis, it is yet unclear what are the full consequences of NS1-mediated PI3K activation during viral infection. Additionally, the role of the different isoforms of p110 (α, β, δ) on NS1-mediated activation of p85β-containing PI3K heterodimers has not been studied. Because of all of this, the objectives of the present study are as follows:

Objective principal

To characterize the pro-viral function of the NS1 protein of influenza viruses via class IA PI3K

Objective specific

1. Establishment of a method to study the interaction between the different catalytic and regulatory subunits of PI3K with NS1.

2. Identification and characterization of the different PI3K signaling pathways associated with NS1 activation

3. Phenotypical and functional comparison of NS1 activation of PI3K and other physiological and pathological stimuli

4. Assessment of fitness of wild-type and PI3K-activating-defective recombinant influenza viruses in stable cell lines with constitutively active PI3K

2. Objectives

3. Materials and Methods

3. Materials and Methods

3.1 Materials

The following materials were used throughout this thesis.

Table 3. List of all the materials and equipment.

Name	Brand
1.5ml microcentrifuge tubes	Nest
15ml conical tubes	Falcon
50ml conical tubes	Falcon
Cell culture treated plates	Corning
Glass bottom plates	MatTek
Table top centrifuge	Eppendorf
Centrifuge	Eppendorf
Flasks	(T75) Nunc, (T175) Falcon
V bottom 96 well plates	Thermo scientific
Petri dish	Falcon
Tubes for minipreps	Falcon
Tubes for transfection	Corning
Pipets tips: micro and serological	ART TIPS Corning (non-filter)
Pipetman	Accu-jet Pro
Pipets	Gilson
Cryovial	Nunc
Incubators for cell	Thermo Scientific NAPCO
Incubators for bacteria	New Brunswick scientific co. Inc.
Shaker with temperature control	Benchmark
Shaker	Benchmark
Erlenmyer flask	Pyrx
Graduated cylinder	Martell
Transiluminator	Analytik jena
Nanodrop	Thermo Scientific
Gel image	Enduro GDS
Film developer	MedXray
Biorad image developer	Biorad
Confocal microscope	Zeiss
Inverted light microscope	Invitrogen
Plate reader for absorbance	BioTek

PCR cycler	Eppendorf
qPCR cycler	Roche
2ml aspirator	Cell treat
Tissue culture dish	Falcon
Solution reservoir	BioTC
Large tissue culture dishes	Falcon
PCR tubes	Nest
Insulin syringes	BD
500ml filter unit	Fisher
Steritop 50ml filter unit	Fisher
Capillary tubes	Fisher
Foam seal for capillary tubes	Leica
Cloning ring	Corning
Vacuum greace	Fisher
Graduated cylinder	Nalgene
Countess 3FL	Invitrogen
Qubit Assay tubes	Invitrogen
Qubit	Invitrogen

3.2 Reagents

The following reagents were used for various experiments described in this thesis.

Table 4. List of all the reagents used.

Name	Brand	Catalog
Qiagen Maxiprep kit	Qiagen	12163
E.Z.N.A. miniprep kit	Omega BioTek	D6942-01
E.Z.N.A. viral RNA kit	Omega BioTek	R6874-01
E.Z.N.A. gel purification kit	Omega BioTek	D2500-01
E.Z.N.A. PCR purification kit	Omega BioTek	D6492-01
One step RTPCR kit	Invitrogen	12574-026
Hercules PCR kit	Agilent	600677
T4 DNA ligase	New England Biolabs	M0202S
Lipofectamine 2000	Invitrogen	11668500
Lipofectamine 3000	Invitrogen	L3000015
TransIT-LT1	Mirus	MIR2305
OptiMEM I	Gibco	31985-062
TRI Reagent	Invitrogen	9738G
BCA kit	Thermo Scientific	23225
Sterile water	Corning	46-000-CV
Oxoid Agar	Oxoid	LP0028B

Agarose I	Thermo Scientific	17852
DEAE-Dextran	MedChemExpress	HY-W134327A
Sodium Bicarbonate	Fisher	S233-3
HEPES	Corning	25-060-CI
L-Glutamine	Gibco	25030-081
1Kb plus DNA ladder	New England Bio Labs	N3200S
Protein ladder	Thermo Scientific	26619
Western Gels	BioRad	varied (4-20%, 4-15%, 10%)
Trans-Blot Turbo Mini 0.2 µm PVDF Transfer Packs	BioRad	1704156
Non-fat Milk	Research Products international	M17200-500.0
BSA	Gemini Bio	700-100P
35% Bovine serum albumin	MP Biomedicals	810063
PBS (1X)	Corning	21-040-CV
Triton x-100	Fisher	BP151-500
Saponin	Sigma	47036-50G-F
Paraformaldehyde	Electron Microscopy Sciences	157-4-100
Methanol	Fisher	A433P-4
2-propanol	Fisher	A464SK-4
Ethanol	Decon	2701G
TPCK (tosylsulfonyl phenylalanyl chloromethyl ketone)-trypsin	Sigma	T-8802
Trypsin-EDTA	Corning	25-052-CI
Wortmannin	Sigma	681675-1MG
Ampicillin	Sigma	A0166-25G
Antartic Phosphatase	New England Bio Labs	M0289L
Puromycin	Gibco	A11138-03
6x Orange DNA dye	Thermo Scientific	R0631
Tween20	Fisher	NP-337-500
MEM NEAA	Gibco	11140-050
TrueBlue	Sera Care	5510-0030
Crystal Violet	Fisher	C581-100
LB agar powder	Fisher	BP1425-2
2XYT Broth powder	Fisher	BP9743-2
HRP Chemiluminescent ECL	BrightStar	XR92
Pierce™ Lane Marker Reducing Sample Buffer	Thermo Fisher	39000
Running buffer (WB) 10x Tris/Glycine/SDS	BioRad	1610772
TAE	Boston BioProducts	BM-250
TBS	Boston BioProducts	BM-301X-4L

Polybrene	Millipore	TR-1003G
Taq2x	New England Biolabs	M0270L
In-Fusion snap assembly	Takara	638951
S.O.C. media	Invitrogen	15-544-034
BCA standards	Thermo Scientific	23208
DNTPs	Invitrogen	18-427-013
Protease/Phosphatase Inhibitor Cocktail (100X)	Cell signaling technology	5872
Ripa buffer	Sigma	R0278-500ML
DMSO (Dimethyl sulfoxide)	Sigma	D2650-100ml
Trypan Blue	Gibco	15250-061
Parafin	Fisher	P31-500
Superscript IV one-step RT-PCR system	Invitrogen	12594100
AMPure XP	Fisher	NC9959336
Direct-zol RNA miniprep kit	Zymol	R2052
Qubit dsDNA quantification assay kit	Invitrogen	Q32854

3.3 Biological Materials

3.3.1 Cells

Table 5. List of all the cell lines used in this work.

Cell line	**Background**	**ATCC**
A549	Epithelial cells isolated from a patient with lung carcinoma in 1972	CCL-185
293T	Epithelial cells isolated from the kidney of a patient in 1987	CRL-3216
HeLa	Epithelial cells isolated from a patient with cervical carcinoma in 1951 and these were the first immortal human cells grown in culture for basic research.	CCL-2
MDCK	Epithelial cells isolated from a normal kidney tissue from a female cocker spaniel in 1966.	CCL-34

A large stock of each cell line was prepared at an early passage and stored at -80°C. Cells were cultured at 37°C with 5% CO_2 and sub-cultured with fresh media two to three times per week. Passage numbers were recorded, and upon reaching passage 20, cells were discarded and replaced with a newly thawed aliquot from the original stock.

3.3.2 Bacteria

- **DH5α:** *Escherichia coli (*E. coli*)* cells purchased from Thermo Scientific, are a standard laboratory strain used for cloning applications and are known for their high transformation efficiency. These cells provide α-complementation of the β-galactosidase gene to allow blue/white colony screening.
- **Stellar competent cells:** *E. coli* HST08 strain purchased from Takara, are optimized for high-efficiency transformation, particularly of large plasmids and ligation products. These cells also provide α-complementation of the β-galactosidase gene to allow blue/white colony screening.

3.4 Media

3.4.1 Media for cells

DMEM/10%FBS/PS: 450ml DMEM (Gibco); 50ml fetal bovine serum (FBS) (HyClone); 5ml 100x Penicillin (10U/mL)/Streptomycin (10mg/mL) (Gibco). **(Maintaining cells)**

2xMEM: 100ml 10x MEM (Gibco); 10ml 100x Penicillin (10U/mL)/Streptomycin (10mg/mL) (Gibco); 10ml 100x L-Glutamine (Gibco); 6ml 35% Bovine Serum Albumin (MPI); 10ml 1M HEPES (Gibco); 25ml 5% $NaHCO_3$; 340ml Sterile water (Gibco). **(Plaque assay)**

1xMEM/0.2%BA/PS: 500ml 1x MEM (Gibco); 2.9ml 35% Bovine Serum Albumin (MPI); 5ml 100x Penicillin (10U/mL)/Streptomycin (10mg/mL) (Gibco). **(Infection assay)**

Agar overlay media: 25ml 2xMEM; 8.5ml sterile H_2O; 1ml 5% $NaHCO_3$; 0.5ml 1% DEAE-dextran; 15ml 2% Oxoid agar; (titrated based on cell type) TPCK-trypsin

1% DEAE-dextran: Dissolve 0.4g of DEAE-dextran in 40ml of sterile H_2O and filter using 0.22uM filter unit.

5% $NaHCO_3$: Dissolve 2g of $NaHCO_3$ in 40ml of sterile H_2O and filter using 0.22uM filter unit.

TPCK-trypsin: Reconstitute 50g of trypsin with 5ml of sterile H_2O to prepare 10mg/ml (10x) stock solution and aliquot 1ml/tube and store at -20°C. Dilute 1 tube of 10x stock into 1x using sterile H_2O and store small aliquots of 1x working solution at -20°C. Test different concentrations

of working solution of trypsin on mock cells to determine the concentration that does not detach the monolayer.

3.4.2 Media for Bacteria

LB: Luria-Bertani broth for culturing bacteria based on Dr. Bertani's recipe containing tryptone (10g/L), yeast extract (5g/L) and sodium chloride (10g/L).
2XYT: Luria-Bertani broth modified to contain higher concentrations of casein peptone (16g/L), yeast extract (10g/L) and sodium chloride (5g/L).
S.O.C. medium: Super optimal broth with catabolite repression medium is used after heat shock to recover cells from stress. The components of this media are: 2% tryptone, 0.5% yeast extract, 10 mM NaCl, 2.5 mM KCl, 10 mM MgCl2, 10 mM MgSO4, and 20 mM glucose. This is purchased from Invitrogen.

3.5 Viruses

- **rA/Puerto Rico/8/1934**
- **rA/Puerto Rico/8/1935 Y89F**

Viruses were propagated in 10-day old embryonated chicken eggs for 48hrs at 37°C (**Section 3.8.1**). Following incubation, allantoic fluid was harvested, and the presence of virus was confirmed by HA assay (**Section 3.9.2**). Small aliquots of the confirmed stocks were prepared and stored at –80°C. Viral titers were determined by plaque assay (**Section 3.9.3**).

3.6 Plasmids

3.6.1 pCAGGS

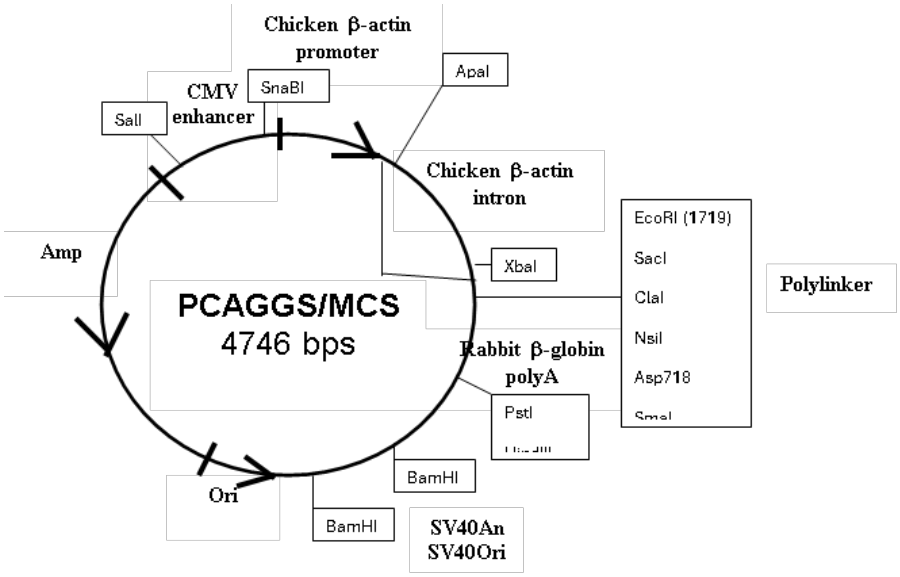

Figure 16. Map of pCAGGS expression vector.
This vector was used to generate all the expression plasmids and BiFC constructs used in this study.

The pCAGGS mammalian expression vector was generated by Niwa *et al.* (122) in 1991. This expression vector contains chicken β-actin promoter and CMV enhancer, enabling strong and ubiquitous expression in mammalian cells. All constructs used in this study were cloned or subcloned into this vector.

3.6.2 pLVX-IRES-Puro

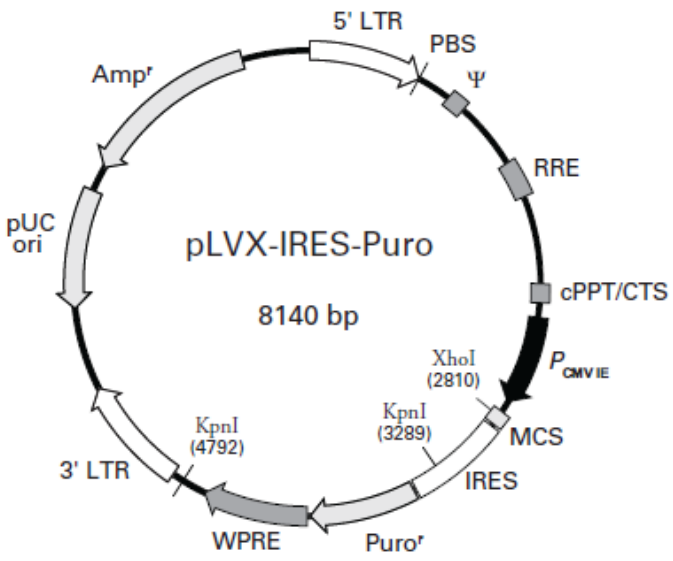

Figure 17. Map of pLVX-IRES-Puro plasmid.
This vector was used for lentivirus production and the generation of a stable cell line. It was purchased from Takara Bio, and the map is adapted from the manufacturer's website.

Table 6. List of all the plasmids used in this thesis.

Name	Source
pCAGGS-p110α-YN	Aslam et al. 2025
pCAGGS-p110α H1047R-YN	Aslam et al. 2025
pCAGGS-V5-p110α H1047R	Aslam et al. 2025
pCAGGS-p110β-YN	Aslam et al. 2025
pCAGGS-p110δ -YN	Aslam et al. 2025
pCAGGS-p85α-YC	Aslam et al. 2025
pCAGGS-p85α-FLAG	Turkington et al. 2018
pCAGGS-p85β-YC	Aslam et al. 2025
pCAGGS-p85β-FLAG	Turkington et al. 2018
pCAGGS-p85β N561D-YC	Aslam et al. 2025
pCAGGS-HA-p85β N561D	Aslam et al. 2025

pCAGGS-p85β R355A R647A (RARA)-YC	Aslam et al. 2025
pCAGGS-NS1-V5 (PR8)	Hale et al. 2006
pCAGGS-NS1 Y89F-V5 (PR8)	Hale et al. 2006
pCAGGS-NS1 W187A-V5 (PR8)	Kerry et al. 2011
pCAGGS-A/Brevig Mission/1/1918 NS1	Dr. Juan Ayllon
pCAGGS-A/Wilson-Smith/1933 NS1	Ayllon et al. 2012
pCAGGS-A/California/04/2009 NS1	Ayllon et al. 2014
pCAGGS-A/Wyoming/03/2003 NS1	Ayllon et al. 2014
pCAGGS-A/Hong Kong/156/1997 NS1	Ayllon et al. 2014
pCAGGS-A/Vietnam/1203/2004 NS1	Ayllon et al. 2014
pCAGGS- mCherry HRAS C12V T40C	Aslam et al. 2025/Origene
pCAGGS-Src Y530F- mCherry	Aslam et al. 2025/Origene
pCAGGS-Zyxin-N-RFP	Aslam et al. 2025/Origene
pCAGGS-Rab5-N-RFP	Aslam et al. 2025/Origene
pLVX-IRES-Puro-HA-p85β-N561D	Aslam et al. 2025
pLVX-IRES-Puro	Dr. Melissa Uccellini
lenti-gag/pol	Dr. Melissa Uccellini
pMD2VSV-G	Dr. Melissa Uccellini

3.7 Antibodies

See the following table for all the antibodies used for this work.

Table 7. List of primary and secondary antibodies

Antibody	**Catalog/Origin**	**Working concentration/application**	**Primary/Secondary**
Anti-V5	460705; Invitrogen	1:500/IF	Primary
Anti-V5	MCA1360, Bio-Rad		Primary
Anti-HA	326700; Invitrogen	1:500/IF; 1:1000/WB	Primary
Anti-HA-tag-HRP	2999S; Cell signaling technology	1:1000/WB	
Anti-p85β	MS53215; Invitrogen	1:500/IF; 1:1000/WB	Primary
Anti-PIP3	Echelon	1:200/IF	Primary

Anti-pAkt (Ser473)	4060S; Cell signaling technology	1:200/IF; 1:1000/WB	Primary
DAPI	D1306; Invitrogen	1:1000/IF	
Anti-NP	PA532242; Invitrogen	1:1000/Immunostaining	Primary
Anti-FLAG	F1804; Sigma-Aldich	N/A	Primary
Anti-NS1	PA532243; Invitrogen	1:1000/IF	Primary
Anti-NS1	GT1653; Invitrogen	1:1000/WB	Primary
Anti-YFP	Ab1218; Abcam		Primary
Beta-actin-HRP	12262; Cell signaling technology	1:2000/WB	Primary
Phalloidin Alexa fluor 568	A12380; Invitrogen	1:40/IF	
Anti-mouse Alexa fluor 633	A21052; Invitrogen	1:1000/IF	Secondary
Anti-rabbit Alexa fluor 647	A21443; Invitrogen	1:1000/IF	Secondary
Pacific Blue anti-mouse	P31582; Initrogen	1:1000/IF	Secondary
anti-rabbit Alexa fluor 488	A-11034; Invitrogen	1:1000/IF	Secondary
anti-mouse-HRP		1:2000/WB	Secondary
fluorochrome-conjugated anti-mouse immunoglobulin	35519; Thermo Fisher Scientific	N/A	Secondary
anti-rabbit immunoglobulin	SA5-10036; Thermo Fisher Scientific	N/A	Secondary

3.8 Method for virus amplification in embryonated chicken eggs

3.8.1 Inoculation of embryonated chicken eggs

Specific pathogen free (SPF) embryonated chicken eggs, 8 to 10 days old, were purchased from Charles River, PA. Eggs were visualized using a flashlight and the space between the air sack and embryo was marked with an "X" using a pencil. Eggs were surface sterilized with 70% ethanol, and a small hole was made at the marked location using a sharp-edged tool. A sterile 500 µL syringe was used to inoculate 100-200 µL of virus (pre-diluted with PBS) into the allantoic cavity. The hole was then sealed with warm wax, paraffin or glue. Eggs were incubated at 37°C for 48 hours. After 48 hours, eggs were transferred to 4°C for at least 3-4 hours to euthanize the embryo and coagulate the blood.

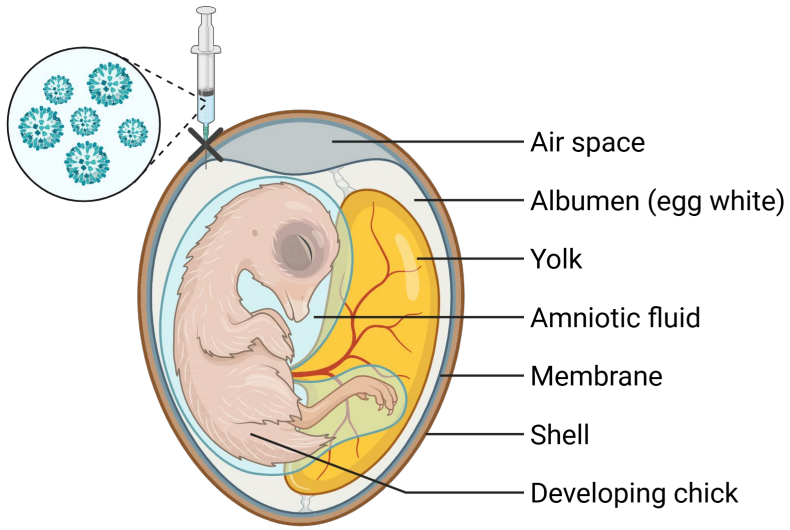

Figure 18. Schematic of embryonated chicken egg inoculation.
An embryonated chicken egg is checked using a flashlight to locate the air sac, and an "X" is marked at the space between air sac and membrane. Using a sharp tool a small hole is made to allow the needle to pass through. The virus inoculation occurs at this site followed by sealing with paraffin or glue.
(Generated using Biorender).

3.8.2 Harvesting of allantoic fluid

After incubation at 4°C for several hours, the eggs were opened at the air sack end, and the initial membrane was removed using a tweezer, carefully avoiding the yolk. The allantoic fluid was collected using a serological pipet and the yolk and embryo were gently pushed to the side with a sterile spatula to provide access to the fluid. The fluid was collected in 15 mL conical tubes and centrifuged for 5 min at 1200 rpm. Samples were stored at 4°C until further titration and aliquoting.

3.9 Methods for titrating influenza virus

3.9.1 Preparation of blood

Chicken blood in alseveres's (117) buffer was purchased from Lampire. Red blood cell (RBC) content was quantified using a hematocrit and capillary reader. Two capillary tubes were filled with blood, and the ends were sealed with foam plugs. The tubes were spun in a tabletop centrifuge for 1 min at 1300 rpm. The percentage of RBCs was then determined using a capillary reader. Calculations were performed to prepare 0.5% RBC in PBS for hemagglutination (HA) assay. To exchange buffer, the required volume of blood was diluted in 50 mL of PBS and centrifuged for 5 mins at 1200 rpm. The supernatant was discarded, and the RBC pellet was resuspended in PBS to the final desired concentration.

3.9.2 Hemagglutination assay

To confirm the presence of virus in the allantoic fluid and to determine the HA titer, an HA assay was performed. In a 96 well V-bottom plate, 50 µL of PBS was added to each well. Then, 50 µL of allantoic fluid or PBS (negative control) was added to the wells in the first column. A two-fold serial dilution was performed across the plate. Following the dilution, 50 µL of 0.5% chicken red blood cells (as described in 3.9.1) were added to all the wells and the plate was incubated at 4°C for 30-45 mins. After incubation, the plate was tilted to observe RBC sedimentation. The last well showing complete hemagglutination (i.e., no teardrop formation) was considered positive. The HA titer was expressed in hemagglutination units (HAU), based on the dilution factor of the last positive well (**Figure 19**).

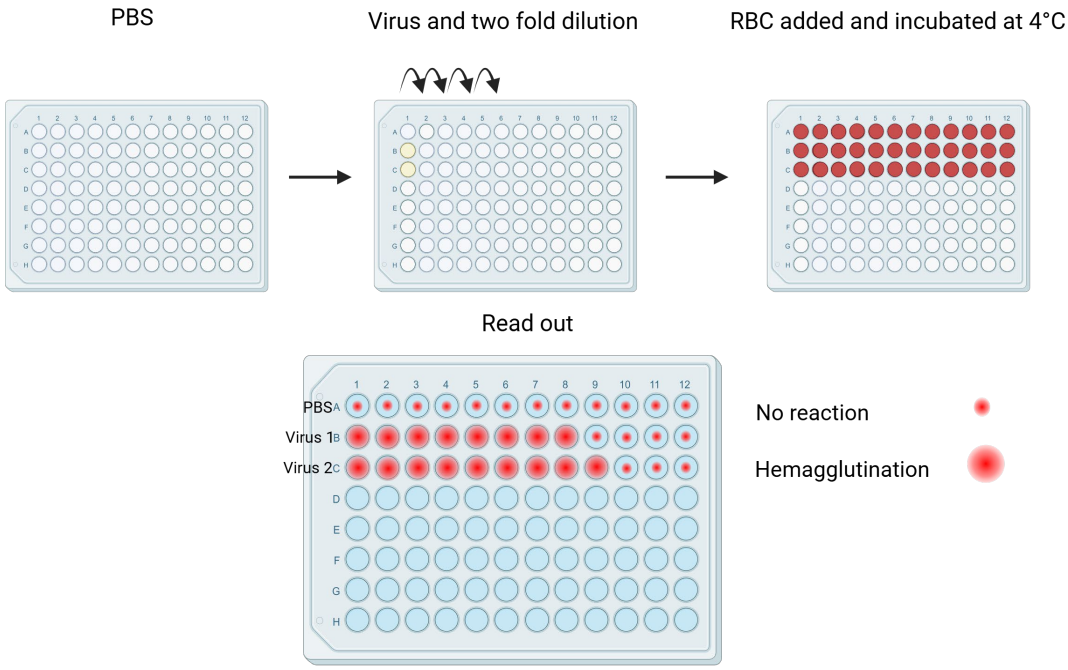

Figure 19. Schematic of HA assay.
PBS is added to the wells of a 96 well plate, followed by serial dilution of the virus and the addition of red blood cells. After incubation, the plate is assessed for hemagglutination to determine the relative amount of virus present in the sample. *(Generated using Biorender)*.

3.9.3 Plaque assay

Influenza virus plaque assays were performed on MDCK cells. A total of $1.5x10^6$ cells per well were seeded into 6-well plates and incubated overnight at 37°C/5% CO_2. Ten-fold serial dilutions (10^{-1} to 10^{-6}) of the virus samples were prepared in OPTI-MEM I in 1.5 mL microcentrifuge tubes. Cells were washed twice with OPTI-MEM I to remove any residual serum and then, 500 µl of virus dilution was added to the corresponding well. Plates were incubated at 37°C for 1 hour to allow absorption of the virus. The plate(s) were rocked every 10-15 mins to prevent cells from drying and to ensure even distribution of the inoculum. After the incubation, the inoculum was removed, and an agar overlay was added to each well. Once the overlay solidified, the plates were incubated at 37°C/5% CO_2 for 2 days for plaque formation (**Figure 20**). Plaques were visualized by immunostaining (See 3.9.4).

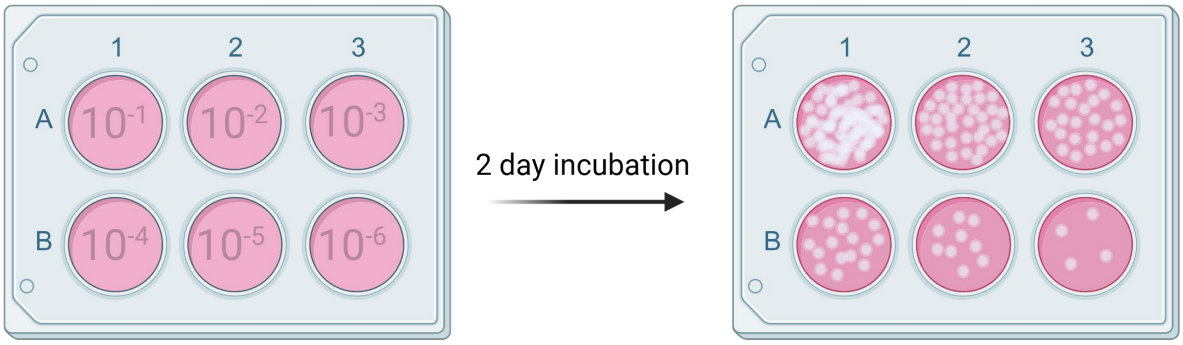

Figure 20. Plaque assay
A plaque assay of influenza virus was performed using MDCK cells. Cells were infected with serial dilutions of the virus, followed by incubation with an agar overlay. Plaques were subsequently visualized by immunostaining. *(Generated using Biorender)*.

3.9.4 Immunostaining

Plaque assay plates were fixed with 4% paraformaldehyde (PFA) for 30 minutes. After fixation, PFA is removed, and the agar overlay was gently removed with tap water. Cells were washed with PBS and permeabilized with 0.1% Triton X-100 in PBS for 15 minutes at room temperature. Following permeabilization, cells were washed with PBS and blocked with 1% bovine serum albumin (BSA) in PBS for 1 hour at room temperature. Primary antibody (against viral protein, ex. HA, NP, or NS1) was diluted in 1% BSA/PBS and added to each of the wells for 1 hour. Following incubation, the cells were washed with PBS and incubated with a secondary antibody conjugated with a horseradish peroxidase (HRP) (diluted in 1% BSA/PBS) for 1 hour at room temperature. Following the secondary antibody incubation, cells were washed with PBS and then developed with TrueBlue peroxidase substrate for 30 mins. until plaques were visible by eye. The reaction was stopped by rinsing with water. The plates were dried, and then plaques were counted, and the titer was determined taking into account the initial dilution. In this thesis, the primary antibody used was against NP (PA532242, 1:1000) and the secondary was anti-rabbit-HRP (1:1000) (**Table 7**).

3.10 Molecular biology

3.10.1 Primer list

Table 8. List of primers used for generation of plasmids, mutagenesis and cell line

P85aN564Dfrwrd	gaaattgacaaacgtatggacagcattaaaccag
P85aN564Drev	ctggtttaatgctgtccatacgtttgtcaatttc
P85bN561Dfrwrd	gatcgacaagcgcatggacagcctcaagccgg
P85bN561Drev	ccggcttgaggctgtccatgcgcttgtcgatc
P110aH1047Rfrwrd	caaatgaatgatgcacgtcatggtggctggac
P110aH1047Rrev	gtccagccaccatgacgtgcatcattcatttg
P85b-R355Afrwrd	caccttcctagtcgcagatgcttctagcaag
P85b-R355Arev	cttgctagaagcatctgcgactaggaaggtg
P85b-R647Afrwrd	caccttcctcatcgccgagagcagccagcgg
P85b-R647Arev	ccgctggctgctctcggcgatgaggaaggtg
P110dXholLinkfrwrd	gcctctcgagctcaagcttcgaattctatgccccctggggtggac
P110dBamHIrev	ggccggatccctactgcctgttgtctttgg
P110d1frwrd	caacctcagcaccatc
P110d2frwrd	caaaccacctcccattc
P110d3rev	ggagcgagccttcttgg
P110d4frwrd	gtgcatgtcaccgagg
P110d5frwrd	cactcgaccccagcac
P110d6frwrd	gaagtccaagaacccgg
ClalV5p110afrwrd	ggccatcgatatgggaaagccgatcccaaacccctattaggtctggactccacccctccacg accatcatcagg
Nhep110arev	ggccgctagctcagttcaatgcatgctgtttaattg
Xhollinkp110arev	ggccctcgagatctgagtccggagttcaatgcatgctgtttccttg
XhollinkRFPfrwrd	ggccctcgagctcaagcttcgaattctatggcctcctccgaggacg
NheRFPrev	ggccgctagcttaggcgccggtggagtgg
ClalV5p110bfrwrd	ccggatcgatatgggaaagccgatcccaaacccctattaggtctggactccacctgcttcagtt tcataatgcc
Nhep110brev	ccgggctagcttaagatctgtagtctttcc

Xhollinkp110brev	ccggctcgagatctgagtccggaagatctgtagtctttcc
EcoR1HAp85afrwrd	ggccgaattcatgtacccttatgatgtgccagattatgccagtgctgaggggtaccag
Nhep85arev	ggccgctagctcatcgcctctgctgtgcatatactgg
EcoRllinkp85arev	ggccgaattcgaagcttgagctcgagatctgagtccggatcgcctctgctgtgcatatactgg
ClalHAp85afrwrd	ggccatcgatatgtacccttatgattgccagattatgccgcgggccctgagggcttccag
Xhollinkp110afrwrd	ggccctcgagctcaagcttcgaattctcctccacgaccatcatcagg
Xhollinkp110bfrwrd	ggccctcgagctcaagcttcgaattcttgattcagtttcataatgcc
Bglillinkp85afrwrd	ggccagatctcgagctcaagcttcgaattctagtgctgaggggtaccag
BgIllp85arev	ggccagatcttcatcgectctgctgtgcatatactgg
Clalp110afrwrd	ggccatcgatatgcctccacgaccatcatcagg
Clalp110bfrwrd	ccggatcgatatgtgcttcagtttcataatgcc
ECORIp85afrwrd	ggccgaattcatgagtgctgaggggtaccag
p85aS1frwrd	tgaaaccacaggggaaaggggg
p85aS2frwrd	gccctatgcttttcag
p85aS3frwrd	gaatatacccgcacatcccag
p85aS4frwrd	gtggacggcgaagtaaag
p85aS5rev	gctggaatgacaggatttgg
p110aS1frwrd	gtaagtgttactcaagaag
p110aS2frwrd	gagtcagtataagtatataag
p110aS3frwrd	gaaactccatgcttagag
p110aS4frwrd	ggcatttaaaatctgagatg
p110aS5frwrd	gtgcactgcagttcaacag
p110aS6frwrd	gacattgcatacattcg
p110aS7rev	ggagaaactattacccag
p110bS1frwrd	ggatattgactcctatatg
p110bS2frwrd	ggaacttgtgatgaacag
p110bS3frwrd	gaactcgaagaaatgttg
p110bS4frwrd	ggcagtttctattttgg
p110bS5frwrd	gcaatgtggctgctgcagcag
p110bS6frwrd	gatatacagtatcttaagg

p110bS7rev	gatgagctttcccccataaag
p85ClaI	ggccatcatatggcgggccctgagggcttccag
p85XholrevI	ggccctcgagatctgagtccggagcgggcggcaggcggcggg
HA-p85bfrwrd	ggccatcgatgccaccatgtacccttatgatgtgccagattatgccgcgggccctgagggcttccag
HA-p85brev	gcccgctagctcagcgggcggcagg
pLVX-puroseqfrwrd	tccacgctgttttgacctc
pLVX-puroseqrev	aaaagacggcaatatggtgg
HA-p85beta-lenti frwrd	ggccctcgaggccaccatgtacccttatgatgtgccagattatgccgcgggccctgagggcttccag
HA-p85beta-lenti rev	gcccgcggccgctcagcgggcggcagg
pCAGGS frwrd	ccttcttctttttcctacagc
pCAGGS rev	cctttattagccagaagtcag

3.10.2 Restriction enzyme list

Table 9. List of restriction enzymes used.

Enzyme	Recognition site
NheI	G|CTAGC
XhoI	C|TCGAG
BamHI	G|GATCC
BglII	A|GATCT
ClaI	A|TCGAT
NotI	GC|GGCC|GC

Table 10. Sequence of the tags used in some of the constructs.

Tag	Sequence
HA	ATG TAC CCT TAT GAT GTG CCA GAT TAT GCC
V5	ATG GGA AAG CCG ATC CCA AAC CCT CTA TTA GGT CTG GAC TCC ACC

3.10.3 Accession number for the constructs/ORF

Table 11. GenBank accession number for proteins that were used in this study.

Protein	Accession number
p110α	NM_006218
p110β	BC114432
p110δ	BC132919
p85α	BC094795
p85β	BC070082.1
A/Puerto Rico/8/1934 NS1	AF389122.1
A/Wyoming/03/2003 NS1	EU268231.1
A/Wilson-Smith/1933 NS1	LC333189.1
A/Hong Kong/156/1997 NS1	AF036360.1
A/California/04/2009 NS1	MN371614.1
A/Brevig Mission/1/1918 NS1	AF333238.1
Ras	NM_005343.4
Src	NM_005417
Rab5	NM_004162
Zyxin	NM_003461

3.10.4 Viral RNA extraction

Viral RNA was extracted from allantoic fluid using the E.Z.N.A. viral RNA kit following the manufacturer's protocol. Briefly, 150 µL of allantoic fluid was mixed with 500 µL of QVL lysis buffer containing carrier RNA (poly(A)). The mixture was incubated at room temperature. Following incubation, 350 µL of 100% ethanol was added to the lysate and mixed thoroughly. The lysate was transferred to a silica-based column and centrifuged using a tabletop microcentrifuge. The column was subsequently washed with 500 µL of VHB buffer, followed by two washes with 500 µl of RNA wash buffer II. The column was centrifuged to remove any

residual buffer. Finally, RNA was eluted with 30ul of nuclease free water. RNA concentration was measured using a NanoDrop spectrophotometer.

3.10.5 Cloning

3.10.5.1 RTPCR

Extracted RNA was reverse transcribed into complementary DNA (cDNA) and amplified using superscript one step RTPCR kit according to the manufacturer's instructions (see details in **Table 8**, **Table 12** and **Table 13**). The products were analyzed by agarose gel electrophoresis, and bands of expected size were excised and purified. Purified DNA was stored at -20°C.

Table 12. RTPCR thermocycler setup

Step	Temp	Time	No. Cycle
RT	45	45 min	1
Denaturation	92	2 min	
Amplification	94	30 s	35
	55	30 s	
	72	3 min	
Final extension	72	10 min	1
Hold	4	infinity	

Table 13. RTPCR reaction mix.

Reagent	Volume (ul)
Buffer (2x)	12.5
RNA	2
Primer 5' (10uM)	1.5
Primer 3' (10uM)	1.5
Water	7.5
Enzyme	0.5

3.10.5.2 PCR

PCR was performed for DNA amplification and site-directed mutagenesis. PCR products were analyzed by agarose gel electrophoresis, and bands excised and purified. Purified DNA was stored at -20°C for further use (see **Table 8**, **Table 14** and **Table 15**).

Table 14. PCR thermocycler setup.

Step	Temp (°C)	Time	Number of cycles
Denaturation	95	5 min	1
Amplification	94	30 s	35
	55	30 s	
	72	1	
Final extension	72	7 min	1
Hold	4	Pause	

Table 15. PCR reaction mix.

Reagent	Volume (ul)
Buffer (10x)	10
DNA/Template	2
Primer 5' (10uM)	1
Primer 3' (10uM)	1
DNTP	1
DMSO	5
Water	30
Enzyme	0.5

3.10.5.3 Digestion

Plasmid vectors were digested with restriction enzymes to linearize the DNA and generate overhangs for ligating desired inserts. DNA inserts were similarly digested to create compatible overhangs. Following digestion, all samples were run on agarose, and the appropriate bands were excised and gel purified. For plasmid vectors, a phosphatase treatment was performed after digestion to prevent self-ligation. Digested vectors were treated with phosphatase for 1 hour at 37°C prior to gel purification. Majority of the restriction enzyme digestions, as well as the phosphatase treatment, were carried out at 37°C (see **Table 16**).

Table 16. Digestion reaction mix.

Reagent	Volume (µL) for insert digest	Volume (µL) for vector digest
Buffer (10x)	5	5
DNA (insert/vector)	43	4 (µg)
Enzyme 1	1	2.5
Enzyme 2	1	2.5
Water	0	36

3.10.5.4 Ligation

Desired DNA inserts were ligated into linearized vectors with compatible overhangs using T4 DNA ligase according to the manufacturer's protocol. Ligation reactions were incubated overnight at 4°C (See **Table 17**).

Table 17. Ligation reaction mix.

Reagent	Volume (µL)
Insert	10
Vector	1
Ligase	1
Buffer (10x)	2
water	7

3.10.5.5 Transformation

Plasmids were transformed into *E. coli* strains (DH5α or Stellar) either for propagation of plasmids or for cloning. Bacteria was heat shocked to allow the integration of DNA. For propagating more plasmid, 0.5 µg of plasmid DNA was mixed with 50 µL of chemically competent cells. The mixture was incubated on ice for 5 mins, followed by heat shock at 42℃ for 1 min. Immediately after the heat shock, the cells were placed on ice for 5 mins. Subsequently, 900 µL of S.O.C. media was added to the transformed cells, and the suspension was incubated for 1hour at 30℃ at 140 rpm to allow bacterial recovery. Following the incubation, 50 µl of the transformed cells was plated on LB agar plates with the appropriate antibiotic (ampicillin in this case (100 µg/mL)). Plates were first allowed to sit at room temperature for absorption, then incubated overnight at 33℃. For products of ligation, the same protocol was followed with the following modifications: 10 µL of ligation product was mixed with 50 µL of competent cells. After the recovery step, the cells were pelleted, and most of the supernatant was discarded. The cell pellet was then resuspended in the remaining supernatant (~100 µL) and plated.

3.10.5.6 Colony PCR

After transformation and incubation, individual bacterial colonies were screened via colony PCR to confirm the presence of the desired constructs. PCR reactions were prepared using a 2× Taq polymerase master mix, with one primer annealing to the plasmid backbone and the other to the insert sequence. Individual colonies were picked using 200 µL pipette tips, which were then placed directly into PCR tubes and kept on ice. To preserve the colonies, the tips were subsequently touched to a freshly prepared LB agar plate marked with a numerical grid and incubated overnight. PCR amplification was performed, and the products were analyzed by agarose gel electrophoresis to assess fragment size. Colonies producing PCR products of the expected size were selected for inoculation into liquid cultures for plasmid minipreps (**Section 3.10.6.7**) and sequencing.

3.10.5.7 Miniprep

Plasmid DNA was extracted from E. coli cultures using the QIAGEN QIAprep Spin Miniprep Kit, following the manufacturer's protocol. Briefly, 3 mL of overnight bacterial culture was pelleted

by centrifugation and resuspended in 250 µL of Buffer P1. Cells were lysed with 250 µL of Buffer P2 and neutralized with 350 µL of Buffer N3. The lysate was centrifuged to pellet cell debris, and the supernatant was transferred to the spin columns. The column was washed twice with 500 µL of Buffer PB followed by 750 µL of Buffer PE. The columns were centrifuged to remove residual wash buffer, and the plasmid DNA was eluted in 50 µL of nuclease-free water. Plasmid DNA quality was analyzed by NanoDrop spectrophotometer and sanger sequence.

3.10.5.8 Maxiprep

Plasmid DNA was isolated using the QIAGEN Maxiprep Kit, following the manufacturer's instructions. Briefly, 200 mL of overnight E. coli culture was harvested by centrifugation at 4500 rpm for 30 mins. The bacterial pellet was resuspended in 10 mL of Buffer P1 (containing RNase A), lysed with 13 mL of Buffer P2, and neutralized with 13 mL of Buffer P3. The lysate was clarified by first centrifugation at 3000 rpm for 30 mins and then by filtration through 70 µM filter into the anion-exchange columns for gravity flow. The column was pre-equilibrated before the lysate with 15 mL of equilibration buffer. The column was washed with Buffer QC to remove contaminants, and plasmid DNA was eluted with 15 mL of Buffer QF. DNA was then precipitated by adding 13 mL of isopropanol, followed by centrifugation at 18000 rpm for 45 mins. The DNA pellet was transferred to an Eppendorf tube with 1ml of 70% ethanol and centrifuged for 10 mins. The supernatant was discarded and the pellet was air-dried and resuspended in 200 µL of nuclease-free water. DNA concentration and purity were measured using a spectrophotometer and sanger sequenced.

3.10.6 Subcloning

Constructs encoding the ORFs of human p85α, p85β, p110α, p110β, p110δ and Src were purchased from OriGene and subcloned into pCAGGS (**Table 11**) (91). Constructs encoding the ORF of human Ras V12 was purchased from Clontech and subcloned into pCAGGS with an mCherry tag. NS1 ORF from A/Puerto Rico/8/1934 was cloned into pCAGGS with an N-terminal V5 tag. The Y89F, W187A, N561D, H1047R, T40C and Y530F mutations were introduced by site directed mutagenesis using overlapping primers. Zyxin-N-RFP and Rab5-N-RFP constructs were purchased from OriGene and subcloned into pCAGGS.

3.10.6.1 BiFC complex cloning design

The bimolecular fluorescence complementation system was originally established by Hu and colleagues in 2002 to visualize the interactions among bZIP and Rel family proteins (68). In this assay, the researchers split yellow fluorescent protein (YFP), a variant of the green fluorescent protein (GFP) that was first identified in the jellyfish *Aequorea victoria* in 1962 by Osamu Shimomura, Martin Chalfie, and Roger Y. Tsien (150). Since its introduction, the BiFC technique has evolved to include different variants of fluorescent proteins, enabling the use of various fluorophores such as mRFP (74). It has also been modified in several ways, including TriFC (184)and BiFC-TALE (69). We generated our BiFC system (142, 146) by adding N-terminus (YN) of YFP (amino acids 1-154) to the N-terminus of p110s (YN- p110α, YN-p110β, YN-p110δ) and the C-terminus of YFP (YC) (amino acids 155-end) to the C-terminus of the p85s (YC-p85α, YC-p85β) by polymerase chain reaction (PCR). A short linker region (SGLRSRAQASIS) and XhoI restriction site was included after the YN sequence in the YN constructs, while in the YC it was included prior to the YC sequence (**Figure 21**). The original split YFP system was kindly provided by Dr. Thorstenn Wolff.

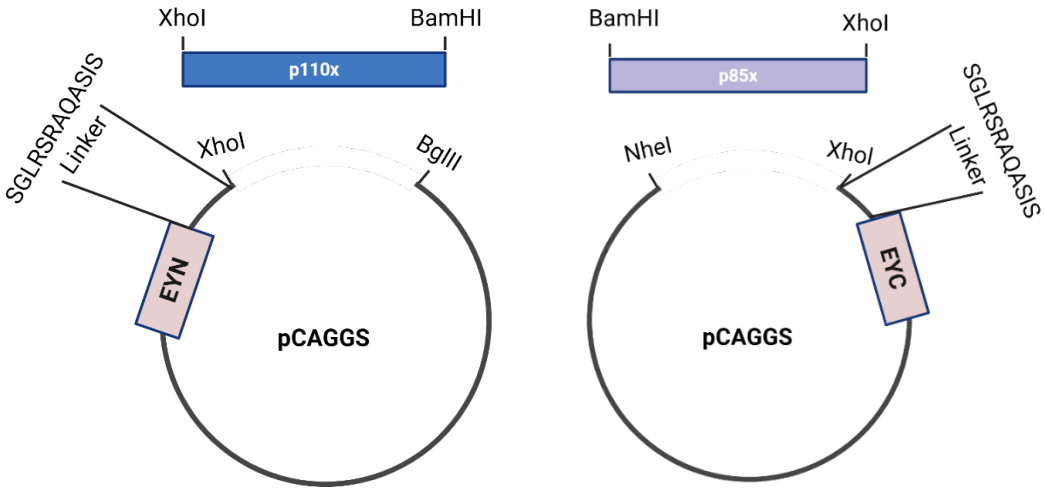

Figure 21. Schematic of the BiFC construction.
The YC or YN portions of the YFP were cloned into the pCAGGS expression vector followed by a small linker. The catalytic subunit was cloned downstream of the YN and linker region, while p85 was cloned upstream of the linker and YC region. All possible combinations were originally cloned and tested, however, this combination was selected due to the signal strength and structural knowledge of the p85-p110 interaction. *(Generated using Biorender)*.

3.11 Transfection for BiFC with lipofectamine 2000 and 3000

Cells were transfected with lipofectamine 2000 or 3000 according to the manufacturer's instructions. Briefly, 1 μg of each plasmid was mixed with OPTI-MEM I to a final volume of 50 μL. In a separate tube, with 3 μL of lipofectamine was mixed with 200 μL of OPTI-MEM I (1:3 (DNA:lipofectamine) ratio) and incubated for 5 mins. Following incubation, the lipofectamine/OPTI-MEM I mixture was combined with DNA/OPTI-MEM I and incubated for 30-45 mins at room temperature. During this incubation, cells were trypsinized, resuspended in fresh media and counted. After the 30-minute incubation, the desired concentration of cells was mixed with the DNA/lipofectamine/OPTI-MEM I mixture and plated onto appropriate plates. At 6 hours post transfection, or the following day, the media was replaced and cells were processed for the desired assays. For lipofectamine 3000, the same protocol was followed, except that P3000 reagent was added with to the DNA/OPTI-MEM I mixture at a 1:2 ratio (DNA:P3000).

3.12 BiFC reconstruction and staining

HeLa cells were co-transfected with plasmids encoding p110s, p85s and/or NS1 using Lipofectamine 2000 or 3000, as described in **section 3.11**. The following DNA concentrations were used: 1 μg of plasmids expressing YN-p110s and YC-p85s, and 0.5 μg of plasmid expressing NS1. Between 8-16 hours post transfection, media was changed and after 16hrs the cells were placed at 33 °C for 3 hours to allow reconstitution of YFP. Cells were washed with PBS and fixed with ice cold methanol for 20 minutes at 4 °C. Following fixation, the cells were washed with PBS and blocked with 1% BSA/PBS for 1 hour at room temperature (RT). After blocking, the primary antibody (V5-tag (Invitrogen, 460705)) was diluted 1:500 in 1% BSA/PBS and added to the cells for 1 hour at RT. After incubation, the cells were washed again and incubated with a fluorophore conjugated secondary antibody (anti-mouse Alexa 633 (Invitrogen, A21052)) and 4′,6-diamidino-2-phenylindole (DAPI) (Invitrogen, D1306), both diluted 1:1000 in 1% BSA/PBS, for 1 hour at RT, followed by three PBS washes. Samples were stored in PBS at 4°C and protected from light. Fluorescence was observed using confocal microscope (LSM 580 and LSM880), and images were acquired. Z-stack images were collected and processed using Fiji (ImageJ).

3.12.1 Wortmannin treatment

HeLa cells were co-transfected to generate the indicated BiFC complexes with NS1, as described above (**Section 3.12**). Prior to fixation and staining, cells were treated with 10 μM of wortmannin according to the manufacturer's instructions, and the fixation protocol was modified as described below (**Section 3.12.2**).

3.12.2 PIP3 staining

HeLa cells were co-transfected to generate the indicated BiFC complexes with NS1, as described above (**Section 3.12**). Cells were fixed with 2.5% paraformaldehyde (PFA) (Polyscience, 04018-1) for 5 mins at RT, washed three times with PBS, and permeabilized with 0.5% saponin in PBS for 15 mins at RT. The remaining steps were performed as described in **section 3.12**, with the following antibodies and incubation conditions: cells were blocked with 10% BSA/PBS overnight at 4°C; the primary antibody (Echelon Biosciences) was diluted 1:200 in 1% BSA/PBS and incubated at 37°C for 1 hour; the secondary antibody (anti-mouse Alexa Fluor 633, 1:1000) and DAPI (1:2000) were diluted in 1% BSA/PBS incubated at RT for 30 mins.

3.12.3 pAkt staining

HeLa cells expressing BiFC complexes with and without NS1 were fixed with 4% PFA for 10 mins at RT followed by three PBS washes. Cells were then permeabilized with 0.1% Triton X-100 in PBS (Fisher, BP151-500) for 5 min at RT. The rest was as described above (**Section 3.12**), with the following changes: the cells were blocked with 1% BSA/PBS overnight at 4°C; the primary antibodies V5-tag (1:500) and pAkt (1:200) (cell signaling technology, 4060) was diluted in 1% BSA/PBS and incubated for 1 hour at RT; the secondary antibodies anti-rabbit Alexa Fluor 647 (1:1000) (Invitrogen, A21443), Pacific Blue anti-mouse (1:1000) (Invitrogen, P31582), and Phalloidin Alexa Fluor 568 (1:40) (Invitrogen, A12380) were diluted in 1% BSA/PBS and incubated at RT for 1 hour.

3.13 Generation of stable cell line

3.13.1 Cloning of pLVX-IRES-puro construct

To generate a stable cell line constitutively expressing HA-p85β-N561D, we used the lentiviral system (158). The HA-p85β-N561D ORF was cloned into pLVX-IRES-Puro lentiviral vector (Takara), as described above (**Section 3.10.6**). The lentiviral system is widely used to generate stable cell lines. It is based on a replication incompetent lentivirus, safely modified by splitting the viral components among different plasmids. This three-plasmid system includes: a packaging plasmid encoding viral structural and enzymatic proteins (Gag/Pol), an envelope plasmid encoding a viral surface protein (VSV-G), and a transfer plasmid encoding the gene of interest (pLVX-IRES-puro-HA-p85β-N561D).

3.13.2 Co-transfection to produce lentivirus

293T cells were co-transfected with pLVX-IRES-Puro-HA-p85β-N561D, lenti-Gag/Pol, and pMD2VSV-G using TransIT-LT1 (Mirus) according to the manufacturer's guidelines. Briefly, 3 µg of lenti-Gag/Pol, 3 µg of pMD2-VSV-G, and 5 µg of pLVX-IRES-Puro-HA-p85β-N561D were mixed with 250 µL of OPTI-MEM I and 33 µL of TransIT-LT1, and incubated for 20-30 min at RT. During this incubation, 293T cells were trypsinized, resuspended in fresh medium and counted. After incubation, $1x10^6$ cells were mixed with DNA/OPTI-MEM I/TransIT-LT1 mixture, and plated in a 6 well plate, and incubated at 37°C/5% CO_2. Between 8-16 hours post transfection, the medium was replaced with fresh cDMEM, and the cells were incubated at 37°C/5% CO_2. The supernatant was collected at 48 hours post transfection, fresh medium was added, and a second collection was at 60 hours post transfection. Both supernatants were combined and centrifuged at 1200 rpm for 10 min using a tabletop centrifuge (Eppendorf). The supernatant was filtered through a 0.45 µm cellulose acetate filter, aliquoted and stored at -80 °C until further use.

3.13.3 Transduction of A549 and clonal population selection

A549 cells were seeded in a 6 well plate at 50-70% confluency. The medium was replaced with cDMEM containing 700 µL of lentivirus (**Section 3.13.2**) and 1 µL of polybrene (stock 12 mg/mL; Millipore, TR-1003G), and the cells were incubated at 37°C/5% CO_2. Twenty-four hours after transduction, the medium was replaced with fresh cDMEM. Four days post transduction, the medium was replaced with cDMEM containing the selection antibiotic puromycin, and cells were maintained under selection until all untransduced cells had died, with media changes and passaging as needed. The resulting polyclonal population was tested for expression of HA-p85β-N561D by indirect immunofluorescence (**Section 3.15**). Once the expression was confirmed, cells were seeded at a very low density in a large tissue culture dish to allow clonal population generation. Once individual clones became visible, they were transferred to 24 well plates for expansion. Clones were screened by indirect immunofluorescence, and the best expressing clones were expanded and several aliquots were frozen.

3.14 Growth curve

A549 WT and A549-p85β-N561D cells were seeded in 6 well plates at a density of 1.5 x 10^6 cells per well, in triplicates for each virus and mock. Cells were washed with PBS and starved for 24 hours (**Section 3.14.1**). Following starvation, cells were washed with OPTI-MEM I and infected with A/Puerto Rico/8/134 (rPR8 WT) or A/Puerto Rico/8/1935-NS1-Y89F (rPR8-Y89F) at an MOI of 0.01 for 1 hour and incubated at 37°C/5% CO_2, with intermittent rocking. After adsorption, the inoculum was removed and replaced with infection medium containing TPCK-treated trypsin, and cells were incubated at 37°C/5% CO_2. Supernatants were collected at 8, 24, 32-, 48-, 56-, and 72-hours post infection, aliquoted, and stored at -80°C. Viral titers were determined by plaque assay (**Section 3.9.3**).

3.14.1 Starvation protocol

A549 WT and A549-p85β-N561D cells were seeded in 6 well plates at a density of 1.5 x 10^6 cells per well and incubated at 37°C/5% CO_2. Following day, cells were washed with PBS to remove any residual serum, and starvation medium (1xMEM + P/S + 0.2% BA) was added. The cells were then incubated for 24 hours. Starvation was confirmed by running the cell lysate on an SDS-PAGE gel and probing for pAkt (**Section 3.16**).

3.14.2 Infection of BiFC-transfected cells

HeLa cells were co-transfected with the various BiFC constructs using Lipofectamine 3000 (Invitrogen) according to the manufacturer's guidelines (**Section 3.11**). At 16 hours post transfection, the medium was replaced with fresh media, and the cells were incubated at 33°C for 3 hours to allow reconstitution of YFP. Following incubation, the cells were washed twice with OPTI-MEM I (Gibco, 31985-062) and then infected with rPR8 WT and rPR8-Y89F with a MOI of 10 PFU/cell for 1 hour at 37°C/5% CO_2. After infection, the inoculum was removed, infection medium (1xMem+0.2% BA+P/S) was added, and the cells were incubated at 33°C or 37°C for 24 hours. At 24 hours p.i., cells were processed for immunofluorescence using an anti-NS1 antibody (Invitrogen, PA532243).

3.15 Immunofluorescence for cell line validation

A549 WT and A549-p85β-N561D cells were seeded on 12 well glass bottom plates and incubated at 37°C/5% CO_2. The following day, cells were fixed with 4% PFA without methanol for 30 minutes. Following fixation, cells were permeabilized with 0.1% triton X-100 in PBS for 15 mins and then washed with PBS. Blocking was performed with 1% BSA/PBS for 1 hour at RT. Primary antibodies (HA tag, Invitrogen, 326700), and p85β (Invitrogen, MS53215)) were diluted 1:1000 in 1% BSA/PBS, and cells were incubated for 1 hour at RT. After washing with PBS, secondary antibodies (anti-rabbit Alexa Fluor 488 (Invitrogen, A-11034)) and DAPI were diluted 1:1000 in 1% BSA/PBS and incubated for 1 hour at RT. Cells were washed three times with PBS and stored

in PBS at 4℃, protected from light. Fluorescence was observed using LSM880 confocal microscope, and images were acquired and processed with ImageJ.

3.16 Western Blot

3.16.1 Sample collection

A549 WT and A549-p85β-N561D cells were seeded in 6 well plates and starved for 24 hours as described in **section 3.14.1**. Following starvation, cells were infected with rPR8 WT and rPR8-Y89F at an MOI of 2 for 1 hour, after which the medium was with infection media. Cell lysates were collected at 0, 2, 4, 6, 8 hours post-infection. At the appropriate time points, infection media was aspirated, and 300 µL of RIPA buffer containing protease/phosphatase inhibitor (cell signaling technology) was added to each well. The cells were incubated for 5 min, after which they were scraped, and the mixture was transferred to microcentrifuge tubes. Samples were centrifuged at 13,000 rpm for 10 mins at 4℃, and the supernatant was transferred to a new tube. The samples were stored at -80℃ until further processing.

3.16.2 Protein quantification

Proteins from the cell lysate were quantified using the Pierce BCA Protein Assay Kit (Thermo fisher), following the manufacturer's guidelines. Briefly, solution A and solution B were mixed in a conical tube at a 50:1 ratio. Next, 10 µL of either the sample or standard was added to a well in a 96 well cell culture plate, and 200 µL of reagent (solution A/B) was added to each well using a multichannel pipette, followed by mixing. The plate was incubated at 37℃ for 30 minutes. After incubation, the plate was brought to room temperature, and the absorbance was read at 562 nm using a plate reader. All samples, standards, and mock samples were run in triplicates. The total protein concentration in each sample was calculated using the standard curve generated from the standards.

3.16.3 Sample preparation, gel loading and transfer

Based on the BCA assay, 10 µg of total protein was mixed with Pierce Lane marker reducing sample buffer (5x) (Thermo fisher), diluted with water to a final volume of 30 µL. The samples were boiled for 5 mins at 100℃, then transferred to ice and centrifuged briefly. The samples were run on 4-20% reducing denaturing sodium dodecyl sulfate polyacrylamide gel electrophoresis (SDS-PAGE) gel (Bio-Rad), and the protein was transferred onto a polyvinylidene difluoride (PVDF) membrane (Bio-Rad) using the turbo transfer system (Bio-Rad) with mixed molecular weight settings for 7 min.

3.16.4 Blotting

Following the transfer of proteins to the PVDF membrane, the membrane was blocked with 5% (w/v) BSA in PBS containing 0.1% (v/v) Tween 20 (PBST) for 1 hour at RT on a shaker. The membrane was incubated overnight with pAkt (Ser473) (cell signaling technology, 4060S) diluted 1:1000 in 5% BSA in PBST at 4℃ on a shaker. The membrane was washed three times with PBST (5-minute incubation each time) on a shaker at RT. Next, the membrane was incubated with anti-mouse-HRP IgG diluted 1:2000 in 5% BSA in PBST for 1 hour at RT on a shaker. The membrane was washed three times with PBST and developed using Brightstar HCL (ASI). The HRP was activity was quenched by incubating the membrane with 1% sodium azide for 15 minutes on a shaker at RT. The membrane was washed overnight with PBST (changing the buffer several times) on a shaker. The membrane was then incubated overnight with a monoclonal antibody against NS1 (Invitrogen, GT1653) diluted 1:1000 in 5% milk/PBST at 4℃ on a shaker. The membrane was washed three times and incubated with anti-mouse-HRP (Kindlebio) diluted 1:1000 in 5% milk/PBST for 1 hour at RT on a shaker. The membrane was washed three times and developed with Brightstar HCL. The membrane was washed for 24 hours with frequent changes of PBST. Finally, the membrane was incubated with β-actin-HRP (cell signaling technology, 12262) antibody diluted 1:2000 in 5% milk/PBST for 1 hour at RT on a shaker. The membrane was washed three times and developed with Brightstar HCL (ASI). Cell line validation by Western blot was performed as described above, with the following modifications: blocking was done with 5% milk/PBST and the following antibodies were used: HA-tag-HRP conjugated (Cell signaling

technology, 2999S), p85β (Invitrogen, MA53215), and loading control β-actin-HRP (Cell signaling technology, 12262).

3.17 Competition assay

To perform the competition assay with both viruses in two different cell lines, A549 WT and A549-p85β-N561D cells were seeded in 6-well plates at a density of 1.5 X 10^6 cells per well and incubated overnight. The next day, rPR8 WT and rPR8-Y89F viruses were diluted to 10^7 PFU/mL in Opti-MEM I. Equal volume of each virus were mixed to achieve a 50:50 ratio. The mixed virus was then diluted to 10^3 PFU/mL, which was considered the input. A549 WT and A549-p85β-N561D cells were washed with Opti-MEM I to remove any residual serum and then infected for 1 hour. Following infection, the inoculum was removed and replaced with infection medium, and cells were incubated for 12, 24, and 48 hours. At each respective time, the supernatant was aspirated, and the cells were collected in 500 µL of TRI Reagent (Invitrogen, 9738G). RNA extraction was performed using the Direct-zol RNA miniprep extraction kit (Zymol, R2052) according to manufacturer's instructions. Briefly, 500 µL of 100% ethanol was added to each samples and mixed, then transferred to spin columns and centrifuged. DNase I treatment was performed on-column for 15 mins. Following DNase treatment, the columns were washed twice with 400 µL of Pre Wash buffer and then with 700 µL of wash buffer. The columns were centrifuged for 1 minute to remove any residual buffer, and RNA was eluted in 30 µL of water. Samples were then prepared for MinION Oxford Nanopore sequencing (**Section 3.18**) (**Figure 22**).

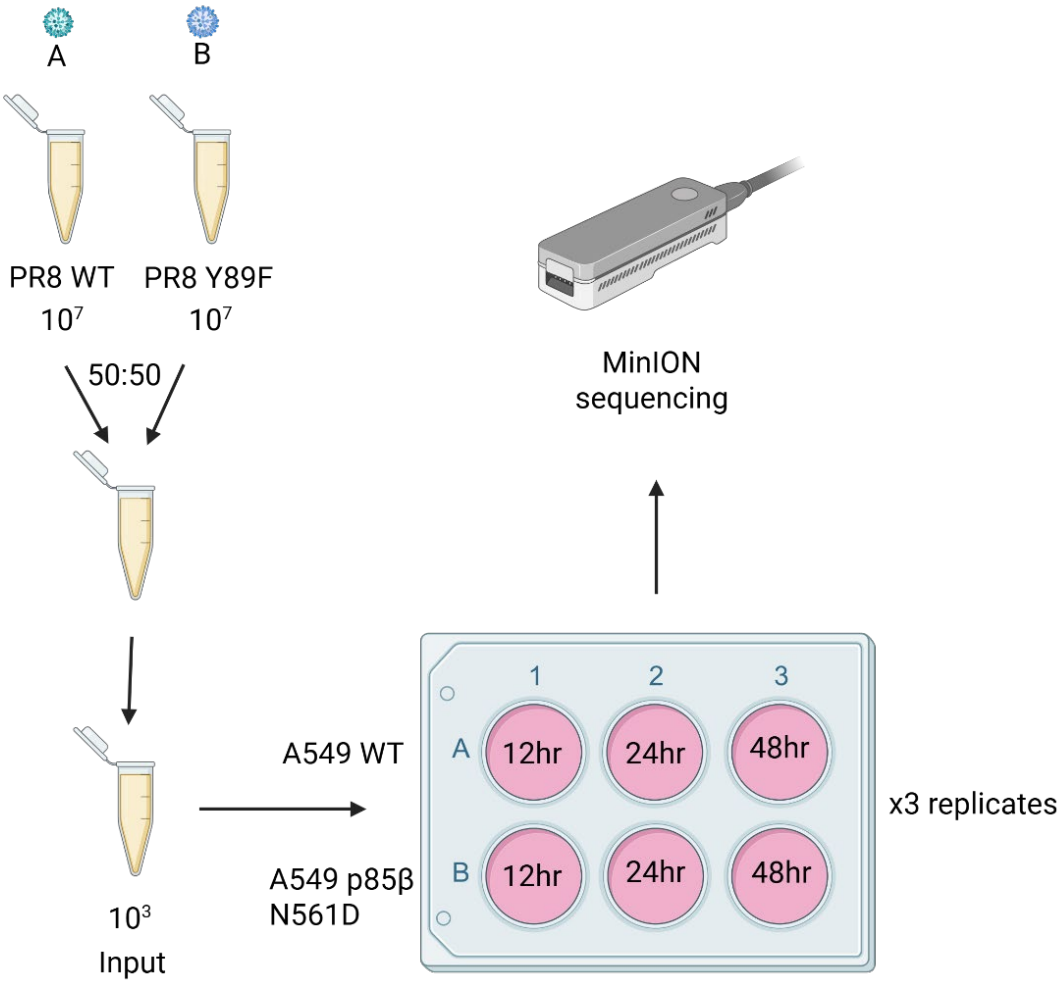

Figure 22. Schematic representation of the competition assay
Competition assay was performed by first diluting PR8 WT and PR8 Y89F to 10^7 PFU/mL and then the two viruses were mixed in a 50:50 ratio. The mixed virus was further diluted to 10^3 PFU/mL and A549 WT and A549 p85β N561D cells were infected for 12, 24, and 48hrs. Cells were harvested at the indicated time points and processed for MinIon sequencing. The percentage of reads for NS1 Y89F versus NS1 WT were quantified. *(Generated using Biorender)*.

3.18 MinION sequencing

5 µL of each viral RNA sample was used for RT-PCR using SuperScript IV One-Step RT-PCR System (Invitrogen). Each PCR product was purified using AMPure XP (Beckman Coulter) according to the manufacturer's instructions and quantified using a Qubit (Thermo Fisher Scientific). The library of purified samples was prepared for sequencing using the Native Barcoding Kit 96 V14 (SQK-NBD114.96, Oxford Nanopore) (187, 188) as per the

manufacturer's instructions. The library was loaded onto a MinION flow cell (R10.4.1, Oxford Nanopore) following the recommended protocol. FASTQ were obtained for each sample, and Geneious Prime (2025.1.1) was used to perform reference-based alignment. The number of reads corresponding to rPR8 WT and rPR8-Y89F were subsequently identified.

3.19 BiFC quantification

HeLa cells were co-transfected with indicated p110s, p85s and NS1 WT using Lipofectamine 3000 (Invitrogen), according to the manufacturer's guidelines (**Section 3.11**). Then, 16 hours post transfection, media was changed, and the cells were placed at 33°C for 3 hours. At 19 hours p.t., cells were processed for fluorescence microscopy following the previously described BiFC assay protocol, using antibodies against V5 tag. Using an LSM880 confocal microscope, 30 cells per condition were first assessed for positive BiFC and NS1 signals. Subsequently, the phenotype of each cell was checked to determine whether it displayed the relocalization pattern. Each condition was quantified in triplicate (30 cells/replicate/condition).

3.20 Co-Immunoprecipitation assay (Co-IP)

Co-IPs were performed as described previously (6). In brief, using 293T cells transfected with 2 μg of the pLVX-IRES-ZsGreen1 plasmid (Clontech, CA) carrying V5-tagged NS1 proteins or GST (as appropriate), 1 μg of the p3×FLAG-CMV7.1 plasmid (Sigma-Aldrich, MO) expressing FLAG-tagged human p85β or human p85α (provided by Hannah L. Turkington, University of Zurich, Zurich, Switzerland) (7) and 1 μg of the plasmid expressing one of the YN-tagged p110 subunits. Protein lysates (total and IP fractions) were resolved by SDS-PAGE on NuPAGE 4 to 12% Bis-Tris protein gels (Thermo Fisher), followed by transfer to nitrocellulose membranes. Proteins were detected by Western blotting using the following primary antibodies: mouse anti-V5 (cat# MCA1360; Bio-Rad), mouse anti-FLAG (cat# F1804; Sigma-Aldrich) and anti-YFP (cat# ab1218; Abcam). Secondary antibodies were fluorochrome-conjugated anti-mouse immunoglobulin (cat# 35519; Thermo Fisher Scientific) and anti-rabbit immunoglobulin (cat#

SA5-10036; Thermo Fisher Scientific,). A Li-Cor Odyssey scanner was used for detection. *Experiment performed by Dr. Nikos Tsolakos at the University of Zurich, Switzerland.*

3.21 Baculovirus generation and amplification

The plasmids harboring class IA PI3K catalytic and regulatory subunits were transformed into DH10MultiBac cells (MultiBac, Geneva Biotech) containing the baculovirus viral genome (bacmid) and a helper plasmid expressing transposase to transpose the expression cassette harboring the gene of interest into the baculovirus genome. Bacmids with successful incorporation of the expression cassette of pFastBac/ pACEBac1 into the viral genome was identified by blue-white screening and were purified from a single white colony using a standard isopropanol-ethanol extraction method. Briefly, colonies were grown overnight (~16 hours) in 3-5 mL 2xYT (BioBasic #SD7019). Cells were pelleted by centrifugation, and the pellet was resuspended in 225 µL P1 Buffer (Qiagen MiniPrep Kit, #27106), chemically lysed by the addition of 225 µL Buffer P2, and the lysis reaction was neutralized by addition of 300 µL Buffer N3. Following centrifugation at 21130 rcf and 4°C (Rotor #5424 R), the supernatant was separated and mixed with 600 µL isopropanol to precipitate the DNA out of solution. Further centrifugation at the same temperature and speed pelleted the bacmid DNA, which was then washed with 500 µL 70% ethanol three times. The Bacmid DNA pellet was then dried for 1 minute and re-suspended in 50 µL Buffer EB. Purified bacmid was then transfected into Sf9 cells. 2 mL of Sf9 cells between 0.3-0.5X10^6 cells/mL were aliquoted into the wells of a 6-well plate and allowed to attach, creating a monolayer of cells at ~ 70-80% confluency. Transfection reactions were prepared by the addition of 2-10 ug of bacmid DNA to 100 µL 1xPBS and 12 µL polyethyleneimine (PEI) at 1 mg/mL (Polyethyleneimine "Max" MW 40.000, Polysciences #24765, USA) to 100 µL 1xPBS. The bacmid-PBS and the PEI-PBS solutions were mixed, and the reaction occurred for 20-30 minutes before addition drop-by-drop to an Sf9 monolayer containing well. Transfections were allowed to proceed for 5-7 days before harvesting virus containing supernatant as a PI viral stock. Viral stocks were amplified by adding P1 viral stock to suspension Sf9 cells between 1- 2x10^6 cells/mL at a 1/100 volume ratio. This amplification produces a P2 stage viral stock that can be used in final protein expression. The amplification proceeded for 4-5 days before harvesting, with cell shaking at 120 RPM in a 27°C shaker (New Brunswick). Harvesting of P2 viral stocks was carried out by

centrifuging cell suspensions in 50 mL Falcon tubes at 2281 RCF (Beckman GS-15), collecting the supernatant in a fresh sterile tube, and adding 5-10% inactivated fetal bovine serum (FBS; VWR Canada #97068-085). *Experiment performed by Dr. Braden D. Siempelkamp and Dr. Gillian L. Dornan at the University of Victoria, British Columbia, Canada.*

3.22 Expression and purification of recombinant proteins

All PI3K constructs were expressed and purified as described previously (8-10). In brief the catalytic subunit and regulatory subunits were expressed using the pFASTBAC/ pACEBac1 expression system in Sf9 cells. After expressing the cells at 27°C for 55 hours the cells were harvested at 1739 x g at 4°C using Eppendorf Centrifuge 5810R and the cells were flash frozen using liquid nitrogen and stored in -80 °C. The frozen pellets were resuspended in lysis buffer containing 20 mM Tris pH 8, 10 mM Imidazole, 100 mM NaCl, 5% glycerol [v/v], 2 mM βME, protease inhibitor [Protease Inhibitor Cocktail Set III, Sigma]) and sonicated for 2 min (15s on, 15 s off, level 4.0, Misonix sonicator 3000). Triton-X 100 was added to the lysate at a final concentration of 0.1% and then clarified by spinning at 15,366xg for 45 min (Beckman Coulter JA-20 rotor). The supernatant was loaded onto a 5 ml crude Ni-NTA column (GE healthcare) equilibrated in NiNTA A buffer containing 20 mM Tris pH 8, 100 mM NaCl, 10 mM Imidazole and 5% glycerol [v/v]. The column was washed using high salt buffer containing 20 mM Tris, 1 M NaCl, 10 mM Imidazole, 5% Glycerol [v/v] followed by NiNTA buffer wash (20 mM Tris pH 8, 100 mM NaCl, 21 mM Imidazole and 5% Glycerol). The protein was eluted using 100% NiNTA B buffer (20 mM Tris pH 8, 100 mM NaCl, 200 mM Imidazole and 5% Glycerol). The elute from the nickel column was loaded onto Streptavidin column (GE healthcare) and subjected to buffer wash using Hep A buffer (20 mM Tris pH 8, 100 mM NaCl, 5% Glycerol and 0.5 mM tris(2-carboxyethyl) phosphine [TCEP]). The column was incubated on ice for 3 hours in the presence of TEV protease and then eluted by a wash with HEP A buffer. Proteins were subjected to gel filtration using SuperdexTM 200 10/300 GL Increase column from GE healthcare. After gel filtration, the protein was concentrated, aliquoted, frozen, and stored at −80°C. NS1 constructs were transformed into Escherichia coli (BL21 (DE3)). Bacterial cultures were induced with 1 mm isopropyl 1-thio-β-d-galactopyranoside after growth to an A600 of 0.6–0.9 in 2× YT (Sigma) broth containing ampicillin at 100 μg/ml. Induction was allowed to proceed for 4 h at 37 °C. The bacteria

were harvested by centrifugation, and the pellets were stored at −80 °C. Frozen E. coli pellets were resuspended in lysis buffer and sonicated on ice for 5 min (10 s on, 10 s off, level 6.0, Misonix sonicator 3000). Triton X-100 was added to the lysate at a concentration of 0.1% and centrifuged at 20 000 × g for 45 min (Beckman Coulter Avanti J-25I, JA 25.50 rotor). The supernatant was then loaded onto a 5-ml GSTrap™ HP Column (cytivia) equilibrated in buffer containing 20 mM Tris pH 8, 100 mM NaCl, and 5% glycerol. The column was washed with 30 ml of this buffer. TEV protease was added to a final concentration of ∼0.3 mg/mL. The cleavage was allowed to proceed overnight at 4 °C. To de-enrich the TEV protease, the protein solution was loaded onto a HisTrapTM FF column and eluted with 10 mL of Ni- NTA A buffer. The elution was concentrated to ∼2 mL. NS1 protein was injected onto a SuperdexTM 75 10/300 GL size exclusion column (GE Healthcare) equilibrated in gel filtration buffer (20 mm HEPES (pH 7.5), 150 mm NaCl, 1 mM TCEP). After gel filtration, the protein was concentrated, aliquoted, frozen, and stored at −80°C. *Experiment performed by Dr. Braden D. Siempelkamp and Dr. Gillian L. Dornan at the University of Victoria, British Columbia, Canada.*

3.23 Lipid Vesicle Preparation

Assays were carried out with PM mimic vesicles consisting of 5% brain PIP2, 20% brain PS, 45% egg yolk PE, 15% egg yolk phosphatidylcholine (PC) (Avanti #840051C), 10% cholesterol (Sigma Aldrich, #47127-U), and 5% egg yolk sphingomyelin (Sigma Aldrich, #S0756). To generate vesicles, the lipid mixtures were combined in organic solvent. The mixture was then evaporated using a stream of argon gas followed by desiccation under vacuum for 45 minutes. The lipids were resuspended in a lipid buffer (25 mM HEPES pH 7, 100 mM NaCl, 10% Glycerol [v/v]) and the solution was subjected to sonication for 15 mins. The vesicles were subjected to five freeze thaw cycles and extruded 11 times through a 100 nm filter (T and T Scientific: TT-002–0010). The extruded vesicles were sonicated again for 5 min, aliquoted and stored at −80°C. *Experiment performed by Dr. Braden D. Siempelkamp and Dr. Gillian L. Dornan at the University of Victoria, British Columbia, Canada.*

3.24 ATPase assay

All PI3K assays used the Transcreener ADP2 Fluorescence Intensity (FI) assay (Bellbrook labs) which measures formation of ADP. 2 µL of a PI3K solution (final concentration 100nM-400nM) at 2X final concentration was mixed with 2 µL substrate solution containing ATP and lipid vesicles (final concentration of 0.45 vesicles and 100 µM ATP), and the reaction was allowed to proceed for 60 min at 20°C. For experiments examining activation by NS1 protein, the PI3K and NS1 protein were allowed to pre-incubate for 15 minutes before incubation with substrate, with NS1 being present at a final concentration of 1 µM in the kinase reaction.

The reaction was stopped with 4 µL of 2X stop and detect solution containing EDTA (chelates Mg2+, stopping kinase activity) along with 8 nM ADP Alexa Fluor 594 Tracer and 93.7 µg/mL ADP2 Antibody IRDye QC-1, and was allowed to incubate for 60 minutes. The fluorescence intensity was measured using a SpectraMax M5 plate reader at excitation 590 nm and emission 620 nm. This data was normalized against a 0–100% ADP window made using conditions containing a final concentration of 100 µM ATP or ADP. % ATP turnover was interpolated from an ATP standard curve obtained from performing the assay on 100 µM (total) ATP/ADP mixtures with increasing concentrations of ADP. *Experiment performed by Dr. Braden D. Siempelkamp and Dr. Gillian L. Dornan at the University of Victoria, British Columbia, Canada.*

4. Results

4. Results

4.1 Generation of a system to visualize the PI3K complexes

First, we established a system to visualize the isoform-specific p85 and p110 heterodimers by using a bimolecular fluorescence complementation assay (BiFC). A similar assay was previously described by our group to study the cellular behaviors of protein complexes during the induction of the innate immune response (142). We fused the N-terminal (YN) part of yellow fluorescent protein (YFP) to the N-terminus of the p110 subunits (YN-p110α, YN-p110β, YN-p110δ), and the C-terminal (YC) part of YFP to the C-terminus of the p85s (p85α-YC, p85β-YC) (**Figure 23A**). In this way, upon transfection of a p85-p110 pair into cells, only the heterodimer formed by the combination of the specific YN- and YC- tagged subunits can be visualized by a YFP signal, allowing us to ascertain the cellular localization of each PI3K heterodimer (**Figure 23B)**. All the possible p85-p110 BiFC combinations showed a similar fluorescence phenotype when co-expressed by transfection in HeLa cells (**Figure 24**): a diffuse, homogeneous cytoplasmic distribution.

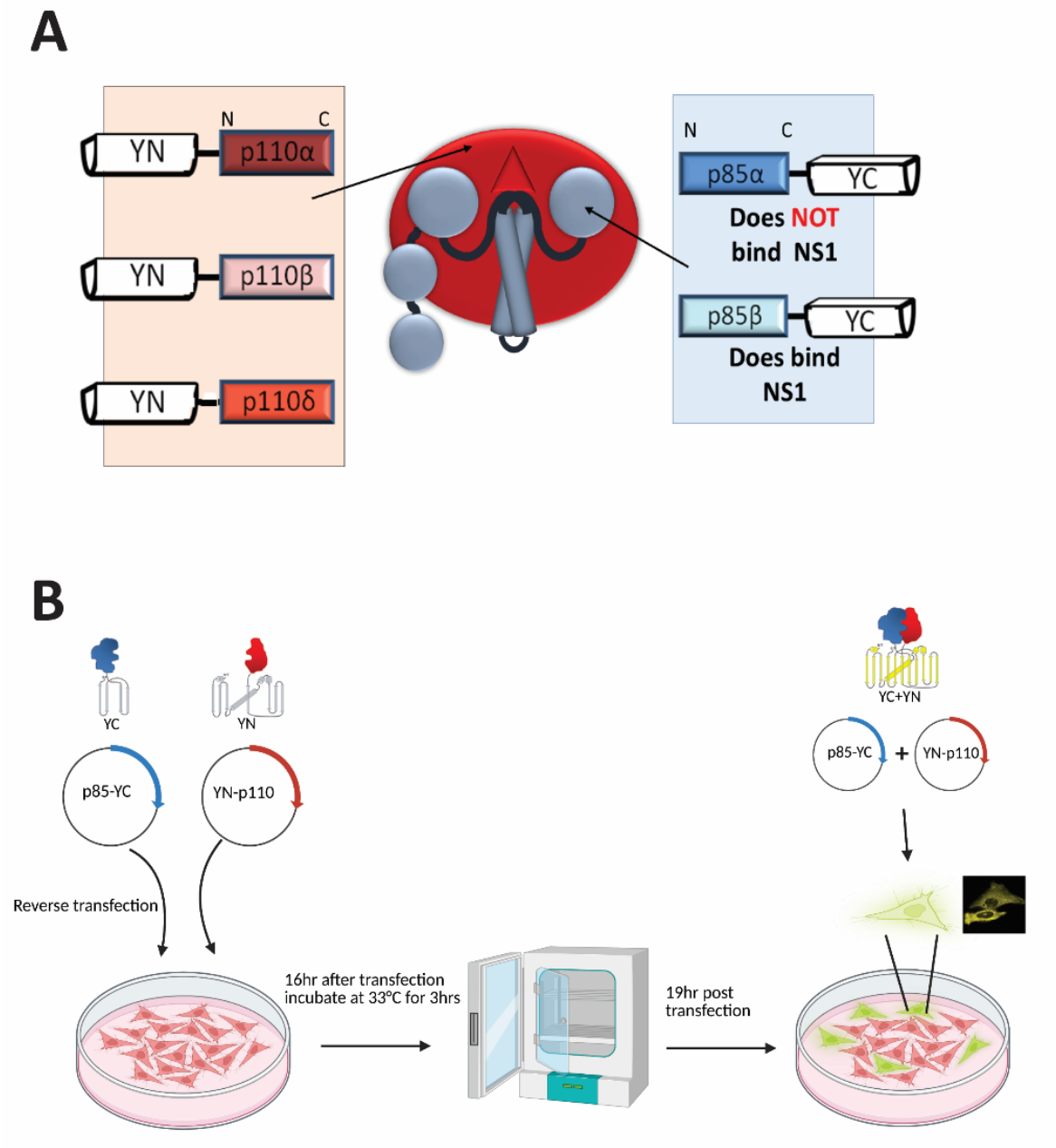

Figure 23. Split YFP system to study specific PI3K heterodimers.
A) A schematic representation of the BiFC system to study the interaction of the catalytic and regulatory subunits of PI3K. N-terminal (YN) and C-terminal (YC) parts of YFP were added to the N- or C-terminus of p110 or p85, respectively.

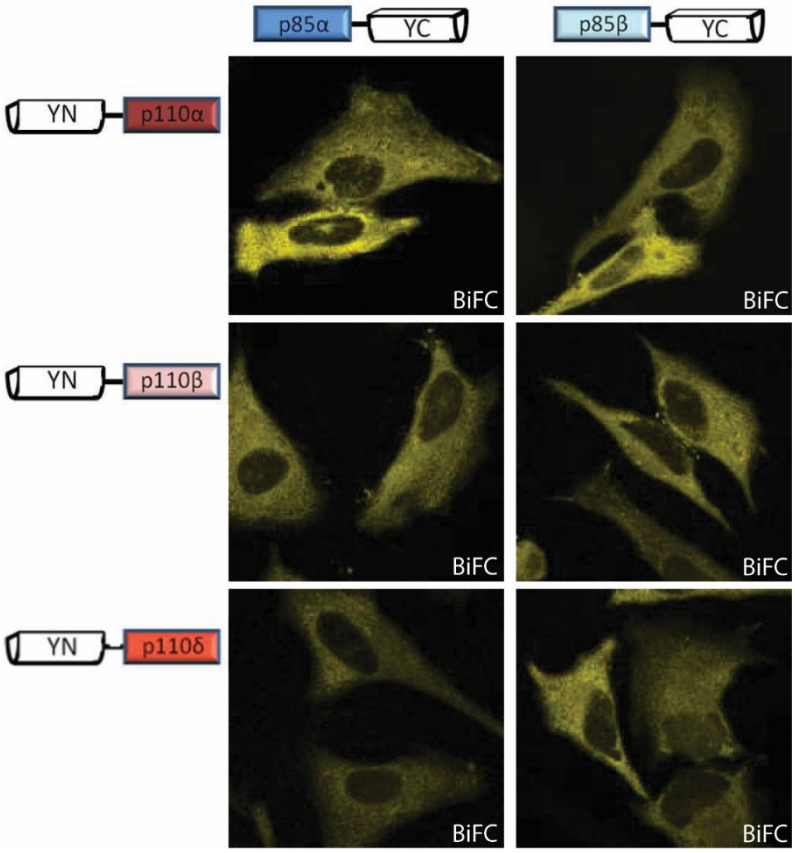

Figure 24. BiFC system tested with different combinations of PI3K isoforms.
HeLa cells were transfected with the different BiFC combinations and processed 19 hr p.t. for fluorescence microscopy. All the heterotypic dimers showed a broad diffused distribution.

4.2 Influenza A virus NS1 relocalizes PI3K complexes in an isoform-specific manner

Then, we assessed changes to these localizations upon co-transfection with the NS1 protein from influenza A/Puerto Rico/8/34 virus (PR8, **Figure 25A**). The presence of NS1 did not affect p85α heterodimers, consistent with the inability of NS1 to bind this specific isoform (61). On the other hand, NS1 expression resulted in a remarkable redistribution of the p85β-containing heterodimers. The redistribution of PI3K in the cytoplasm of NS1-expressing cells from a diffuse to a punctate pattern was different according to the p110 isoform present: those with p110α and p110δ showed accumulation at the edges of the cells, while those with p110β were relocated to a punctate phenotype close to the nucleus. To confirm that these changes were specifically due to

the NS1-p85β interaction, we also co-transfected the PI3K BiFC heterodimers with PR8 NS1 carrying the Y89F mutation, which has previously been shown to abrogate NS1 binding to p85β (10, 61). As expected, NS1-Y89F failed to relocate the different PI3K heterodimers (**Figure 25B**), which remained in the same diffuse cytoplasmic distributions as without any NS1 present.
We quantified the number of cells that were positive for their respective phenotype based on the different PI3K heterodimers being expressed with NS1. We observed that at least 80% of the cells expressing the PI3K BiFC with NS1 displayed either the accumulation at the cell edges (p110α and p110δ) or the punctate close to the nucleus (p110β) (**Figure 26**). We further corroborated the ability of NS1 to bind to a dimer of p85β including any of the three catalytic p110 subunits by co-immunoprecipitation assays. We co-transfected 293T cells with plasmids expressing V5-GST, V5-NS1 wt, or V5-NS1 Y89F, together with Flag-p85α or p85β with each of the p110 isoforms (YN-p110α/β/δ). We confirmed the preferential binding of NS1 to p85β over p85α (**Figure 27A**) as well as the successful precipitation of all the dimer combinations with p85β and each of the different p110 (**Figure 27B**).

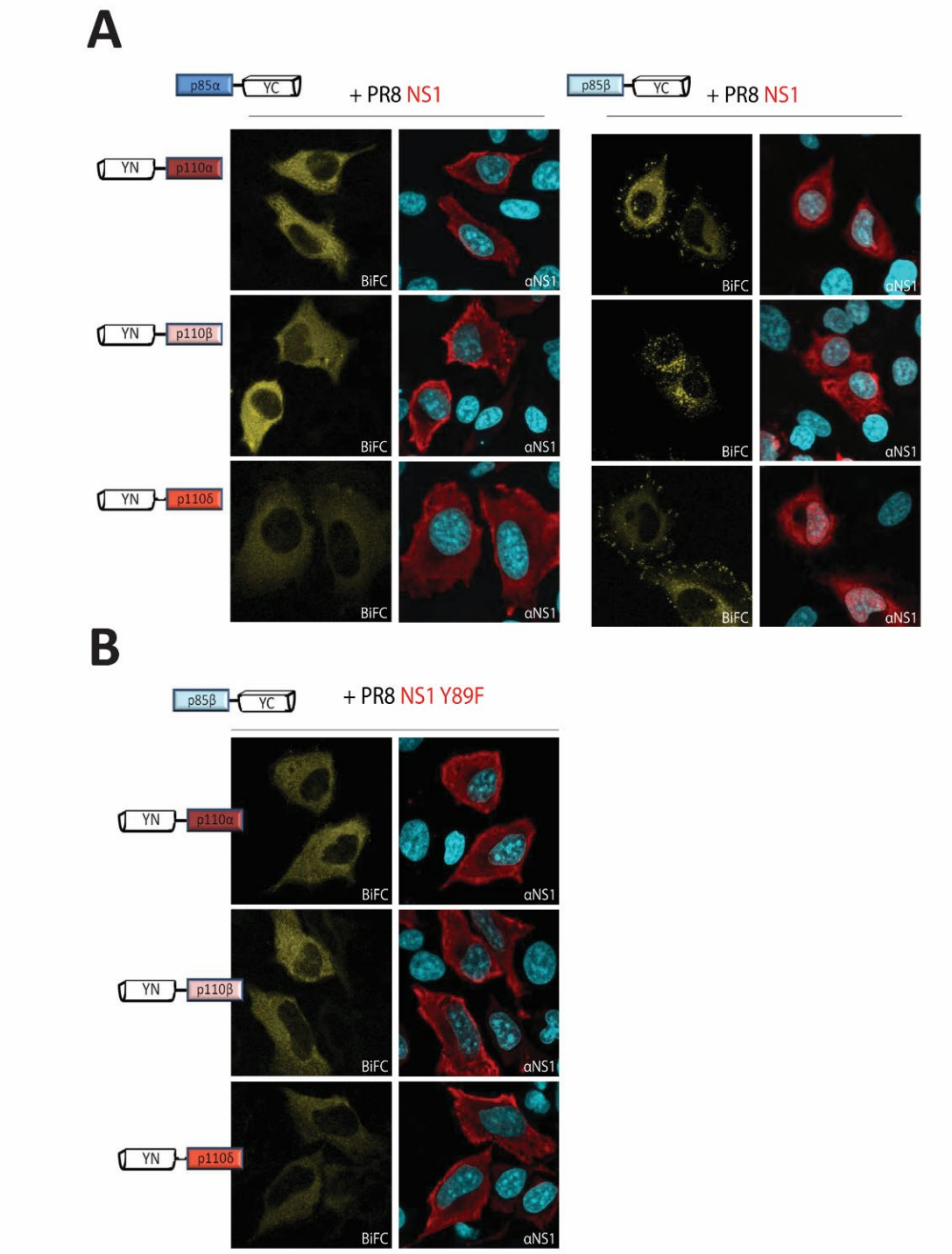

Figure 25. PI3K BiFC complexes with NS1.
A) When co-transfected with NS1, heterodimers containing p85β, but not p85α, were relocated to cell edges (p110α and p110δ) or acquired a punctate localization near the nucleus (p110β). B) None of these phenotypes were observed after co-transfection with an NS1 mutant unable to bind p85β (Y89F substitution). (NS1: red, nucleus: cyan, BiFC: yellow).

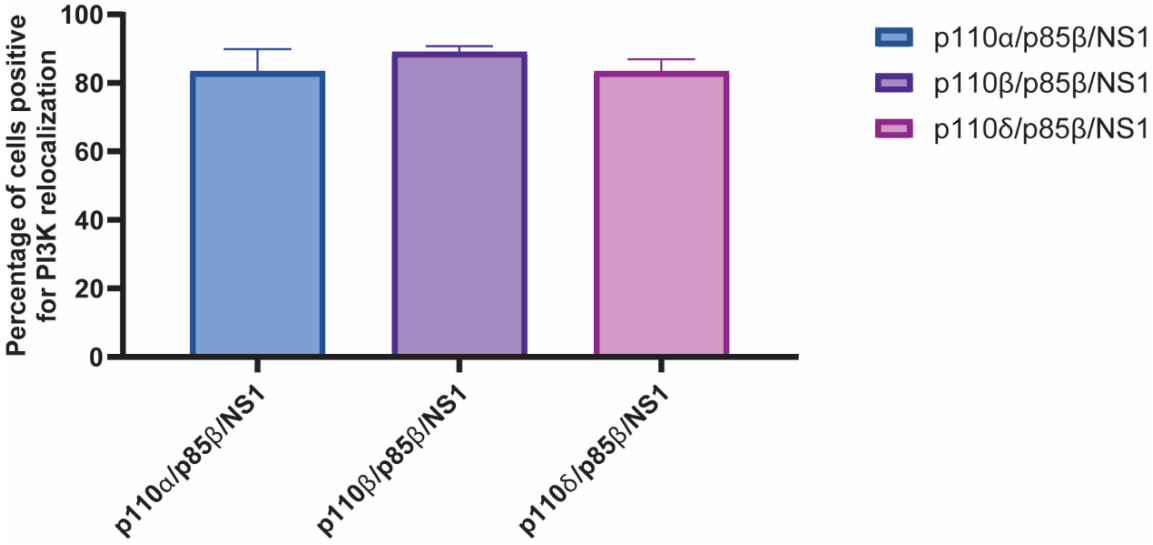

Figure 26. Quantification of the different relocalization pattern of PI3K BiFC.
When cells expressing the different heterodimers with NS1 were quantified, 80% of cells expressing PI3K complexes and NS1 showed a relocalization phenotype. (n = 30 cells/condition, and triplicates, error bars represent standard deviation).

4.3 PI3K complexes have a distinct distribution pattern upon infection with influenza virus

Next, we tested if the distinct distribution of the PI3K heterodimers also occurred when cells were infected with influenza virus. In order to establish the settings for visualizing our BiFC complexes after infection, we first expressed p110α/p85β complexes and infected with rPR8 WT or rPR8-Y89F at a multiplicity of infection (MOI) of 10 PFU/cell and performed immunofluorescence at 3, 6, 16 (incubated at 37°C) and 24 hrs post infection (incubated at 33°C). We observed the presence of relocalized BiFC complexes starting at 3hrs, however, the phenotype was much more evident at later time points (**Figure 28**). We next expressed the indicated BiFC complexes and then infected the cells with rPR8 WT or rPR8-Y89F at a MOI of 10 PFU/cell and as predicted the BiFC complexes relocated to the cell edges for p110α and p110δ combinations when infected with rPR8 WT and closer to the nucleus for p110β. The complexes were in a diffuse, homogenous distribution when infected with rPR8-Y89F, similar to the mock infected cells and this was consistently observed whether the cells were incubated at 33°C or 37°C after infection (**Figure 29**).

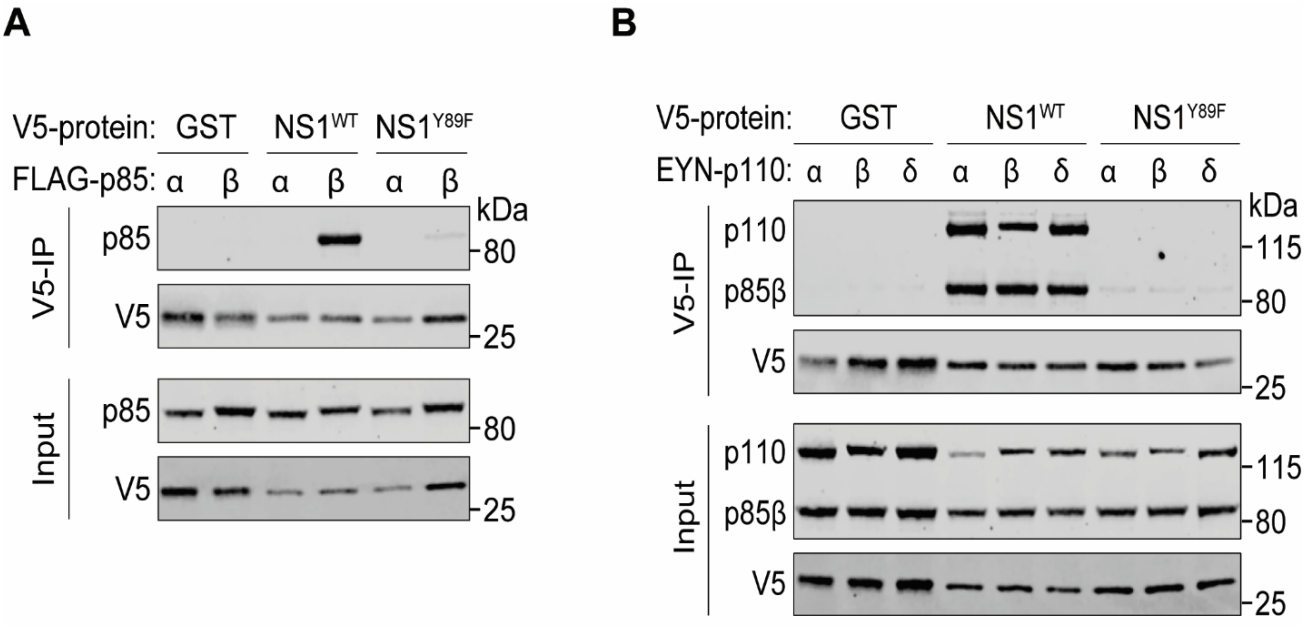

Figure 27. NS1 binds to p85β-p110 dimers with no preference for a specific catalytic subunit.
(A) Assessment of binding of NS1 to p85 subunits using 293T cells co-transfected for 48 h with plasmids expressing the indicated V5-tagged NS1 protein (or GST) and FLAG-tagged p85α or p85β. NS1 preferentially binds to p85β only. (B) 293T cells were co-transfected with plasmids expressing the indicated V5-tagged NS1 protein (or GST), FLAG-tagged p85β and YN-tagged p110α or p110β or p110δ catalytic subunit and cell lysates were co-immunoprecipated with V5 antibody and analyzed by SDS-Page and western blotting (soluble (input) and pulldown (V5-IP)). We detected that NS1 binds to all the p85β-p110x dimers with no preference for a specific catalytic subunit.

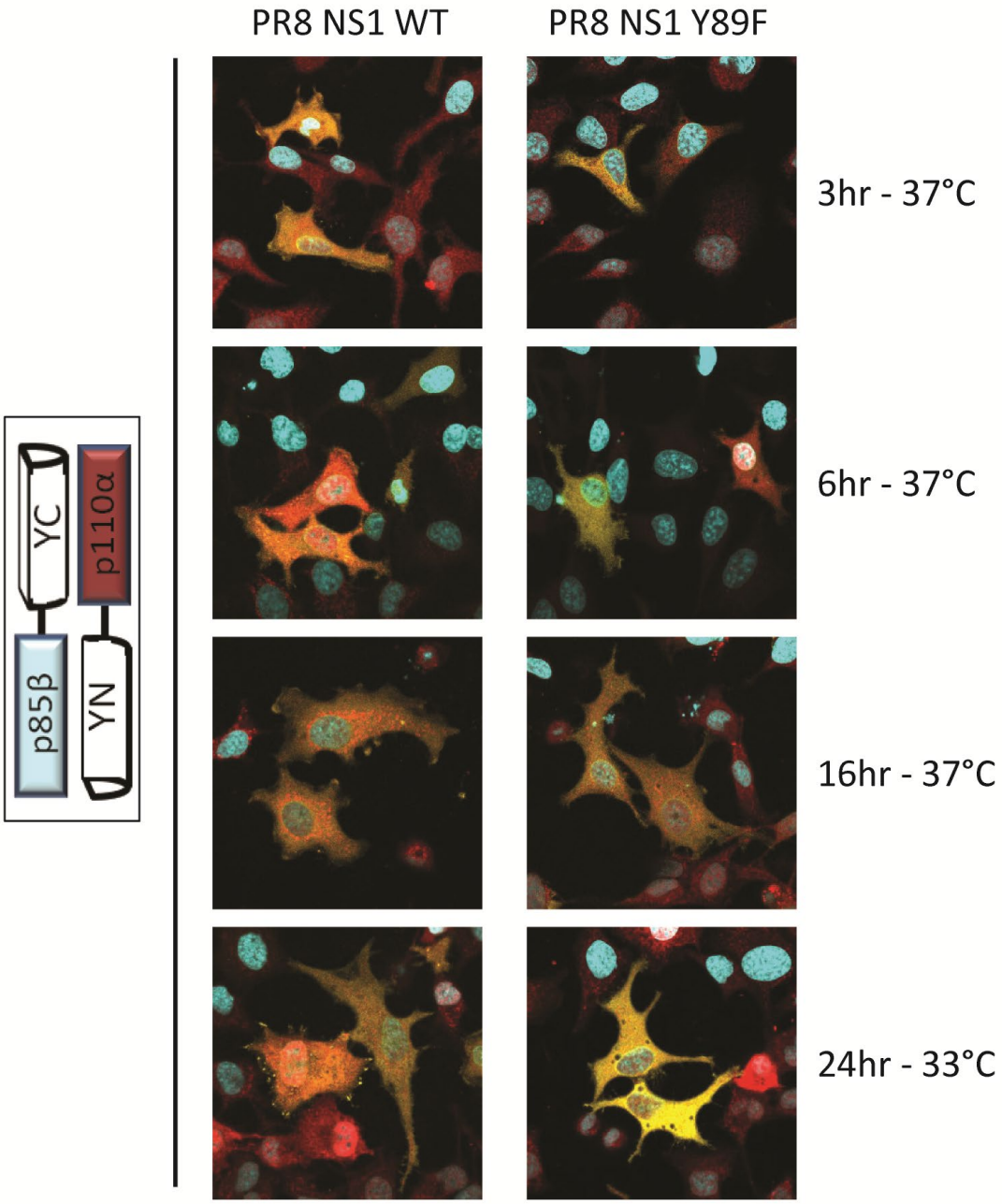

Figure 28. Infection optimization for BiFC PI3K complexes.
HeLa cells were co-transfected with p110α/p85β BiFC complex and 19 hr p.t. cells were infected with an MOI of 10 PFU/cell. 3, 6, 16, and 24 hrs post infection cells were processed for fluorescence microscopy. The 3, 6 and 16 hr samples were incubated at 37°C while the 24hr samples were incubated at 33°C. Cells infected with rPR8 WT led to the distinct relocalization pattern of the PI3K heterodimers but with rPR8-Y89F the complexes were in a homogeneous distribution similar to the mock infected cells. The relocalization pattern is clearer at later time points in comparison to earlier time points. (BiFC in yellow, NS1 in red and nucleus in cyan).

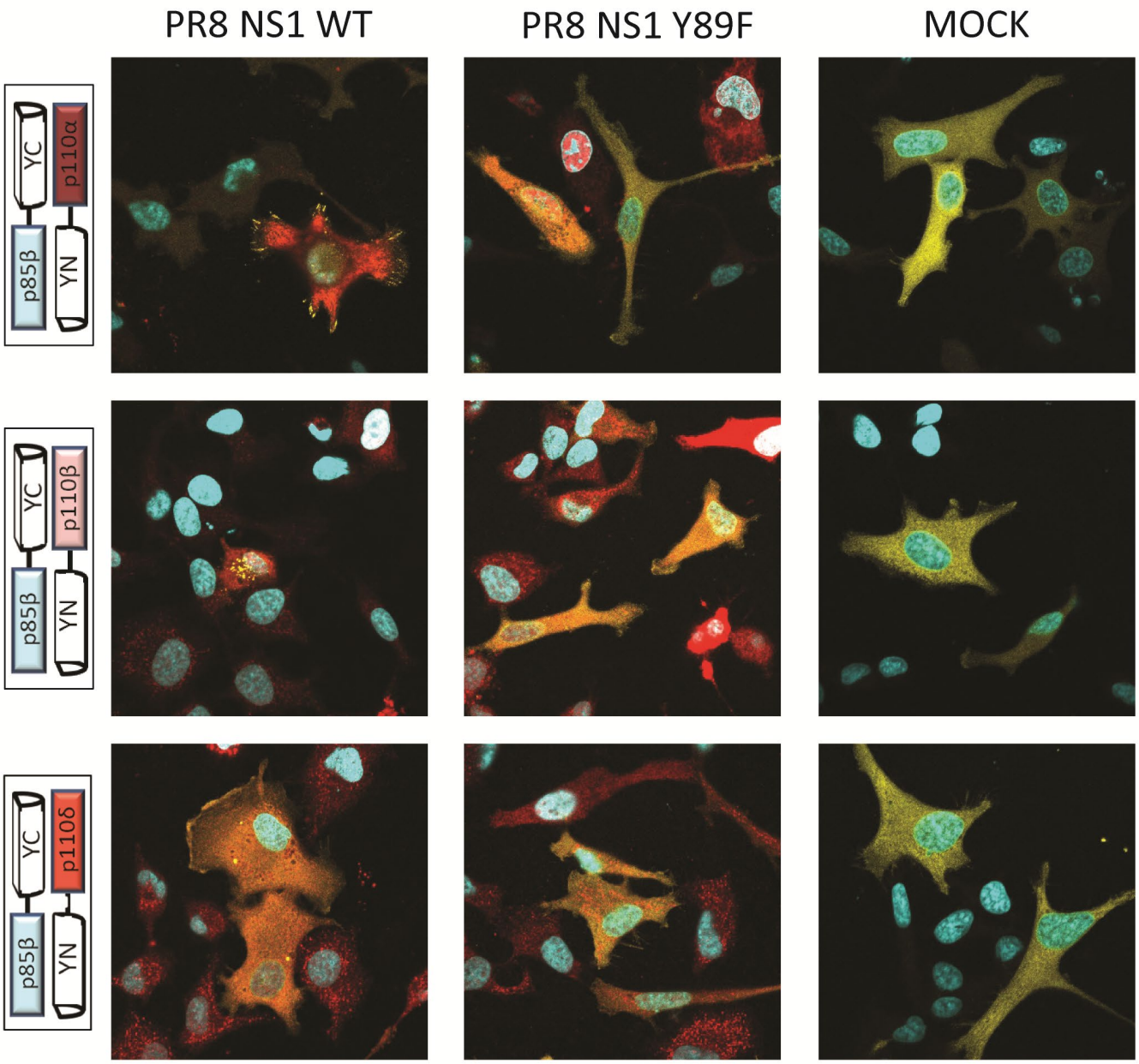
PR8 NS1 WT
PR8 NS1 Y89F
MOCK
YC
p110α
p85β
YN
YC
p110β
p85β
YN
YC
p110δ
p85β
YN

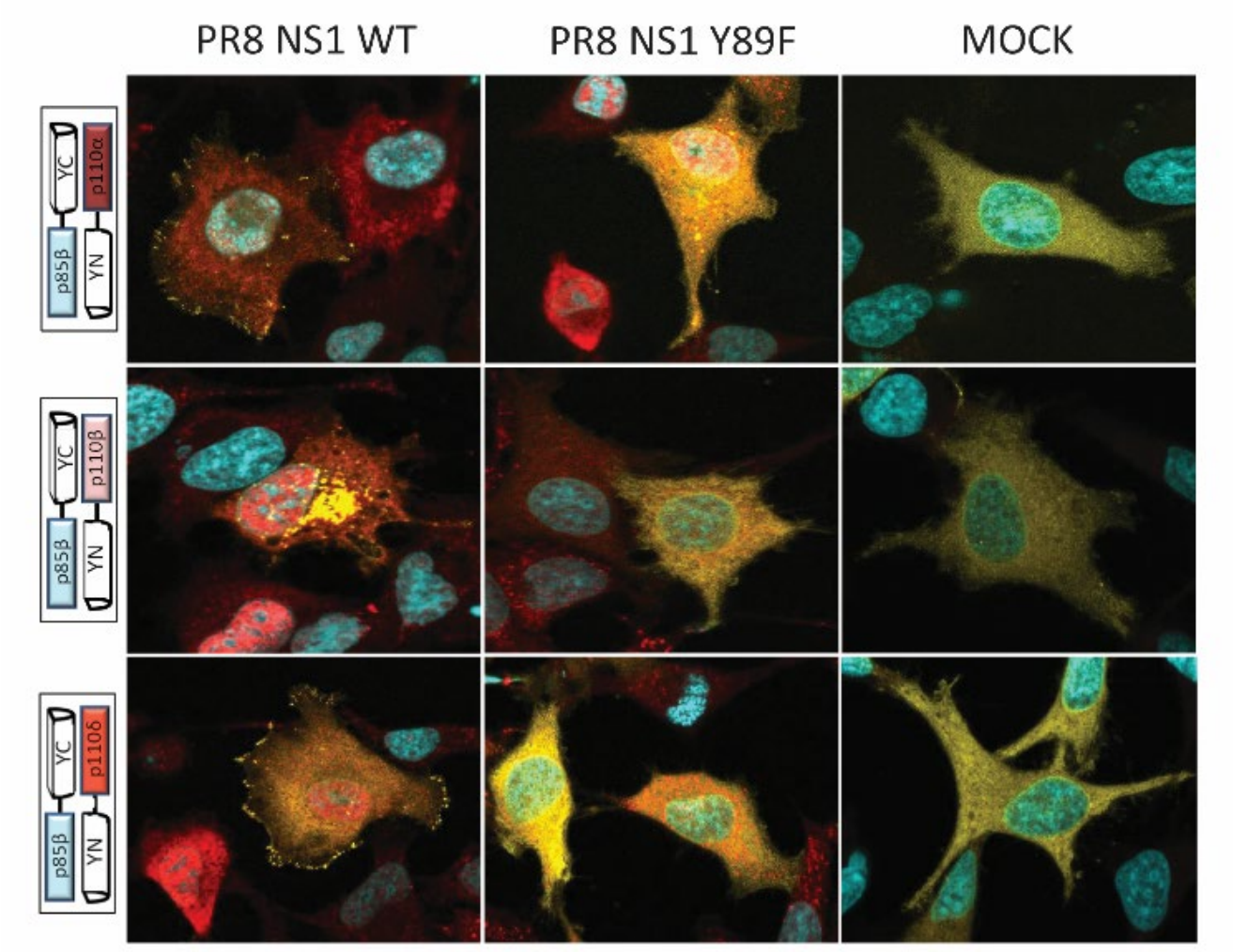

Figure 29. Relocalization of BiFC PI3K heterodimers by infection.
HeLa cells were co-transfected with different BiFC complexes and 19 hr p.t. cells were infected with an MOI of 10 PFU/cell. 24 hrs post infection ((A)incubated at 37°C (B) incubated at 33°C) they were processed for fluorescence microscopy. Cells infected with rPR8 WT led to the distinct relocalization pattern of the PI3K heterodimers but with rPR8-Y89F the complexes were in a homogeneous distribution similar to the mock infected cells. (BiFC in yellow, NS1 in red and nucleus in cyan).

4.4 NS1 drives PI3K heterodimer relocalization in a strain-independent manner.

In order to evaluate whether the NS1-mediated relocalization of PI3K complexes is strain specific, we expressed NS1 proteins from H1 (A/Puerto Rico/8/1934, A/Brevig Mission/1/1918, A/Wilson-Smith/1933, A/California/04/2009), H3 (A/Wyoming/03/2003), and H5 (A/Hong Kong/156/1997, A/Vietnam/1203/2004) subtypes. All different NS1s promoted similar relocalizations of the PI3K heterodimers, indicating that this phenomenon is not strain specific (**Figure 30**), although in the multifactorial context of an infection this might result in different functional phenotypes, as we have previously shown (10).

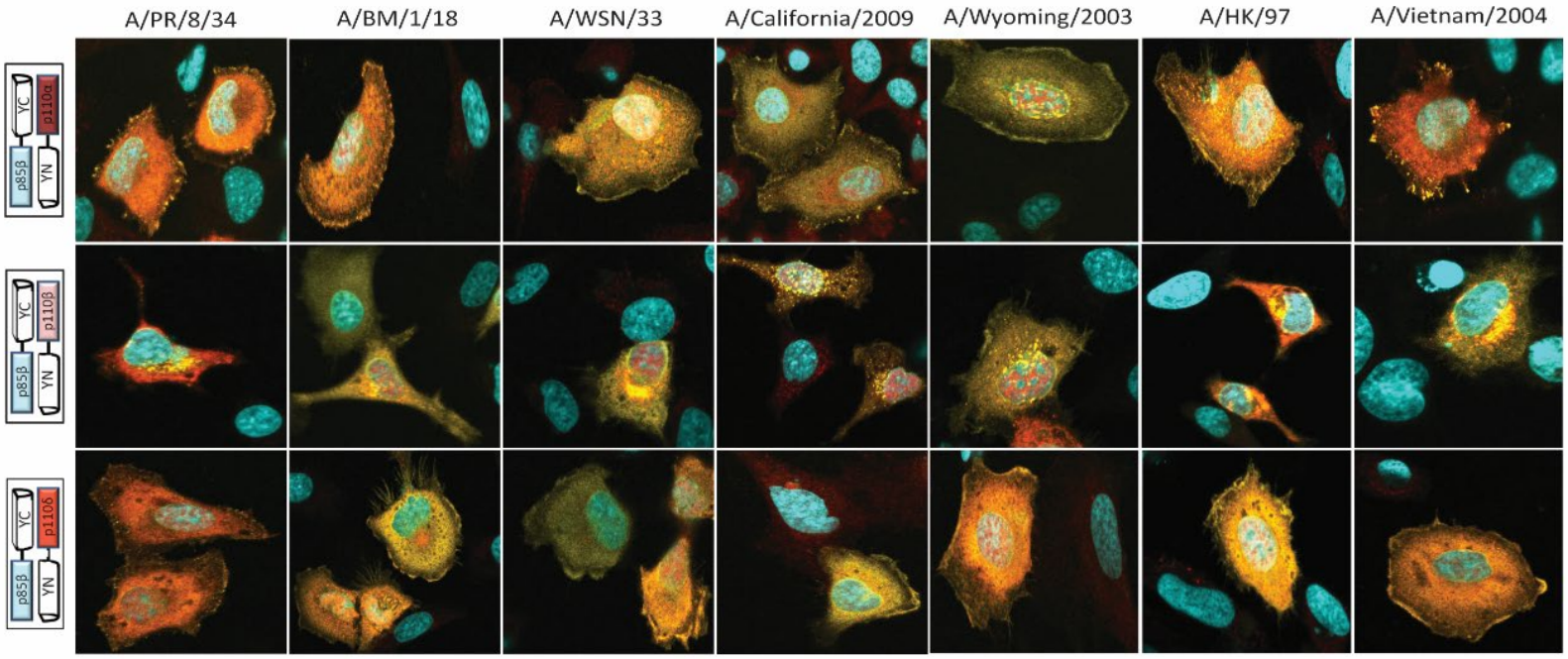

Figure 30. Distinct redistribution of PI3K heterodimers is not strain dependent.
HeLa cells were co-transfected with indicated BiFC constructs and NS1 from different strains. At 19 hr p.t., cells were processed for immunofluorescence with antibody against NS1 (1A7). NS1 from different influenza A strains were able to relocalize the complexes with p110α and p110β to the focal adhesion regions and the complexes with p110β near the endosome in a strain independent manner. (BiFC in yellow, NS1 in red and nucleus in cyan).

4.5 Monomeric effector domain of NS1 is sufficient to redistribute the PI3K complexes.

Structural and biochemical studies have revealed that the NS1 effector domain (ED) located at its carboxy-terminal end is sufficient to bind the inter-SH2 domain of p85β, and does not require dimerization (60, 62). To ascertain whether this NS1 domain has the same impact on PI3K relocalization as the entire NS1, we expressed the NS1 ED on its own, without the N-terminal RNA-binding domain (62), and carrying a known mutation (W187A) to prevent its dimerization (11, 59, 83), in the presence of our diverse PI3K BiFC complexes. As shown in **Figure 31**, we observed that the expression of the NS1 ED induced the same isoform dependent redistribution of the PI3K complexes as full-length NS1, confirming that just binding of p85β to NS1 is enough for isoform-specific PI3K relocalization.

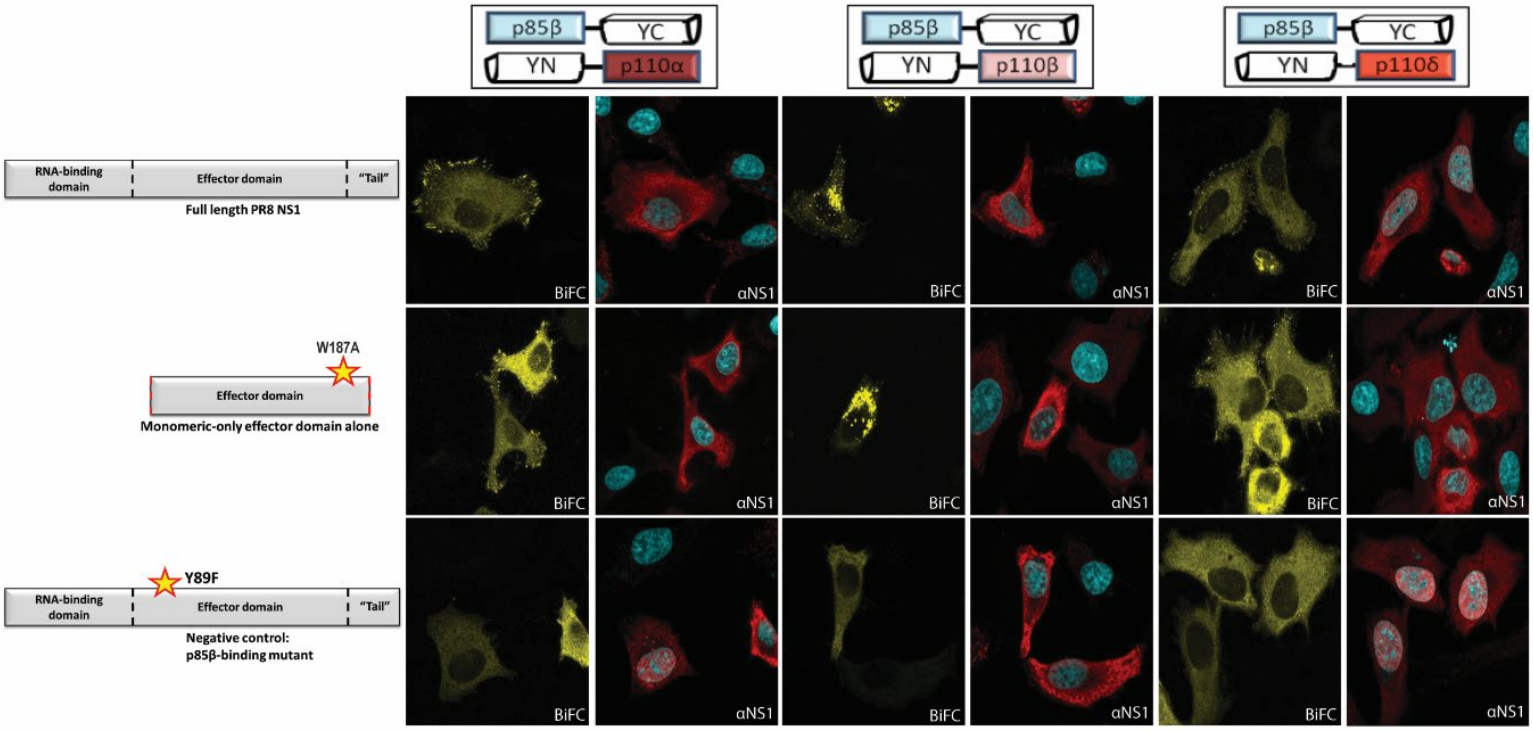

Figure 31. Relocalization of PI3K BiFC with effector domain of NS1.
HeLa cells were transfected with the different PI3K complexes and monomeric effector domain of NS1, NS1 full length and mutant NS1. The monomeric effector domain of NS1 (NS1 ED with W187A) is sufficient to induce the same PI3K heterodimer relocalizations as full length NS1, NS1-Y89F was used as a negative control. (NS1: red, nucleus: cyan, BiFC: yellow).

4.6 Influenza A virus NS1 relocalizes PI3K complexes in proximity to focal adhesions or to endosomes depending on the p110 isoform.

Next, we tried to spatially characterize the different isoform-dependent PI3K redistributions. In order to do that, we co-transfected HeLa cells with the various PI3K-NS1 BiFC combinations in the presence of NS1, and used different cell markers to identify potential colocalization. For p85β/p110α and p85β/p110δ complexes, their localization in the presence of NS1 resembled focal adhesions (174), plasma membrane-associated macromolecular assemblies that serve as sites for sensing and transducing extracellular cues, and therefore we co-expressed our BiFC system together with a focal adhesion marker. For this purpose, we expressed RFP-tagged zyxin, a phosphoprotein that is concentrated at focal adhesions (14) (**Figure 32A and B**). We noted that the expression of zyxin mirrors the pattern we detected with the NS1-relocated PI3K BiFC complexes, and is in high proximity with these complexes. Similarly, we presumed that the distinct p85β/p110β dots we observed in the presence of NS1 could correspond with an endosomal compartment. To test this theory, we co-transfected our BiFC system with NS1 together with the early endosome marker Rab5 fused to RFP (77, 154, 173), and found that indeed the distribution pattern of this NS1-relocated PI3K complex coincides with the distribution of Rab5 (**Figure 32C**). These results indicate that in the presence of NS1, p85β/p110β heterodimers are directed towards early endosomes while p85β/p110α and p85β/p110δ are directed towards focal adhesion regions. Given that the NS1-p85β remains constant in all these scenarios, our data reveal that it is the p110 subunit that determines heterodimer intracellular localization. It should be noted that only a small fraction of the NS1 co-localizes with the PI3K BiFC complexes, as expected for this multi-functional protein that in addition to bind to p85β also associates with several other host factors.

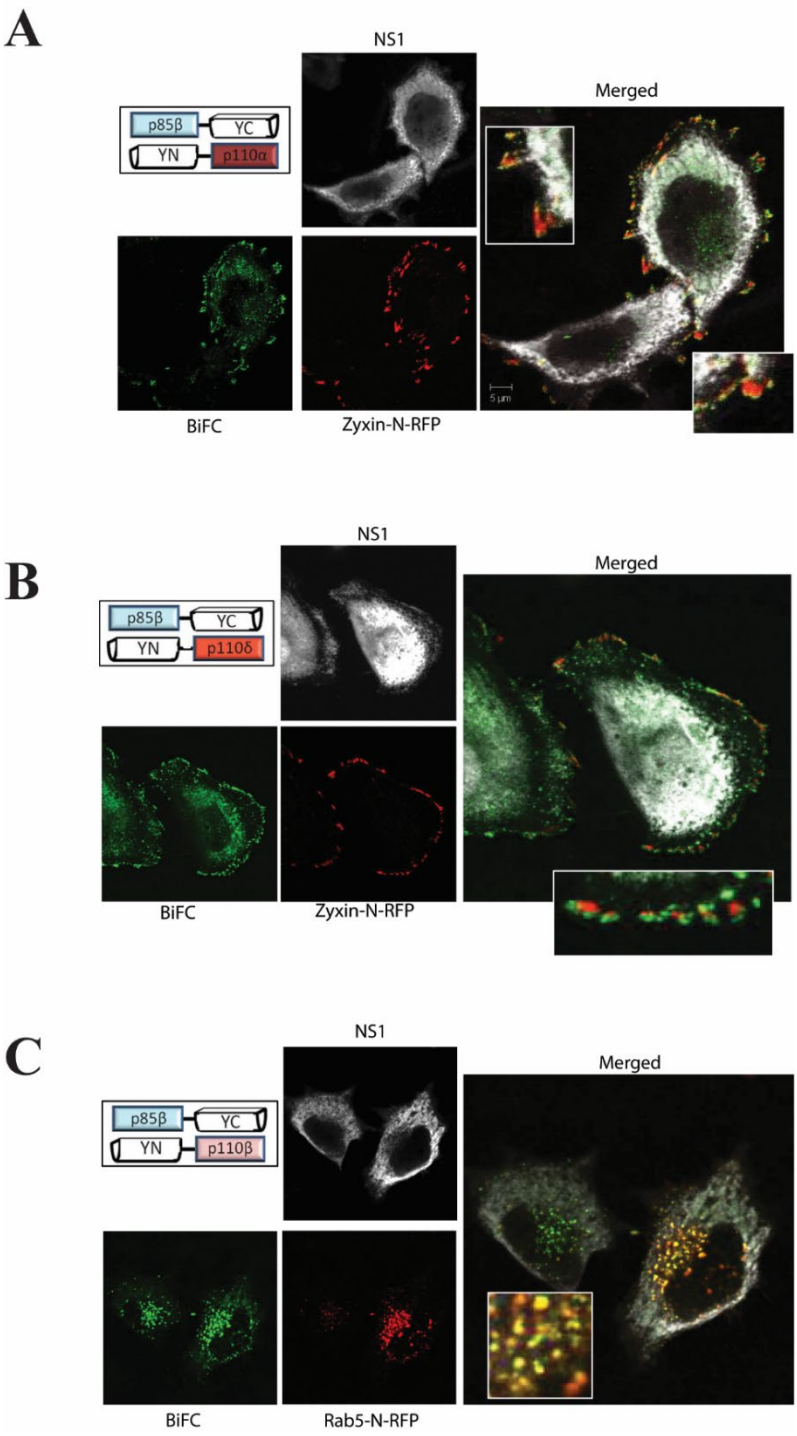

Figure 32. Colocalization of redistributed PI3K complexes with different cellular markers.
HeLa cells were co-transfected with the indicated BiFC constructs, RFP-tagged markers for different cellular compartments and wild type NS1. Cells were processed for confocal microscopy at 19 hr p.t. Cell edge phenotype associated with p110α and p110δ appeared to localize in close proximity to the focal adhesion marker, zyxin (A, B), whereas BiFC complexes with p110β colocalized with the early-endosome-associated small GTPase Rab5 (C). (Green: BiFC, red: Rab5-RFP or Zyxin1-RFP; white on merged pictures: NS1).

4.7 Kinase activity of the isoform-specific PI3K complexes in the presence of NS1

Next, we characterized the functionality of these PI3K complexes within the different relocalization patterns. The canonical signaling of active PI3K is based on the phosphorylation of PIP_2, resulting in the generation of PIP_3, which diffuses and promotes downstream activation and phosphorylation of Akt. Therefore, we expressed p85β in combination with the different isoforms of p110, as well as NS1, and detected the production of PIP_3 by indirect immunofluorescence (**Figure 33A**). We observed production of PIP_3 at the cell periphery when p85β was in complex with p110α and p110δ in the presence of NS1, concomitant with its relocalization to focal adhesions at the cell periphery. However, we were unable to visualize using this technique the production of PIP_3 when NS1 was coexpressed with p110β-containing PI3K heterodimers. In order to confirm that the catalytic activity of each p110 was necessary for the NS1-mediated activation of the PI3K complexes, we treated our PI3K-BiFC/NS1 expressing cells with a PI3K inhibitor (wortmannin, which targets p110) and discerned that the distinct relocalizations of PI3K complexes were still taking place, but that there was no production of PIP_3 (**Figure 33B**).

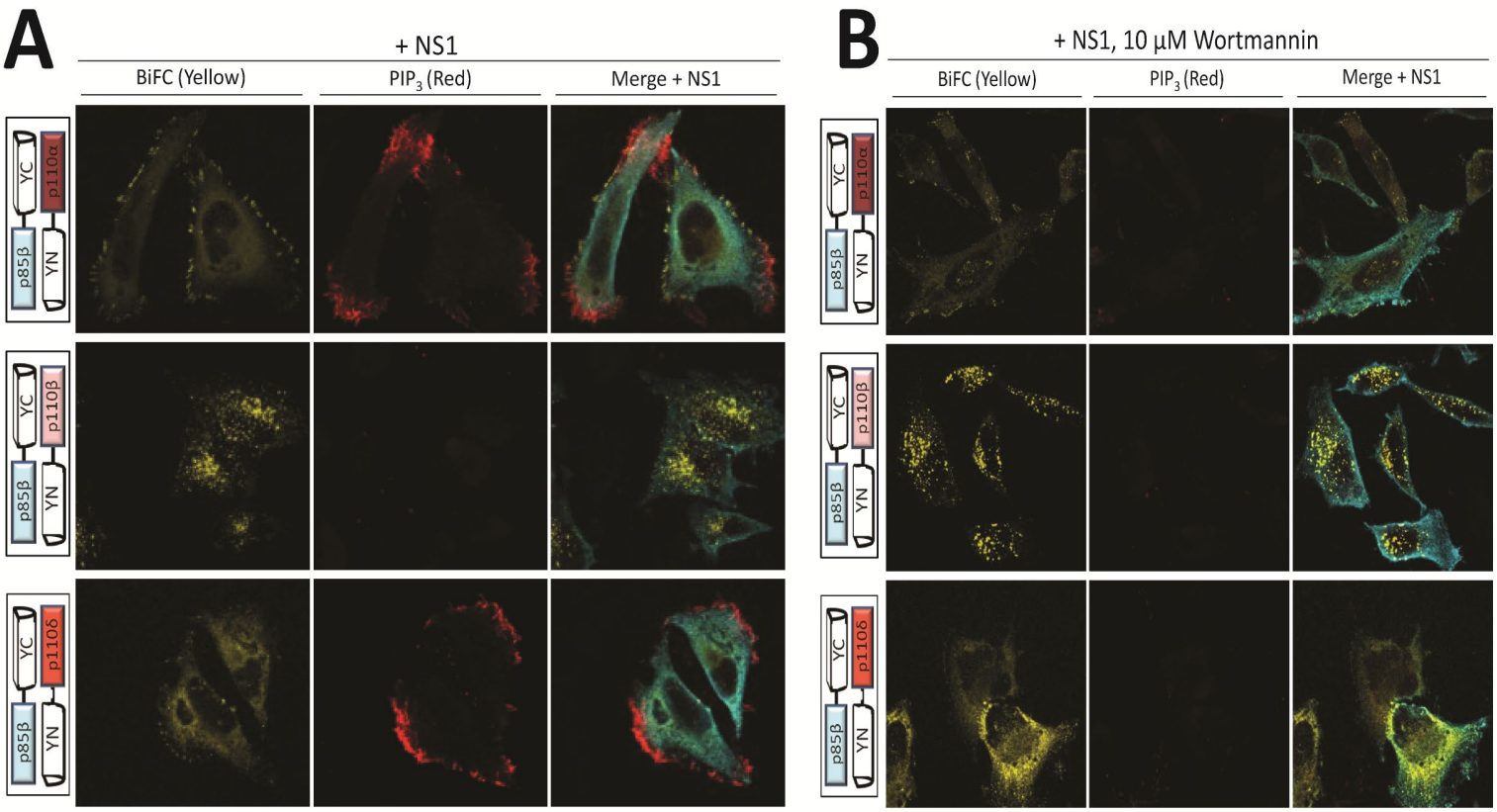

Figure 33. Differential catalytic activity of redistributed PI3K complexes.
HeLa cells were co-transfected with the indicated BiFC constructs and wild type NS1. At 19 hr p.t., cells were processed for immunofluorescence with antibodies against NS1(blue) and (A) PIP3(red). Markedly increased levels of PIP_3 could be appreciated in cells transfected with p110α/δ complexes, but not with p110β. Incubation with the pan-PI3K inhibitor wortmannin abrogated the production of PIP_3, but not the redistribution of the PI3K complexes by NS1 (B). (BiFC in yellow, PIP3 in red and NS1 in cyan).

We further characterized the differential kinase activities using biochemical methods and performed in vitro lipid kinase assays. We measured the turnover of adenosine triphosphate (ATP) in the presence of 5% PIP_2 vesicles by PI3K heterodimers and found that upon addition of NS1, only the activity of p110α/p85β complexes was significantly increased, while there was no significant difference in activity of p110β/p85β complexes or on the p110α/p85α complexes as expected **(Figure 34 A-B)**. The activation of p110α/p85β was dose-dependent on NS1 **(Figure 34C)**. Notably, when we assayed NS1-Y89F in this in vitro system, we did not observe significant activation of p110α/p85β complex (**Figure 34D**), complementary to the results observed in the cell based assay.

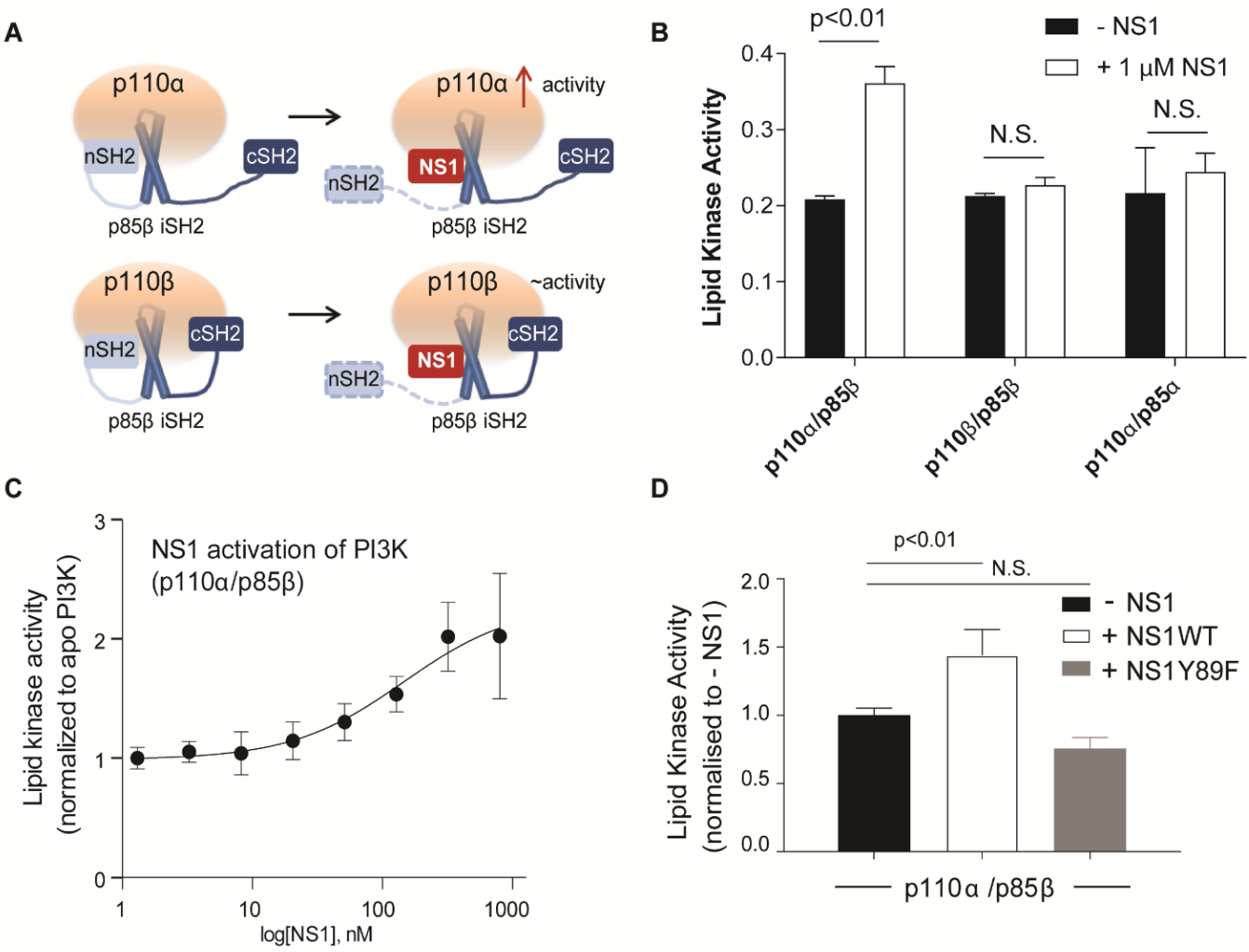

Figure 34. NS1 leads to activation of only p110α/p85β, with no significant activation of p110β/p85β. A) Schematic of NS1 activation of class IA PI3Ks. B) Relative activities of different combinations of catalytic and regulatory subunits of class IA PI3Ks in the presence and absence of 1 μM NS1. Assays measured the turnover of ATP in the presence of PI3K complexes at the following concentrations: 30 nM p110α/p85β, 300 nM p110β/p85β, and 60 nM p110α/p85α. Kinase assays contained 100 μM ATP, and 0.45 mg/ml vesicles containing [5% PIP2 /15% PC/20% PS/45% PE/10% cholesterol/5% sphingomyelin]. C) Dose response of p110α/p85β with increasing amounts of NS1 protein. D) Mutation of Y89F in NS1 prevents PI3K activation. Kinase assays were carried out under the same conditions as panel B, with both wild type and Y89F NS1 present at 1 μM. For all panels, assays were performed in triplicate (error shown as S.D., n = 3), with p values greater than 0.05 shown as not significant (N.S.).

Next, we determined where in the cell activation of Akt occurs in this system. We therefore probed for pAkt (Ser-473) in our BiFC assays by immunostaining with an antibody specific for pAkt. We indeed, detected elevated levels of pAkt in the presence of NS1, especially at the cell periphery with p85β/p110α and p85β/p110δ isoforms, but not with p85β/p110β (**Figure 35**). These

results indicate that p85β/p110α and p85β/p110δ are catalytically active after being bound and relocated by NS1, but that p85β/p110β catalytic activity is not detectable despite its relocalization in the presence of NS1.

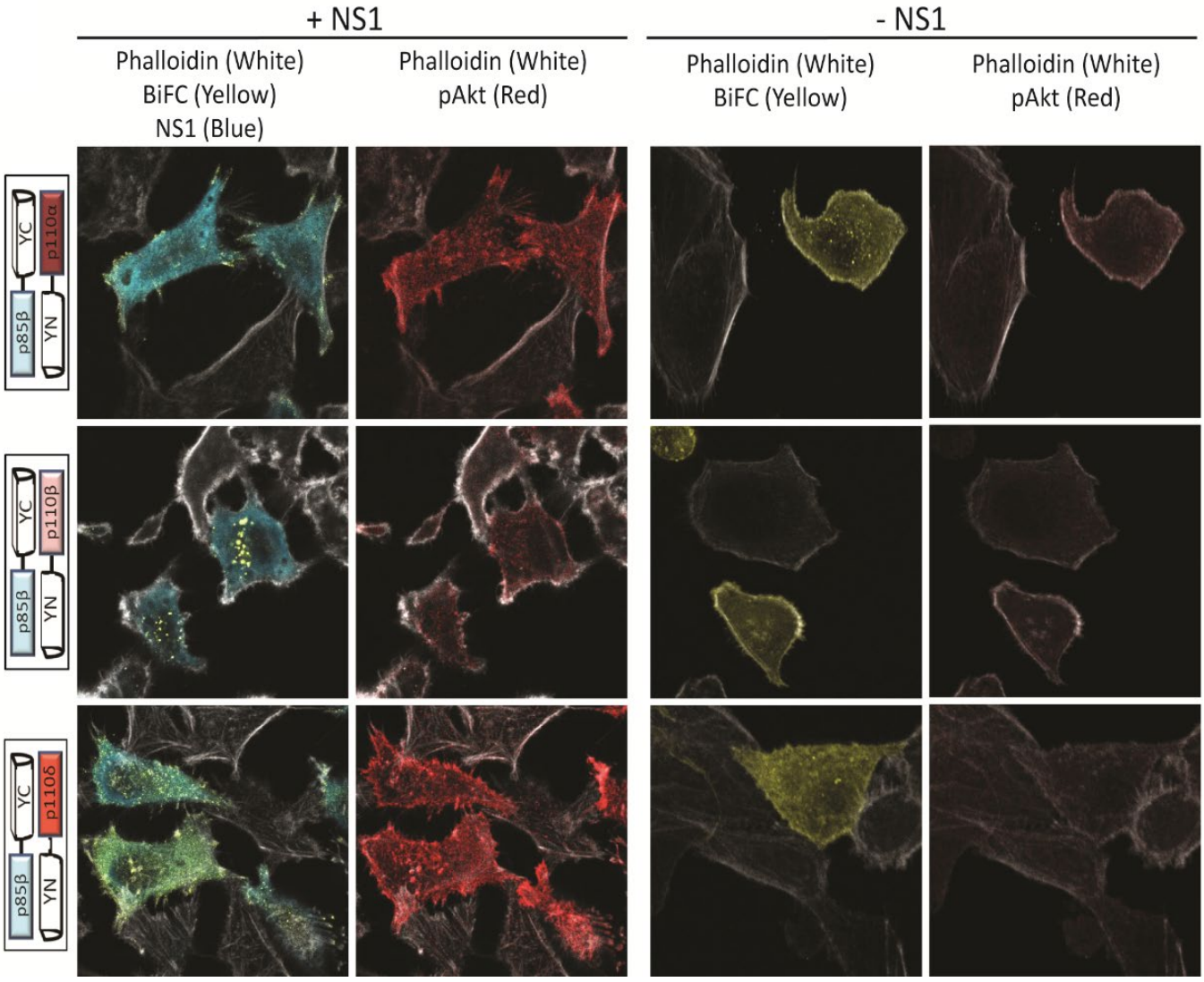

Figure 35. Isoform dependent production of pAkt in relocalized PI3K complexes.
HeLa cells were co-transfected with the indicated BiFC constructs and wild type NS1. At 19 hr p.t., cells were processed for immunofluorescence with antibodies against NS1(blue), pAkt(red) and phalloidin (white). Markedly increased levels of pAkt could be appreciated in cells transfected with p110α/δ complexes, but not with p110β.

4.8 An intact SH2 domain in p85β is required for NS1-mediated redistribution of PI3K complexes containing p110α and p110δ, but not p110β

Canonical activation of PI3K is triggered by p85 binding to phospho-tyrosine (pY) residues via one of its SH2 (Src homology 2) domains, thereby relieving its inhibition of p110. These pY residues are commonly found in the cytoplasmic tails of growth factor receptors which are phosphorylated upon recognition of external growth stimuli. We next investigated whether a functional p85β SH2 domain was required for NS1-mediated relocalization of the different PI3K complexes. For this purpose, we introduced R355A and R647A (RARA) mutations into p85β in order to disrupt the interaction of p85β with pY residues (138). We expressed p85β RARA in our BiFC system along with NS1, and noticed that the mutant p85β nullifies the redistribution of the p110α and p110δ complexes to focal adhesion regions in the presence of NS1. However, the RARA mutations had no effect on the redistribution of p110β-containing complexes with NS1 (**Figure 36**), indicating that there are different requirements for a functional SH2 domain of p85β for the NS1-mediated redistribution of PI3K complexes, and that these appear to be specific to the p110 isoform in the complex.

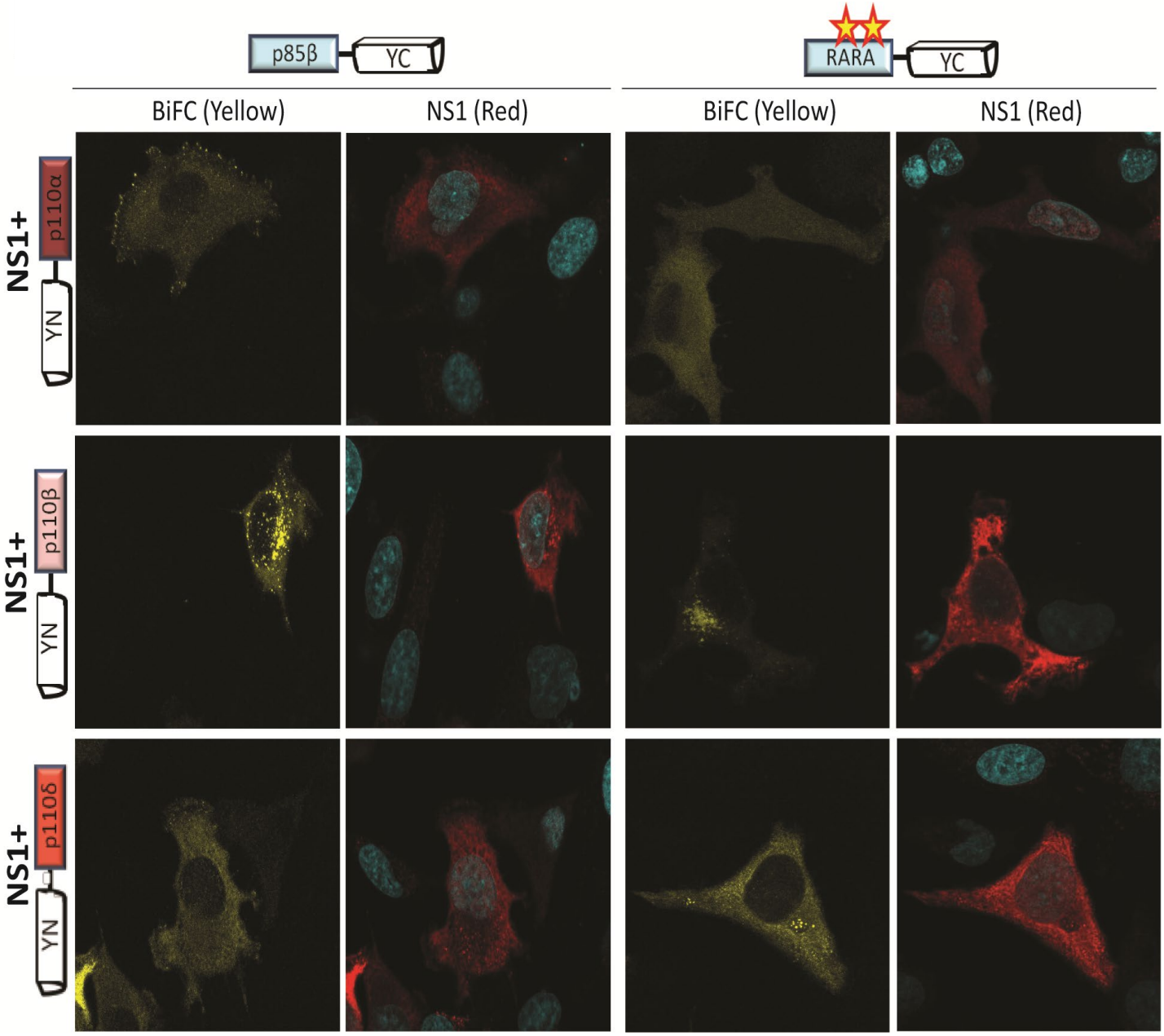

Figure 36. Phosphotyrosine binding is required for 110α and 110δ, but not 110β, BiFC phenotypes. When HeLa cells were co-transfected with NS1, YN-p110α, β or δ and either wild type p85β-YC or the double mutant p85β-YC R355A/R647A (RARA), accumulation of p110α/δ BiFC complexes in membrane focal adhesions was abolished, while it had no effect on the endosome-associated accumulation of p110β complexes. (BiFC in yellow, NS1 in red, and nucleus in cyan).

4.9 PI3K oncogenic mutations phenocopy the NS1-mediated relocalization of PI3K

We next investigated whether activation of PI3K complexes by other known cellular stimuli different to NS1 results in similar redistributions of PI3K in a p110-specific manner. We therefore tested a constitutively-active HRas with previously described point mutations that lead to activation of the PI3K pathway (HRas C12V and T40C) (166). We observed that there was an isoform-independent relocalization of the PI3K complexes to membrane regions in all the combinations tested, including with both p85α and p85β (**Figure 37**). In addition, we assessed the non-receptor tyrosine kinase Src in its constitutively active form (SrcY530F) and observed two distinct phenotypes that were isoform dependent. When we expressed SrcY530F together with p85α and any p110, we detected more membrane localization of the PI3K complexes, while similar complexes with p85β exhibited a more punctate distribution of PI3K near the nucleus and endosomal compartments (**Figure 38**). These relocalization phenotypes are strikingly divergent from what we have observed with NS1.

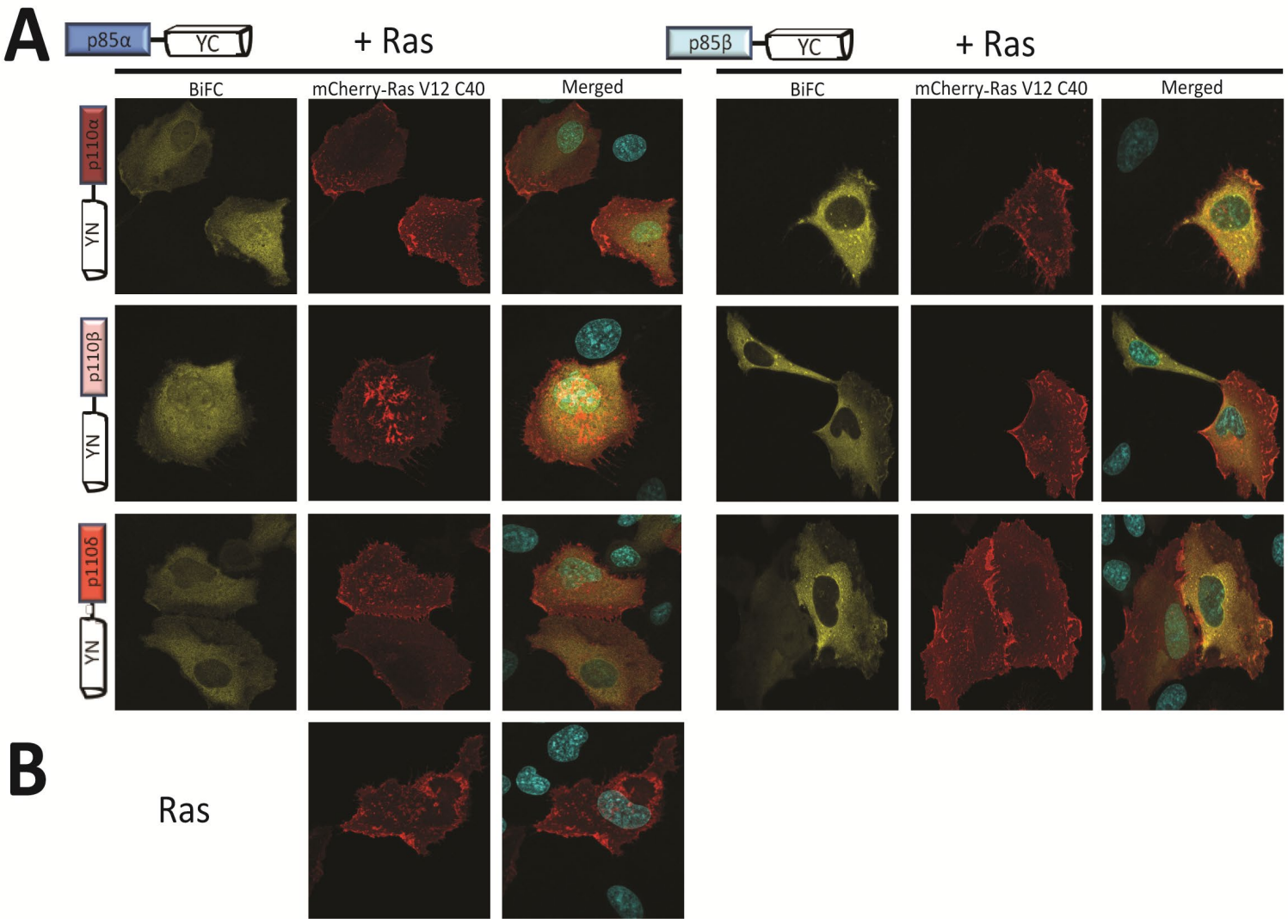

Figure 37. Relocalization of BiFC PI3K heterodimers by different cellular stimuli.
A) HeLa cells were co-transfected with the indicated BiFC constructs together with pCAGGS-mCherry-HRas V12 C40. The PI3K complexes relocalized to similar membrane regions with both p85α and p85β. B) Cells transfected with constitutively active Ras were used as controls. (BiFC in yellow, nucleus in cyan and Ras in red).

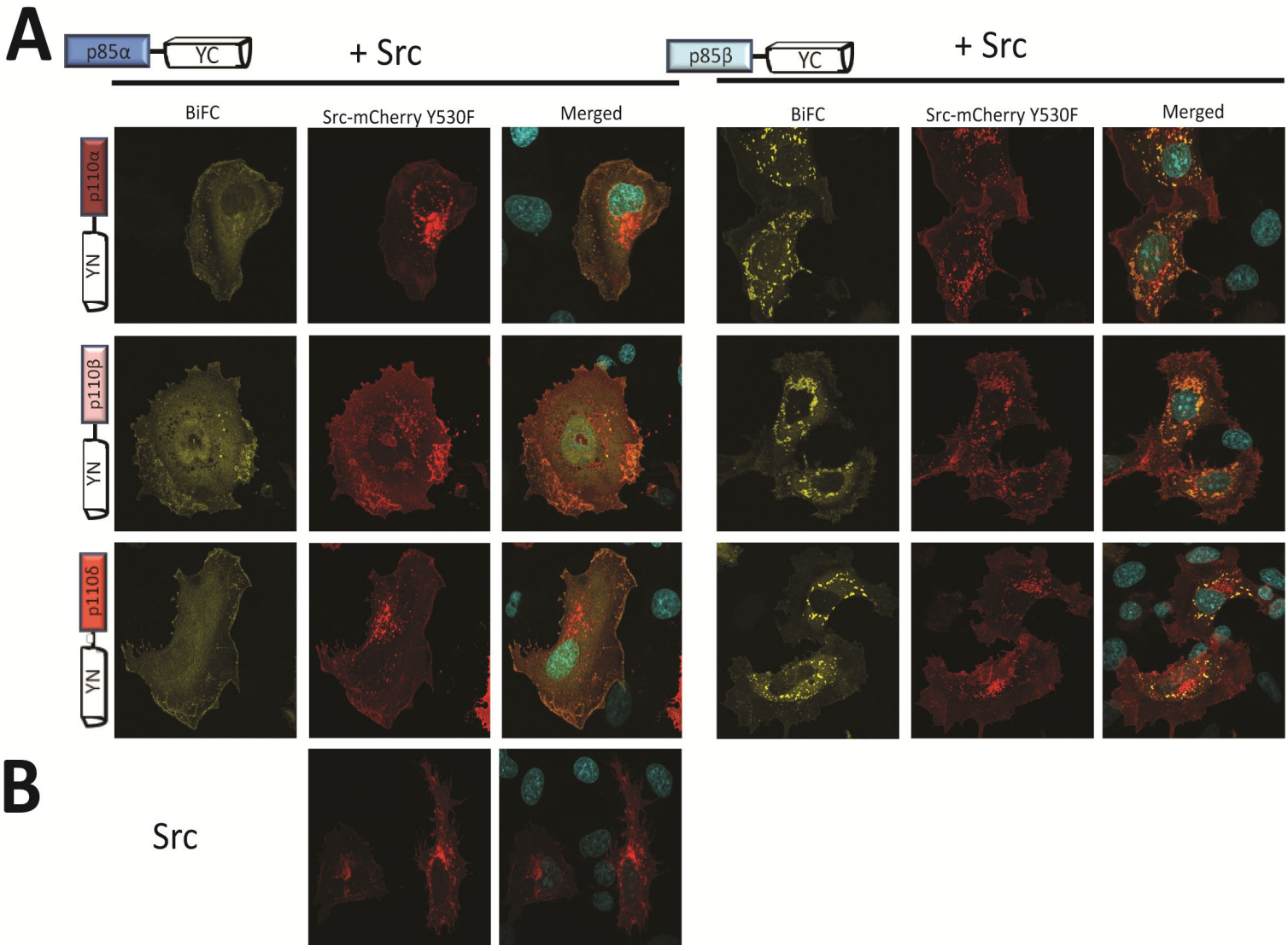

Figure 38. Relocalization of BiFC PI3K heterodimers by different cellular stimuli.
When HeLa cells were co-transfected with PI3K BiFC constructs together with pCAGGS-Src-mCherry Y530F (A), we observed an isoform dependent redistribution of the PI3K complexes. Complexes with p85α redistributed to the cell edges while complexes with p85β formed a punctate distribution near the nucleus. B) Cells transfected with constitutively active Src were used as controls. (BiFC in yellow, nucleus in cyan and Src in red).

There are well characterized mutations in both p110 and p85 subunits that have been shown to play a role in cellular transformation in human cancers. We therefore wondered whether NS1 activation could be reproducing these overactive pathway events. Consequently, we investigated whether PI3K oncogenic mutations could cause the same redistribution pattern of p85β/p110 complexes as with NS1. Substitution H1047R is one of the hot spot mutations found in the kinase domain of p110α (141, 172), and is known to increase lipid kinase activity and potently activate PI3K/Akt signaling (24). This mutation is frequently found in cancers such as colon, lung, breast, ovarian, endometrial and many more (99). We introduced the H1047R (24, 99, 141, 172) mutation into our p110α BiFC construct and then evaluated the intracellular localization of this mutant p110α in combination with p85α or p85β in the absence of NS1 (**Figure 39**). We found that this oncogenic p110α led to the same redistribution to focal adhesion regions as seen when the wild-type p110α:p85β complex was bound by NS1. However, the oncogenic p110α localization phenotype occurred case independently of the regulatory p85 subunit present. Since this mutation does not exactly replicate the activation we had seen with NS1, which is specific to p85β, we assessed whether another oncogenic mutation found in p85, and that could be applied to p85β, would better reflect NS1 action.

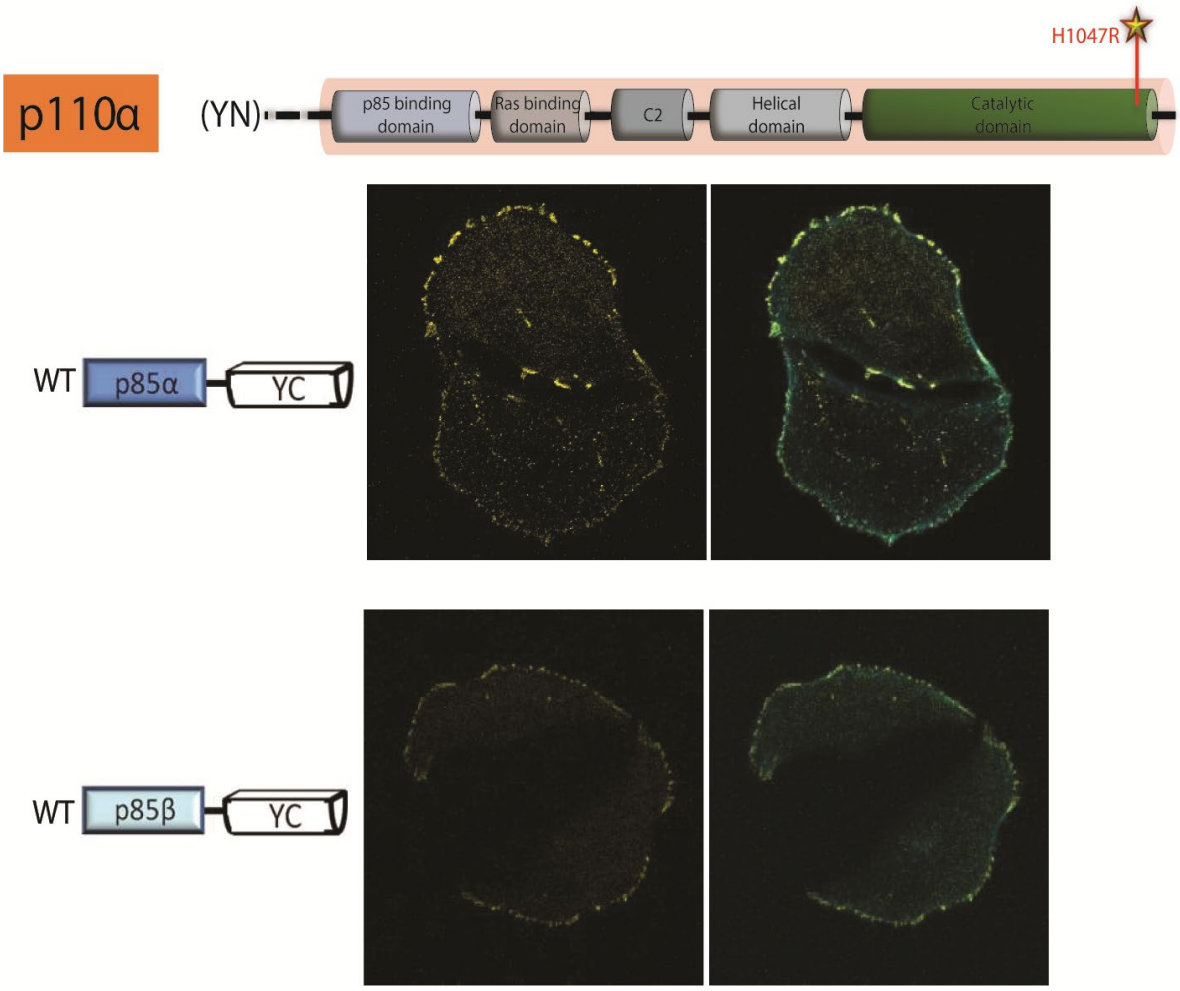

Figure 39. Relocation of BiFC PI3K heterodimers by naturally-occurring oncogenic mutations. HeLa cells were co-transfected with mutant YN-p110α (H1047R) and wild type p85α-YC or p85β-YC. The H1047R mutant generates the same phenotype associated to focal adhesions as the wild type NS1 but with both p85α and β.

We therefore introduced N561D (28, 149) to p85β (**Figure 40**), which is a mutation in the iSH2 region (70) homologous to N564 substitutions found in p85a and naturally occurring in cancers such as endometrial (28) or melanoma (70, 75, 149).When we tested this mutant p85β in our BiFC system, we observed that heterodimers containing p110α and p110δ relocated to focal adhesion regions, similar to the effect of NS1 of wild-type versions of these complexes. Furthermore, the heterodimer of the mutant p85β with p110β also relocated to endosomal regions recreating the exact same phenotypic distribution as detected with NS1 and the wild-type complex. In addition

to the redistribution pattern, we tested the kinase activity of these mutant PI3K complexes and detected the production of PIP_3 when mutant p85β was complexed with p110α and p110δ but not with p110β (**Figure 41**), similar to what we have observed with wild type PI3K heterodimers with NS1 (**Figure 47**). Moreover, we noticed the presence of PIP_3 when mutant p110α was complexed with p85α and p85β (**Figure 41**).

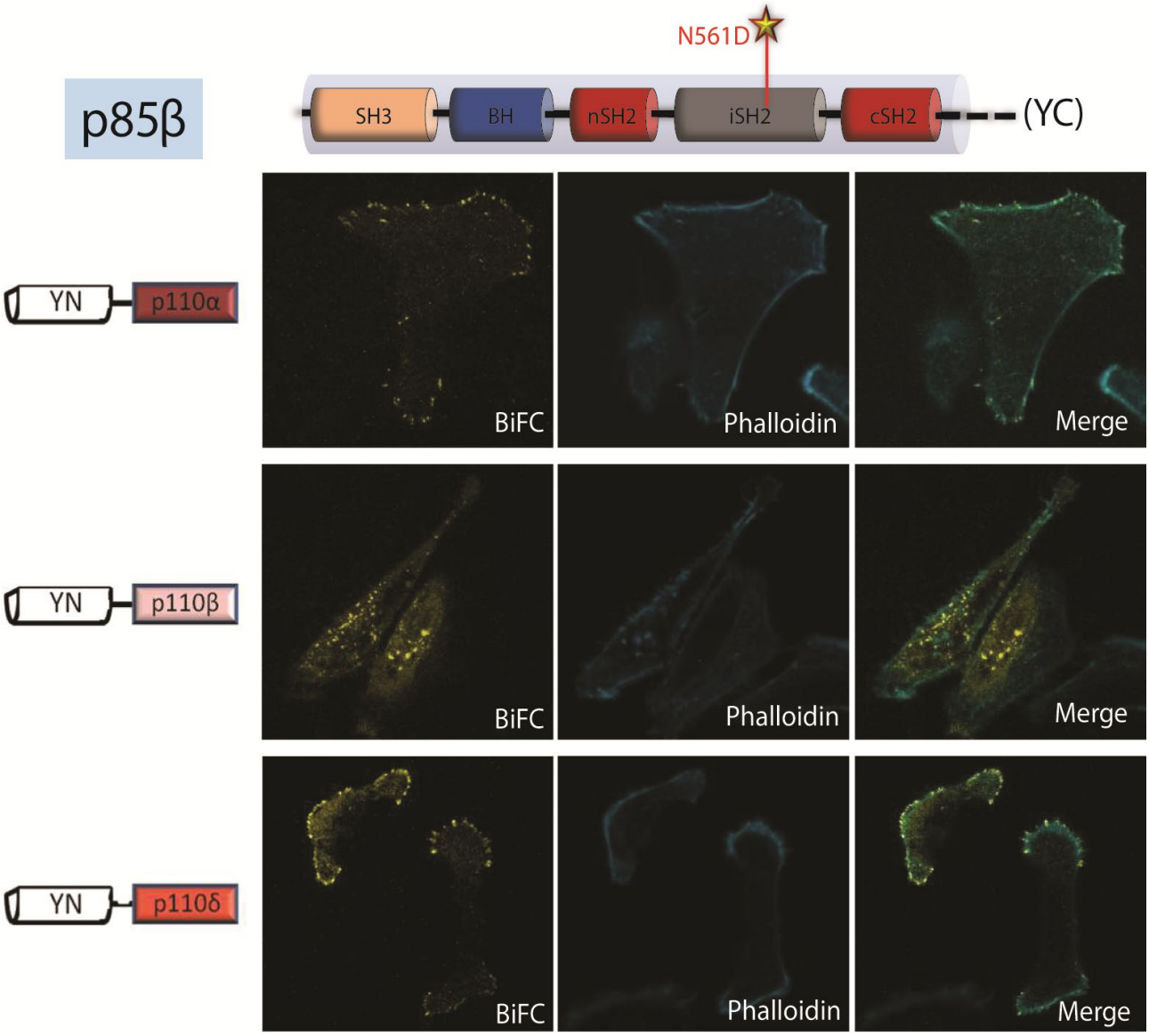

Figure 40. Relocation of BiFC PI3K heterodimers by naturally-occurring oncogenic mutations.
When HeLa cells were co-transfected with mutant p85β-YC (N561D) and wild type YN-p110s, we observed recapitulation of the two distinct outcomes observed with NS1 expression. Actin fibers were stained with phalloidin.

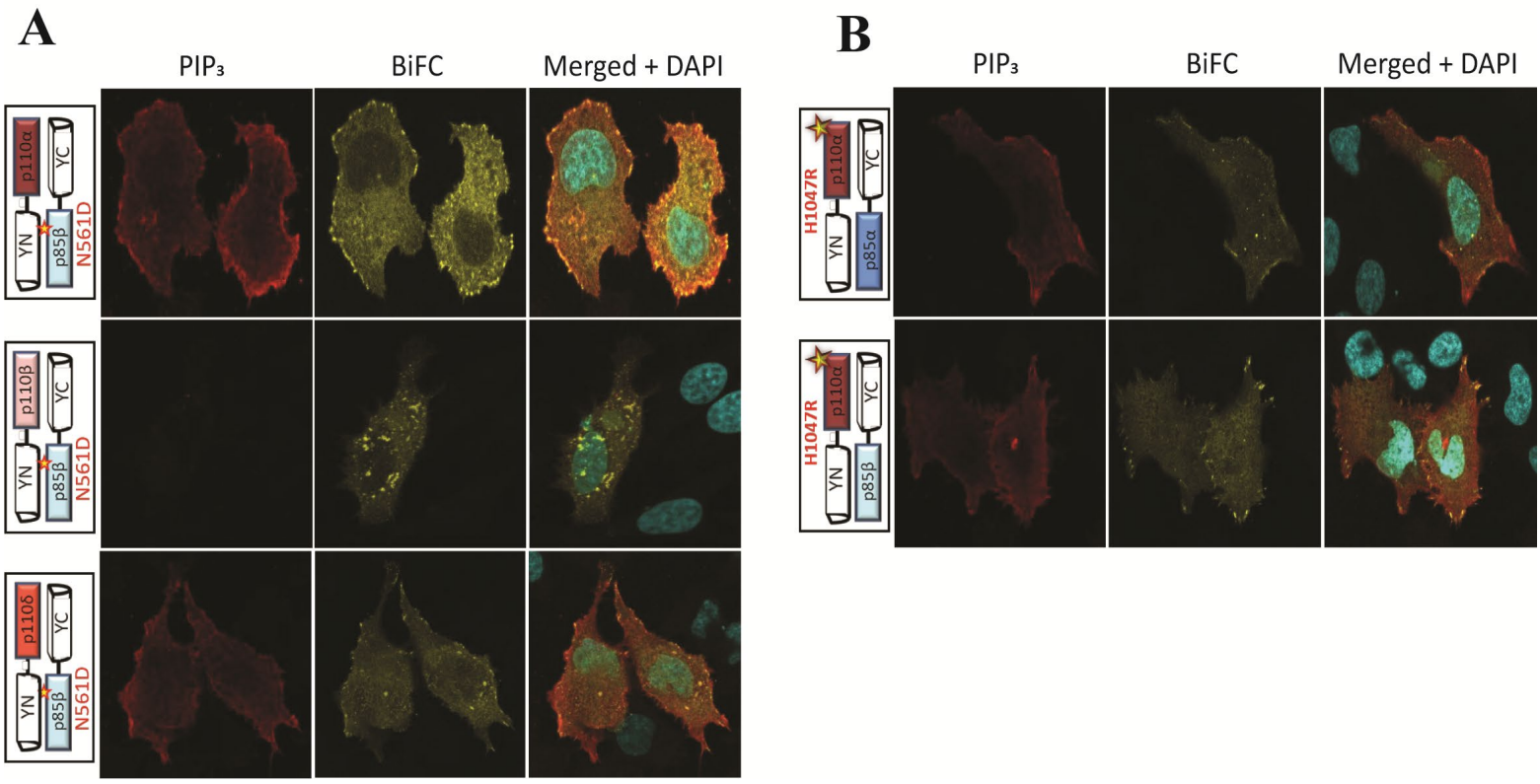

Figure 41. Catalytic activity of mutant PI3K complexes
Catalytic activity of mutant PI3K complexes was tested by co-transfecting HeLa cells with indicated wild type p110 constructs and p85β-N561D and 19 hr p.t. the cells were processed for fluorescence microscopy against PIP_3 (red). As expected, we observed increased levels of PIP_3 with p110α/δ complexes, but not with p110β. We also observed elevated levels of PIP_3 when p110α-H1047R was co-transfected with p85α and p85β. (BiFC in yellow, PIP3 in red, and nucleus in cyan).

4.10 Hyperactivating mutation in p85β partially rescues the growth phenotype of PI3K activation-defective virus.

Finally, we designed a system to test whether the hyperactivating N561D mutation in p85β could rescue the growth phenotype of a recombinant influenza A virus whose NS1 has been engineered to be unable to bind and activate PI3K. Such a virus has been shown previously to suffer a loss in fitness (10, 61) *in vitro* and *in vivo* when compared to wild type viruses (10, 61). We generated a stable A549 cell line constitutively overexpressing HA-p85β-N561D, which was

confirmed by indirect immunofluorescence (**Figure 42A**) and by immunoblotting with specific antibodies (**Figure 42B**).

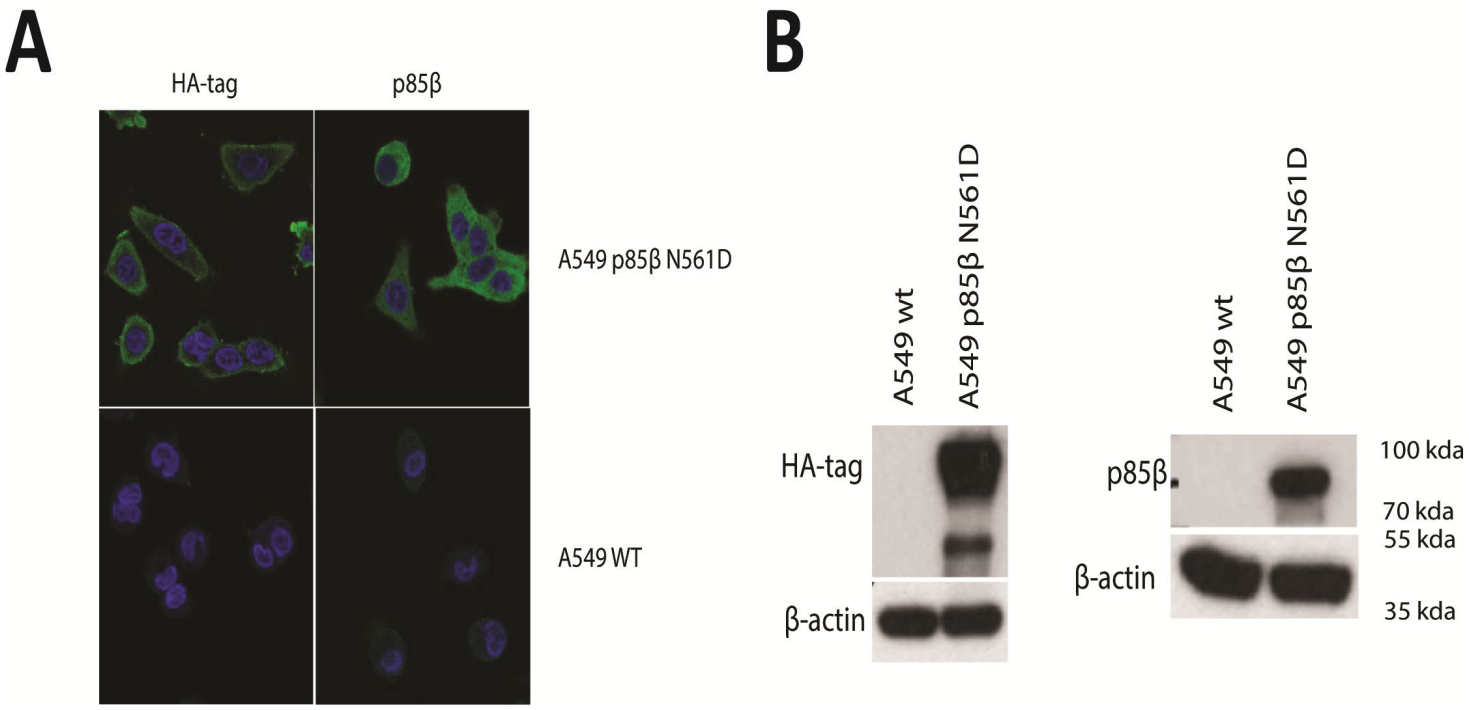

Figure 42. Characterization of A549-p85β N561D cells.
A stable cell line expressing constitutively active HA-p85β N561D in the A549 background was validated by (A) immunofluorescence and (B) western blot. A549 wt was used as a negative control, and staining was performed using antibodies against HA-tag (A, green), p85β (A, green), DAPI (A, blue) and β-actin for western blot loading control (B).

Next, we infected A549 WT and A549-p85β-N561D cells with rPR8 WT and rPR8-Y89F at an MOI of 2 PFU/cell and tested activation of PI3K by assessing levels of pAkt (serine 473) at various time points post-infection (**Figure 43**). As expected, we did not see activation of pAkt in WT cells infected with rPR8-Y89F, but increasing levels of pAkt were detected over time after infection with rPR8 WT virus. On the other hand, we detected higher basal levels of pAkt in A549-p85β-N561D cells as compared to WT cells, and pAkt levels were therefore high whether infected with rPR8-Y89F or rPR8 WT. Additionally, it was notable that we could detect the initial transient phosphorylation of Akt at an early time point (2hr post infection (p.i.)) due to virus entry and attachment in both cell lines and with both viruses (8, 43, 61, 151). However, a second increase in

pAkt levels only occurred in rPR8 WT infected cells, for both cell lines, starting 6hr p.i., consistent with expression of WT NS1.

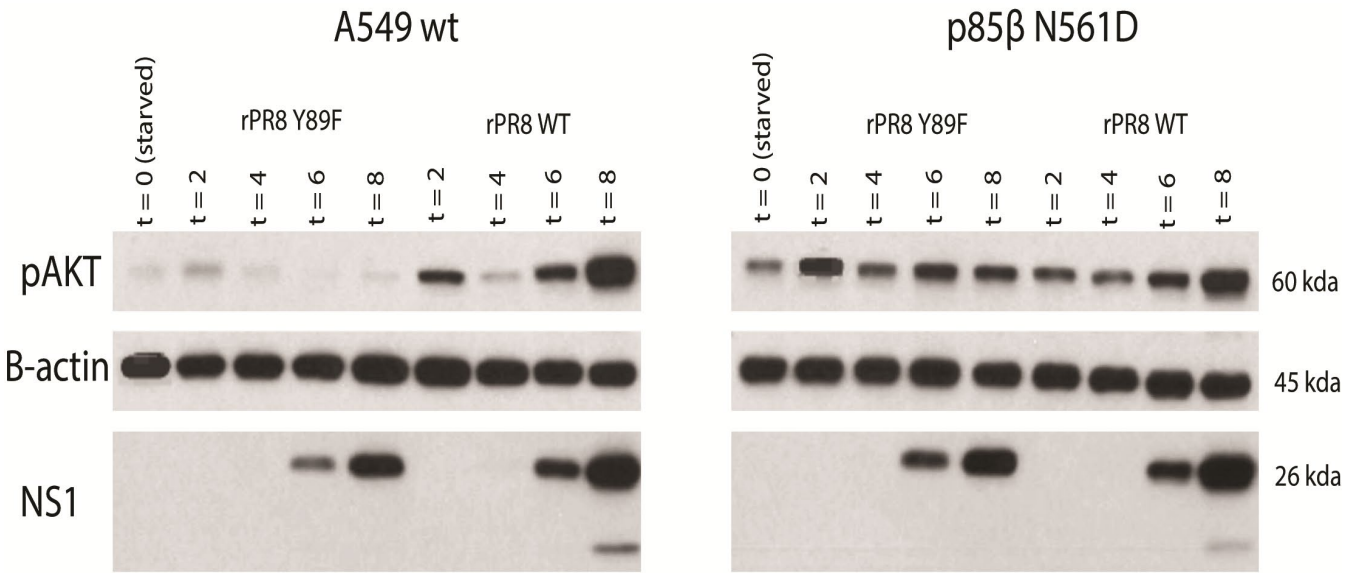

Figure 43. Time course
Time course was performed on serum-starved cells (A549 WT and A549 expressing p85β-N561D) with rPR8 WT and rPR8-Y89F. Cells were infected at a multiplicity of infection of 2 PFU/cell and collected at 0, 2, 4, 6 and 8-hours post infection. Levels of pAkt, NS1 and β-actin were detected by western blot. β-actin was used as a loading control.

We next performed growth kinetics with the two viruses on A549 WT and A549-p85β-N561D cells (**Figure 44**) and observed a partial recovery of rPR8-Y89F fitness in the cells that express constitutively active p85β. Specifically, rPR8-Y89F grew to almost 2 logs lower infectious titers than rPR8 WT in A549 WT cells, while this difference was only of approximately 1 log in A549-p85β-N561D cells. In order to further validate this, we performed a competition assay with rPR8 WT and rPR8-Y89F in A549 wt and A549-p85β-N561D cells. We mixed equal number of PFU of each virus and then infected the different cell lines. We collected cells at 12, 24 and 48 hours post infection and processed them for MinION sequencing. We compared the total number of reads for rPR8 WT versus rPR8-Y89F in the two cell lines. We observed that at 24 and 48 hours post infection, rPR8 WT could outcompete rPR8-Y89F in A549 WT cells, but in A549-p85β-N561D cells, rPR8-Y89F performed slightly better, and was not outcompeted by rPR8 WT as rapidly (**Figure 45**).

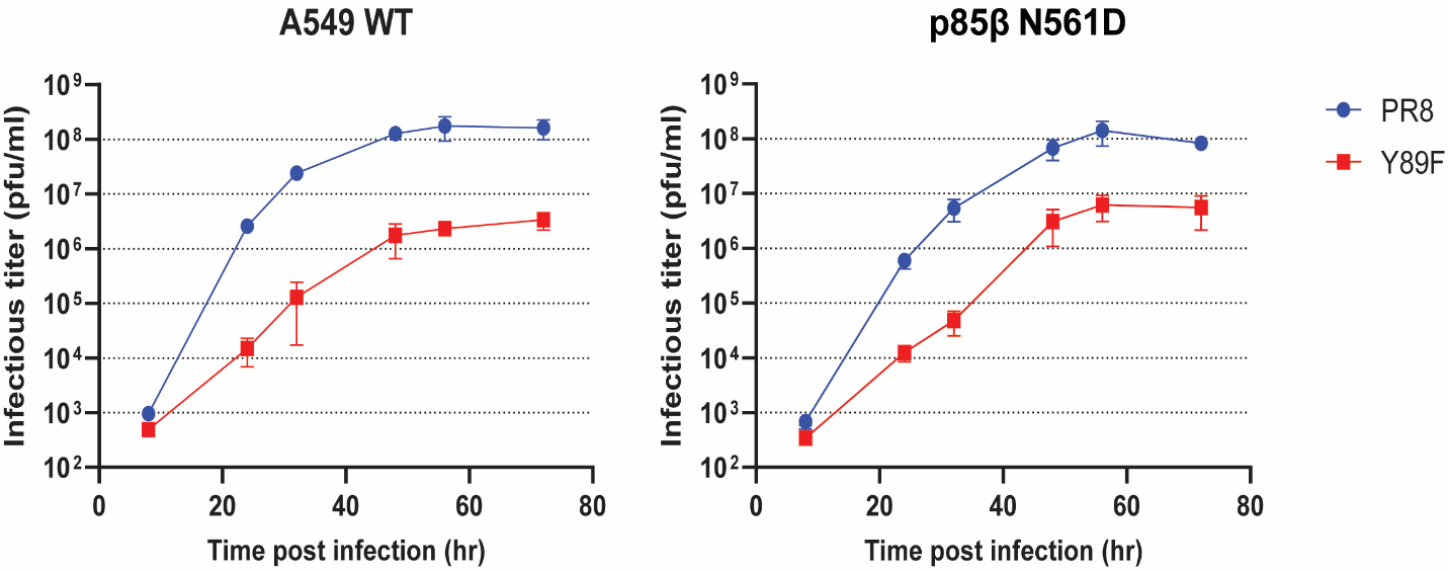

Figure 44. Growth curve
Growth curve was done on serum-starved cells with rPR8 WT and rPR8-Y89F viruses. Supernatant was collected at the indicated times post infection. Plaque assays were performed to determine viral titers. (n=3, error bars represent standard deviation).

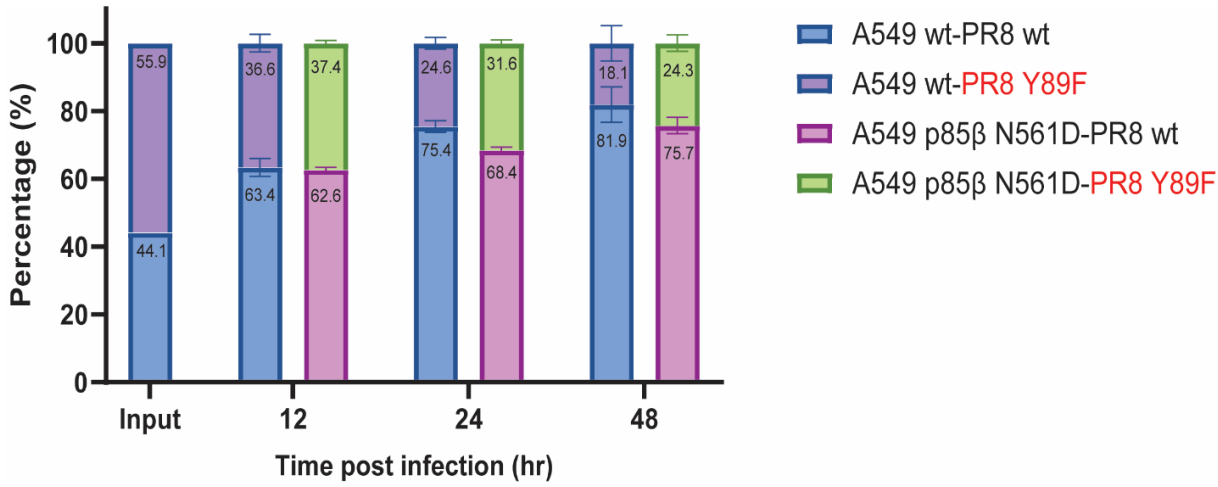

Figure 45. Competition assay
Competition assay was performed to assess viral fitness in A549 wt and A549-p85β-N561D cells. rPR8 WT and rPR8-Y89F were mixed in a 50:50 ratio and cells were infected at 10^3 PFU/mL, cells were collected at 12, 24, and 48 hrs post infection. All the samples were analyzed using MinION nanopore technology and the bars represent percentage of reads present for rPR8 WT and rPR8-Y89F in each sample. (n=3 (except for input), error bars represent standard deviation).

5. Discussion

5. Discussion

The phosphoinositide 3-kinase (PI3K)-Akt signaling cascade serves as a critical checkpoint of multiple cellular processes, including translation, survival, proliferation, migration, and immunity responses. This pathway is also implicated in various pathological processes, such as cancer and diabetes (108). Upon activation, PI3K generates PIP_3, which triggers downstream phosphorylation events leading to Akt activation. Once Akt is activated, it can phosphorylate more than 100 substrates that regulate diverse cellular functions (174). For example, Akt mediates phosphorylation of the pro-apoptotic protein BAD (Bcl-2-associated death promoter), resulting in its release from binding partners and preventing initiation of apoptosis (34). Another such group of proteins are FOXO (Forkhead box O1) proteins, Akt phosphorylates FOXO proteins in the nucleus and displaces FOXO transcription factors from target genes and triggers the translocation of FOXO to the cytoplasm and prevents the production of genes that promote apoptosis and cell-cycle arrest (160). The extensive range of downstream effects posed by this signaling axis highlights the complexity and significance of its regulation. Understanding the variety of outcomes resulting from PI3K-Akt pathway activation remains a fundamental challenge in biological sciences.

Class IA PI3Ks, which act as obligate heterodimers, comprising several isoforms of both catalytic (p110α, p110β and p110δ) and regulatory subunits (mainly, p85α and p85β), leading to various possible combinations of the heterodimers. However, how this heterogeneity translates into potential functional diversity is poorly understood. p110-independent p85 has been shown to perform critical adaptor functions, including the sequestration and compartmentalization of key signaling proteins. Free p85 has roles in glucose homeostasis, cellular stress pathways, receptor trafficking, and cell migration. The balance between p110-independent p85 and p110-bound p85 is essential for maintaining cellular function. Among the isoforms, p85α is the most abundant isoform in normal tissues and functions as a tumor suppressor and its expression is reduced in cancer (164). In contrast, p85β, which is also ubiquitously expressed, is frequently overexpressed in cancers and is considered a proto-oncogene (165). The adaptor functions of p110-independent p85 are localizing proteins and coordinating their activity. Most of these are in cellular stress-induced pathways, such as unfolded protein response (130, 179, 180), p53-mediated senescence

(185), and insulin response. Additionally, critical roles in mediating cytoskeletal changes and endocytic trafficking (50, 76, 109).

Notwithstanding, one of the best characterized examples of specific isoform activation of PI3K is mediated by the influenza A virus NS1 protein, which only binds p85β, and so can only activate p85β- (and not p85α-) heterodimers with p110. Structural and biochemical studies have revealed that this specificity arises from key residues in the regulatory subunit that enable NS1 binding to the iSH2 domain of p85β. However, the mechanisms by which NS1 leverages the diversity of PI3K heterodimer combinations to activate the pathway remain poorly understood.

To investigate whether the NS1-mediated activation of PI3K varies according to the p110 isoform heterodimerizing with p85β, we employed a bimolecular fluorescence complementation (BiFC) assay to specifically tag and visualize each possible p85/p110 combination. The BiFC system, established in 2002, allows direct tracking of protein-protein interactions and their spatial dynamics through fluorescent signal reconstitution upon complex formation (68, 137). Using this approach, we observed that in the absence of NS1, all p85-p110 heterodimers exhibited a diffuse cytoplasmic distribution consistent with an inactive state. Also as expected, the presence of NS1 did not affect the basal distribution of complexes containing p85α, but relocalized those specifically containing p85β, a change that could be prevented by the Y89F substitution in NS1, previously shown to abrogate NS1 binding to p85β (10, 61). This differential relocalization pattern persisted during infection with recombinant influenza virus strains, with wild type NS1 inducing relocalization, whereas the Y89F mutant maintained homogeneous distribution, confirming that the effect is physiologically relevant and not an artifact of NS1 overexpression. Additionally, we observed that the relocalization was strain-independent when we transiently introduced NS1s from different subtypes indicating that the strain-dependent mechanism reported in the context of viral infection might be due to downstream mediators of this pathway leading to differential functional phenotypes. Furthermore, relocalization of the complex only required the monomeric effector domain of NS1, consistent with previously published structural studies demonstrating that other NS1 domains are dispensable for p85β binding and subsequent PI3K activation (60, 62). Notably, we identified two distinct PI3K phenotypes both spatially and functionally associated with NS1 expression, depending on the p110 isoform present in the heterodimer.

The first of these outcomes involved complexes containing p110α or p110δ, that, when engaged by NS1, were relocated to specific regions of the plasma membrane, which we identified

as focal adhesions. Focal adhesions are well characterized scaffolding structures that serve as critical hubs for assembling signaling complexes downstream of cell surface receptors (174). Consistent with this, the translocation of NS1-bound PI3K complexes to the focal adhesions required functional pY-receptor binding sites within the p85β subunit, and resulted in PI3K catalytic activation leading to PIP_3 production and activation of Akt. All of this is consistent with the canonical activation mechanism of PI3K.

Supporting this, recent studies have shown that endogenous p110α labeled with mNeonGreen preferentially localizes to focal adhesions, where it becomes activated by focal adhesion kinase (FAK)-mediated signaling, leading to localized PIP_3 production and Akt recruitment. These studies also observed similar focal adhesion recruitment and activation phenotypes for endogenous p110β and transiently expressed p110δ. The researchers propose that p85α binding to FAK is essential for class IA PI3K recruitment and PIP_3 generation at focal adhesions under basal cellular conditions (174). Our findings corroborate the notion that canonical PI3K activation predominantly occurs at the plasma membrane focal adhesions, initiation subsequent signaling cascades. Although they describe a route of activation that is independent of growth factors and receptor tyrosine kinases, these findings indicate that, despite different upstream activators, the heterodimers are relocated to the focal adhesions. This suggests redundant mechanisms for the canonical mode of activation. Interestingly, when the studies tested epidermal growth factor receptor (EGFR) activation by treating cells with EGF, they did not observe localization at focal adhesion sites, but rather at EGFR spots, suggesting that the mechanism of class IA PI3K spatial targeting differs between basal and stimulated conditions in their system—something that we also observed when we treating our BiFC complexes with EGFR.

The second outcome concerned PI3K heterodimers containing p110β. In this case, in stark contrast to the first outcome, the NS1-activated complexes translocated to punctate perinuclear structures, which we identified as early endosomes. This translocation was independent of functional pY-receptor binding residues in p85β, leaving unclear which factor(s) may serve as anchors of these complexes to the endosome; however, this is likely to be a specific determinant of p110β. Similarly, we did not detect clear production of PIP_3, although others have found pools of this second messenger in endosomal membranes (5), nor could we detect localized activation of Akt. Additionally, no increase in kinase activity was detected in our in vitro lipid kinase assay, which further supports our pY-receptor binding results, considering that this assay tests activity

with vesicles containing PIP_2, a step downstream of activation by pY-receptors (**Figure 46**). The presence of PI3K complexes in the endosome is consistent with previous proteomics studies that found that active p110β binds to Rab5 (13), the same marker we have used to co-localize PI3K complexes containing p110β with early endosomes. This Rab5-p110β interaction has been associated with regulation of autophagy (38) independent of the receptor tyrosine kinase pathway. It has been reported that Rab5 interaction with the catalytic subunit is isoform specific, meaning it interacts with p110β but not with p110α (29, 92). It is important to note that class IA PI3Ks p110α, p110β, and p110δ signal downstream of receptor tyrosine kinase but p110β can also be activated by G-protein coupled receptors (GPCRs) (93), confirming multiple modes of activation for p110β independent of the receptor tyrosine kinase. Jonathan Backer and colleagues (38) proposed that there are two pools of p110β/p85, one that acts through the classical growth factor receptor signaling complex and another intracellular pool that promotes basal autophagy by binding to the small GTPase Rab5. The proposed mechanism is that the intracellular p110β/p85 protects Rab5-GTP (active form) from GAP activity, leading to increased active Rab5 that interacts downstream with effectors like Vsp34 to induce autophagy. Additionally, GTPase Rab5 has been reported to play a critical role in endocytic trafficking and formation of autophagosome (136). They also reported that p110β increases its interaction with Rab5 upon growth factor limitation, indicating a possible regulatory role in balancing cell survival (canonical pathway) and autophagy depending on growth factor availability. These findings suggest that in the context of viral infection or NS1 presence alone, a mechanism may promote p110β's intracellular routing and enhanced interaction with Rab5. Future studies will have to determine if the NS1-relocalized p85β/p110β complexes similarly impact autophagy during influenza A virus infection by looking for the presence of Rab5-GTP or its downstream effectors such as Vps34 and EEA1 (116). Additionally, it would be interesting to investigate whether endogenous p110α/p110β ratios are altered during viral infection to promote PI3K pathway activation, either through canonical or non-canonical mechanisms. It is also possible that this ratio changes in a time-dependent manner—canonically at earlier time points post-infection, to suppress autophagy and support viral replication, and non-canonically at later stages, in response to cellular stress or the depletion of growth factors.

Interestingly in our assays, we did not observe differences between p110α and p110δ-associated phenotypes, so it remains unknown whether their activation could lead to different outcomes. The different p110 subunits have been shown to have different tissue and cell type

distributions, as well as interaction partners, and in addition p110α and p110δ signaling pathways may diverge downstream of Akt phosphorylation, in ways that will require further studies to elucidate. It has been reported that p110α and p110β are ubiquitously expressed in different cell types (145) but p110δ is restricted to the hematopoietic system and multipotential progenitors and to a lesser extent in neurons (12, 129). This possibility suggests that p110δ maybe the equivalent of p110α in immune cells in the context of its role in the PI3K heterodimers. However, it is important to note that PI3K isoforms can take up different roles in different cell contexts (129). For example, p110α is recruited by activated insulin receptor, vascular endothelial growth factor (VEGFR), among others (12, 57). In contrast, less is known about p110β, although it signals downstream of both receptor tyrosine kinases and GPCRs and may have overlapping functions with class IB PI3Kγ (58, 91), though, developmental studies indicate that it is essential for embryonic development, as mice homozygous for deletion alleles exhibit embryonic lethality (17). On the other hand, p110δ is directly or indirectly activated by receptors such as B-cell, T-cell and Toll-like receptors, among others. It has been shown that p110δ plays a critical role in the antiviral response against West Nile Virus (WNV) via the induction of type I interferon (69). Interestingly, in the context of influenza virus, differential immune responses have been observed in a subtype specific manner in dendritic cells (DCs). Viruses expressing NS1 from human strains (H1N1 and H3N2) have higher levels of type I and type III IFNs in comparison to NS1 from avian subtypes (H5N1, H7N9 and H7N2) (113, 159). Further studies would be required to elucidate if this distinct subtype phenotype is dependent on the different catalytic subunits of PI3K and to what extent.

Other studies have shown how specific inputs may act exclusively through some PI3K isoforms, such as HRas only activating p110α and p110δ, but not p110β (152). However, when we tested constitutively active Ras and Src, we were not able to distinguish a specific phenotype to any of the isoforms and this would require additional follow up to see if there is an advantage of one isoform over another in this context. However, our work shows that a single stimulus, NS1, can distinctively affect each p85β-containing complex of the class IA PI3K family, leading to different outcomes according to the p110 isoform. We speculate that the physiological result of the NS1 activation of PI3K would be greatly affected by the balance between the p110α/p110δ "focal adhesion" route or the p110β "endosome" route, a balance that will depend on the basal expression levels of each isoform. These complexities would help to explain how the physiological

impact of PI3K activation by influenza A viruses remains largely obscure, and may not be limited to delaying apoptosis (40, 102).

Our work demonstrates how the BiFC system described here can be used to investigate how PI3K activators differentially affect each hetero-isoformic member of the class IA PI3K family. Notably, the H1047R amino acid substitution in p110α, one of the most prevalent alterations found in colon and breast cancers, relocates PI3K to focal adhesions, regardless of whether it is paired with p85α or p85β. This may be due to the mutation weakening the stabilizing interaction that maintains the p110-p85 in an inhibited state, thereby lowering the activation threshold of the pathway, particularly given that the mutation resides in the kinase domain of p110 (12, 41). H1047R is one of the top four hot spot mutations in p110α, accounting for 80-90% of all mutations found in p110α, and is used as a predictive biomarker in cancers, particularly breast cancer. (82, 141). We also introduced a homologous, naturally-occurring oncogenic mutation in p85β, N561D, which interestingly recapitulated the PI3K phenotypes observed during NS1 co-expression. This result suggests that influenza A virus may have evolved to stimulate PI3K during infection to induce a cellular environment resembling that of cells harboring oncogenic PI3K mutations. It is also noteworthy that this effect is isoform-specific, with NS1 selectively activating the oncogenic properties of p85β. Furthermore, when we tested kinase activities of the oncogenic PI3K constructs, we observed PIP_3 production downstream of the p110α H1047R mutant in complex with either p85α or p85β, confirming the expected active status of the kinase. More interestingly, similar to the relocalization pattern seen in NS1-activated PI3K, we also detected PIP_3 production downstream of p85β N561D in complex with p110α and p110δ but not p110β. Further studies are required to determine the percentage of p110α/δ versus p110β complexes present in an oncogenic state and the downstream functionality of these distinct phenotypes.

In fact, we found that hyperactivated p85β-N561D partially compensated to some extent for the loss of fitness found in an influenza A virus expressing a mutated NS1 protein unable to activate PI3K. This partial incomplete rescue could be due to several factors, including differences in the magnitude and kinetics of p85β activation between virus-infected cells and the constitutively active p85β-N561D cells. Also, although previous studies have not definitively detected other functions of NS1 affected by the Y89F substitution, it cannot be ruled out that this mutation has further impacts than changing the binding to p85β, particularly given the location of Y89 at the interface with other host factors (87). One study has shown that PI3K mutant NS1 (NS1-Y89F) is

able to bind NXF1 but does not promote NXF1 interaction with M and does not promote the translocation of segment 7 (M) mRNA from the nucleus to the cytoplasm (131). This additional function could play a role in viral replication and the lack of complete rescue. In any case, our data are consistent with a role for the influenza A virus NS1 protein in establishing a transient PI3K-driven "transformed-like" phenotype in infected cells that promotes optimal virus replication. Interestingly, some other factors associated with cell transformation, such as deficiencies in the interferon response (78) and oncogenic activation of the Ras/Raf/MEK/ERK signaling pathway (16, 133), have also been associated with increased influenza virus replication.

PI3K heterodimers and individual isoforms have been extensively studied due to the central role of this pathway in processes such as cell survival, proliferation, migration and immune responses. It is also implicated in numerous diseases, including cancer and autoimmune disorders. However, many questions remain unanswered, and recent discoveries have revealed additional roles for these isoforms, both as part of heterodimeric complexes and as independent proteins. These emerging findings underscore the need for new tools to better understand the complexities of this signaling pathway. Current research approaches include the use of transgenic mice, isoform-specific and pan-PI3K inhibitors, endogenous protein tagging, and various biochemical and structural techniques. Here, we propose that our BiFC system can be employed alongside these methods to spatial-temporally track PI3K heterodimers and investigate their distinct phenotypes. More importantly, we suggest that NS1 could be used as a selective activator of PI3K heterodimers in an isoform-specific manner, enabling deeper characterization of the downstream signaling pathways driven by different catalytic isoforms. This strategy could not only enhance our understanding of the role influenza virus infection plays in an oncogenic state but also offer new avenues for dissecting PI3K activation mechanism in health and disease.

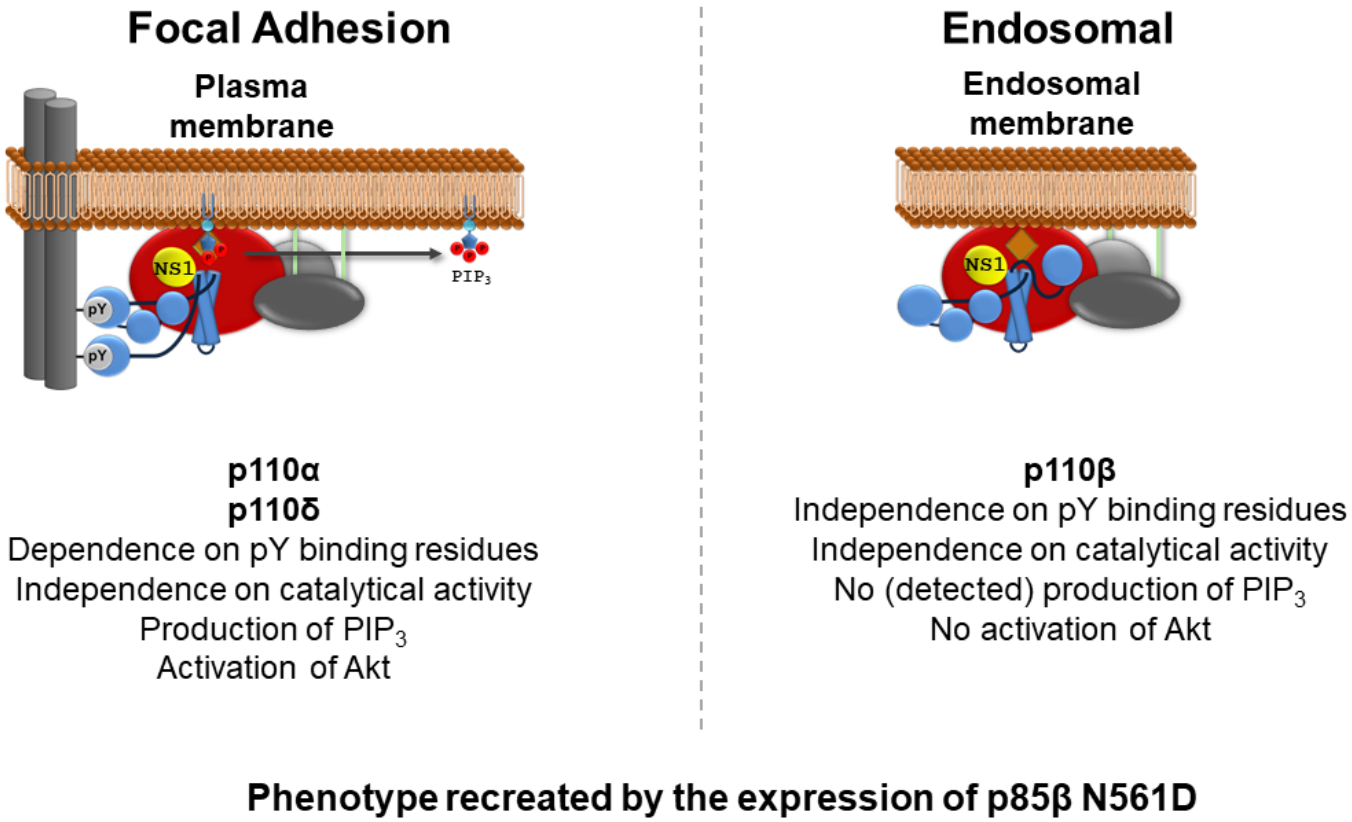

Figure 46. Isoform-specific activation and relocalization of PI3K heterodimers by NS1.
The NS1 protein of influenza A virus activates and relocalizes PI3K complexes in an isoform-specific manner independent of catalytic activity. Complexes containing p110α or p110δ are activated and relocalized to focal adhesions. This leads to a mostly canonical activation of PI3K activity, dependent on binding to pY residues and leading the production of PIP3 and phosphorylated Akt. In contrast, heterodimers containing p110β are relocalized to the endosomal region independently of pY binding residues and do not become catalytically active.

6. Conclusion

6. Conclusion

6. Conclusion

Here we established a Bimolecular Fluorescence Complementation (BiFC) system to spatially visualize the localization of PI3K heterodimers at the cellular level and used this tool in combination with influenza A virus NS1 protein to study the activation of this complex pathway. We posit that the BiFC system we describe in this report can be applied to the study of PI3K signaling regulation beyond the virology field. Considering the central role of PI3K-Akt in some of the most prevalent human maladies, we propose our system as an interesting new tool for further understanding and addressing the role of this pathway in human health and disease.

1. We successfully established a BiFC system to spatially visualize and characterize the location of PI3K heterodimers. In the absence of NS1, we observed inactive PI3K complexes with homogenous expression, whereas in the presence of NS1, we detected activated heterodimers with distinct relocalization.

2. Utilizing the BiFC system, we identified isoform-specific activation of the PI3K signaling pathway by NS1: complexes with p110α/p110δ led to the canonical activation ("focal adhesion"), while complexes with p110β resulted in non-canonical activation ("endosomal").

3. We tested different pathological and physiological stimuli and identified an oncogenic mutation that mimicked the distinct phenotype observed upon NS1-mediated activation of the PI3K heterodimer.

4. We assessed the fitness of wild-type and PI3K-activating mutant recombinant influenza viruses in cells expressing constitutively active p85β (harboring the oncogenic mutation) and wild-type cells. A partial rescue in the viral growth phenotype was observed in cells expressing the mutant p85β.

6. Conclusion

7. References

7. References

7. References

1. **(CDC) CfDCaP**. May 9, 2025 2025. Preliminary Estimated Flu Disease Burden 2024-2025 Flu Season. https://www.cdc.gov/flu-burden/php/data-vis/2024-2025.html. Accessed May 19, 2025.
2. **Alessi DR**. 2001. Discovery of PDK1, one of the missing links in insulin signal transduction. Colworth Medal Lecture. Biochem Soc Trans 29:1-14.
3. **Alessi DR, Andjelkovic M, Caudwell B, Cron P, Morrice N, Cohen P, Hemmings BA**. 1996. Mechanism of activation of protein kinase B by insulin and IGF-1. EMBO J 15:6541-51.
4. **Alessi DR, Cohen P**. 1998. Mechanism of activation and function of protein kinase B. Curr Opin Genet Dev 8:55-62.
5. **Antal CE, Newton AC**. 2013. Spatiotemporal dynamics of phosphorylation in lipid second messenger signaling. Mol Cell Proteomics 12:3498-508.
6. **Aramini JM, Ma LC, Zhou L, Schauder CM, Hamilton K, Amer BR, Mack TR, Lee HW, Ciccosanti CT, Zhao L, Xiao R, Krug RM, Montelione GT**. 2011. Dimer interface of the effector domain of non-structural protein 1 from influenza A virus: an interface with multiple functions. J Biol Chem 286:26050-60.
7. **Arcaro A, Wymann MP**. 1993. Wortmannin is a potent phosphatidylinositol 3-kinase inhibitor: the role of phosphatidylinositol 3,4,5-trisphosphate in neutrophil responses. Biochem J 296 (Pt 2):297-301.
8. **Ayllon J, Garcia-Sastre A**. 2015. The NS1 protein: a multitasking virulence factor. Curr Top Microbiol Immunol 386:73-107.
9. **Ayllon J, Garcia-Sastre A, Hale BG**. 2012. Influenza A viruses and PI3K: are there time, place and manner restrictions? Virulence 3:411-4.
10. **Ayllon J, Hale BG, Garcia-Sastre A**. 2012. Strain-specific contribution of NS1-activated phosphoinositide 3-kinase signaling to influenza A virus replication and virulence. J Virol 86:5366-70.
11. **Ayllon J, Russell RJ, Garcia-Sastre A, Hale BG**. 2012. Contribution of NS1 effector domain dimerization to influenza A virus replication and virulence. J Virol 86:13095-8.
12. **Aytenfisu TY, Campbell HM, Chakrabarti M, Amzel LM, Gabelli SB**. 2022. Class I PI3K Biology. Curr Top Microbiol Immunol 436:3-49.
13. **Backer JM**. 2010. The regulation of class IA PI 3-kinases by inter-subunit interactions. Curr Top Microbiol Immunol 346:87-114.
14. **Beckerle MC**. 1997. Zyxin: zinc fingers at sites of cell adhesion. Bioessays 19:949-57.
15. **Belli C, Repetto M, Anand S, Porta C, Subbiah V, Curigliano G**. 2023. The emerging role of PI3K inhibitors for solid tumour treatment and beyond. Br J Cancer 128:2150-2162.
16. **Bergmann M, Romirer I, Sachet M, Fleischhacker R, Garcia-Sastre A, Palese P, Wolff K, Pehamberger H, Jakesz R, Muster T**. 2001. A genetically engineered influenza A virus with ras-dependent oncolytic properties. Cancer Res 61:8188-93.

17. **Bi L, Okabe I, Bernard DJ, Nussbaum RL**. 2002. Early embryonic lethality in mice deficient in the p110beta catalytic subunit of PI 3-kinase. Mamm Genome 13:169-72.

18. **Bilanges B, Posor Y, Vanhaesebroeck B**. 2019. PI3K isoforms in cell signalling and vesicle trafficking. Nat Rev Mol Cell Biol 20:515-534.

19. **Blanco J, Cameirao C, Lopez MC, Munoz-Barroso I**. 2020. Phosphatidylinositol-3-kinase-Akt pathway in negative-stranded RNA virus infection: a minireview. Arch Virol 165:2165-2176.

20. **Bornholdt ZA, Prasad BV**. 2006. X-ray structure of influenza virus NS1 effector domain. Nat Struct Mol Biol 13:559-60.

21. **Bouvier NM, Palese P**. 2008. The biology of influenza viruses. Vaccine 26 Suppl 4:D49-53.

22. **Cantrell DA**. 2001. Phosphoinositide 3-kinase signalling pathways. J Cell Sci 114:1439-45.

23. **Carpenter CL, Duckworth BC, Auger KR, Cohen B, Schaffhausen BS, Cantley LC**. 1990. Purification and characterization of phosphoinositide 3-kinase from rat liver. J Biol Chem 265:19704-11.

24. **Carson JD, Van Aller G, Lehr R, Sinnamon RH, Kirkpatrick RB, Auger KR, Dhanak D, Copeland RA, Gontarek RR, Tummino PJ, Luo L**. 2008. Effects of oncogenic p110alpha subunit mutations on the lipid kinase activity of phosphoinositide 3-kinase. Biochem J 409:519-24.

25. **Carter T, Iqbal M**. 2024. The Influenza A Virus Replication Cycle: A Comprehensive Review. Viruses 16.

26. **Chauhan RP, Gordon ML**. 2022. An overview of influenza A virus genes, protein functions, and replication cycle highlighting important updates. Virus Genes 58:255-269.

27. **Cheng A, Wong SM, Yuan YA**. 2009. Structural basis for dsRNA recognition by NS1 protein of influenza A virus. Cell Res 19:187-95.

28. **Cheung LW, Hennessy BT, Li J, Yu S, Myers AP, Djordjevic B, Lu Y, Stemke-Hale K, Dyer MD, Zhang F, Ju Z, Cantley LC, Scherer SE, Liang H, Lu KH, Broaddus RR, Mills GB**. 2011. High frequency of PIK3R1 and PIK3R2 mutations in endometrial cancer elucidates a novel mechanism for regulation of PTEN protein stability. Cancer Discov 1:170-85.

29. **Christoforidis S, Miaczynska M, Ashman K, Wilm M, Zhao L, Yip SC, Waterfield MD, Backer JM, Zerial M**. 1999. Phosphatidylinositol-3-OH kinases are Rab5 effectors. Nat Cell Biol 1:249-52.

30. **Cirillo D, Diceglie M, Nazare M**. 2023. Isoform-selective targeting of PI3K: time to consider new opportunities? Trends Pharmacol Sci 44:601-621.

31. **Colgan DF, Manley JL**. 1997. Mechanism and regulation of mRNA polyadenylation. Genes Dev 11:2755-66.

32. **Dar AC, Dever TE, Sicheri F**. 2005. Higher-order substrate recognition of eIF2alpha by the RNA-dependent protein kinase PKR. Cell 122:887-900.

33. **Das K, Ma LC, Xiao R, Radvansky B, Aramini J, Zhao L, Marklund J, Kuo RL, Twu KY, Arnold E, Krug RM, Montelione GT**. 2008. Structural basis for suppression of a host antiviral response by influenza A virus. Proc Natl Acad Sci U S A 105:13093-8.

34. **Datta SR, Katsov A, Hu L, Petros A, Fesik SW, Yaffe MB, Greenberg ME**. 2000. 14-3-3 proteins and survival kinases cooperate to inactivate BAD by BH3 domain phosphorylation. Mol Cell 6:41-51.

35. **DeClue JE, Sadowski I, Martin GS, Pawson T**. 1987. A conserved domain regulates interactions of the v-fps protein-tyrosine kinase with the host cell. Proc Natl Acad Sci U S A 84:9064-8.

36. **Domin J, Waterfield MD**. 1997. Using structure to define the function of phosphoinositide 3-kinase family members. FEBS Lett 410:91-5.

37. **Dou D, Revol R, Ostbye H, Wang H, Daniels R**. 2018. Influenza A Virus Cell Entry, Replication, Virion Assembly and Movement. Front Immunol 9:1581.

38. **Dou Z, Pan JA, Dbouk HA, Ballou LM, DeLeon JL, Fan Y, Chen JS, Liang Z, Li G, Backer JM, Lin RZ, Zong WX**. 2013. Class IA PI3K p110beta subunit promotes autophagy through Rab5 small GTPase in response to growth factor limitation. Mol Cell 50:29-42.

39. **Du R, Cui Q, Chen Z, Zhao X, Lin X, Rong L**. 2023. Revisiting influenza A virus life cycle from a perspective of genome balance. Virol Sin 38:1-8.

40. **Duronio V**. 2008. The life of a cell: apoptosis regulation by the PI3K/PKB pathway. Biochem J 415:333-44.

41. **Echeverria I, Liu Y, Gabelli SB, Amzel LM**. 2015. Oncogenic mutations weaken the interactions that stabilize the p110alpha-p85alpha heterodimer in phosphatidylinositol 3-kinase alpha. FEBS J 282:3528-42.

42. **Ehrhardt C, Ludwig S**. 2009. A new player in a deadly game: influenza viruses and the PI3K/Akt signalling pathway. Cell Microbiol 11:863-71.

43. **Ehrhardt C, Marjuki H, Wolff T, Nurnberg B, Planz O, Pleschka S, Ludwig S**. 2006. Bivalent role of the phosphatidylinositol-3-kinase (PI3K) during influenza virus infection and host cell defence. Cell Microbiol 8:1336-48.

44. **Ehrhardt C, Wolff T, Pleschka S, Planz O, Beermann W, Bode JG, Schmolke M, Ludwig S**. 2007. Influenza A virus NS1 protein activates the PI3K/Akt pathway to mediate antiapoptotic signaling responses. J Virol 81:3058-67.

45. **Engelman JA, Luo J, Cantley LC**. 2006. The evolution of phosphatidylinositol 3-kinases as regulators of growth and metabolism. Nat Rev Genet 7:606-19.

46. **Escobedo JA, Kaplan DR, Kavanaugh WM, Turck CW, Williams LT**. 1991. A phosphatidylinositol-3 kinase binds to platelet-derived growth factor receptors through a specific receptor sequence containing phosphotyrosine. Mol Cell Biol 11:1125-32.

47. **Florian K**. 2021. Orthomyxoviridae: The Viruses and Their Replication. *In* Howley PM (ed), Fields Virology: Emerging Viruses. Lippincott Williams & Wilkins,

48. **Fodor E**. 2013. The RNA polymerase of influenza a virus: mechanisms of viral transcription and replication. Acta Virol 57:113-22.

49. **Fodor E, Devenish L, Engelhardt OG, Palese P, Brownlee GG, Garcia-Sastre A**. 1999. Rescue of influenza A virus from recombinant DNA. J Virol 73:9679-82.

50. **Fox M, Mott HR, Owen D**. 2020. Class IA PI3K regulatory subunits: p110-independent roles and structures. Biochem Soc Trans 48:1397-1417.

51. **Franke TF, Yang SI, Chan TO, Datta K, Kazlauskas A, Morrison DK, Kaplan DR, Tsichlis PN**. 1995. The protein kinase encoded by the Akt proto-oncogene is a target of the PDGF-activated phosphatidylinositol 3-kinase. Cell 81:727-36.

52. **Fresno Vara JA, Casado E, de Castro J, Cejas P, Belda-Iniesta C, Gonzalez-Baron M**. 2004. PI3K/Akt signalling pathway and cancer. Cancer Treat Rev 30:193-204.

53. **Fruman DA, Meyers RE, Cantley LC**. 1998. Phosphoinositide kinases. Annu Rev Biochem 67:481-507.

54. **Gack MU, Albrecht RA, Urano T, Inn KS, Huang IC, Carnero E, Farzan M, Inoue S, Jung JU, Garcia-Sastre A**. 2009. Influenza A virus NS1 targets the ubiquitin ligase TRIM25 to evade recognition by the host viral RNA sensor RIG-I. Cell Host Microbe 5:439-49.

55. **Garcia-Sastre A**. 2010. Influenza virus receptor specificity: disease and transmission. Am J Pathol 176:1584-5.

56. **Garcia-Sastre A, Egorov A, Matassov D, Brandt S, Levy DE, Durbin JE, Palese P, Muster T**. 1998. Influenza A virus lacking the NS1 gene replicates in interferon-deficient systems. Virology 252:324-30.

57. **Graupera M, Guillermet-Guibert J, Foukas LC, Phng LK, Cain RJ, Salpekar A, Pearce W, Meek S, Millan J, Cutillas PR, Smith AJ, Ridley AJ, Ruhrberg C, Gerhardt H, Vanhaesebroeck B**. 2008. Angiogenesis selectively requires the p110alpha isoform of PI3K to control endothelial cell migration. Nature 453:662-6.

58. **Guillermet-Guibert J, Bjorklof K, Salpekar A, Gonella C, Ramadani F, Bilancio A, Meek S, Smith AJ, Okkenhaug K, Vanhaesebroeck B**. 2008. The p110beta isoform of phosphoinositide 3-kinase signals downstream of G protein-coupled receptors and is functionally redundant with p110gamma. Proc Natl Acad Sci U S A 105:8292-7.

59. **Hale BG, Barclay WS, Randall RE, Russell RJ**. 2008. Structure of an avian influenza A virus NS1 protein effector domain. Virology 378:1-5.

60. **Hale BG, Batty IH, Downes CP, Randall RE**. 2008. Binding of influenza A virus NS1 protein to the inter-SH2 domain of p85 suggests a novel mechanism for phosphoinositide 3-kinase activation. J Biol Chem 283:1372-1380.

61. **Hale BG, Jackson D, Chen YH, Lamb RA, Randall RE**. 2006. Influenza A virus NS1 protein binds p85beta and activates phosphatidylinositol-3-kinase signaling. Proc Natl Acad Sci U S A 103:14194-9.

62. **Hale BG, Kerry PS, Jackson D, Precious BL, Gray A, Killip MJ, Randall RE, Russell RJ**. 2010. Structural insights into phosphoinositide 3-kinase activation by the influenza A virus NS1 protein. Proc Natl Acad Sci U S A 107:1954-9.

63. **Hale BG, Randall RE, Ortin J, Jackson D**. 2008. The multifunctional NS1 protein of influenza A viruses. J Gen Virol 89:2359-2376.

64. **Haller O**. 2015. A tribute to Jean Lindenmann, co-discoverer of interferon (1924-2015). Cytokine 76:113-5.

65. **Hawkins PT, Anderson KE, Davidson K, Stephens LR**. 2006. Signalling through Class I PI3Ks in mammalian cells. Biochem Soc Trans 34:647-62.

66. **Hiles ID, Otsu M, Volinia S, Fry MJ, Gout I, Dhand R, Panayotou G, Ruiz-Larrea F, Thompson A, Totty NF, et al.** 1992. Phosphatidylinositol 3-kinase: structure and expression of the 110 kd catalytic subunit. Cell 70:419-29.

67. **Horisberger MA, Staeheli P, Haller O**. 1983. Interferon induces a unique protein in mouse cells bearing a gene for resistance to influenza virus. Proc Natl Acad Sci U S A 80:1910-4.

68. **Hu CD, Chinenov Y, Kerppola TK**. 2002. Visualization of interactions among bZIP and Rel family proteins in living cells using bimolecular fluorescence complementation. Mol Cell 9:789-98.

69. **Hu H, Zhang H, Wang S, Ding M, An H, Hou Y, Yang X, Wei W, Sun Y, Tang C**. 2017. Live visualization of genomic loci with BiFC-TALE. Sci Rep 7:40192.

70. **Huang CH, Mandelker D, Schmidt-Kittler O, Samuels Y, Velculescu VE, Kinzler KW, Vogelstein B, Gabelli SB, Amzel LM**. 2007. The structure of a human p110alpha/p85alpha complex elucidates the effects of oncogenic PI3Kalpha mutations. Science 318:1744-8.

71. **Inglis SC, Barrett T, Brown CM, Almond JW**. 1979. The smallest genome RNA segment of influenza virus contains two genes that may overlap. Proc Natl Acad Sci U S A 76:3790-4.

72. **Isaacs A, Lindenmann J**. 1957. Virus interference. I. The interferon. Proc R Soc Lond B Biol Sci 147:258-67.

73. **Isaacs A, Lindenmann J, Valentine RC**. 1957. Virus interference. II. Some properties of interferon. Proc R Soc Lond B Biol Sci 147:268-73.

74. **Jach G, Pesch M, Richter K, Frings S, Uhrig JF**. 2006. An improved mRFP1 adds red to bimolecular fluorescence complementation. Nat Methods 3:597-600.

75. **Jaiswal BS, Janakiraman V, Kljavin NM, Chaudhuri S, Stern HM, Wang W, Kan Z, Dbouk HA, Peters BA, Waring P, Dela Vega T, Kenski DM, Bowman KK, Lorenzo M, Li H, Wu J, Modrusan Z, Stinson J, Eby M, Yue P, Kaminker JS, de Sauvage FJ, Backer JM, Seshagiri S**. 2009. Somatic mutations in p85alpha promote tumorigenesis through class IA PI3K activation. Cancer Cell 16:463-74.

76. **Jimenez C, Portela RA, Mellado M, Rodriguez-Frade JM, Collard J, Serrano A, Martinez AC, Avila J, Carrera AC**. 2000. Role of the PI3K regulatory subunit in the control of actin organization and cell migration. J Cell Biol 151:249-62.

77. **Jovic M, Sharma M, Rahajeng J, Caplan S**. 2010. The early endosome: a busy sorting station for proteins at the crossroads. Histol Histopathol 25:99-112.

78. **Kabiljo J, Laengle J, Bergmann M**. 2020. From threat to cure: understanding of virus-induced cell death leads to highly immunogenic oncolytic influenza viruses. Cell Death Discov 6:48.

79. **Kaplan DR, Whitman M, Schaffhausen B, Pallas DC, White M, Cantley L, Roberts TM**. 1987. Common elements in growth factor stimulation and oncogenic transformation: 85 kd phosphoprotein and phosphatidylinositol kinase activity. Cell 50:1021-9.

80. **Karakus U, Mena I, Kottur J, El Zahed SS, Seoane R, Yildiz S, Chen L, Plancarte M, Lindsay L, Halpin R, Stockwell TB, Wentworth DE, Boons GJ, Krammer F, Stertz S, Boyce W, de Vries RP, Aggarwal AK, Garcia-Sastre A**. 2024. H19 influenza A virus exhibits species-specific MHC class II receptor usage. Cell Host Microbe 32:1089-1102 e10.

81. **Katze MG, Detjen BM, Safer B, Krug RM**. 1986. Translational control by influenza virus: suppression of the kinase that phosphorylates the alpha subunit of initiation factor eIF-2 and selective translation of influenza viral mRNAs. Mol Cell Biol 6:1741-50.

82. **Keraite I, Alvarez-Garcia V, Garcia-Murillas I, Beaney M, Turner NC, Bartos C, Oikonomidou O, Kersaudy-Kerhoas M, Leslie NR**. 2020. PIK3CA mutation enrichment and quantitation from blood and tissue. Sci Rep 10:17082.

83. **Kerry PS, Ayllon J, Taylor MA, Hass C, Lewis A, Garcia-Sastre A, Randall RE, Hale BG, Russell RJ**. 2011. A transient homotypic interaction model for the influenza A virus NS1 protein effector domain. PLoS One 6:e17946.

84. **Kochs G, Garcia-Sastre A, Martinez-Sobrido L**. 2007. Multiple anti-interferon actions of the influenza A virus NS1 protein. J Virol 81:7011-21.

85. **Kok K, Geering B, Vanhaesebroeck B**. 2009. Regulation of phosphoinositide 3-kinase expression in health and disease. Trends Biochem Sci 34:115-27.

86. **Kok K, Nock GE, Verrall EA, Mitchell MP, Hommes DW, Peppelenbosch MP, Vanhaesebroeck B**. 2009. Regulation of p110delta PI 3-kinase gene expression. PLoS One 4:e5145.

87. **Koliopoulos MG, Lethier M, van der Veen AG, Haubrich K, Hennig J, Kowalinski E, Stevens RV, Martin SR, Reis e Sousa C, Cusack S, Rittinger K**. 2018. Molecular mechanism of influenza A NS1-mediated TRIM25 recognition and inhibition. Nat Commun 9:1820.

88. **Krammer F, Smith GJD, Fouchier RAM, Peiris M, Kedzierska K, Doherty PC, Palese P, Shaw ML, Treanor J, Webster RG, Garcia-Sastre A**. 2018. Influenza. Nat Rev Dis Primers 4:3.

89. **Krammer FP, Peter**. 2021. Orthomyxoviridae: The Viruses and Their Replication. *In* Howley PMK, David M. (ed), Fields Virology: Emerging viruses. Lippincott Willians & Wilkins, Philadelphia.

90. **Krug RM**. 2014. Viral proteins that bind double-stranded RNA: countermeasures against host antiviral responses. J Interferon Cytokine Res 34:464-8.

91. **Kubo H, Hazeki K, Takasuga S, Hazeki O**. 2005. Specific role for p85/p110beta in GTP-binding-protein-mediated activation of Akt. Biochem J 392:607-14.

92. **Kurosu H, Katada T**. 2001. Association of phosphatidylinositol 3-kinase composed of p110beta-catalytic and p85-regulatory subunits with the small GTPase Rab5. J Biochem 130:73-8.

93. **Kurosu H, Maehama T, Okada T, Yamamoto T, Hoshino S, Fukui Y, Ui M, Hazeki O, Katada T**. 1997. Heterodimeric phosphoinositide 3-kinase consisting of p85 and p110beta is synergistically activated by the betagamma subunits of G proteins and phosphotyrosyl peptide. J Biol Chem 272:24252-6.

94. **Lamb RA, Choppin PW**. 1979. Segment 8 of the influenza virus genome is unique in coding for two polypeptides. Proc Natl Acad Sci U S A 76:4908-12.

95. **Lamb RA, Lai CJ**. 1980. Sequence of interrupted and uninterrupted mRNAs and cloned DNA coding for the two overlapping nonstructural proteins of influenza virus. Cell 21:475-85.

96. **Lazarowitz SG, Compans RW, Choppin PW**. 1971. Influenza virus structural and nonstructural proteins in infected cells and their plasma membranes. Virology 46:830-43.

97. **Li S, Min JY, Krug RM, Sen GC**. 2006. Binding of the influenza A virus NS1 protein to PKR mediates the inhibition of its activation by either PACT or double-stranded RNA. Virology 349:13-21.

98. **Li Y, Anderson DH, Liu Q, Zhou Y**. 2008. Mechanism of influenza A virus NS1 protein interaction with the p85beta, but not the p85alpha, subunit of phosphatidylinositol 3-kinase (PI3K) and up-regulation of PI3K activity. J Biol Chem 283:23397-409.

99. **Ligresti G, Militello L, Steelman LS, Cavallaro A, Basile F, Nicoletti F, Stivala F, McCubrey JA, Libra M**. 2009. PIK3CA mutations in human solid tumors: role in sensitivity to various therapeutic approaches. Cell Cycle 8:1352-8.

100. **Lindenmann J**. 1962. Resistance of mice to mouse-adapted influenza A virus. Virology 16:203-4.

101. **Liu J, Lynch PA, Chien CY, Montelione GT, Krug RM, Berman HM**. 1997. Crystal structure of the unique RNA-binding domain of the influenza virus NS1 protein. Nat Struct Biol 4:896-9.

102. **Liu R, Chen Y, Liu G, Li C, Song Y, Cao Z, Li W, Hu J, Lu C, Liu Y**. 2020. PI3K/AKT pathway as a key link modulates the multidrug resistance of cancers. Cell Death Dis 11:797.

103. **Lowen AC**. 2017. Constraints, Drivers, and Implications of Influenza A Virus Reassortment. Annu Rev Virol 4:105-121.

104. **Lu Y, Wambach M, Katze MG, Krug RM**. 1995. Binding of the influenza virus NS1 protein to double-stranded RNA inhibits the activation of the protein kinase that phosphorylates the elF-2 translation initiation factor. Virology 214:222-8.

105. **Ludwig S, Schultz U, Mandler J, Fitch WM, Scholtissek C**. 1991. Phylogenetic relationship of the nonstructural (NS) genes of influenza A viruses. Virology 183:566-77.

106. **Maehama T, Dixon JE**. 1999. PTEN: a tumour suppressor that functions as a phospholipid phosphatase. Trends Cell Biol 9:125-8.

107. **Matsuda M, Mayer BJ, Fukui Y, Hanafusa H**. 1990. Binding of transforming protein, P47gag-crk, to a broad range of phosphotyrosine-containing proteins. Science 248:1537-9.

108. **McMullen JR, Shioi T, Zhang L, Tarnavski O, Sherwood MC, Kang PM, Izumo S**. 2003. Phosphoinositide 3-kinase(p110alpha) plays a critical role for the induction of physiological, but not pathological, cardiac hypertrophy. Proc Natl Acad Sci U S A 100:12355-60.

109. **Mellor P, Furber LA, Nyarko JN, Anderson DH**. 2012. Multiple roles for the p85alpha isoform in the regulation and function of PI3K signalling and receptor trafficking. Biochem J 441:23-37.

110. **Mibayashi M, Martinez-Sobrido L, Loo YM, Cardenas WB, Gale M, Jr., Garcia-Sastre A**. 2007. Inhibition of retinoic acid-inducible gene I-mediated induction of beta interferon by the NS1 protein of influenza A virus. J Virol 81:514-24.

111. **Min JY, Krug RM**. 2006. The primary function of RNA binding by the influenza A virus NS1 protein in infected cells: Inhibiting the 2'-5' oligo (A) synthetase/RNase L pathway. Proc Natl Acad Sci U S A 103:7100-5.

112. **Min JY, Li S, Sen GC, Krug RM**. 2007. A site on the influenza A virus NS1 protein mediates both inhibition of PKR activation and temporal regulation of viral RNA synthesis. Virology 363:236-43.

113. **Monteagudo PL, Munoz-Moreno R, Fribourg M, Potla U, Mena I, Marjanovic N, Hartmann BM, Sealfon SC, Garcia-Sastre A, Ramos I, Fernandez-Sesma A**. 2019. Differential Modulation of Innate Immune Responses in Human Primary Cells by Influenza A Viruses Carrying Human or Avian Nonstructural Protein 1. J Virol 94.

114. **Mora A, Komander D, van Aalten DM, Alessi DR**. 2004. PDK1, the master regulator of AGC kinase signal transduction. Semin Cell Dev Biol 15:161-70.

115. **Moran MF, Koch CA, Anderson D, Ellis C, England L, Martin GS, Pawson T**. 1990. Src homology region 2 domains direct protein-protein interactions in signal transduction. Proc Natl Acad Sci U S A 87:8622-6.

116. **Murray JT, Panaretou C, Stenmark H, Miaczynska M, Backer JM**. 2002. Role of Rab5 in the recruitment of hVps34/p150 to the early endosome. Traffic 3:416-27.

117. **Nagappan R, Flegel WA, Srivastava K, Williams EC, Ryzhov I, Tuzikov A, Galanina O, Shilova N, Sukhikh G, Perry H, Bovin NV, Henry SM**. 2021. COVID-19 antibody screening with SARS-CoV-2 red cell kodecytes using routine serologic diagnostic platforms. Transfusion 61:1171-1180.

118. **Nemeroff ME, Barabino SM, Li Y, Keller W, Krug RM**. 1998. Influenza virus NS1 protein interacts with the cellular 30 kDa subunit of CPSF and inhibits 3'end formation of cellular pre-mRNAs. Mol Cell 1:991-1000.

119. **Neumann G, Treanor, John J. & Kawaoka, Yoshihiro**. 2021. Orthomyxoviruses. *In* Howley PMK, David M. (ed), Fields Virology: Emerging Viruses. Lippincott Willians & Wilkins, Philadelphia.

120. **Neumann G, Watanabe T, Ito H, Watanabe S, Goto H, Gao P, Hughes M, Perez DR, Donis R, Hoffmann E, Hobom G, Kawaoka Y**. 1999. Generation of influenza A viruses entirely from cloned cDNAs. Proc Natl Acad Sci U S A 96:9345-50.

121. **Newcomb LL, Kuo RL, Ye Q, Jiang Y, Tao YJ, Krug RM**. 2009. Interaction of the influenza a virus nucleocapsid protein with the viral RNA polymerase potentiates unprimed viral RNA replication. J Virol 83:29-36.

122. **Niwa H, Yamamura K, Miyazaki J**. 1991. Efficient selection for high-expression transfectants with a novel eukaryotic vector. Gene 108:193-9.

123. **Noda T, Kawaoka Y**. 2010. Structure of influenza virus ribonucleoprotein complexes and their packaging into virions. Rev Med Virol 20:380-91.

124. **Noorolyai S, Shajari N, Baghbani E, Sadreddini S, Baradaran B**. 2019. The relation between PI3K/AKT signalling pathway and cancer. Gene 698:120-128.

125. **Nypaver C, Dehlinger C, Carter C**. 2021. Influenza and Influenza Vaccine: A Review. J Midwifery Womens Health 66:45-53.

126. **O'Brien MC, Fukui Y, Hanafusa H**. 1990. Activation of the proto-oncogene p60c-src by point mutations in the SH2 domain. Mol Cell Biol 10:2855-62.

127. **Osaki M, Oshimura M, Ito H**. 2004. PI3K-Akt pathway: its functions and alterations in human cancer. Apoptosis 9:667-76.

128. **Otsu M, Hiles I, Gout I, Fry MJ, Ruiz-Larrea F, Panayotou G, Thompson A, Dhand R, Hsuan J, Totty N, et al.** 1991. Characterization of two 85 kd proteins that associate with receptor tyrosine kinases, middle-T/pp60c-src complexes, and PI3-kinase. Cell 65:91-104.

129. **Papakonstanti EA, Zwaenepoel O, Bilancio A, Burns E, Nock GE, Houseman B, Shokat K, Ridley AJ, Vanhaesebroeck B**. 2008. Distinct roles of class IA PI3K isoforms in primary and immortalised macrophages. J Cell Sci 121:4124-33.

130. **Park SW, Zhou Y, Lee J, Lu A, Sun C, Chung J, Ueki K, Ozcan U**. 2010. The regulatory subunits of PI3K, p85alpha and p85beta, interact with XBP-1 and increase its nuclear translocation. Nat Med 16:429-37.

131. **Pereira CF, Wise HM, Kurian D, Pinto RM, Amorim MJ, Gill AC, Digard P**. 2018. Effects of mutations in the effector domain of influenza A virus NS1 protein. BMC Res Notes 11:673.

132. **Pflug A, Lukarska M, Resa-Infante P, Reich S, Cusack S**. 2017. Structural insights into RNA synthesis by the influenza virus transcription-replication machine. Virus Res 234:103-117.

133. **Pleschka S, Wolff T, Ehrhardt C, Hobom G, Planz O, Rapp UR, Ludwig S**. 2001. Influenza virus propagation is impaired by inhibition of the Raf/MEK/ERK signalling cascade. Nat Cell Biol 3:301-5.

134. **Rajsbaum R, Albrecht RA, Wang MK, Maharaj NP, Versteeg GA, Nistal-Villan E, Garcia-Sastre A, Gack MU**. 2012. Species-specific inhibition of RIG-I ubiquitination and IFN induction by the influenza A virus NS1 protein. PLoS Pathog 8:e1003059.

135. **Rascio F, Spadaccino F, Rocchetti MT, Castellano G, Stallone G, Netti GS, Ranieri E**. 2021. The Pathogenic Role of PI3K/AKT Pathway in Cancer Onset and Drug Resistance: An Updated Review. Cancers (Basel) 13.

136. **Ravikumar B, Imarisio S, Sarkar S, O'Kane CJ, Rubinsztein DC**. 2008. Rab5 modulates aggregation and toxicity of mutant huntingtin through macroautophagy in cell and fly models of Huntington disease. J Cell Sci 121:1649-60.

137. **Ren H, Ou Q, Pu Q, Lou Y, Yang X, Han Y, Liu S**. 2024. Comprehensive Review on Bimolecular Fluorescence Complementation and Its Application in Deciphering Protein-Protein Interactions in Cell Signaling Pathways. Biomolecules 14.

138. **Rordorf-Nikolic T, Van Horn DJ, Chen D, White MF, Backer JM**. 1995. Regulation of phosphatidylinositol 3'-kinase by tyrosyl phosphoproteins. Full activation requires occupancy of both SH2 domains in the 85-kDa regulatory subunit. J Biol Chem 270:3662-6.

139. **Safaroghli-Azar A, Sanaei MJ, Pourbagheri-Sigaroodi A, Bashash D**. 2023. Phosphoinositide 3-kinase (PI3K) classes: From cell signaling to endocytic recycling and autophagy. Eur J Pharmacol 953:175827.

140. **Samji T**. 2009. Influenza A: understanding the viral life cycle. Yale J Biol Med 82:153-9.

141. **Samuels Y, Wang Z, Bardelli A, Silliman N, Ptak J, Szabo S, Yan H, Gazdar A, Powell SM, Riggins GJ, Willson JK, Markowitz S, Kinzler KW, Vogelstein B, Velculescu VE**. 2004. High frequency of mutations of the PIK3CA gene in human cancers. Science 304:554.

142. **Sanchez-Aparicio MT, Ayllon J, Leo-Macias A, Wolff T, Garcia-Sastre A**. 2017. Subcellular Localizations of RIG-I, TRIM25, and MAVS Complexes. J Virol 91.

143. **Sarbassov DD, Guertin DA, Ali SM, Sabatini DM**. 2005. Phosphorylation and regulation of Akt/PKB by the rictor-mTOR complex. Science 307:1098-101.

144. **Saunders-Hastings PR, Krewski D**. 2016. Reviewing the History of Pandemic Influenza: Understanding Patterns of Emergence and Transmission. Pathogens 5.

145. **Sawyer C, Sturge J, Bennett DC, O'Hare MJ, Allen WE, Bain J, Jones GE, Vanhaesebroeck B**. 2003. Regulation of breast cancer cell chemotaxis by the phosphoinositide 3-kinase p110delta. Cancer Res 63:1667-75.

146. **Schmidt U, Richter K, Berger AB, Lichter P**. 2006. In vivo BiFC analysis of Y14 and NXF1 mRNA export complexes: preferential localization within and around SC35 domains. J Cell Biol 172:373-81.

147. **Selman M, Dankar SK, Forbes NE, Jia JJ, Brown EG**. 2012. Adaptive mutation in influenza A virus non-structural gene is linked to host switching and induces a novel protein by alternative splicing. Emerg Microbes Infect 1:e42.

148. **Shaw ML, & Palese, Peter**. 2013. Orthomyxoviridae, Fields Virology, sixth ed, vol 1. Wolters Kluwer Health Adis (ESP).

149. **Shi H, Hugo W, Kong X, Hong A, Koya RC, Moriceau G, Chodon T, Guo R, Johnson DB, Dahlman KB, Kelley MC, Kefford RF, Chmielowski B, Glaspy JA, Sosman JA, van Baren N, Long GV, Ribas A, Lo RS**. 2014. Acquired resistance and clonal evolution in melanoma during BRAF inhibitor therapy. Cancer Discov 4:80-93.

150. **Shimomura O, Johnson FH, Saiga Y**. 1962. Extraction, purification and properties of aequorin, a bioluminescent protein from the luminous hydromedusan, Aequorea. J Cell Comp Physiol 59:223-39.

151. **Shin YK, Liu Q, Tikoo SK, Babiuk LA, Zhou Y**. 2007. Influenza A virus NS1 protein activates the phosphatidylinositol 3-kinase (PI3K)/Akt pathway by direct interaction with the p85 subunit of PI3K. J Gen Virol 88:13-18.

152. **Siempelkamp BD, Rathinaswamy MK, Jenkins ML, Burke JE**. 2017. Molecular mechanism of activation of class IA phosphoinositide 3-kinases (PI3Ks) by membrane-localized HRas. J Biol Chem 292:12256-12266.

153. **Silverman RH**. 2007. Viral encounters with 2',5'-oligoadenylate synthetase and RNase L during the interferon antiviral response. J Virol 81:12720-9.

154. **Simonsen A, Lippe R, Christoforidis S, Gaullier JM, Brech A, Callaghan J, Toh BH, Murphy C, Zerial M, Stenmark H**. 1998. EEA1 links PI(3)K function to Rab5 regulation of endosome fusion. Nature 394:494-8.

155. **Skolnik EY, Margolis B, Mohammadi M, Lowenstein E, Fischer R, Drepps A, Ullrich A, Schlessinger J**. 1991. Cloning of PI3 kinase-associated p85 utilizing a novel method for expression/cloning of target proteins for receptor tyrosine kinases. Cell 65:83-90.

156. **Songyang Z, Shoelson SE, Chaudhuri M, Gish G, Pawson T, Haser WG, King F, Roberts T, Ratnofsky S, Lechleider RJ, et al.** 1993. SH2 domains recognize specific phosphopeptide sequences. Cell 72:767-78.

157. **Stommel JM, Kimmelman AC, Ying H, Nabioullin R, Ponugoti AH, Wiedemeyer R, Stegh AH, Bradner JE, Ligon KL, Brennan C, Chin L, DePinho RA**. 2007. Coactivation of receptor tyrosine kinases affects the response of tumor cells to targeted therapies. Science 318:287-90.

158. **Tandon N, Thakkar KN, LaGory EL, Liu Y, Giaccia AJ**. 2018. Generation of Stable Expression Mammalian Cell Lines Using Lentivirus. Bio Protoc 8.

159. **Thitithanyanont A, Engering A, Ekchariyawat P, Wiboon-ut S, Limsalakpetch A, Yongvanitchit K, Kum-Arb U, Kanchongkittiphon W, Utaisincharoen P, Sirisinha S, Puthavathana P, Fukuda MM, Pichyangkul S**. 2007. High susceptibility of human dendritic cells to avian influenza H5N1 virus infection and protection by IFN-alpha and TLR ligands. J Immunol 179:5220-7.

160. **Tran H, Brunet A, Griffith EC, Greenberg ME**. 2003. The many forks in FOXO's road. Sci STKE 2003:RE5.

161. **Treanor JJ, Snyder MH, London WT, Murphy BR**. 1989. The B allele of the NS gene of avian influenza viruses, but not the A allele, attenuates a human influenza A virus for squirrel monkeys. Virology 171:1-9.

162. **Twu KY, Kuo RL, Marklund J, Krug RM**. 2007. The H5N1 influenza virus NS genes selected after 1998 enhance virus replication in mammalian cells. J Virol 81:8112-21.

163. **Twu KY, Noah DL, Rao P, Kuo RL, Krug RM**. 2006. The CPSF30 binding site on the NS1A protein of influenza A virus is a potential antiviral target. J Virol 80:3957-65.

164. **Ueki K, Fruman DA, Brachmann SM, Tseng YH, Cantley LC, Kahn CR**. 2002. Molecular balance between the regulatory and catalytic subunits of phosphoinositide 3-kinase regulates cell signaling and survival. Mol Cell Biol 22:965-77.

165. **Vallejo-Diaz J, Chagoyen M, Olazabal-Moran M, Gonzalez-Garcia A, Carrera AC**. 2019. The Opposing Roles of PIK3R1/p85alpha and PIK3R2/p85beta in Cancer. Trends Cancer 5:233-244.

166. **Vandal G, Geiling B, Dankort D**. 2014. Ras effector mutant expression suggest a negative regulator inhibits lung tumor formation. PLoS One 9:e84745.

167. **Vanhaesebroeck B, Leevers SJ, Panayotou G, Waterfield MD**. 1997. Phosphoinositide 3-kinases: a conserved family of signal transducers. Trends Biochem Sci 22:267-72.

168. **Vanhaesebroeck B, Stephens L, Hawkins P**. 2012. PI3K signalling: the path to discovery and understanding. Nat Rev Mol Cell Biol 13:195-203.

169. **Vlahos CJ, Matter WF, Hui KY, Brown RF**. 1994. A specific inhibitor of phosphatidylinositol 3-kinase, 2-(4-morpholinyl)-8-phenyl-4H-1-benzopyran-4-one (LY294002). J Biol Chem 269:5241-8.

170. **Wahle E, Keller W**. 1996. The biochemistry of polyadenylation. Trends Biochem Sci 21:247-50.

171. **Walker EH, Perisic O, Ried C, Stephens L, Williams RL**. 1999. Structural insights into phosphoinositide 3-kinase catalysis and signalling. Nature 402:313-20.

172. **Wan G, Pehlke C, Pepermans R, Cannon JL, Lidke D, Rajput A**. 2015. The H1047R point mutation in p110 alpha changes the morphology of human colon HCT116 cancer cells. Cell Death Discov 1:15044.

173. **Wang C, Puerta-Guardo H, Biering SB, Glasner DR, Tran EB, Patana M, Gomberg TA, Malvar C, Lo NTN, Espinosa DA, Harris E**. 2019. Endocytosis of flavivirus NS1 is required for NS1-mediated endothelial hyperpermeability and is abolished by a single N-glycosylation site mutation. PLoS Pathog 15:e1007938.

174. **Wang J, An Z, Wu Z, Zhou W, Sun P, Wu P, Dang S, Xue R, Bai X, Du Y, Chen R, Wang W, Huang P, Lam SM, Ai Y, Liu S, Shui G, Zhang Z, Liu Z, Huang J, Fang X, He K**. 2024. Spatial organization of PI3K-PI(3,4,5)P(3)-AKT signaling by focal adhesions. Mol Cell 84:4401-4418 e9.

175. **Wang W, Riedel K, Lynch P, Chien CY, Montelione GT, Krug RM**. 1999. RNA binding by the novel helical domain of the influenza virus NS1 protein requires its dimer structure and a small number of specific basic amino acids. RNA 5:195-205.

176. **Weis S, Te Velthuis AJW**. 2021. Influenza Virus RNA Synthesis and the Innate Immune Response. Viruses 13.

177. **Whitman M, Downes CP, Keeler M, Keller T, Cantley L**. 1988. Type I phosphatidylinositol kinase makes a novel inositol phospholipid, phosphatidylinositol-3-phosphate. Nature 332:644-6.

178. **Wille M, Holmes EC**. 2020. The Ecology and Evolution of Influenza Viruses. Cold Spring Harb Perspect Med 10.

179. **Winnay JN, Boucher J, Mori MA, Ueki K, Kahn CR**. 2010. A regulatory subunit of phosphoinositide 3-kinase increases the nuclear accumulation of X-box-binding protein-1 to modulate the unfolded protein response. Nat Med 16:438-45.

180. **Winnay JN, Kahn CR**. 2011. PI 3-kinase regulatory subunits as regulators of the unfolded protein response. Methods Enzymol 490:147-58.

181. **Wright SCE, Vasilevski N, Serra V, Rodon J, Eichhorn PJA**. 2021. Mechanisms of Resistance to PI3K Inhibitors in Cancer: Adaptive Responses, Drug Tolerance and Cellular Plasticity. Cancers (Basel) 13.

182. **Wu NC, Wilson IA**. 2020. Influenza Hemagglutinin Structures and Antibody Recognition. Cold Spring Harb Perspect Med 10.

183. **Yano H, Nakanishi S, Kimura K, Hanai N, Saitoh Y, Fukui Y, Nonomura Y, Matsuda Y**. 1993. Inhibition of histamine secretion by wortmannin through the blockade of phosphatidylinositol 3-kinase in RBL-2H3 cells. J Biol Chem 268:25846-56.

184. **Yin J, Zhu D, Zhang Z, Wang W, Fan J, Men D, Deng J, Wei H, Zhang XE, Cui Z**. 2013. Imaging of mRNA-protein interactions in live cells using novel mCherry trimolecular fluorescence complementation systems. PLoS One 8:e80851.

185. **Yin Y, Terauchi Y, Solomon GG, Aizawa S, Rangarajan PN, Yazaki Y, Kadowaki T, Barrett JC**. 1998. Involvement of p85 in p53-dependent apoptotic response to oxidative stress. Nature 391:707-10.

186. **York A, Hengrung N, Vreede FT, Huiskonen JT, Fodor E**. 2013. Isolation and characterization of the positive-sense replicative intermediate of a negative-strand RNA virus. Proc Natl Acad Sci U S A 110:E4238-45.

187. **Zhou B, Donnelly ME, Scholes DT, St George K, Hatta M, Kawaoka Y, Wentworth DE**. 2009. Single-reaction genomic amplification accelerates sequencing and vaccine production for classical and Swine origin human influenza a viruses. J Virol 83:10309-13.

188. **Zhou B, Lin X, Wang W, Halpin RA, Bera J, Stockwell TB, Barr IG, Wentworth DE**. 2014. Universal influenza B virus genomic amplification facilitates sequencing, diagnostics, and reverse genetics. J Clin Microbiol 52:1330-7.

189. **Zvelebil MJ, MacDougall L, Leevers S, Volinia S, Vanhaesebroeck B, Gout I, Panayotou G, Domin J, Stein R, Pages F, et al.** 1996. Structural and functional diversity of phosphoinositide 3-kinases. Philos Trans R Soc Lond B Biol Sci 351:217-23.

7. References

8. Publications

8. Publications

List of scientific publications co-authored during the development of this thesis.

1. **Aslam, S.**, Sánchez-Aparicio MT, Siempelkamp BD, Dornan GL, Tsolakos N, Burke JE, Hale BG, García-Sastre A, Ayllon J. *Influenza A virus NS1 protein mimics oncogenic PI3K resulting in isoform specific cellular redistribution and activation*. *Proc Natl Acad Sci U S A*. 2025 Aug 12;122(32):e2423066122. doi: 10.1073/pnas.2423066122. Epub 2025 Aug 4. PMID: 40758871.
2. Zhang K, Cagatay T, Xie D, Angelos AE, Cornelius S, Aksenova V, **Aslam, S.**, He Z, Esparza M, Vazhavilla A, Dasso M, García-Sastre A, Ren Y, Fontoura BMA. *Cellular NS1-BP protein interacts with the mRNA export receptor NXF1 to mediate nuclear export of influenza virus M mRNAs*. *J Biol Chem*. 2024 Nov;300(11):107871. doi: 10.1016/j.jbc.2024.107871. Epub 2024 Oct 9. PMID: 39384042.
3. Rathnasinghe R, Chang LA, Pearl R, Jangra S, Aspelund A, Hoag A, Yildiz S, Mena I, Sun W, Loganathan M, Crossland NA, Gertje HP, Tseng AE, **Aslam, S.**, Albrecht RA, Palese P, Krammer F, Schotsaert M, Muster T, García-Sastre A. *Sequential immunization with chimeric hemagglutinin ΔNS1 attenuated influenza vaccines induces broad humoral and cellular immunity*. *NPJ Vaccines*. 2024 Sep 16;9(1):169. doi: 10.1038/s41541-024-00952-7. PMID: 39300090.
4. Mei M, Cupic A, Miorin L, Ye C, Cagatay T, Zhang K, Patel K, Wilson N, McDonald WH, Crossland NA, Lo M, Rutkowska M, **Aslam, S.**, Mena I, Martinez-Sobrido L, Ren Y, García-Sastre A, Fontoura BMA. *Inhibition of mRNA nuclear export promotes SARS-CoV-2 pathogenesis*. *Proc Natl Acad Sci U S A*. 2024 May 28;121(22):e2314166121. doi: 10.1073/pnas.2314166121. Epub 2024 May 20. PMID: 38768348.
5. Diego JG, Singh G, Jangra S, Handrejk K, Laporte M, Chang LA, El Zahed SS, Pache L, Chang MW, Warang P, **Aslam, S.**, Mena I, Webb BT, Benner C, García-Sastre A, Schotsaert M. *Breakthrough infections by SARS-CoV-2 variants boost cross-reactive hybrid immune responses in mRNA-vaccinated Golden Syrian hamsters*. *PLoS Pathog*. 2024 Jan 10;20(1):e1011805. doi: 10.1371/journal.ppat.1011805. PMID: 38198521.
6. Kehrer T, Cupic A, Ye C, Yildiz S, Bouhaddou M, Crossland NA, Barrall EA, Cohen P, Tseng A, Çağatay T, Rathnasinghe R, Flores D, Jangra S, Alam F, Mena I, **Aslam, S.**, Saqi A, Rutkowska M, Ummadi MR, Pisanelli G, Richardson RB, et al. *Impact of SARS-CoV-2 ORF6 and its variant polymorphisms on host responses and viral pathogenesis*. *Cell Host Microbe*. 2023 Oct 11;31(10):1668-1684.e12. doi: 10.1016/j.chom.2023.08.003. PMID: 37738983.
7. Bouhaddou M, Reuschl AK, Polacco BJ, Thorne LG, Ummadi MR, Ye C, Rosales R, Pelin A, Batra J, Jang GM, Xu J, Moen JM, Richards AL, Zhou Y, Harjai B, Stevenson E, Rojc A, Ragazzini R, Whelan MVX, Furnon W, De Lorenzo G, Cowton V, Syed AM, Ciling A, Deutsch N, Pirak D, Dowgier G, Mesner D, Turner JL, McGovern BL, Rodriguez ML, Leiva-Rebollo R, Dunham AS, Zhong X, Eckhardt M, Fossati A, Liotta NF, Kehrer T, Cupic A, Rutkowska M, Mena I, **Aslam, S.**, Hoffert A, Foussard H, Olwal CO, Huang W, Zwaka T, Pham J, Lyons M, Donohue L, Griffin A, Nugent R, Holden K, Deans R, Aviles P, Lopez-Martin JA, Jimeno JM, Obernier K, Fabius JM, Soucheray M, Hüttenhain R,

Jungreis I, Kellis M, Echeverria I, Verba K, Bonfanti P, Beltrao P, Sharan R, Doudna JA, Martinez-Sobrido L, Patel AH, Palmarini M, Miorin L, White K, Swaney DL, Garcia-Sastre A, Jolly C, Zuliani-Alvarez L, Towers GJ, Krogan NJ. *SARS-CoV-2 variants evolve convergent strategies to remodel the host response*. *Cell*. 2023 Oct 12;186(21):4597-4614.e26. doi: 10.1016/j.cell.2023.08.026. PMID: 37738970.

8. Bhat P, Aksenova V, Gazzara M, Rex EA, **Aslam, S.**, Haddad C, Gao S, Esparza M, Cagatay T, Batten K, El Zahed SS, Arnaoutov A, Zhong H, Shay JW, Tolbert BS, Dasso M, Lynch KW, García-Sastre A, Fontoura BMA. *Influenza virus mRNAs encode determinants for nuclear export via the cellular TREX-2 complex*. *Nat Commun*. 2023 Apr 21;14(1):2304. doi: 10.1038/s41467-023-37911-0. PMID: 37085480.

9. **Aslam, S.**, Rajendran M, Kriti D, Kurland A, Johnson J, van Bakel H, Krammer F, García-Sastre A, Ayllon J. *Generation of a high yield vaccine backbone for influenza B virus in embryonated chicken eggs*. *NPJ Vaccines*. 2023 Feb 10;8(1):12. doi: 10.1038/s41541-023-00603-3. PMID: 36765053.

10. Rathnasinghe R, Jangra S, Ye C, Cupic A, Singh G, Martínez-Romero C, Mulder LCF, Kehrer T, Yildiz S, Choi A, Yeung ST, Mena I, Gillespie V, De Vrieze J, **Aslam, S.**, Stadlbauer D, Meekins DA, McDowell CD, Balaraman V, Corley MJ, Richt JA, De Geest BG, Miorin L; PVI study group; Krammer F, Martinez-Sobrido L, Simon V, García-Sastre A, Schotsaert M. *Characterization of SARS-CoV-2 Spike mutations important for infection of mice and escape from human immune sera*. *Nat Commun*. 2022 Jul 7;13(1):3921. doi: 10.1038/s41467-022-30763-0. PMID: 35798721.

11. van der Heide V, Jangra S, Cohen P, Rathnasinghe R, **Aslam, S.**, Aydillo T, Geanon D, Handler D, Kelley G, Lee B, Rahman A, Dawson T, Qi J, D'Souza D, Kim-Schulze S, Panzer JK, Caicedo A, Kusmartseva I, Posgai AL, Atkinson MA, Albrecht RA, García-Sastre A, Rosenberg BR, Schotsaert M, Homann D. *Limited extent and consequences of pancreatic SARS-CoV-2 infection*. *Cell Rep*. 2022 Mar 15;38(11):110508. doi: 10.1016/j.celrep.2022.110508. PMID: 35247306.

12. Escalera, A., Gonzalez-Reiche, A. S., **Aslam, S.**, Mena, I., Laporte, M., Pearl, R. L., Fossati, A., Rathnasinghe, R., Alshammary, H., van de Guchte, A., Farrugia, K., Qin, Y., Bouhaddou, M., Kehrer, T., Zuliani-Alvarez, L., Meekins, D. A., Balaraman, V., McDowell, C., Richt, J. A., Bajic, G., … Aydillo, T. (2022). Mutations in SARS-CoV-2 variants of concern link to increased spike cleavage and virus transmission. Cell host & microbe, 30(3), 373–387.e7. https://doi.org/10.1016/j.chom.2022.01.006

8. Publications

9. Appendix I

9. Appendix I

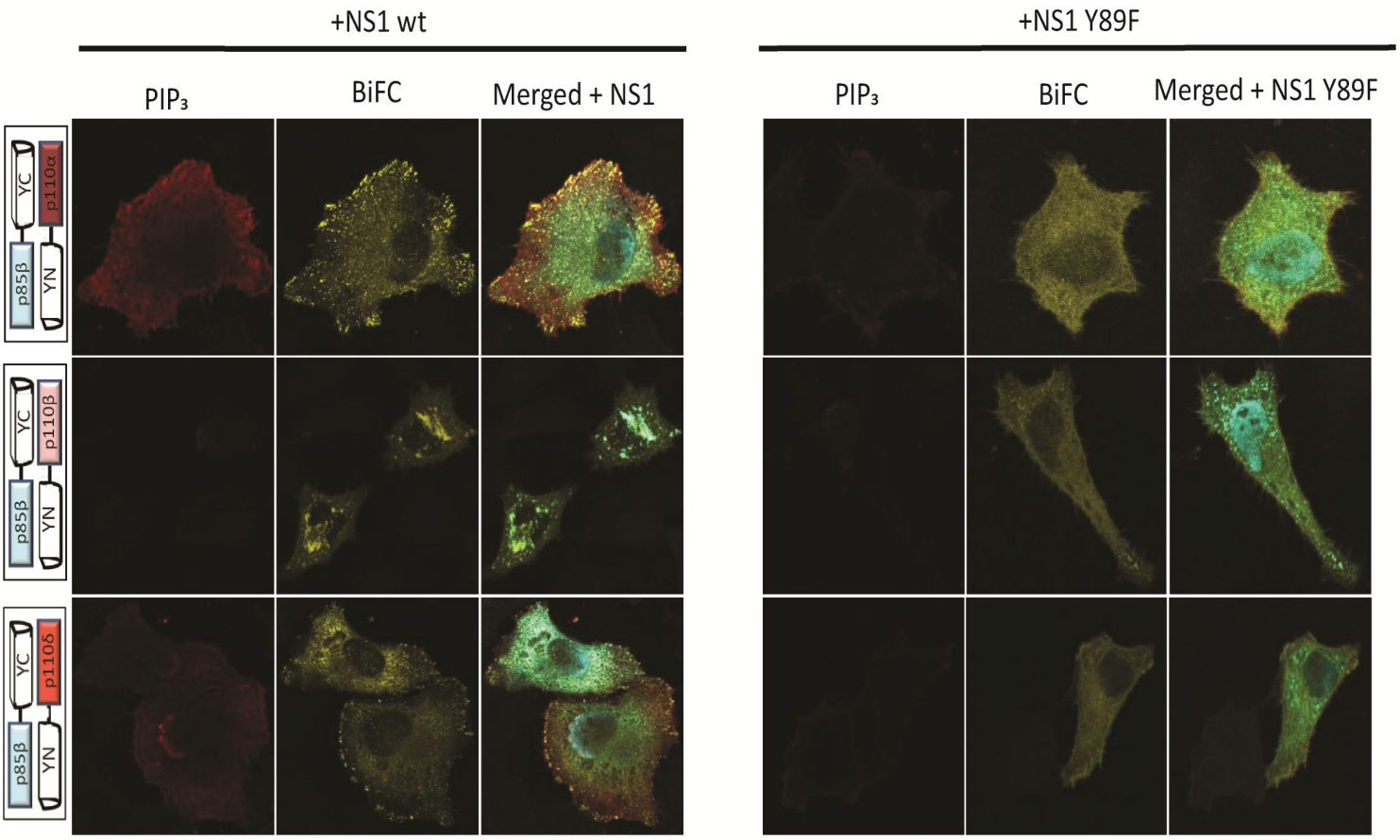

Figure 47. Controls
We tested wt p110x and wild type p85β with NS1 as controls (D). (PIP_3 in red, NS1 and DAPI in cyan, BiFC in yellow and Phalloidin in cyan).

9. Appendix I

10. Appendix II

Sequences used in the generation of the split YFP system

The YFP sequence was obtained from GenBank (GQ221700.1) to generate the YFP system as described by Hu et al (68).

YN (Amino acid 1-154)

Nucleotide sequence

atgtccaagggcgaggagctgttcaccggcgtggtgcctatcctcgtggagctcgacggcgacgtgaacggccacaagttcagcgtgtcc
ggcgagggcgagggcgacgccacctacggcaagctgaccctgaagttcatctgcaccaccggcaagctcccggtgccatggccaaccc
tggtgaccaccttcggctacggcctgcagtgcttcgccaggtaccccgaccacatgaagaggcacgacttcttcaagagcgccatgccag
agggctacgtgcaggagaggaccatcttcttcaaggacgacggcaactacaagaccagggccgaggtgaagttcgagggcgacaccct
ggtgaacaggatcgagctgaagggcatcgacttcaaggaggacggcaacatcctgggccacaagctggagtacaactacaactcccaca
acgtgtacatcatggcc

Amino acid sequence

MSKGEELFTGVVPILVELDGDVNGHKFSVSGEGEGDATYGKLTLKFICTTGKLPVPWPTLVTTFG
YGLQCFARYPDHMKRHDFFKSAMPEGYVQERTIFFKDDGNYKTRAEVKFEGDTLVNRIELKGID
FKEDGNILGHKLEYNYNSHNVYIMA

YC (Amino acid 155-238)

Nucleotide sequence

gacaagcagaagaacggcatcaaggtgaacttcaagatccgccacaacatcgaggacggctccgtgcagctggccgaccactaccagc
agaacaccccaatcggcgacggcccggtgctcctccctgacaaccactacctcagctaccagtccgccctcagcaaggacccgaacgag
aagagggaccacatggtgctgctggagttcgtgaccgccgccggcatcacccacggcatggacgagctctacaag

Amino acid sequence

DKQKNGIKVNFKIRHNIEDGSVQLADHYQQNTPIGDGPVLLPDNHYLSYQSALSKDPNEKRDHM
VLLEFVTAAGITHGMDELYK

10. Appendix II

11. Appendix III

11. Appendix III

Influenza A virus NS1 protein mimics oncogenic PI3K resulting in isoform specific cellular redistribution and activation

Sadaf Aslam[1,2,7], María T. Sánchez-Aparicio[1,2], Braden D. Siempelkamp[8], Gillian L. Dornan[8], Nikos Tsolakos[10], John E. Burke[8,9], Benjamin G. Hale[10], Adolfo García-Sastre[1,2,3,4,5,6*] and Juan Ayllon[1,2,7*]

Affiliation: [1]Department of Microbiology, [2]Global Health and Emerging Pathogens Institute, [3]Department of Pathology, Molecular and Cell-Based Medicine, [4]Department of Medicine, Division of Infectious Diseases, [5]The Icahn Genomics Institute and [6]The Tisch Cancer Institute, Icahn School of Medicine at Mount Sinai, One Gustave L. Levy Place, New York, NY 10029, USA. [7]Department of Health Sciences, University of Burgos, Burgos, Spain. [8]Department of Biochemistry and Microbiology, University of Victoria, Victoria, British Columbia, V8W 2Y2, Canada. [9]Department of Biochemistry and Molecular Biology, The University of British Columbia, Vancouver, British Columbia V6T 1Z3, Canada. [10]Institute of Medical Virology, University of Zurich, Winterthurerstrasse 190, Zurich, 8057, Switzerland.

*Correspondence to: jayllon@ubu.es; Adolfo.garcia-sastre@mssm.edu

Keywords: Influenza A virus, non-structural protein 1 (NS1), phosphoinositide-3-kinases (PI3K), bimolecular fluorescence complementation (BiFC)

Abstract

The non-structural protein 1 (NS1) of influenza A virus performs a broad variety of pro-viral activities in the infected cell, primarily mediating evasion from the host innate immune response by being the main viral interferon antagonist. However, there are several interactions whose biological relevance remains obscure, such as the ability of NS1 to bind and activate class IA phosphoinositide 3-kinases (PI3Ks). PI3Ks are highly regulated lipid kinases that act as critical nodes in multiple cell signaling networks and are also important proto-oncogenes. This activation is mediated by NS1 binding specifically to the p85β subunit. To better understand the consequences of this interaction, we developed a bimolecular fluorescence complementation (BiFC) assay to selectively track the different PI3K heterodimers and, using this system, we found that NS1 induces an isoform-specific relocation and activation of the different PI3K heterodimers. We found that clinically relevant oncogenic mutations in both catalytic and regulatory subunits of PI3K could mimic the effect caused by NS1, and partially rescue the loss of viral fitness in a recombinant virus encoding a p85β-binding deficient NS1.

Significance

Using a new cell biology system to locate PI3K complexes, we found that the behavior of these complexes during influenza infection and in the presence of NS1 is different not only depending on p85beta for activation, but also depending on the type of p110 isoform they have (alpha, beta or delta). By comparing the phenotypic behavior of PI3K complexes upon activation by diverse stimuli, we discovered that oncogenic mutations of PI3K best mimic the activation induced by influenza infection, suggesting that infection induces a transient PI3K transformed state in infected cells to increase viral replication. We believe this finding will inspire further research on the non-redundant role that the different subunits and complexes of PI3K have in the cell.

Introduction

Influenza A viruses are negative-sense, segmented single-stranded RNA viruses belonging to the *Orthomyxoviridae* family (1). Non-structural protein 1 (NS1) is encoded by segment 8 (NS) through alternative splicing. NS1 mRNA is translated into a 26 kDa polypeptide which consists of two functionally distinct globular domains separated by a linker region: an N-terminal RNA binding domain (RBD) and a C-terminal effector domain (ED) (2). NS1 is a multifunctional protein that is involved in various mechanisms to aid virus replication (3). Among these, NS1 is well characterized as an antagonist of the

host interferon response, it inhibits the host innate immune response by repressing type I/III interferon pathways (3). NS1 inhibits the interferon system both pre-transcriptionally through impeding the activation of the cytoplasmic viral RNA sensor, retinoic acid-inducible gene I (RIG-I), and post-transcriptionally by interfering with the pre-mRNA processing and mRNA nucleo-cytoplasmic export machinery of the host and suppressing expression of cellular genes (3-6).

An intriguing function of NS1 is related to the phosphoinositide 3-kinase (PI3K) pathway. PI3Ks are lipid kinases that are involved in cell growth, proliferation, and survival (7). Due to the critical role of this pathway in cellular processes, it is also one of the most over-activated pathways in oncogenic transformation (8-10). Over-activated PI3K has been found in many human cancers such as colon, lung, ovarian, and many more (9, 11); as an example, up to 40% of breast cancers present mutations in PI3K (12, 13). Class IA PI3Ks are comprised of heterodimers that consist of a regulatory (p85) and a catalytic (p110) subunit. In its basal state, the heterodimers are inactive, with p85 inhibiting p110. The best characterized mechanism of activation of class IA PI3K involves translocation to the membrane upon certain stimuli (e.g. growth factors). The p85 subunit then binds to phosphotyrosine (pY) residues in activated tyrosine receptors, inducing a conformational change in the heterodimer and releasing the inhibition of the active site in p110, which in turn leads to production of the second messenger phosphatidylinositol-3,4,5-trisphosphate (PIP3) and downstream activation of protein kinase B (PKB or Akt) (14-16). Class IA PI3K activation and regulation is complicated by the existence of several isoforms of each subunit (p85α, p85β, p110α, p110β, p110δ), some of which are more or less abundant in different cell types, allowing for different combinations of catalytic and regulatory subunits with either distinct or redundant functions. The functional consequences of this PI3K diversity are not yet fully understood (17-19).

The interaction of influenza A viruses with PI3K is an interesting example of how such diversity can influence PI3K activation, as it has been shown that NS1 binds exclusively to p85β and not p85α (20). Through this interaction, influenza A virus infection activates the PI3K pathway, as measured by downstream phosphorylation of Akt (pAkt) (20). It has been suggested that such activation prevents, or at least delays, virus-induced apoptosis, thereby enhancing viral replication (21). However, the extent of impact of this activation on viral fitness is strain-specific, as observed with recombinant viruses carrying the NS1-p85β abrogating mutation, Y89F (20, 22), or with naturally-evolving strains in humans (23). Given the variety of processes regulated by PI3K, including cell survival, translation, endocytosis, vesicle trafficking, cell motility, innate immunity and oncogenesis, it is yet unclear what are the full consequences of NS1-mediated PI3K activation during viral infection. Additionally, the role of the different isoforms of p110 (α, β, δ) on NS1-mediated activation of p85β-containing PI3K heterodimers has not been studied. In order to deepen our understanding of the role of the p110 isoform in PI3K activation by NS1, here we established an in vitro system to visualize PI3K heterodimers with specific isoform combinations, assess their behavior in the presence or absence of NS1, and compare this with other known PI3K activating stimuli. Our observations should aid in ultimately characterizing the functional meaning of the NS1:PI3K interaction during viral infection, and may dissect the specific and common roles of the multiple PI3K isoforms.

Results

Influenza A virus NS1 relocalizes PI3K complexes in an isoform-specific manner

First, we established a system to visualize the isoform-specific p85 and p110 heterodimers by using a bimolecular fluorescence complementation assay (BiFC). A similar assay was previously described by our group to study to the cellular behaviors of protein complexes during the induction of the innate immune response (24). We fused the N-terminal (YN) part of yellow fluorescent protein (YFP) to the N-terminus of the p110 subunits (YN-p110α, YN-p110β, YN-p110δ), and the C-terminal (YC) part of YFP to the C-terminus of the p85s (p85α-YC, p85β-YC) (Fig. 1A). In this way, upon transfection of a p85-p110 pair into cells, only the heterodimer formed by the combination of the specific YN- and YC- tagged subunits can be visualized by a YFP signal, allowing us to ascertain the cellular localization of each PI3K heterodimer. All the possible p85-p110 BiFC combinations showed a similar fluorescence phenotype when co-expressed by transfection in HeLa cells (Fig. 1B): a diffuse, homogeneous cytoplasmic

distribution. Then, we assessed changes to these localizations upon co-transfection with the NS1 protein from influenza A/Puerto Rico/8/34 virus (PR8, Fig. 1C). The presence of NS1 did not affect p85α heterodimers, consistent with the inability of NS1 to bind this specific isoform (20). On the other hand, NS1 expression resulted in a remarkable redistribution of the p85β-containing heterodimers. The redistribution of PI3K in the cytoplasm of NS1-expressing cells from a diffuse to a punctate pattern was different according to the p110 isoform present: those with p110α and p110δ showed accumulation at the edges of the cells, while those with p110β were relocated to a punctate phenotype close to the nucleus. To confirm that these changes were specifically due to the NS1-p85β interaction, we also co-transfected the PI3K BiFC heterodimers with PR8 NS1 carrying the Y89F mutation, which has previously been shown to abrogate NS1 binding to p85β (20, 22). As expected, NS1-Y89F failed to relocate the different PI3K heterodimers (Fig. 1D), which remained in the same diffuse cytoplasmic distributions as without any NS1 present. We quantified the number of cells that were positive for their respective phenotype based on the different PI3K heterodimers being expressed with NS1. We observed that at least 80% of the cells expressing the PI3K BiFC with NS1 displayed either the accumulation at the cell edges (p110α and p110δ) or the punctate close to the nucleus (p110β) (Fig. 1E). We further corroborated the ability of NS1 to bind to a dimer of p85β including any of the three catalytic p110 subunits by co-immunoprecipitation assays. We co-transfected 293T cells with plasmids expressing V5-GST, V5-NS1 wt, or V5-NS1 Y89F, together with Flag-p85α or p85β with each of the p110 isoforms (YN-p110α/β/δ). We confirmed the preferential binding of NS1 to p85β over p85α (SI Appendix, Fig. S1a) as well as the successful precipitation of all the dimer combinations with p85β and each different p110 (SI Appendix, Fig. S1b).

Next, we tested if the distinct distribution of the PI3K heterodimers also occurred when cells were infected with influenza virus. We expressed the indicated PI3K complexes then infected cells with rPR8 WT or rPR8-Y89F at a multiplicity of infection (MOI) of 10 PFU/cell and as predicted the BiFC complexes relocated to the cell edges for p110α and p110δ combinations when infected with rPR8 WT and closer to the nucleus for p110β. The complexes were in a diffuse, homogenous distribution when infected with rPR8-Y89F, similar to the mock infected cells (SI Appendix, Fig. S2).

In order to evaluate whether the NS1-mediated relocalization of PI3K complexes is strain specific, we expressed NS1 proteins from H1 (A/Puerto Rico/8/1934, A/Brevig Mission/1/1918, A/Wilson-Smith/1933, A/California/04/2009), H3 (A/Wyoming/03/2003), and H5 (A/Hong Kong/156/1997, A/Vietnam/1203/2004) subtypes. All different NS1s promoted similar relocalizations of the PI3K heterodimers, indicating that this phenomenon is not strain specific (SI Appendix, Fig. S3), although in the multifactorial context of an infection this might result in different functional phenotypes, as we have previously shown (22).

Structural and biochemical studies have revealed that the NS1 effector domain (ED) located at its carboxy-terminal end is sufficient to bind the inter-SH2 domain of p85β, and does not require dimerization (25, 26). To ascertain whether this NS1 domain has the same impact on PI3K relocalization as the entire NS1, we expressed the NS1 ED on its own, without the N-terminal RNA-binding domain (26), and carrying a known mutation (W187A) to prevent its dimerization (27-29), in the presence of our diverse PI3K BiFC complexes. As shown in SI Appendix, Fig. S4, we observed that the expression of the NS1 ED induced the same isoform dependent redistribution of the PI3K complexes as full-length NS1, confirming that just binding of p85β to NS1 is enough for isoform-specific PI3K relocalization.

Influenza A virus NS1 relocalizes PI3K complexes in proximity to focal adhesions or to endosomes depending on the p110 isoform.

Next, we tried to spatially characterize the different isoform-dependent PI3K redistributions. In order to do that, we co-transfected HeLa cells with the various PI3K-NS1 BiFC combinations in the presence of NS1, and used different cell markers to identify potential colocalization. For p85β/p110α and p85β/p110δ complexes, their localization in the presence of NS1 resembled focal adhesions, and therefore we co-expressed our BiFC system together with a focal adhesion marker. For this purpose, we expressed RFP-tagged zyxin, a phosphoprotein that is concentrated at focal adhesions (30) (Fig. 2A and B). We noted that the expression of zyxin mirrors the pattern we detected with the NS1-relocated PI3K BiFC complexes, and is in high proximity with these complexes. Similarly, we presumed that the distinct p85β/p110β dots we observed in the presence of NS1 could correspond with an endosomal

compartment. To test this theory, we co-transfected our BiFC system with NS1 together with the early endosome marker Rab5 fused to RFP (31-33), and found that indeed the distribution pattern of this NS1-relocated PI3K complex coincides with the distribution of Rab5 (Fig. 2C). These results indicate that in the presence of NS1, p85β/p110β heterodimers are directed towards early endosomes while p85β/p110α and p85β/p110δ are directed towards focal adhesion regions. Given that the NS1-p85β remains constant in all these scenarios, our data reveal that it is the p110 subunit that determines heterodimer intracellular localization. It should be noted that only a small fraction of the NS1 co-localizes with the PI3K BiFC complexes, as expected for this multi-functional protein that in addition to bind to p85β also associates with several other host factors.

Kinase activity of the isoform-specific PI3K complexes in the presence of NS1

Next, we characterized the functionality of these PI3K complexes within the different relocalization patterns. The canonical signaling of active PI3K is based on the phosphorylation of PIP_2, resulting in the generation of PIP_3, which diffuses and promotes downstream activation and phosphorylation of Akt. Therefore, we expressed p85β in combination with the different isoforms of p110, as well as NS1, and detected the production of PIP_3 by indirect immunofluorescence (Fig. 3A). We detected production of PIP_3 at the cell periphery when p85β was in complex with p110α and p110δ in the presence of NS1, concomitant with its relocalization to focal adhesions at the cell periphery. However, we were unable to visualize using this technique the production of PIP_3 when NS1 was coexpressed with p110β-containing PI3K heterodimers. In order to confirm that the catalytic activity of each p110 was necessary for the NS1-mediated activation of the PI3K complexes, we treated our PI3K-BiFC/NS1 expressing cells with a PI3K inhibitor (wortmannin, which targets p110) and discerned that the distinct relocalizations of PI3K complexes were still taking place, but that there was no production of PIP_3 (Fig. 3B). We further characterized the differential kinase activities using biochemical methods and performed *in vitro* lipid kinase assays. We measured the turnover of adenosine triphosphate (ATP) in the presence of 5% PIP_2 vesicles by PI3K heterodimers and found that upon addition of NS1, only the activity of p110α/p85β complexes was significantly increased, while there was no significant difference in activity of p110β/p85β complexes or on the p110α/p85α complexes as expected (SI Appendix, Fig. S5a-b). The activation of p110α/p85β was dose-dependent on NS1 (SI Appendix, Fig. S5c). Notably, when we assayed NS1-Y89F in this *in vitro* system, we did not observe significant activation of p110α/p85β complex (SI Appendix, Fig. S5d), complementary to the results observed in the cell based assay.

Next, we determined where in the cell activation of Akt occurs in this system. We therefore probed for pAkt (Ser-473) in our BiFC assays by immunostaining with an antibody specific for pAkt. We indeed, detected elevated levels of pAkt in the presence of NS1, especially at the cell periphery with p85β/p110α and p85β/p110δ isoforms, but not with p85β/p110β (Fig. 3C). These results indicate that p85β/p110α and p85β/p110δ are catalytically active after being bound and relocated by NS1, but that p85β/p110β catalytic activity is not detectable despite its relocalization in the presence of NS1.

An intact SH2 domain in p85β is required for NS1-mediated redistribution of PI3K complexes containing p110α and p110δ, but not p110β

Canonical activation of PI3K is triggered by p85 binding to phospho-tyrosine (pY) motifs via one of its SH2 (Src homology 2) domains, thereby relieving its inhibition of p110. These pY motifs are commonly found in the cytoplasmic tails of growth factor receptors which are activated upon recognition of external growth stimuli. We next investigated whether a functional p85β SH2 domain was required for NS1-mediated relocalization of the different PI3K complexes. For this purpose, we introduced R355A and R647A (RARA) mutations into p85β in order to disrupt the interaction of p85β with pY motifs (34). We expressed p85β RARA in our BiFC system along with NS1, and noticed that the mutant p85β nullifies the redistribution of the p110α and p110δ complexes to focal adhesion regions in the presence of NS1. However, the RARA mutations had no effect on the redistribution of p110β-containing complexes with NS1 (Fig. 3D), indicating that there are different requirements for a functional SH2 domain of p85β for the NS1-mediated redistribution of PI3K complexes, and that these appear to be specific to the p110 isoform in the complex.

PI3K oncogenic mutations phenocopy the NS1-mediated relocalization of PI3K

We next investigated whether activation of PI3K complexes by other known cellular stimuli different to NS1 results in similar redistributions of PI3K in a p110-specific manner. We therefore tested a constitutively-active HRas with previously described point mutations that lead to activation of the PI3K pathway (HRas C12V and T40C) (35). We observed that there was an isoform-independent relocalization of the PI3K complexes to membrane regions in all the combinations tested, including with both p85α and p85β (SI Appendix, Fig. S6A/B). In addition, we assessed the non-receptor tyrosine kinase Src in its constitutively active form (SrcY530F) and observed two distinct phenotypes that were isoform dependent. When we expressed SrcY530F together with p85α and any p110, we detected more membrane localization of the PI3K complexes, while similar complexes with p85β exhibited a more punctate distribution of PI3K near the nucleus and endosomal compartments (SI Appendix, Fig. S6B/C). These relocalization phenotypes are strikingly divergent from what we have observed with NS1.

There are well characterized mutations in both p110 and p85 subunits that have been shown to play a role in cellular transformation in human cancers. We therefore wondered whether NS1 activation could be reproducing these overactive pathway events. Consequently, we investigated whether PI3K oncogenic mutations could cause the same redistribution pattern of p85β/p110 complexes as with NS1. Substitution H1047R is one of the hot spot mutations found in the kinase domain of p110α (36, 37), and is known to increase lipid kinase activity and potently activate PI3K/Akt signaling (38). This mutation is frequently found in cancers such as colon, lung, breast, ovarian, endometrial and many more (12). We introduced the H1047R (12, 36-38) mutation into our p110α BiFC construct and then evaluated the intracellular localization of this mutant p110α in combination with p85α or p85β in the absence of NS1 (Fig. 4A). We found that this oncogenic p110α led to the same redistribution to focal adhesion regions as seen when the wild-type p110α:p85β complex was bound by NS1. However, the oncogenic p110α localization phenotype occurred case independently of the regulatory p85 subunit present. Since this mutation does not exactly replicate the activation we had seen with NS1, which is specific to p85β, we assessed whether another oncogenic mutation found in p85, and that could be applied to p85β, would better reflect NS1 action. We therefore introduced N561D (39, 40) to p85β (Fig. 4B), which is a mutation in the iSH2 region (41) that naturally occurs in cancers such as endometrial (39) or melanoma (40), and is homologous to the N564 substitutions found in p85a (41, 42).When we tested this mutant p85β in our BiFC system, we observed that heterodimers containing p110α and p110δ relocated to focal adhesion regions, similar to the effect of NS1 of wild-type versions of these complexes. Furthermore, the heterodimer of the mutant p85β with p110β also relocated to endosomal regions recreating the exact same phenotypic distribution as detected with NS1 and the wild-type complex. In addition to the redistribution pattern, we tested the kinase activity of these mutant PI3K complexes and detected the production of PIP_3 when mutant p85β was complexed with p110α and p110δ but not with p110β (Fig. 4C), similar to what we have observed with wild type PI3K heterodimers with NS1 (Fig. 4D). Moreover, we noticed the presence of PIP_3 when mutant p110α was complexed with p85α and p85β (Fig. 4C).

Finally, we designed a system to test whether the hyperactivating N561D mutation in p85β could rescue the growth phenotype of a recombinant influenza A virus whose NS1 has been engineered to be unable to bind and activate PI3K. Such a virus has been shown previously to suffer a loss in fitness (20, 22) in vitro and in vivo when compared to wild type viruses (20, 22). We generated a stable A549 cell line constitutively overexpressing HA-p85β-N561D, which was confirmed by indirect immunofluorescence (Fig. 5A) and by immunoblotting with specific antibodies (Fig. 5B). Next, we infected A549 WT and A549-p85β-N561D cells with rPR8 WT and rPR8-Y89F at an MOI of 2 PFU/cell and tested activation of PI3K by assessing levels of pAkt (serine 473) at various time points post-infection (Fig. 5C). As expected, we did not see activation of pAkt in WT cells infected with rPR8-Y89F, but increasing levels of pAkt were detected over time after infection with rPR8 WT virus. On the other hand, we detected higher basal levels of pAkt in A549-p85β-N561D cells as compared to WT cells, and pAkt levels were therefore high whether infected with rPR8-Y89F or rPR8 WT. Additionally, it was notable that we could detect the initial transient phosphorylation of Akt at an early time point (2hr post infection (p.i.)) due to virus entry and attachment in both cell lines and with both viruses (3, 7, 20, 43). However, a second increase in pAkt levels only occurred in rPR8 WT infected cells, for both cell lines, starting 6hr p.i., consistent with expression of WT NS1. We next performed growth kinetics with the two viruses on A549 WT and A549-p85β-N561D cells (Fig. 5D) and observed a partial recovery of rPR8-Y89F fitness in the cells that express constitutively active p85β. Specifically, rPR8-Y89F grew to almost 2 logs lower infectious titers than rPR8 WT in A549 WT cells, while this difference was only of approximately 1 log in A549-p85β-N561D cells. In order to further validate this, we performed a competition assay with rPR8 WT and rPR8-Y89F in A549 wt and

A549-p85β-N561D cells. We mixed equal number of PFU of each virus and then infected the different cell lines. We collected cells at 12, 24 and 48 hours post infection and processed them for MinION sequencing. We compared the total number of reads for rPR8 WT versus rPR8-Y89F in the two cell lines. We observed that at 24 and 48 hours post infection, rPR8 WT could outcompete rPR8-Y89F in A549 wt cells, but in A549-p85β-N561D cells, rPR8-Y89F performed slightly better, and was not outcompeted by rPR8 WT as rapidly (Fig. 5E).

Discussion

The PI3K-Akt signaling cascade is critical as a checkpoint of multiple cellular processes, including translation, survival, proliferation, migration, and immunity. It is also involved in several pathological processes. To understand the variety of outcomes associated with the activation of this pathway remains a challenge across multiple fields of biological sciences. Class IA PI3Ks, which act as obligate heterodimers, comprise several isoforms of both catalytic (p110α, p110β and p110δ) and regulatory subunits (mainly, p85α and p85β), but how this heterogeneity translates into potential functional diversity is poorly understood. Notwithstanding, one of the few well characterized examples of specific isoform activation of PI3K is mediated by the influenza A virus NS1 protein, which only binds p85β, and so can only activate p85β- (and not p85α-) heterodimers with p110.

Here, we wanted to investigate whether the NS1-mediated activation of PI3K has different consequences based on the p110 isoform heterodimerizing with p85β. By using a bimolecular fluorescence complementation system to specifically tag each possible p85/p110 combination, we managed to track by microscopy the spatial changes of these complexes in the presence of NS1, as well as partially characterize their functionality. As expected, every p85-p110 combination when expressed alone had a diffuse cytoplasmic distribution, most probably in their inactive form. Also as expected, the presence of NS1 did not affect the basal distribution of complexes containing p85α, but relocalized those specifically containing p85β, a change that could be prevented by the Y89F substitution in NS1, previously shown to abrogate NS1 binding to p85β (20, 22). This pattern was consistently observed when cells expressing different PI3K complexes were infected with rPR8 wt (relocalized) or rPR8-Y89F (homogeneous). Relocalization of the complex only required the monomeric effector domain of NS1, consistent with previously published structural studies showing that other NS1 domains are dispensable for p85β binding and PI3K activation (25, 26). However, we observed two clearly distinct PI3K phenotypes both spatially and functionally associated with NS1 expression, depending on the p110 isoform present on the heterodimers.

The first of these outcomes involved complexes containing p110α or p110δ, that, when engaged by NS1, were relocated to specific regions of the plasma membrane, which we identified as focal adhesions. These are well known structures that can act as scaffolding centers for the assembly of signaling complexes downstream of receptors. Indeed, movement of NS1-bound PI3K to the focal adhesions required functional pY-receptor binding residues in p85β, and resulted in PI3K catalytic activation leading to PIP_3 production and activation of Akt. All of this is consistent with the canonical activation mechanism of PI3K. In our assays, we did not find differences between p110α and p110δ-associated phenotypes, so it remains unknown whether their activation could lead to different outcomes. The different p110 subunits have been shown to have different tissue and cell type distributions, as well as interaction partners, and in addition p110α and p110δ signaling pathways may diverge downstream of Akt phosphorylation, in ways that will require further studies to elucidate.

The second outcome concerned PI3K heterodimers containing p110β. In this case, in stark contrast with the first outcome, the NS1-activated complexes moved to punctate perinuclear structures, which we identified as early endosomes. This translocation proved to be independent of having functional pY-receptor binding residues in p85β, so it remains unclear which factor(s) may serve as anchors of these complexes to the endosome, but it is likely to be a specific determinant of p110β. Also in this case, we could not detect clear production of PIP_3, although others have found pools of this second messenger in endosomal membranes (44), nor could we detect localized activation of Akt. The presence of PI3K complexes in the endosome is consistent with previous proteomics studies that found that active p110β binds to Rab5 (45), the same marker we have used to co-localize PI3K complexes containing p110β with early endosomes. This Rab5-p110β interaction has been associated with regulation of autophagy (46), and future studies will have to determine if the NS1-relocalized p85β/p110β complexes similarly impact autophagy during influenza A virus infection.

Other studies have shown how specific inputs may act exclusively through some PI3K isoforms, such as HRas only activating p110α and p110δ, but not p110β (47), but our work shows that a single stimulus, NS1, can distinctively affect each p85β-containing complex of the class IA PI3K family, leading to different outcomes according to the p110 isoform. We speculate that the physiological result of the NS1 activation of PI3K would be greatly affected by the balance between the p110α/p110δ "focal adhesion" route or the p110β "endosome" route, a balance that will depend on the basal expression levels of each isoform. These complexities would help to explain how the physiological impact of PI3K activation by influenza A viruses remains largely obscure, and may not be limited to delaying apoptosis (48, 49).

Our work shows how the BiFC system described here can be used to explore how PI3K activators can differentially impact each hetero-isoformic member of the class IA PI3K family. Indeed, the H1047R amino acid substitution in p110α, one of the most prevalent alterations found in human cancers, relocated PI3K to focal adhesions, independent of whether it paired with p85α or p85β. We also introduced a naturally-occurring oncogenic mutation in p85β, N561D, which interestingly recapitulated the PI3K phenotypes found with NS1 co-expression. This result suggests that influenza A virus may have evolved to stimulate PI3K during infection to induce a cellular environment similar to that present in cells containing oncogenic p85 mutations. In fact, we found that hyperactivated p85β-N561D partially compensated to some extent for the loss of fitness found in an influenza A virus expressing a mutated NS1 protein unable to activate PI3K. This partial incomplete rescue could be due to several factors, including differences in the magnitude and kinetics of p85β activation between virus-infected cells and the constitutively active p85β-N561D cells. Also, although previous studies have not definitively detected other functions of NS1 affected by the Y89F substitution, it cannot be ruled out that this substitution has further impacts than changing the binding to p85β, particularly given the location of Y89 at the interface with other host factors (50). In any case, our data are consistent with a role for the influenza A virus NS1 protein in establishing a transient PI3K-driven oncogenic phenotype in infected cells that promotes optimal virus replication. Interestingly, some other factors associated with cell transformation, such as deficiencies in the interferon response (51) and oncogenic activation of the Ras/Raf/MEK/ERK signaling pathway (52, 53), have also been associated with increased influenza virus replication.

Conclusion

Here we established a Bimolecular Fluorescence Complementation (BiFC) system to spatially visualize the localization of PI3K heterodimers at the cellular level and used this tool in combination with influenza A virus NS1 protein to study the activation of this complex pathway. Our findings show how a single PI3K stimulus can direct the signaling cascade induced by this kinase family into at least two different functional directions depending on the exact composition of the PI3K heterodimers. We have also shown how naturally-occurring hyperactivating mutations in p85β recapitulate the outcomes of NS1-mediated PI3K activation found in our BiFC system, and can partially compensate for a loss of function mutation in a recombinant IAV. Moreover, we posit that the BiFC system we describe in this report can be applied to the study of PI3K signaling regulation beyond the virology field. Considering the central role of PI3K-Akt in some of the most prevalent human maladies, we propose our system as an interesting new tool for further understanding and addressing the role of this pathway in human health and disease.

Figure Legends

Figure 1. Split YFP system to study specific PI3K heterodimers. A) A schematic representation of the BiFC system to study the interaction of the catalytic and regulatory subunits of PI3K. N-terminal (YN) and C-terminal (YC) parts of YFP were added to the N- or C-terminus of p110 or p85, respectively. B) HeLa cells were transfected with the different BiFC combinations and processed 19 hr p.t. for fluorescence microscopy. All the heterotypic dimers showed a broad diffused distribution. C) When co-transfected with NS1, heterodimers containing p85β, but not p85α, were relocated to cell edges (p110α and p110δ) or acquired a punctate localization near the nucleus (p110β). D) None of these phenotypes were observed after co-transfection with an NS1 mutant unable to bind p85β (Y89F substitution). (NS1: red, DAPI: cyan, BiFC: yellow). E) When cells expressing the different heterodimers with NS1 were quantified, 80% of cells expressing PI3K complexes and NS1 showed a relocalization phenotype. (n = 30 cells/condition, and triplicates, error bars represent standard deviation).

Figure 2. Colocalization of redistributed PI3K complexes with different cellular markers. HeLa cells were co-transfected with the indicated BiFC constructs, RFP-tagged markers for different cellular compartments and wild type NS1. Cells were processed for confocal microscopy at 19 hr p.t. Cell edge phenotype associated with p110α and p110δ appeared to localize in close proximity to the focal adhesion marker, zyxin (A, B), whereas BiFC complexes with p110β colocalized with the early-endosome-associated small GTPase Rab5 (C). (Green: BiFC, red: Rab5-RFP or Zyxin1-RFP; white on merged pictures: NS1).

Figure 3. Differential catalytic activity of redistributed PI3K complexes. HeLa cells were co-transfected with the indicated BiFC constructs and wild type NS1. At 19 hr p.t., cells were processed for immunofluorescence with antibodies against NS1(blue) and (A) PIP3(red). Markedly increased levels of PIP_3 could be appreciated in cells transfected with p110α/δ complexes, but not with p110β. Incubation with the pan-PI3K inhibitor wortmannin abrogated the production of PIP_3, but not the redistribution of the PI3K complexes by NS1 (B). Similar results were obtained when assessing activation of Akt (C). When HeLa cells were co-transfected with NS1, YN-p110α, β or δ and either wild type p85β-YC or the double mutant p85β-YC R355A/R647A (RARA) (D), accumulation of p110α/δ BiFC complexes in membrane focal adhesions was abolished, while it had no effect on the endosome-associated accumulation of p110β complexes.

Figure 4. Relocation of BiFC PI3K heterodimers by naturally-occurring oncogenic mutations. A) HeLa cells were co-transfected with mutant YN-p110α (H1047R) and wild type p85α-YC or p85β-YC. The H1047R mutant generates the same phenotype associated to focal adhesions as the wild type NS1 but with both p85α and β. B) When HeLa cells were co-transfected with mutant p85β-YC (N561D) and wild type YN-p110s, we observed recapitulation of the two distinct outcomes observed with NS1 expression. Actin fibers were stained with phalloidin. Catalytic activity of mutant PI3K complexes was tested by co-transfecting HeLa cells with indicated wild type p110 constructs and p85β-N561D and 19 ht p.t. the cells were processed for fluorescence microscopy against PIP_3 (red). As expected, we observed increased levels of PIP_3 with p110α/δ complexes, but not with p110β. We also observed elevated levels of PIP_3 when p110α-H1047R was co-transfected with p85α and p85β (C). We tested wt p110x and wild type p85β with NS1 as controls (D). (PIP_3 in red, NS1 and DAPI in cyan, BiFC in yellow and Phalloidin in cyan).

Figure 5. Characterization of A549-p85β N561D cells. A stable cell line expressing constitutively active HA-p85β N561D in the A549 background was validated by (A) immunofluorescence and (B) western blot. A549 wt was used as a negative control, and staining was performed using antibodies against HA-tag (A, green), p85β (A, green), DAPI (A, blue) and β-actin for western blot loading control (B). C) Time course was performed on serum-starved cells (A549 WT and A549 expressing p85β-N561D) with rPR8 WT and rPR8-Y89F. Cells were infected at a multiplicity of infection of 2 PFU/cell and collected at 0, 2, 4, 6 and 8-hours post infection. Levels of pAkt, NS1 and β-actin were detected by western blot. β-actin was used as a loading control. D) Growth curve was done on serum-starved cells with rPR8 WT and rPR8-Y89F viruses. Supernatant was collected at the indicated times post infection. Plaque assays were performed to determine viral titers. (n=3, error bars represent standard deviation). E) Competition assay was performed to assess viral fitness in A549 wt and A549-p85β-N561D cells. rPR8 WT and rPR8-Y89F were mixed in a 50:50 ratio and cells were infected at 10^3 PFU/mL, cells were collected at 12, 24, and 48 hrs post infection. All the samples were analyzed using MinION nanopore technology and the bars represent percentage of reads present for rPR8 WT and rPR8-Y89F in each sample. (n=3 (except for input), error bars represent standard deviation).

Material and Methods

A detailed description of the *Materials and Methods* is available in *SI Appendix*. Cell culture, BiFC assays, immunofluorescence, viral infection, growth kinetics, Western blotting, RNA-sequencing, Co-IP, Baculovirus generation and amplification, expression and purification of recombinant proteins, lipid vesicle preparation and ATPase assays were performed.

Acknowledgements:

We thank Richard Cadagan, Elena Moreno and Sara El Zahed for technical assistance. Confocal laser scanning microscopy was performed at the Icahn School of Medicine Microscopy Shared Resource facility.

Author contributions: J.A., B. G. H. and A. G.-S. conceived and designed the project. J. A., S. A., B. G. H., N. T., M. S.-A., B.D.S., G.L.D. and J.E,B. performed all the experiments and analyzed the data. S. A. and J. A. wrote the manuscript and prepared the figures. All authors reviewed and edited the manuscript.

Funding: This work was partly supported by CRIPT (Center for Research on Influenza Pathogenesis and Transmission), a NIAID funded Center of Excellence for Influenza Research and Response (CEIRR, contract #75N93021C00014) to AG-S. The work was also partially supported by the Swiss National Science Foundation (grant 31003A_159993 to BGH) and the Cancer Research Society (CRS- CRS-1052949 to JEB).

Competing interests: The A.G.-S. laboratory has received research support from GSK, Pfizer, Senhwa Biosciences, Kenall Manufacturing, Blade Therapeutics, Avimex, Johnson & Johnson, Dynavax, 7Hills Pharma, Pharmamar, ImmunityBio, Accurius, Nanocomposix, Hexamer, N-fold LLC, Model Medicines, Atea Pharma, Applied Biological Laboratories and Merck, outside of the reported work. A.G.-S. has consulting agreements for the following companies involving cash and/or stock: Castlevax, Amovir, Vivaldi Biosciences, Contrafect, 7Hills Pharma, Avimex, Pagoda, Accurius, Esperovax, Applied Biological Laboratories, Pharmamar, CureLab Oncology, CureLab Veterinary, Synairgen, Paratus, Pfizer and Prosetta, outside of the reported work. A.G.-S. has been an invited speaker in meeting events organized by Seqirus, Janssen, Abbott, Astrazeneca and Novavax. A.G.-S. is inventor on patents and patent applications on the use of antivirals and vaccines for the treatment and prevention of virus infections and cancer, owned by the Icahn School of Medicine at Mount Sinai, New York, outside of the reported work.

References

1. Florian K. 2021. Orthomyxoviridae: The Viruses and Their Replication. *In* Howley PM (ed), Fields Virology: Emerging Viruses. Lippincott Williams & Wilkins,
2. Hale BG. 2014. Conformational plasticity of the influenza A virus NS1 protein. J Gen Virol 95:2099-2105.
3. Ayllon J, Garcia-Sastre A. 2015. The NS1 protein: a multitasking virulence factor. Curr Top Microbiol Immunol 386:73-107.
4. Hale BG, Randall RE, Ortin J, Jackson D. 2008. The multifunctional NS1 protein of influenza A viruses. J Gen Virol 89:2359-2376.
5. Krug RM. 2015. Functions of the influenza A virus NS1 protein in antiviral defense. Curr Opin Virol 12:1-6.
6. Bhat P, Aksenova V, Gazzara M, Rex EA, Aslam S, Haddad C, Gao S, Esparza M, Cagatay T, Batten K, El Zahed SS, Arnaoutov A, Zhong H, Shay JW, Tolbert BS, Dasso M, Lynch KW, Garcia-Sastre A, Fontoura BMA. 2023. Influenza virus mRNAs encode determinants for nuclear export via the cellular TREX-2 complex. Nat Commun 14:2304.
7. Ehrhardt C, Marjuki H, Wolff T, Nurnberg B, Planz O, Pleschka S, Ludwig S. 2006. Bivalent role of the phosphatidylinositol-3-kinase (PI3K) during influenza virus infection and host cell defence. Cell Microbiol 8:1336-48.
8. Rascio F, Spadaccino F, Rocchetti MT, Castellano G, Stallone G, Netti GS, Ranieri E. 2021. The Pathogenic Role of PI3K/AKT Pathway in Cancer Onset and Drug Resistance: An Updated Review. Cancers (Basel) 13.
9. Noorolyai S, Shajari N, Baghbani E, Sadreddini S, Baradaran B. 2019. The relation between PI3K/AKT signalling pathway and cancer. Gene 698:120-128.

10. Stommel JM, Kimmelman AC, Ying H, Nabioullin R, Ponugoti AH, Wiedemeyer R, Stegh AH, Bradner JE, Ligon KL, Brennan C, Chin L, DePinho RA. 2007. Coactivation of receptor tyrosine kinases affects the response of tumor cells to targeted therapies. Science 318:287-90.
11. Martini M, De Santis MC, Braccini L, Gulluni F, Hirsch E. 2014. PI3K/AKT signaling pathway and cancer: an updated review. Ann Med 46:372-83.
12. Ligresti G, Militello L, Steelman LS, Cavallaro A, Basile F, Nicoletti F, Stivala F, McCubrey JA, Libra M. 2009. PIK3CA mutations in human solid tumors: role in sensitivity to various therapeutic approaches. Cell Cycle 8:1352-8.
13. Keraite I, Alvarez-Garcia V, Garcia-Murillas I, Beaney M, Turner NC, Bartos C, Oikonomidou O, Kersaudy-Kerhoas M, Leslie NR. 2020. PIK3CA mutation enrichment and quantitation from blood and tissue. Sci Rep 10:17082.
14. Alessi DR, Cohen P. 1998. Mechanism of activation and function of protein kinase B. Curr Opin Genet Dev 8:55-62.
15. Osaki M, Oshimura M, Ito H. 2004. PI3K-Akt pathway: its functions and alterations in human cancer. Apoptosis 9:667-76.
16. Fresno Vara JA, Casado E, de Castro J, Cejas P, Belda-Iniesta C, Gonzalez-Baron M. 2004. PI3K/Akt signalling pathway and cancer. Cancer Treat Rev 30:193-204.
17. Bilanges B, Posor Y, Vanhaesebroeck B. 2019. PI3K isoforms in cell signalling and vesicle trafficking. Nat Rev Mol Cell Biol 20:515-534.
18. Safaroghli-Azar A, Sanaei MJ, Pourbagheri-Sigaroodi A, Bashash D. 2023. Phosphoinositide 3-kinase (PI3K) classes: From cell signaling to endocytic recycling and autophagy. Eur J Pharmacol 953:175827.
19. Cirillo D, Diceglie M, Nazare M. 2023. Isoform-selective targeting of PI3K: time to consider new opportunities? Trends Pharmacol Sci 44:601-621.
20. Hale BG, Jackson D, Chen YH, Lamb RA, Randall RE. 2006. Influenza A virus NS1 protein binds p85beta and activates phosphatidylinositol-3-kinase signaling. Proc Natl Acad Sci U S A 103:14194-9.
21. Ehrhardt C, Wolff T, Pleschka S, Planz O, Beermann W, Bode JG, Schmolke M, Ludwig S. 2007. Influenza A virus NS1 protein activates the PI3K/Akt pathway to mediate antiapoptotic signaling responses. J Virol 81:3058-67.
22. Ayllon J, Hale BG, Garcia-Sastre A. 2012. Strain-specific contribution of NS1-activated phosphoinositide 3-kinase signaling to influenza A virus replication and virulence. J Virol 86:5366-70.
23. Lopes AM, Domingues P, Zell R, Hale BG. 2017. Structure-Guided Functional Annotation of the Influenza A Virus NS1 Protein Reveals Dynamic Evolution of the p85beta-Binding Site during Circulation in Humans. J Virol 91.
24. Sanchez-Aparicio MT, Ayllon J, Leo-Macias A, Wolff T, Garcia-Sastre A. 2017. Subcellular Localizations of RIG-I, TRIM25, and MAVS Complexes. J Virol 91.
25. Hale BG, Batty IH, Downes CP, Randall RE. 2008. Binding of influenza A virus NS1 protein to the inter-SH2 domain of p85 suggests a novel mechanism for phosphoinositide 3-kinase activation. J Biol Chem 283:1372-1380.
26. Hale BG, Kerry PS, Jackson D, Precious BL, Gray A, Killip MJ, Randall RE, Russell RJ. 2010. Structural insights into phosphoinositide 3-kinase activation by the influenza A virus NS1 protein. Proc Natl Acad Sci U S A 107:1954-9.
27. Kerry PS, Ayllon J, Taylor MA, Hass C, Lewis A, Garcia-Sastre A, Randall RE, Hale BG, Russell RJ. 2011. A transient homotypic interaction model for the influenza A virus NS1 protein effector domain. PLoS One 6:e17946.

28. Ayllon J, Russell RJ, Garcia-Sastre A, Hale BG. 2012. Contribution of NS1 effector domain dimerization to influenza A virus replication and virulence. J Virol 86:13095-8.
29. Hale BG, Barclay WS, Randall RE, Russell RJ. 2008. Structure of an avian influenza A virus NS1 protein effector domain. Virology 378:1-5.
30. Beckerle MC. 1997. Zyxin: zinc fingers at sites of cell adhesion. Bioessays 19:949-57.
31. Wang C, Puerta-Guardo H, Biering SB, Glasner DR, Tran EB, Patana M, Gomberg TA, Malvar C, Lo NTN, Espinosa DA, Harris E. 2019. Endocytosis of flavivirus NS1 is required for NS1-mediated endothelial hyperpermeability and is abolished by a single N-glycosylation site mutation. PLoS Pathog 15:e1007938.
32. Jovic M, Sharma M, Rahajeng J, Caplan S. 2010. The early endosome: a busy sorting station for proteins at the crossroads. Histol Histopathol 25:99-112.
33. Simonsen A, Lippe R, Christoforidis S, Gaullier JM, Brech A, Callaghan J, Toh BH, Murphy C, Zerial M, Stenmark H. 1998. EEA1 links PI(3)K function to Rab5 regulation of endosome fusion. Nature 394:494-8.
34. Rordorf-Nikolic T, Van Horn DJ, Chen D, White MF, Backer JM. 1995. Regulation of phosphatidylinositol 3'-kinase by tyrosyl phosphoproteins. Full activation requires occupancy of both SH2 domains in the 85-kDa regulatory subunit. J Biol Chem 270:3662-6.
35. Vandal G, Geiling B, Dankort D. 2014. Ras effector mutant expression suggest a negative regulator inhibits lung tumor formation. PLoS One 9:e84745.
36. Wan G, Pehlke C, Pepermans R, Cannon JL, Lidke D, Rajput A. 2015. The H1047R point mutation in p110 alpha changes the morphology of human colon HCT116 cancer cells. Cell Death Discov 1:15044.
37. Samuels Y, Wang Z, Bardelli A, Silliman N, Ptak J, Szabo S, Yan H, Gazdar A, Powell SM, Riggins GJ, Willson JK, Markowitz S, Kinzler KW, Vogelstein B, Velculescu VE. 2004. High frequency of mutations of the PIK3CA gene in human cancers. Science 304:554.
38. Carson JD, Van Aller G, Lehr R, Sinnamon RH, Kirkpatrick RB, Auger KR, Dhanak D, Copeland RA, Gontarek RR, Tummino PJ, Luo L. 2008. Effects of oncogenic p110alpha subunit mutations on the lipid kinase activity of phosphoinositide 3-kinase. Biochem J 409:519-24.
39. Cheung LW, Hennessy BT, Li J, Yu S, Myers AP, Djordjevic B, Lu Y, Stemke-Hale K, Dyer MD, Zhang F, Ju Z, Cantley LC, Scherer SE, Liang H, Lu KH, Broaddus RR, Mills GB. 2011. High frequency of PIK3R1 and PIK3R2 mutations in endometrial cancer elucidates a novel mechanism for regulation of PTEN protein stability. Cancer Discov 1:170-85.
40. Shi H, Hugo W, Kong X, Hong A, Koya RC, Moriceau G, Chodon T, Guo R, Johnson DB, Dahlman KB, Kelley MC, Kefford RF, Chmielowski B, Glaspy JA, Sosman JA, van Baren N, Long GV, Ribas A, Lo RS. 2014. Acquired resistance and clonal evolution in melanoma during BRAF inhibitor therapy. Cancer Discov 4:80-93.
41. Huang CH, Mandelker D, Schmidt-Kittler O, Samuels Y, Velculescu VE, Kinzler KW, Vogelstein B, Gabelli SB, Amzel LM. 2007. The structure of a human p110alpha/p85alpha complex elucidates the effects of oncogenic PI3Kalpha mutations. Science 318:1744-8.
42. Jaiswal BS, Janakiraman V, Kljavin NM, Chaudhuri S, Stern HM, Wang W, Kan Z, Dbouk HA, Peters BA, Waring P, Dela Vega T, Kenski DM, Bowman KK, Lorenzo M, Li H, Wu J, Modrusan Z, Stinson J, Eby M, Yue P, Kaminker JS, de Sauvage FJ, Backer JM, Seshagiri S. 2009. Somatic mutations in p85alpha promote tumorigenesis through class IA PI3K activation. Cancer Cell 16:463-74.
43. Shin YK, Liu Q, Tikoo SK, Babiuk LA, Zhou Y. 2007. Influenza A virus NS1 protein activates the phosphatidylinositol 3-kinase (PI3K)/Akt pathway by direct interaction with the p85 subunit of PI3K. J Gen Virol 88:13-18.
44. Antal CE, Newton AC. 2013. Spatiotemporal dynamics of phosphorylation in lipid second messenger signaling. Mol Cell Proteomics 12:3498-508.

559 45. Backer JM. 2010. The regulation of class IA PI 3-kinases by inter-subunit interactions. Curr Top
560 Microbiol Immunol 346:87-114.
561 46. Dou Z, Pan JA, Dbouk HA, Ballou LM, DeLeon JL, Fan Y, Chen JS, Liang Z, Li G, Backer JM, Lin RZ,
562 Zong WX. 2013. Class IA PI3K p110beta subunit promotes autophagy through Rab5 small GTPase
563 in response to growth factor limitation. Mol Cell 50:29-42.
564 47. Siempelkamp BD, Rathinaswamy MK, Jenkins ML, Burke JE. 2017. Molecular mechanism of
565 activation of class IA phosphoinositide 3-kinases (PI3Ks) by membrane-localized HRas. J Biol Chem
566 292:12256-12266.
567 48. Liu R, Chen Y, Liu G, Li C, Song Y, Cao Z, Li W, Hu J, Lu C, Liu Y. 2020. PI3K/AKT pathway as a key
568 link modulates the multidrug resistance of cancers. Cell Death Dis 11:797.
569 49. Duronio V. 2008. The life of a cell: apoptosis regulation by the PI3K/PKB pathway. Biochem J
570 415:333-44.
571 50. Koliopoulos MG, Lethier M, van der Veen AG, Haubrich K, Hennig J, Kowalinski E, Stevens RV,
572 Martin SR, Reis e Sousa C, Cusack S, Rittinger K. 2018. Molecular mechanism of influenza A NS1-
573 mediated TRIM25 recognition and inhibition. Nat Commun 9:1820.
574 51. Kabiljo J, Laengle J, Bergmann M. 2020. From threat to cure: understanding of virus-induced cell
575 death leads to highly immunogenic oncolytic influenza viruses. Cell Death Discov 6:48.
576 52. Bergmann M, Romirer I, Sachet M, Fleischhacker R, Garcia-Sastre A, Palese P, Wolff K,
577 Pehamberger H, Jakesz R, Muster T. 2001. A genetically engineered influenza A virus with ras-
578 dependent oncolytic properties. Cancer Res 61:8188-93.
579 53. Pleschka S, Wolff T, Ehrhardt C, Hobom G, Planz O, Rapp UR, Ludwig S. 2001. Influenza virus
580 propagation is impaired by inhibition of the Raf/MEK/ERK signalling cascade. Nat Cell Biol 3:301-
581 5.

582

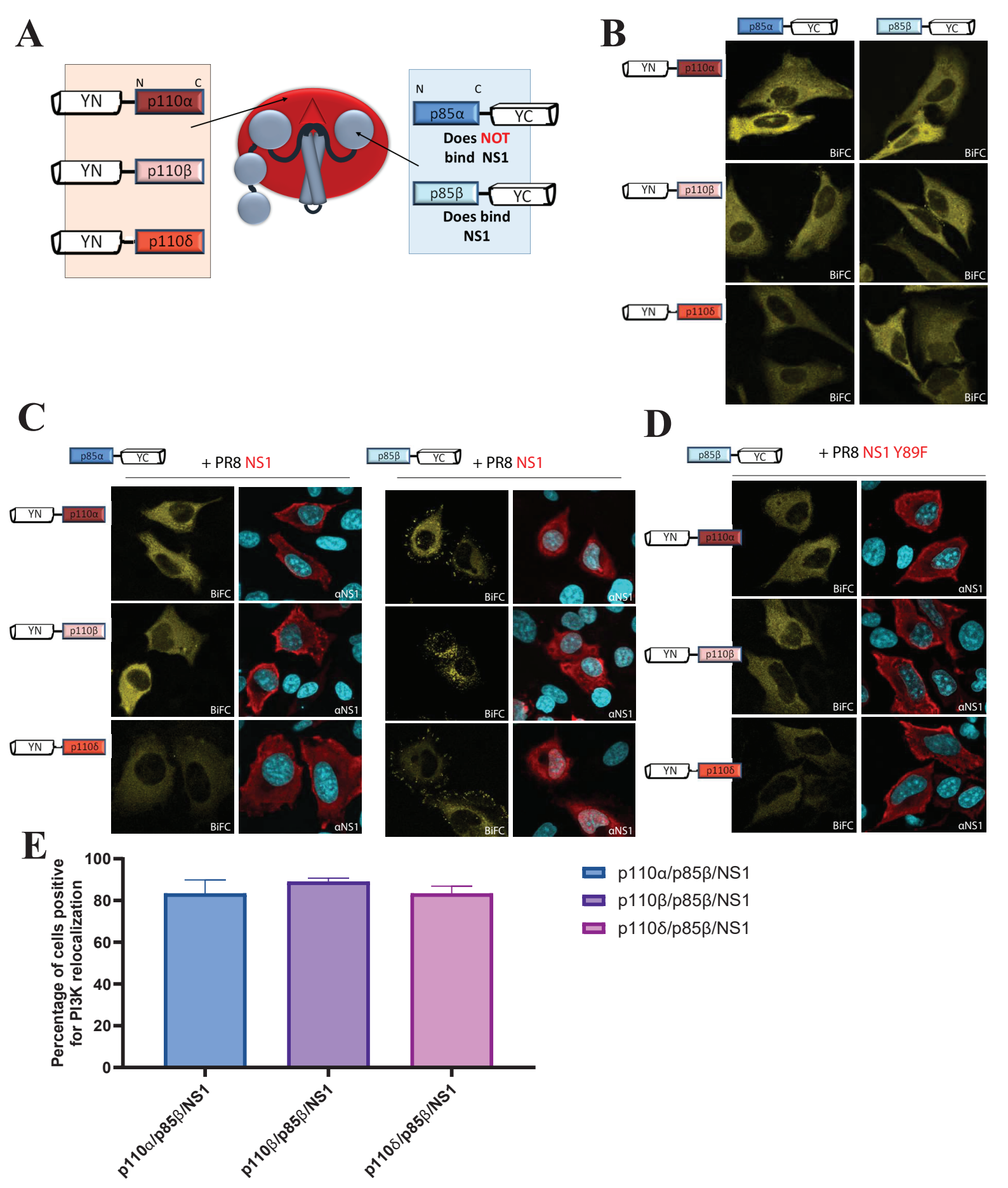
A
N
C
YN
p110α
YN
p110β
YN
p110δ
N
C
p85α
YC
Does NOT bind NS1
p85β
YC
Does bind NS1
B
p85α
YC
p85β
YC
YN
p110α
YN
p110β
YN
p110δ
BiFC
C
p85α
YC
+ PR8 NS1
p85β
YC
+ PR8 NS1
YN
p110α
YN
p110β
YN
p110δ
BiFC
αNS1
D
p85β
YC
+ PR8 NS1 Y89F
YN
p110α
YN
p110β
YN
p110δ
BiFC
αNS1
E
Percentage of cells positive for PI3K relocalization
100
80
60
40
20
0
p110α/p85β/NS1
p110β/p85β/NS1
p110δ/p85β/NS1
p110α/p85β/NS1
p110β/p85β/NS1
p110δ/p85β/NS1

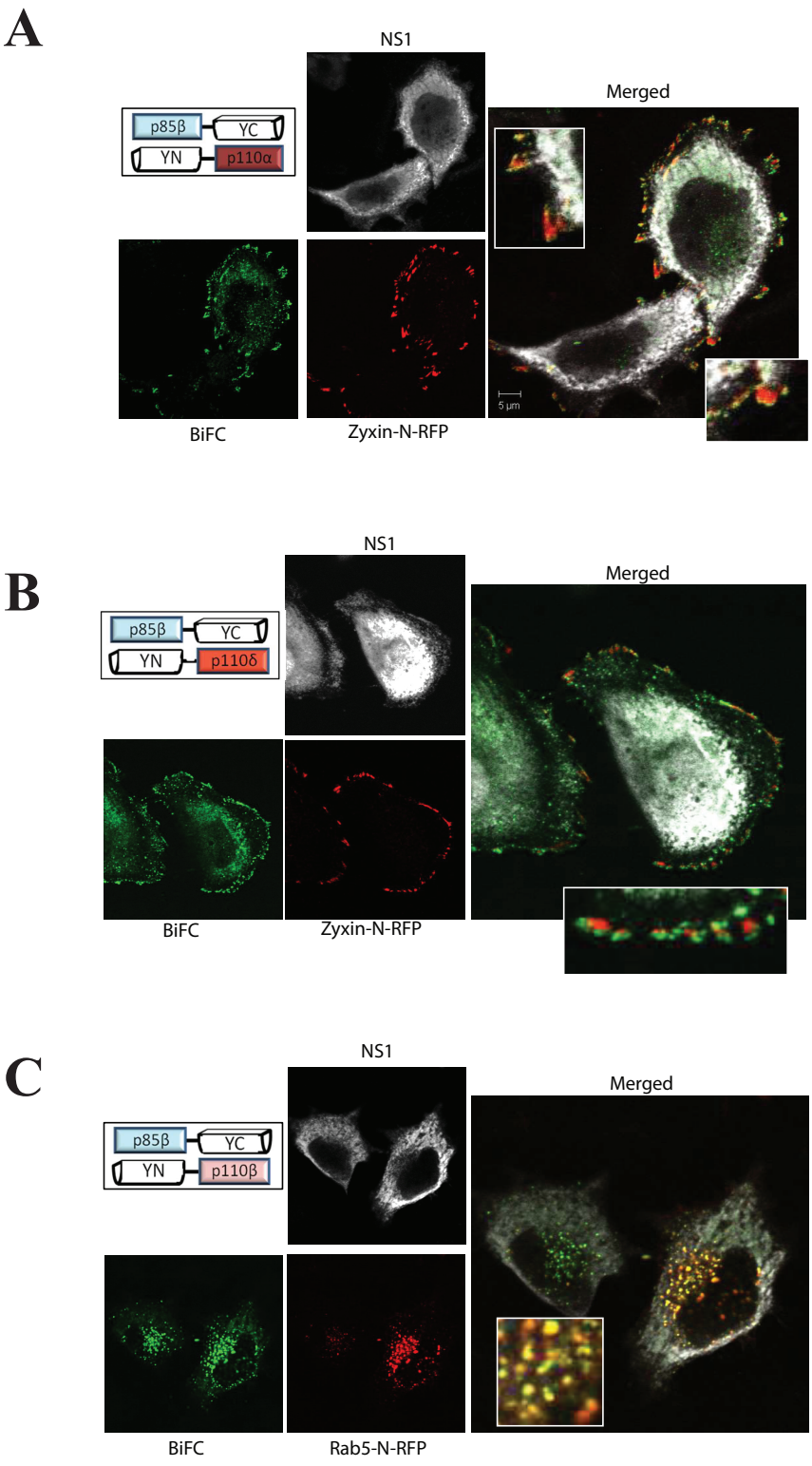
A
NS1
Merged
p85β
YC
YN
p110α
5 μm
BiFC
Zyxin-N-RFP
B
NS1
Merged
p85β
YC
YN
p110δ
BiFC
Zyxin-N-RFP
C
NS1
Merged
p85β
YC
YN
p110β
BiFC
Rab5-N-RFP

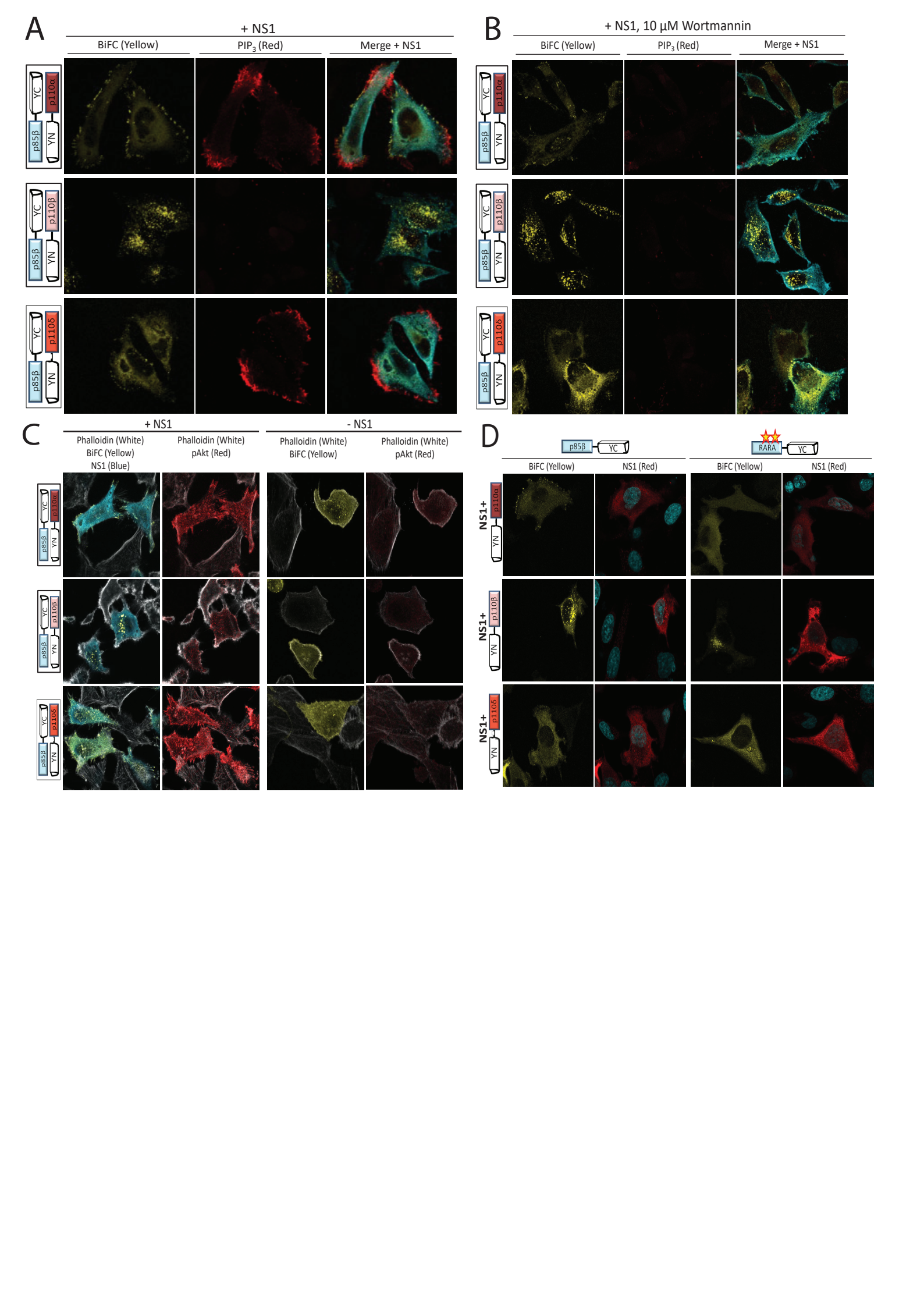
A
+ NS1
BiFC (Yellow)
PIP3 (Red)
Merge + NS1
YC
p110α
p85β
YN
p110β
p110δ
B
+ NS1, 10 µM Wortmannin
C
+ NS1
- NS1
Phalloidin (White)
BiFC (Yellow)
NS1 (Blue)
pAkt (Red)
D
p85β
YC
RARA
NS1 (Red)
NS1+

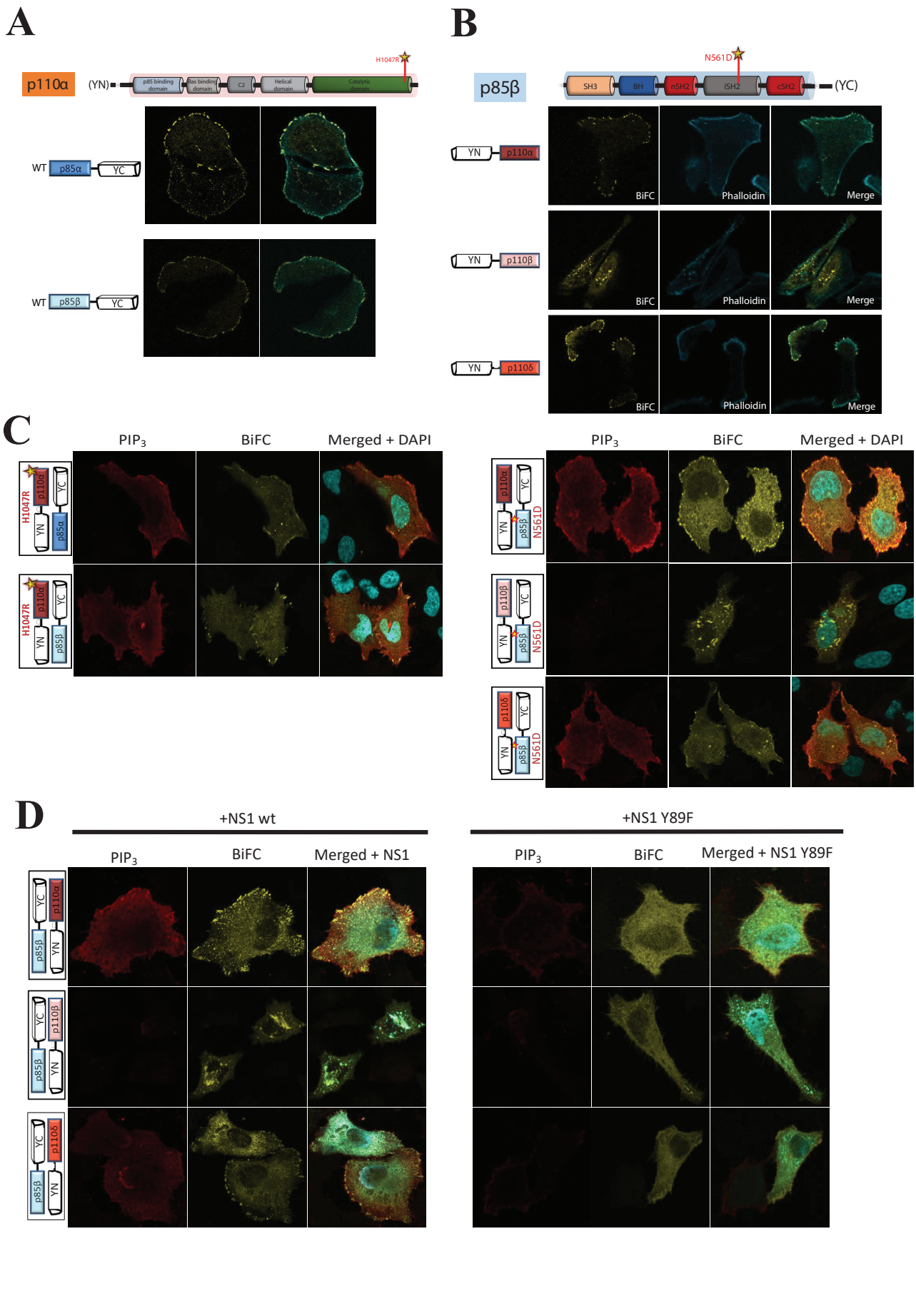
A
p110α
(YN)
H1047R
p85 binding domain
Ras binding domain
C2
Helical domain
Catalytic domain
WT
p85α
YC
WT
p85β
YC
B
p85β
N561D
SH3
BH
nSH2
iSH2
cSH2
(YC)
YN
p110α
BiFC
Phalloidin
Merge
YN
p110β
BiFC
Phalloidin
Merge
YN
p110δ
BiFC
Phalloidin
Merge
C
PIP3
BiFC
Merged + DAPI
H1047R
p110α
YC
YN
p85α
H1047R
p110α
YC
YN
p85β
PIP3
BiFC
Merged + DAPI
p110α
YC
YN
p85β
N561D
p110β
YC
YN
p85β
N561D
p110δ
YC
YN
p85β
N561D
D
+NS1 wt
+NS1 Y89F
PIP3
BiFC
Merged + NS1
PIP3
BiFC
Merged + NS1 Y89F
YC
p110α
p85β
YN
YC
p110β
p85β
YN
YC
p110δ
p85β
YN

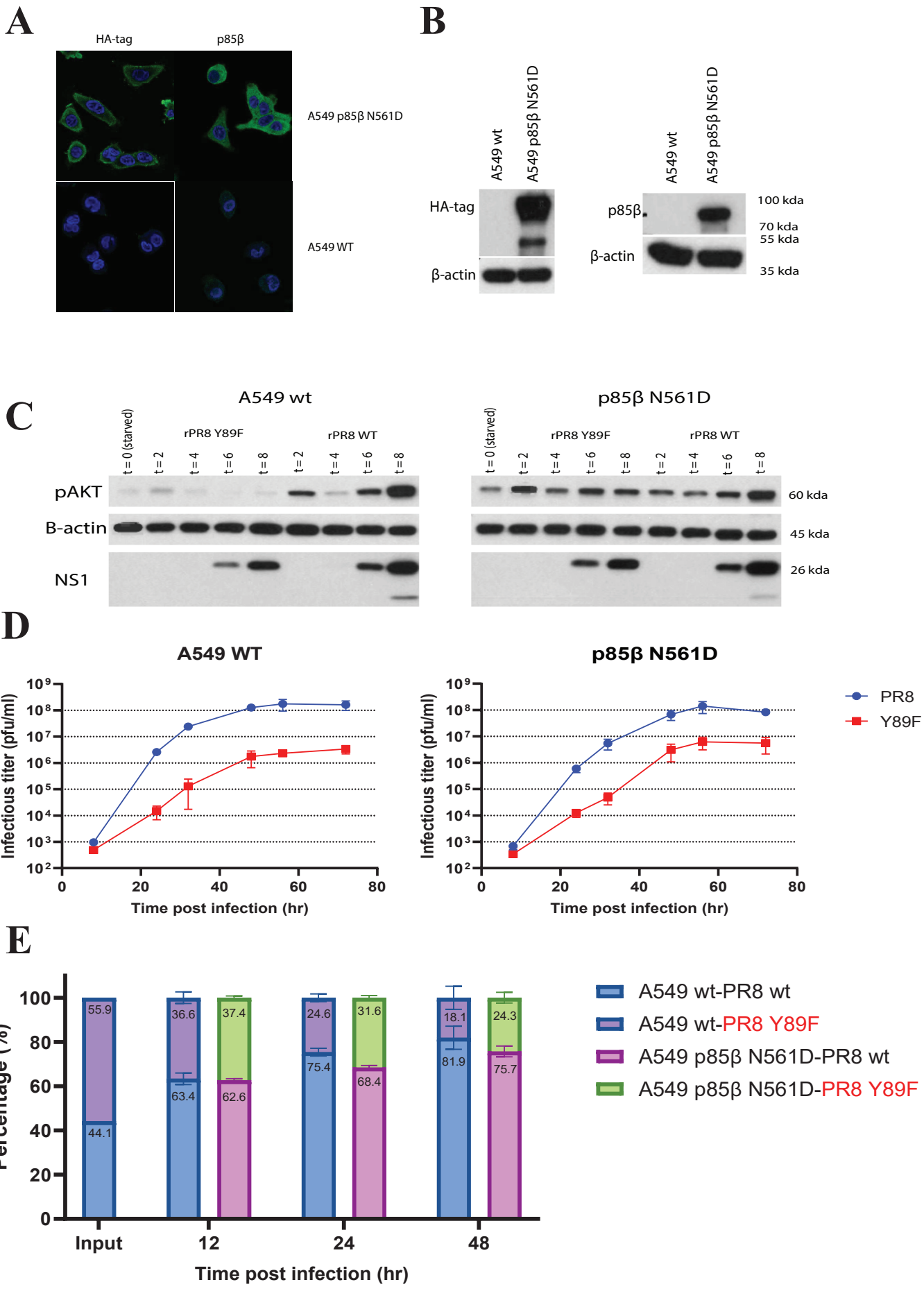
A
HA-tag
p85β
A549 p85β N561D
A549 WT
B
A549 wt
A549 p85β N561D
HA-tag
β-actin
p85β
100 kda
70 kda
55 kda
35 kda
C
A549 wt
p85β N561D
rPR8 Y89F
rPR8 WT
t = 0 (starved)
t = 2
t = 4
t = 6
t = 8
pAKT
B-actin
NS1
60 kda
45 kda
26 kda
D
A549 WT
p85β N561D
Infectious titer (pfu/ml)
Time post infection (hr)
PR8
Y89F
E
Percentage (%)
55.9
44.1
36.6
63.4
37.4
62.6
24.6
75.4
31.6
68.4
18.1
81.9
24.3
75.7
Input
12
24
48
Time post infection (hr)
A549 wt-PR8 wt
A549 wt-PR8 Y89F
A549 p85β N561D-PR8 wt
A549 p85β N561D-PR8 Y89F

Influenza A virus NS1 protein mimics oncogenic PI3K resulting in isoform specific cellular redistribution and activation

Sadaf Aslam[a,b,c], María T. Sánchez-Aparicio[a,b], Braden D. Siempelkamp[d], Gillian L. Dornan[d], Nikos Tsolakos[e], John E. Burke[d,f], Benjamin G. Hale[e], Adolfo García-Sastre[a,b,g,h,i,j,1] and Juan Ayllon[a,b,c,1]

Affiliation:

[a]Department of Microbiology, Icahn School of Medicine at Mount Sinai, New York, NY 10029

[b]Global Health and Emerging Pathogens Institute, Icahn School of Medicine at Mount Sinai, New York, NY 10029

[c]Department of Health Sciences, University of Burgos, Burgos, Spain, 09001

[d]Department of Biochemistry and Microbiology, University of Victoria, Victoria, BC, V8W 2Y2, Canada

[e]Institute of Medical Virology, University of Zurich, Winterthurerstrasse 190, Zurich, 8057, Switzerland

[f]Department of Biochemistry and Molecular Biology, The University of British Columbia, Vancouver, BC V6T 1Z3, Canada

[g]Department of Pathology, Molecular and Cell-Based Medicine, Icahn School of Medicine at Mount Sinai, New York, NY 10029

[h]Department of Medicine, Division of Infectious Diseases, Icahn School of Medicine at Mount Sinai, New York, NY 10029

[i]The Icahn Genomics Institute, Icahn School of Medicine at Mount Sinai, New York, NY 10029

[j]The Tisch Cancer Institute, Icahn School of Medicine at Mount Sinai, New York, NY 10029

[1]Correspondence to: jayllon@ubu.es; Adolfo.garcia-sastre@mssm.edu

Keywords: Influenza A virus, non-structural protein 1 (NS1), phosphoinositide-3-kinases (PI3K), bimolecular fluorescence complementation (BiFC)

This supplementary appendix contains:

Supplementary figures

Material and Methods

Supplementary references

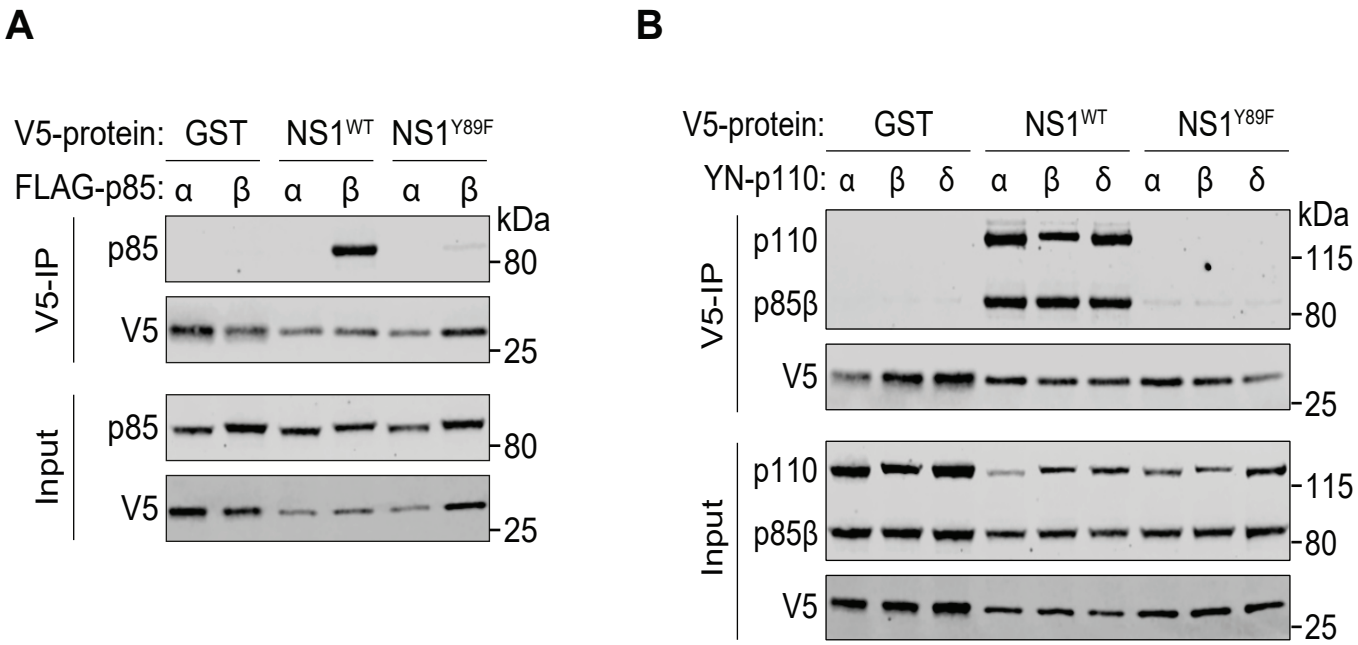

Figure S1. NS1 binds to p85β-p110 dimers with no preference for a specific catalytic subunit. (A) Assessment of binding of NS1 to p85 subunits using 293T cells co-transfected for 48 h with plasmids expressing the indicated V5-tagged NS1 protein (or GST) and FLAG-tagged p85α or p85β. NS1 preferentially binds to p85β only. (B) 293T cells were co-transfected with plasmids expressing the indicated V5-tagged NS1 protein (or GST), FLAG-tagged p85β and YN-tagged p110α or p110β or p110δ catalytic subunit and cell lysates were co-immunoprecipated with V5 antibody and analyzed by SDS-Page and western blotting (soluble (input) and pulldown (V5-IP)). We detected that NS1 binds to all the p85β-p110x dimers with no preference for a specific catalytic subunit.

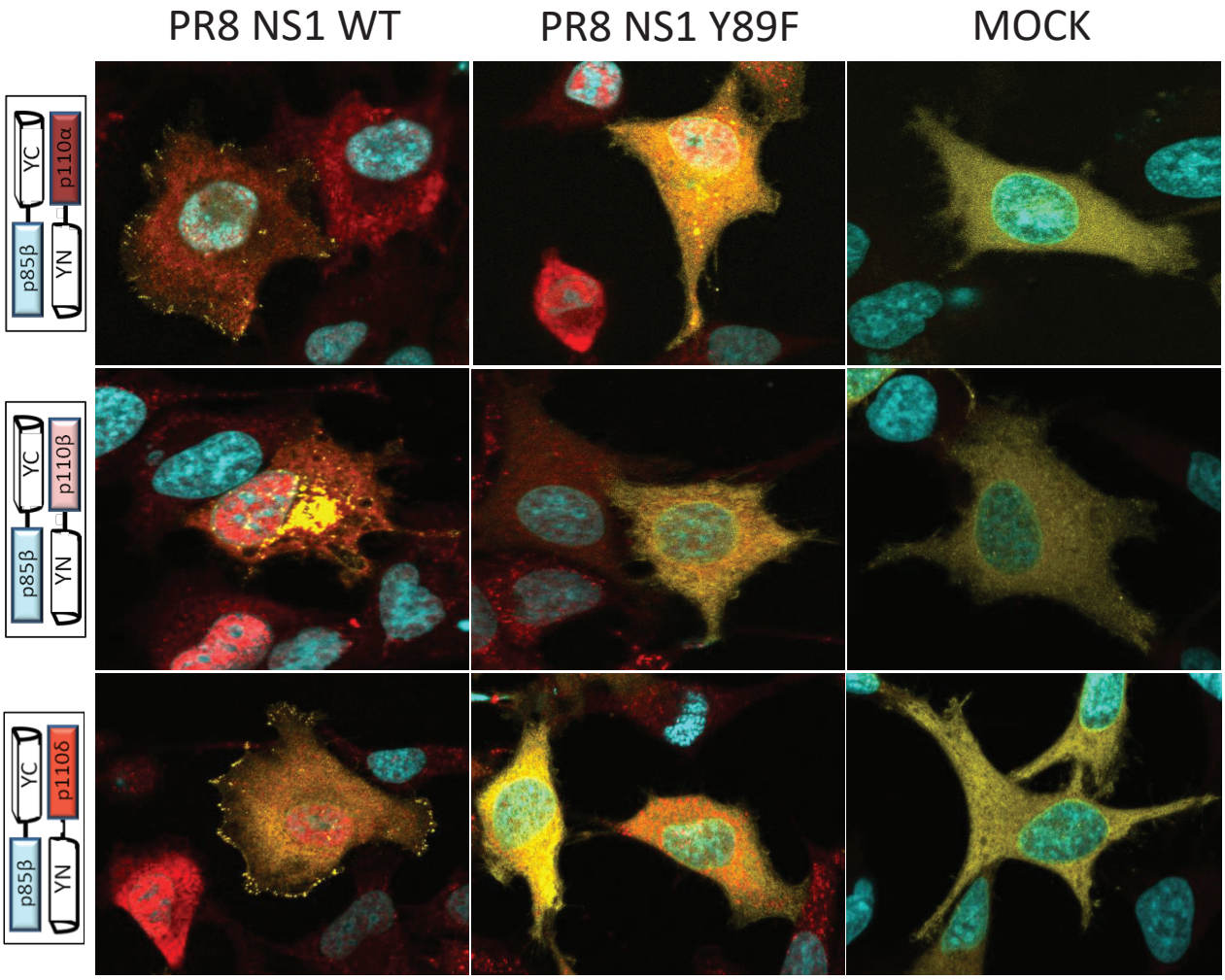

Figure S2. Relocalization of BiFC PI3K heterodimers by infection. HeLa cells were co-transfected with different BiFC complexes and 19 hr p.t. cells were infected with an MOI of 10 PFU/cell. 24 hrs post infection they were processed for fluorescence microscopy. Cells infected with rPR8 WT led to the distinct relocalization pattern of the PI3K heterodimers but with rPR8-Y89F the complexes were in a homogeneous distribution similar to the mock infected cells. (BiFC in yellow, NS1 in red and DAPI in cyan).

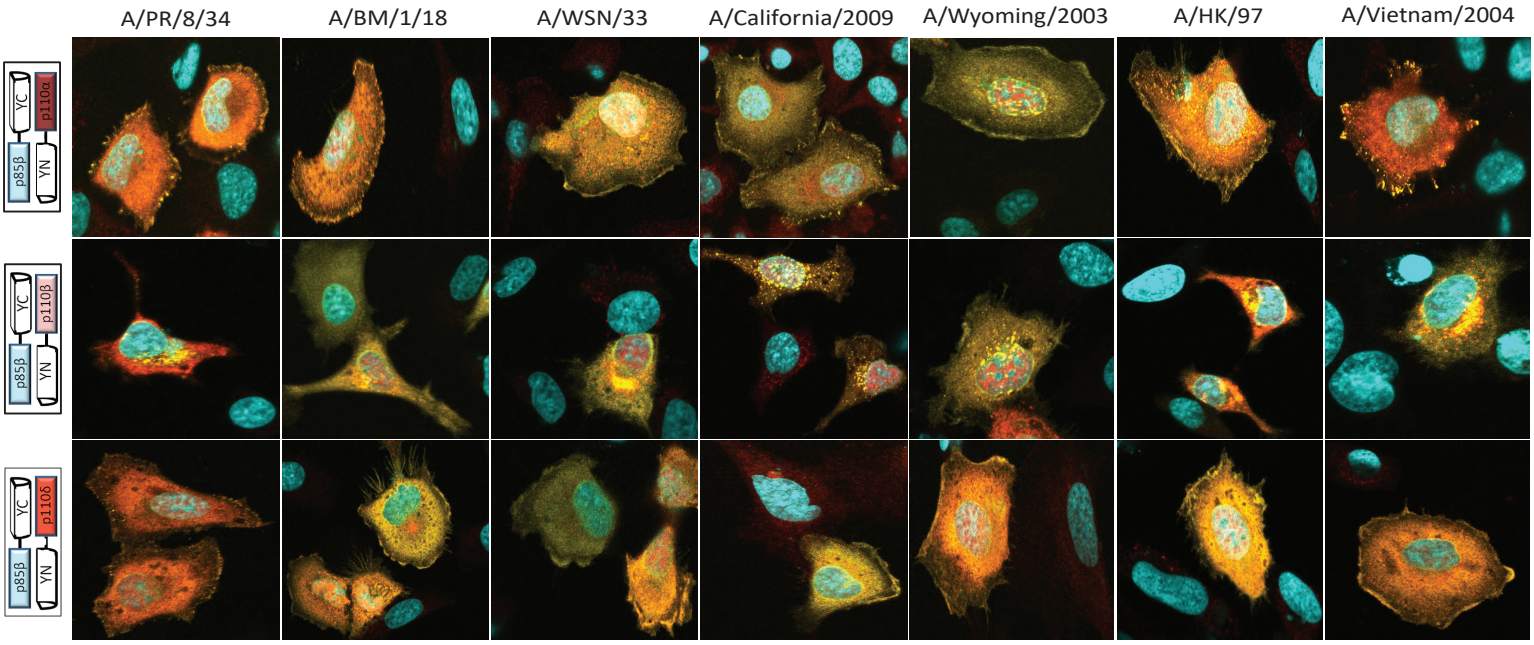

Figure S3. Distinct redistribution of PI3K heterodimers is not strain dependent. HeLa cells were co-transfected with indicated BiFC constructs and NS1 from different strains. At 19 hr p.t., cells were processed for immunofluorescence with antibody against NS1 (1A7). NS1 from different influenza A strains were able to relocalize the complexes with p110α and p110β to the focal adhesion regions and the complexes with p110β near the endosome in a strain independent manner. (BiFC in yellow, NS1 in red and DAPI in cyan).

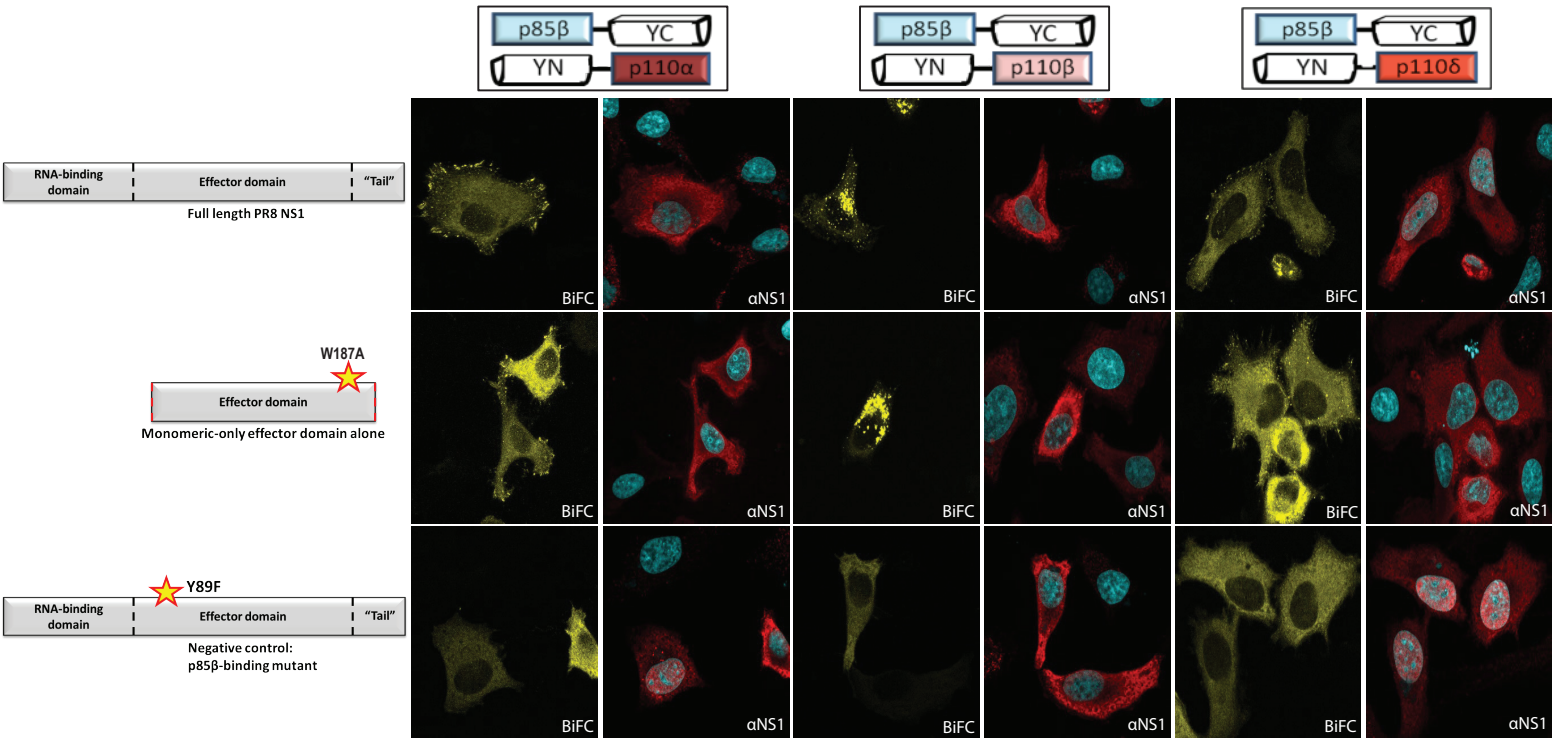

Figure S4. Relocalization of PI3K BiFC with effector domain of NS1. HeLa cells were transfected with the different PI3K complexes and monomeric effector domain of NS1, NS1 full length and mutant NS1. The monomeric effector domain of NS1 (NS1 ED with W187A) is sufficient to induce the same PI3K heterodimer relocalizations as full length NS1, NS1-Y89F was used as a negative control. (NS1: red, DAPI: cyan, BiFC: yellow).

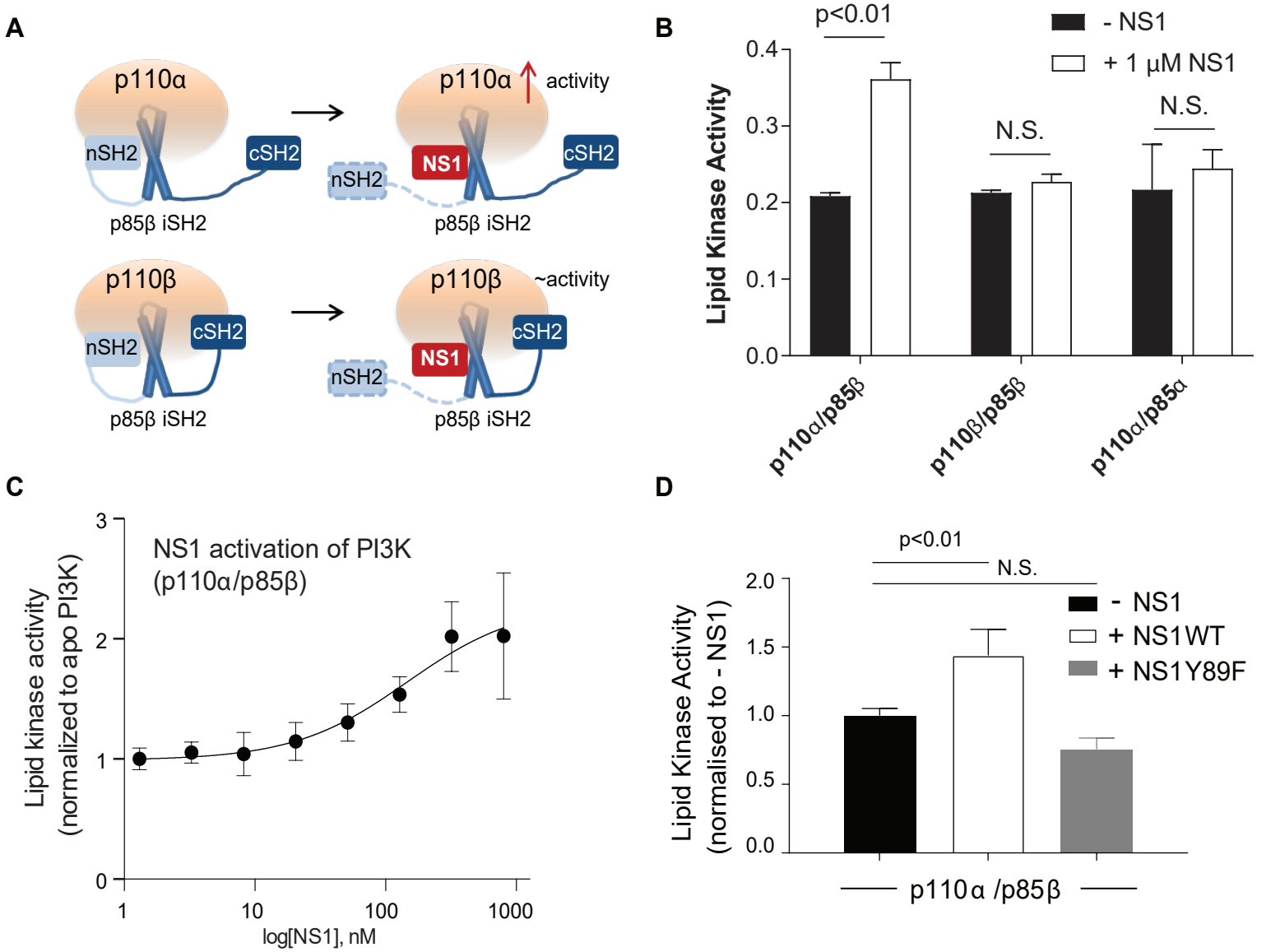

Figure S5. NS1 leads to activation of only p110α/p85β, with no significant activation of p110β/p85β. A) Schematic of NS1 activation of class IA PI3Ks. B) Relative activities of different combinations of catalytic and regulatory subunits of class IA PI3Ks in the presence and absence of 1 μM NS1. Assays measured the turnover of ATP in the presence of PI3K complexes at the following concentrations: 30 nM p110α/p85β, 300 nM p110β/p85β, and 60 nM p110α/p85α. Kinase assays contained 100 μM ATP, and 0.45 mg/ml vesicles containing [5% PIP2 /15% PC/20% PS/45% PE/10% cholesterol/5% sphingomyelin]. C) Dose response of p110α/p85β with increasing amounts of NS1 protein. D) Mutation of Y89F in NS1 prevents PI3K activation. Kinase assays were carried out under the same conditions as panel B, with both wild type and Y89F NS1 present at 1 μM. For all panels, assays were performed in triplicate (error shown as S.D., n = 3), with p values greater than 0.05 shown as not significant (N.S.).

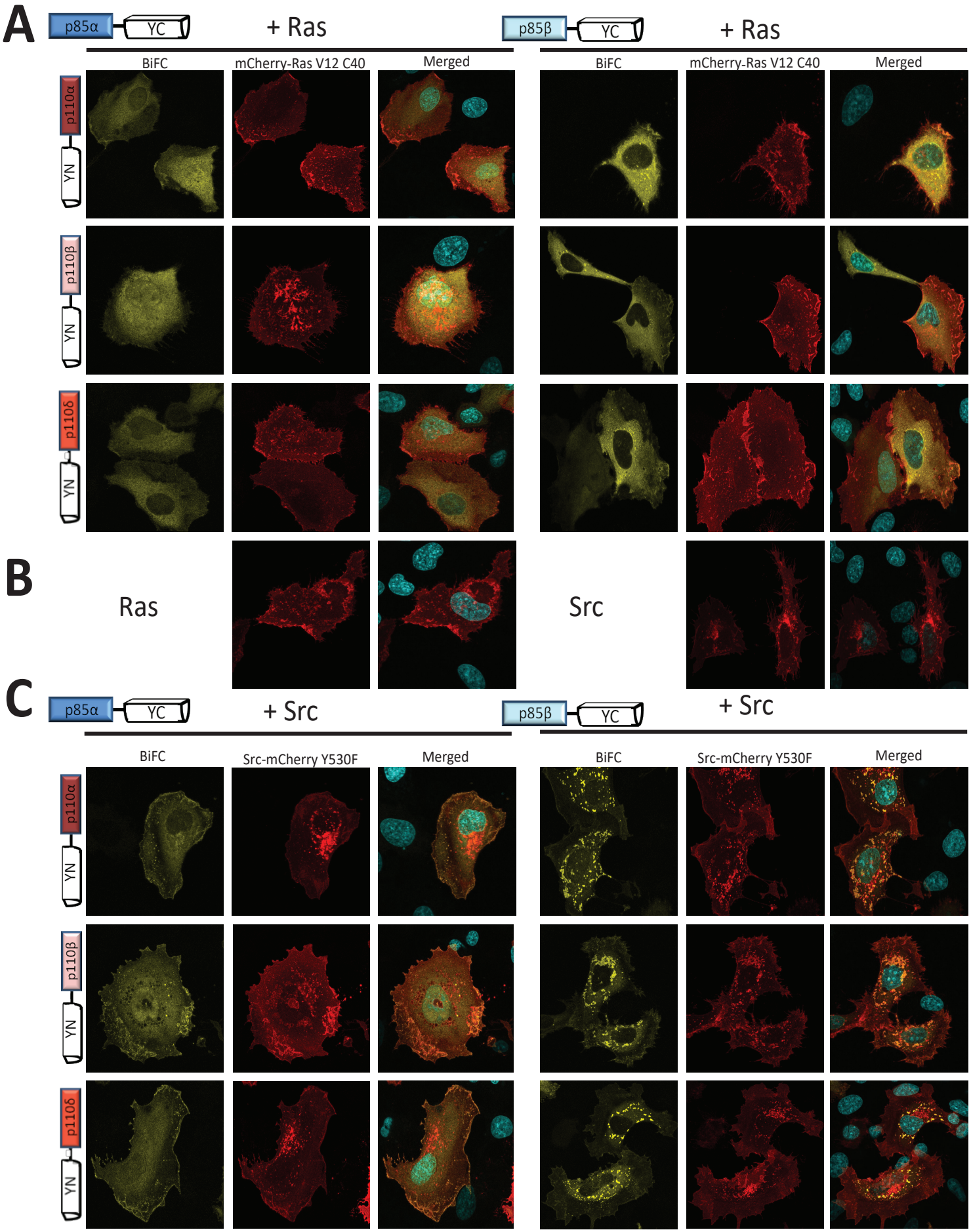

Figure S6. Relocalization of BiFC PI3K heterodimers by different cellular stimuli. A) HeLa cells were co-transfected with the indicated BiFC constructs together with pCAGGS-mCherry-HRas V12 C40. The PI3K complexes relocalized to similar membrane regions with both p85α and p85β. B) When HeLa cells were co-transfected with PI3K BiFC constructs together with pCAGGS-Src-mCherry Y530F, we observed an isoform dependent redistribution of the PI3K complexes. Complexes with p85α redistributed to the cell edges while complexes with p85β formed a punctate distribution near the nucleus. (BiFC in yellow, DAPI in blue and Ras/Src in Red).

Material and Methods

Cell lines and viruses
A549, 293T, MDCK and HeLa cells were obtained from ATCC and were cultured in Dulbecco's Modified Eagle Medium (DMEM, Gibco) supplemented with 10% fetal bovine serum (FBS, HyClone), 10 U penicillin per mL, 10 mg streptomycin per mL (Gibco) and grown at 37°C and 5% CO_2. Influenza A viruses were grown in 8-10 day old embryonated chicken eggs (Charles River) for 2 days at 37 °C. Allantoic fluid was harvested and spun at 290 x g for 5 min at 4°C and supernatant was aliquoted and frozen at -80°C. Viral titers were determined using standard plaque assay on MDCK cells and immunostained using antibody against NP (PA532242, Invitrogen).

Plasmids
Constructs encoding the ORF of human p85α, p85β, p110α, p110β, p110δ and Src were purchased from OriGene and subcloned into pCAGGS (1). Constructs encoding the ORF of human Ras V12 was purchased from Clontech and subcloned into pCAGGS with an mCherry tag. The N-terminus (YN) of YFP was added to the N-terminus of p110s (YN- p110α, YN-p110β, YN-p110δ) and the C-terminus of YFP (YC) was added to the C-terminus of the p85s (YC-p85α, YC-p85β) by polymerase chain reaction (PCR). NS1 ORF from A/Puerto Rico/8/1934 was cloned into pCAGGS with a V5 tag at the N-terminus. Y89F, W187A, N561D, H1047R, T40C and Y530F mutations were introduced by site directed mutagenesis using overlapping primers. Zyxin-N-RFP and Rab5-N-RFP constructs were purchased from OriGene and subcloned into pCAGGS. pCAGGS with NS1 from A/Puerto Rico/8/1934, A/Brevig Mission/1/1918, A/Wilson-Smith/1933, A/California/04/2009, A/Wyoming/03/2003, A/Hong Kong/156/1997 and A/Vietnam/1203/2004 have been previously described (2).

Bimolecular fluorescence complementation (BiFC) assay
HeLa cells were co-transfected with plasmids containing p110s, p85s and/or NS1 using Lipofectamine 2000 (Invitrogen) according to the manufacturer's guidelines. 8-16 hrs post transfection, media was changed. 16 hrs post transfection cells were placed at 33 °C for 3 hrs. Cells were washed with phosphate buffer saline (PBS, Gibco) and fixed with ice cold methanol (sigma) for 20 minutes at 4 °C. Then they were washed with PBS and blocked with 1% bovine serum albumin (BSA)/PBS for 1 hr at room temperature (RT). Primary antibody (V5-tag (Invitrogen, 460705)) was diluted (1:500) in 1% BSA/PBS and added to the cells for 1 hr at RT. Cells were washed with PBS and incubated with secondary antibody (anti-mouse Alexa 633 (Invitrogen, A21052)) and 4′,6-diamidino-2-phenylindole (DAPI) (Invitrogen, D1306) diluted (1:1000) in 1% BSA/PBS for 1 hr at RT, followed by three PBS washes. Samples were stored in PBS at 4℃ and protected from light. Fluorescence was observed using confocal microscope (LSM 580 and LSM880) and images were acquired. For experiments involving wortmannin (Sigma, 681675-1MG), treatment was performed according to manufacturer's instructions. For experiments involving different NS1 plasmids, 1A7 (anti-NS1) was used at 1:500 and anti-mouse Alexa 633 (1:1000) as the secondary antibody (3).

Modifications for PIP_3 staining
Cells were fixed with 2.5% paraformaldehyde (PFA) (Polyscience, 04018-1) for 5 mins at RT. Then they were washed with PBS three times and permeabilized with 0.5% saponin in PBS for 15 mins at RT. The rest was as described above, with the following antibodies and incubation conditions: Blocked with 10% BSA/PBS overnight at 4°C, primary antibody (Echelon Biosciences**)** diluted (1:200) in 1% BSA/PBS at 37°C for 1hr, secondary antibody (anti-mouse Alexa 633, 1:1000) and DAPI (1:2000) diluted in 1% BSA/PBS at RT for 30 mins.

Modifications for pAKT staining
Cells were fixed with PFA 4% for 10 mins at RT followed by three PBS washes. They were permeabilized with 0.1% Triton X-100 (Fisher, BP151-500) for 5 min at RT. The rest was as described above, with the following changes: Blocked with 1% BSA/PBS overnight at 4℃, primary antibodies V5-tag (1:500), pAkt (1:200) (Cell Signaling Technology, 4060) diluted in 1% BSA/PBS for 1hr at RT, secondary antibodies anti-rabbit Alexa fluor 647 (1:1000) (Invitrogen, A21443), Pacific Blue anti-mouse (1:1000) (Invitrogen, P31582), and Phalloidin Alexa fluor 568 (1:40) (Invitrogen, A12380), diluted in 1% BSA/PBS at RT for 1hr.

BiFC with infection
HeLa cells were co-transfected with the different BiFC constructs using Lipofectamine 3000 (Invitrogen) according to the manufacturer's guidelines. 8-16 hrs post transfection, media was changed. 16 hrs post transfection cells were placed at 33 °C for 3 hrs. Cells were washed twice with OPTI-MEM I (Gibco, 31985-062) and then infected with rPR8 WT and rPR8-Y89F with an MOI of 10 PFU/cell. At 1 hr p.i., the inoculum was removed and infection media (1xMem+0.2% BA+P/S) added and the cells were incubated at 33 °C for 24 hrs. At 24 hrs p.i., cells were processed for immunofluorescence with anti-NS1 antibody (Invitrogen, PA532243).

Generation of a stable cell line
HA-p85β-N561D ORF was cloned into pLVX-IRES-Puro lentivirus vector (Takara). 293T cells were co-transfected with pLVX-IRES-Puro-HA-p85β-N561D, lenti-gag/pol, and pMD2VSV-G using TransIT-LT1 (Mirus) according to the manufacturer's guidelines. Supernatant was collected at 48 hrs post transfection and fresh media was added and collected at 60 hrs post transfection. Both supernatants were combined and spun at 1200 rpm for 10 min in a tabletop centrifuge (Eppendorf). The supernatant was filtered through a 0.45 µm cellulose acetate filter and aliquoted and frozen at -80 °C. A549 cells were seeded in a 6 well plate and fresh media, lentivirus and polybrene (1ul of 12mg/ml stock) (Millipore, TR-1003G) were added. Four days post transduction cells were selected with puromycin. Clonal population was generated, and clones were tested by indirect immunofluorescence using anti-HA antibody (Invitrogen).

Growth curve
A549 wt and A549-p85β-N561D cells were seeded in 6 well plates in triplicates for each virus. They were washed with PBS and starvation media was added (1xMEM + P/S + 0.2% BA) for 24 hrs. Following starvation, cells were infected with A/Puerto Rico/8/134 (rPR8 wt) or A/Puerto Rico/8/1935-NS1-Y89F (rPR8-Y89F) at an MOI of 0.01 PFU/cell and supernatants were collected at 8, 24, 32, 48, 56, and 72 hr post infection. Plaque assays were performed on MDCK cells for viral titers.

Immunofluorescence
A549 wt and A549-p85β-N561D cells were seeded on 12 well glass bottom plates. Cells were fixed with 4% PFA without methanol for 30 minutes. Cells were permeabilized with 0.1% triton x-100 for 15 mins and then washed with PBS. Cells were blocked with 1% BSA/PBS for 1 hr at RT. Primary antibodies (HA tag, Invitrogen, 326700), and p85β (Invitrogen, MS53215)) were diluted (1:1000) in 1% BSA/PBS and incubated for 1 hr at RT. Cells were washed with PBS and secondary antibodies (anti-rabbit Alexa 488 (Invitrogen, A-11034)) and DAPI were diluted (1:1000) in 1% BSA/PBS and incubated for 1 hr at RT. Cells were washed with PBS three times and were stored in PBS at 4℃ (protected from light). Fluorescence was observed with LSM880, and images were acquired. Images were processed with ImageJ.

Western blot and protein quantification
A549 WT and A549-p85β-N561D cells were starved for 24 hrs with starvation media (1xMEM + P/S + 0.2% BA) and then infected with A/Puerto Rico/8/1934 and A/Puerto Rico/8/1934-NS1-Y89F at an MOI of 2 PFU/cell. Cells were collected at 0, 2, 4, 6, 8 hours post infection. Cells were lysed in RIPA buffer with protease/phosphatase inhibitor (Cell Signaling Technology) according to the manufacturer's guidelines. Proteins from cell lysates were quantified using Pierce BCA protein assay kit (Thermo fisher) and 10 µg of total protein was mixed with Pierce lane marker reducing sample buffer (Thermo fisher). Samples were run on 4-20% reducing denaturing sodium dodecyl sulfate polyacrylamide gel electrophoresis (SDS-PAGE) (Bio-Rad) and the proteins were transferred onto a polyvinylidene difluoride (PVDF) membrane (Bio-Rad) using turbo transfer system (Bio-Rad). The membrane was blocked with 5% (w/v) BSA in PBS containing 0.1% (v/v) Tween 20 (PBST) for 1 hr at RT on a shaker. The membrane was incubated with pAkt (Ser473) (1:1000) (Cell Signaling Technology, 4060S) diluted in 5% BSA in PBST overnight at 4℃ on a shaker. The membrane was washed with PBST three times (5 minutes incubation each time) on a shaker at RT. The membrane was incubated with anti-mouse-HRP (horseradish peroxidase) IgG diluted in 5% BSA in PBST (1:2000) for 1 hr at RT on a shaker. The membrane was washed three times with PBST and developed using Brightstar HCL (ASI). The HRP was inactivated by incubating the membrane with 1% sodium azide for 15 minutes on a shaker at RT. The membrane was washed overnight with

PBST (changed several times) on a shaker. The membrane was incubated with monoclonal antibody against NS1 (Invitrogen, GT1653) diluted in 5% Milk/PBST (1:1000) overnight at 4℃ on a shaker. The membrane was washed three times and incubated with anti-mouse-HRP (Kindlebio) diluted in 5% milk/PBST (1:1000) and incubated for 1hr at RT on a shaker. The membrane was washed three times and developed with Brightstar HCL. The membrane was washed for 24 hrs with frequent change with PBST. The membrane was incubated with B-actin-HRP (Cell Signaling Technology, 12262) antibody diluted (1:2000) in 5% non-fat milk/PBST for 1 hr at RT on a shaker. The membrane was washed three times and developed with Brightstar HCL (ASI). Cell line validation western blot was performed as described above and the antibodies used were HA-tag-HRP conjugated (Cell Signaling Technology, 2999S), p85β (Invitrogen, MA53215), and loading control β-actin-HRP (Cell Signaling Technology, 12262).

Competition assay
rPR8 WT and rPR8-Y89F were diluted to 10^7 PFU/mL and then equal amounts of each virus was mixed for a 50:50 ratio. The mixed virus was diluted to 10^3 PFU/mL and A549 WT and A549-p85β-N561D cells were infected, and cells were collected in TRI Reagent (Invitrogen, 9738G) at 12, 24, and 48 hrs post infection. RNA extraction was performed using Direct-zol RNA miniprep extraction kit (Zymol, R2052) according to manufacturer's instructions. Samples were prepared for MinION Oxford Nanopore sequencing.

MinION sequencing
5 µL of each viral RNA sample was used for RT-PCR using SuperScript IV One-Step RT-PCR System (Invitrogen). Each PCR product was purified using AMPure XP (Beckman Coulter) according to the manufacturer's instructions and quantified by Qubit (Thermo Fisher Scientific). The library of purified samples was prepared for sequencing using the Native Barcoding Kit 96 V14 (SQK-NBD114.96, Oxford Nanopore) (4, 5) as per the manufacturer's instructions. The library was loaded onto a MinION flow cell (R10.4.1, Oxford Nanopore), according to the manufacturer's instructions. FASTQ were obtained for each samples and Geneious Prime (2025.1.1) was used to perform reference based alignment and the number of reads for rPR8 WT and rPR8-Y89F were identified.

BiFC quantification
HeLa cells were co-transfected with indicated p110s and p85s and NS1 wt using Lipofectamine 2000 (Invitrogen) according to the manufacturer's guidelines. 8-16 hrs post transfection, media was changed. 16 hrs post transfection cells were placed at 33 °C for 3 hrs. At 19 hrs p.t., cells were processed for fluorescence microscopy following the protocol described above (BiFC assay) using antibodies against V5 tag. 30 cells per condition were checked first for positive BiFC and NS1 signals then their phenotype was checked to determine if they express the relocalization or not, each condition was quantified in triplicates (30 cells/replicate/condition).

Co-Immunoprecipitation assay (Co-IP)
Co-IPs were performed as described previously (6). In brief, using 293T cells transfected with 2 µg of the pLVX-IRES-ZsGreen1 plasmid (Clontech, CA) carrying V5-tagged NS1 proteins or GST (as appropriate), 1 µg of the p3×FLAG-CMV7.1 plasmid (Sigma-Aldrich, MO) expressing FLAG-tagged human p85β or human p85α (provided by Hannah L. Turkington, University of Zurich, Zurich, Switzerland) (7) and 1 µg of the plasmid expressing one of the YN-tagged p110 subunits. Protein lysates (total and IP fractions) were resolved by SDS-PAGE on NuPAGE 4 to 12% Bis-Tris protein gels (Thermo Fisher), followed by transfer to nitrocellulose membranes. Proteins were detected by Western blotting using the following primary antibodies: mouse anti-V5 (cat# MCA1360; Bio-Rad), mouse anti-FLAG (cat# F1804; Sigma-Aldrich) and anti-YFP (cat# ab1218; Abcam). Secondary antibodies were fluorochrome-conjugated anti-mouse immunoglobulin (cat# 35519; Thermo Fisher Scientific) and anti-rabbit immunoglobulin (cat# SA5-10036; Thermo Fisher Scientific,). A Li-Cor Odyssey scanner was used for detection.

Baculovirus Generation and Amplification
The plasmids harboring class IA PI3K catalytic and regulatory subunits were transformed into DH10MultiBac cells (MultiBac, Geneva Biotech) containing the baculovirus viral genome (bacmid) and a

helper plasmid expressing transposase to transpose the expression cassette harboring the gene of interest into the baculovirus genome. Bacmids with successful incorporation of the expression cassette of pFastBac/ pACEBac1 into the viral genome was identified by blue-white screening and were purified from a single white colony using a standard isopropanol-ethanol extraction method. Briefly, colonies were grown overnight (~16 hours) in 3-5 mL 2xYT (BioBasic #SD7019). Cells were pelleted by centrifugation and the pellet was resuspended in 225 µL P1 Buffer (Qiagen MiniPrep Kit, #27106), chemically lysed by the addition of 225 µL Buffer P2, and the lysis reaction was neutralized by addition of 300 µL Buffer N3. Following centrifugation at 21130 rcf and 4°C (Rotor #5424 R), the supernatant was separated and mixed with 600 µL isopropanol to precipitate the DNA out of solution. Further centrifugation at the same temperature and speed pelleted the bacmid DNA, which was then washed with 500 µL 70% ethanol three times. The Bacmid DNA pellet was then dried for 1 minute and re-suspended in 50 µL Buffer EB. Purified bacmid was then transfected into Sf9 cells. 2 mL of Sf9 cells between 0.3-0.5X106 cells/mL were aliquoted into the wells of a 6-well plate and allowed to attach, creating a monolayer of cells at ~ 70-80% confluency. Transfection reactions were prepared by the addition of 2-10 ug of bacmid DNA to 100 µl 1xPBS and 12 µL polyethyleneimine (PEI) at 1 mg/mL (Polyethyleneimine “Max” MW 40.000, Polysciences #24765, USA) to 100 µL 1xPBS. The bacmid-PBS and the PEI-PBS solutions were mixed, and the reaction occurred for 20-30 minutes before addition drop-by-drop to an Sf9 monolayer containing well. Transfections were allowed to proceed for 5-7 days before harvesting virus containing supernatant as a PI viral stock. Viral stocks were amplified by adding P1 viral stock to suspension Sf9 cells between 1-2x106 cells/mL at a 1/100 volume ratio. This amplification produces a P2 stage viral stock that can be used in final protein expression. The amplification proceeded for 4-5 days before harvesting, with cell shaking at 120 RPM in a 27°C shaker (New Brunswick). Harvesting of P2 viral stocks was carried out by centrifuging cell suspensions in 50 mL Falcon tubes at 2281 RCF (Beckman GS-15), collecting the supernatant in a fresh sterile tube, and adding 5-10% inactivated fetal bovine serum (FBS; VWR Canada #97068-085).

Expression and purification of recombinant proteins

All PI3K constructs were expressed and purified as described previously (8-10). In brief the catalytic subunit and regulatory subunits were expressed using the pFASTBAC/ pACEBac1 expression system in Sf9 cells. After expressing the cells at 27°C for 55 hrs the cells were harvested at 1739 x g at 4°C using Eppendorf Centrifuge 5810R and the cells were flash frozen using liquid nitrogen and stored in -80 °C. The frozen pellets were resuspended in lysis buffer containing 20 mM Tris pH 8, 10 mM Imidazole, 100 mM NaCl, 5% glycerol [v/v], 2 mM βME, protease inhibitor [Protease Inhibitor Cocktail Set III, Sigma]) and sonicated for 2 min (15s on, 15 s off, level 4.0, Misonix sonicator 3000). Triton-X 100 was added to the lysate at a final concentration of 0.1% and then clarified by spinning at 15,366xg for 45 min (Beckman Coulter JA-20 rotor). The supernatant was loaded onto a 5 ml crude Ni-NTA column (GE healthcare) equilibrated in NiNTA A buffer containing 20 mM Tris pH 8, 100 mM NaCl, 10 mM Imidazole and 5% glycerol [v/v]. The column was washed using high salt buffer containing 20 mM Tris, 1 M NaCl, 10 mM Imidazole, 5% Glycerol [v/v] followed by NiNTA buffer wash (20 mM Tris pH 8, 100 mM NaCl, 21 mM Imidazole and 5% Glycerol). The protein was eluted using 100% NiNTA B buffer (20 mM Tris pH 8, 100 mM NaCl, 200 mM Imidazole and 5% Glycerol). The elute from the nickel column was loaded onto Streptavidin column (GE healthcare) and subjected to buffer wash using Hep A buffer (20 mM Tris pH 8, 100 mM NaCl, 5% Glycerol and 0.5 mM tris(2-carboxyethyl) phosphine [TCEP]). The column was incubated on ice for 3 hours in the presence of TEV protease and then eluted by a wash with HEP A buffer. Proteins were subjected to gel filtration using SuperdexTM 200 10/300 GL Increase column from GE healthcare. After gel filtration, the protein was concentrated, aliquoted, frozen, and stored at −80°C. NS1 constructs were transformed into Escherichia coli (BL21 (DE3)). Bacterial cultures were induced with 1 mm isopropyl 1-thio-β-d-galactopyranoside after growth to an A600 of 0.6–0.9 in 2× YT (Sigma) broth containing ampicillin at 100 µg/ml. Induction was allowed to proceed for 4 h at 37 °C. The bacteria were harvested by centrifugation, and the pellets were stored at −80 °C. Frozen E. coli pellets were resuspended in lysis buffer and sonicated on ice for 5 min (10 s on, 10 s off, level 6.0, Misonix sonicator 3000). Triton X-100 was added to the lysate at a concentration of 0.1% and centrifuged at 20 000 × g for 45 min (Beckman Coulter Avanti J-25I, JA 25.50 rotor). The supernatant was then loaded onto a 5-ml GSTrap™ HP Column (cytivia) equilibrated in buffer containing 20 mM Tris pH 8, 100 mM NaCl, and 5% glycerol. The column was washed with 30 ml of this buffer. TEV protease was added to a final concentration of ~0.3 mg/ml. The cleavage was allowed to proceed overnight at 4 °C. To de-enrich the

TEV protease, the protein solution was loaded onto a HisTrapTM FF column and eluted with 10 ml of Ni-NTA A buffer. The elution was concentrated to ~2 ml. NS1 protein was injected onto a SuperdexTM 75 10/300 GL size exclusion column (GE Healthcare) equilibrated in gel filtration buffer (20 mm HEPES (pH 7.5), 150 mm NaCl, 1 mM TCEP). After gel filtration, the protein was concentrated, aliquoted, frozen, and stored at −80°C.

Lipid Vesicle Preparation
Assays were carried out with PM mimic vesicles consisting of 5% brain PIP2, 20% brain PS, 45% egg yolk PE, 15% egg yolk phosphatidylcholine (PC) (Avanti #840051C), 10% cholesterol (Sigma Aldrich, #47127-U), and 5% egg yolk sphingomyelin (Sigma Aldrich, #S0756). To generate vesicles, the lipid mixtures were combined in organic solvent. The mixture was then evaporated using a stream of argon gas followed by desiccation under vacuum for 45 minutes. The lipids were resuspended in a lipid buffer (25 mM HEPES pH 7, 100 mM NaCl, 10% Glycerol [v/v]) and the solution was subjected to sonication for 15 mins. The vesicles were subjected to five freeze thaw cycles and extruded 11 times through a 100 nm filter (T and T Scientific: TT-002–0010). The extruded vesicles were sonicated again for 5 min, aliquoted and stored at −80°C.

ATPase assay
All PI3K assays used the Transcreener ADP2 Fluorescence Intensity (FI) assay (Bellbrook labs) which measures formation of ADP. 2 µL of a PI3K solution (final concentration 100nM-400nM) at 2X final concentration was mixed with 2 µL substrate solution containing ATP and lipid vesicles (final concentration of 0.45 vesicles and 100 µM ATP), and the reaction was allowed to proceed for 60 min at 20°C. For experiments examining activation by NS1 protein, the PI3K and NS1 protein were allowed to pre-incubate for 15 minutes before incubation with substrate, with NS1 being present at a final concentration of 1 µM in the kinase reaction.
The reaction was stopped with 4 µL of 2X stop and detect solution containing EDTA (chelates Mg2+, stopping kinase activity) along with 8 nM ADP Alexa Fluor 594 Tracer and 93.7 µg/mL ADP2 Antibody IRDye QC-1, and was allowed to incubate for 60 minutes. The fluorescence intensity was measured using a SpectraMax M5 plate reader at excitation 590 nm and emission 620 nm. This data was normalized against a 0–100% ADP window made using conditions containing a final concentration of 100 µM ATP or ADP. % ATP turnover was interpolated from an ATP standard curve obtained from performing the assay on 100 µM (total) ATP/ADP mixtures with increasing concentrations of ADP.

References

1. Niwa H, Yamamura K, Miyazaki J. 1991. Efficient selection for high-expression transfectants with a novel eukaryotic vector. Gene 108:193-9.
2. Ayllon J, Domingues P, Rajsbaum R, Miorin L, Schmolke M, Hale BG, Garcia-Sastre A. 2014. A single amino acid substitution in the novel H7N9 influenza A virus NS1 protein increases CPSF30 binding and virulence. J Virol 88:12146-51.
3. Kerry PS, Ayllon J, Taylor MA, Hass C, Lewis A, Garcia-Sastre A, Randall RE, Hale BG, Russell RJ. 2011. A transient homotypic interaction model for the influenza A virus NS1 protein effector domain. PLoS One 6:e17946.
4. Zhou B, Lin X, Wang W, Halpin RA, Bera J, Stockwell TB, Barr IG, Wentworth DE. 2014. Universal influenza B virus genomic amplification facilitates sequencing, diagnostics, and reverse genetics. J Clin Microbiol 52:1330-7.
5. Zhou B, Donnelly ME, Scholes DT, St George K, Hatta M, Kawaoka Y, Wentworth DE. 2009. Single-reaction genomic amplification accelerates sequencing and vaccine production for classical and Swine origin human influenza a viruses. J Virol 83:10309-13.
6. Lopes AM, Domingues P, Zell R, Hale BG. 2017. Structure-Guided Functional Annotation of the Influenza A Virus NS1 Protein Reveals Dynamic Evolution of the p85beta-Binding Site during Circulation in Humans. J Virol 91.
7. Turkington HL, Juozapaitis M, Tsolakos N, Corrales-Aguilar E, Schwemmle M, Hale BG. 2018. Unexpected Functional Divergence of Bat Influenza Virus NS1 Proteins. J Virol 92.

8. Dornan GL, Stariha JTB, Rathinaswamy MK, Powell CJ, Boulanger MJ, Burke JE. 2020. Defining How Oncogenic and Developmental Mutations of PIK3R1 Alter the Regulation of Class IA Phosphoinositide 3-Kinases. Structure 28:145-156 e5.
9. Dornan GL, Siempelkamp BD, Jenkins ML, Vadas O, Lucas CL, Burke JE. 2017. Conformational disruption of PI3Kdelta regulation by immunodeficiency mutations in PIK3CD and PIK3R1. Proc Natl Acad Sci U S A 114:1982-1987.
10. Jenkins ML, Ranga-Prasad H, Parson MAH, Harris NJ, Rathinaswamy MK, Burke JE. 2023. Oncogenic mutations of PIK3CA lead to increased membrane recruitment driven by reorientation of the ABD, p85 and C-terminus. Nat Commun 14:181.